Disorder effects in unconventional superconductors

Zur Erlangung des akademischen Grades eines

Doktors der Naturwissenschaften

von der Fakultät für Physik
des Karlsruher Instituts für Technologie

genehmigte

Dissertation

von

Mareike Hoyer, M. Sc.
aus Kassel

Tag der mündlichen Prüfung: 10.02.2017

Referent: Prof. Dr. Jörg Schmalian
Korreferent: Prof. Dr. Matthieu Le Tacon

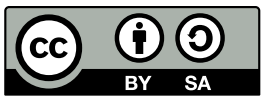

Introduction

Condensed matter physics is dedicated to much more than merely the investigation of *the* condensed state of matter and its properties: The vast number of electrons and their mutual interaction can give rise to a multitude of different phases of matter with interesting and surprising characteristics [1]. The discovery of ever more such *emergent* states of matter has kept physicists fascinated over many decades now and regularly renewed the interest in the field.

One of the most famous examples of the condensation into such a new phase of matter characterized by unexpected properties is the superconducting phase transition observed in many materials at low temperatures: Upon cooling these materials below a critical temperature, they become perfect conductors [2–4] as well as perfect diamagnets [5]. What seems highly promising for applications at first glance unfortunately happens at rather low temperatures – a few Kelvin in the case of the first known superconductors. Moreover, superconductivity is also destroyed by magnetic fields exceeding a critical field strength. In 1986, the interest in superconductivity was immensely boosted again by the discovery of transition temperatures around 30 K in cuprate materials [6]. The intense follow-up research indeed resulted in the development of a large class of copper-based high-temperature superconducting materials some of which may be cooled to operating temperature already by liquid nitrogen. Yet another class of high-temperature superconductors based on iron was discovered in 2008 [7], even though their transition temperatures do not reach up to the boiling point of nitrogen yet.

The interest in these new superconducting materials is however not limited to materials science and engineering. Cuprate and iron-based superconductors are in fact part of a much larger group of materials in which the properties of the superconducting state qualitatively differ from the conventional superconductors. Hence, these *unconventional* superconductors cannot be understood in terms of the standard theory for superconductivity, and in particular, a different mechanism must be responsible for the formation of the superconducting condensate. The explanation of unconventional superconductivity is one of the questions that has been pestering condensed matter physicists for decades now and at present, despite all progress, it seems that this quest may well last a while longer – just as it took almost half a century to find a microscopic explanation for conventional superconductivity [8, 9]. Another interesting aspect of unconventional superconductivity is that it is often observed in close vicinity to (and sometimes even in coexistence with) other ordered phases, such as magnetic order. Consequently, the properties of these materials can be tuned by doping or application of pressure, and the resulting phase diagrams can be quite complex. However, since this variety of phases arises from the same electrons, the investigation of their interplay is hoped to further elucidate the nature of unconventional superconductivity.

Doping a material means that a certain fraction of one type of atoms in the chemical compound is substituted by a similar element in order to manipulate the properties of the material. For example, this is routinely used in semiconductors to add or remove charge carriers. Furthermore, as the dopant atoms are distributed randomly throughout the material and locally change the crystal structure, doping introduces *disorder* to the system: The itinerant electrons that are responsible for the macroscopic properties of the sample might be scattered off these impurities. Therefore, one of the questions that arises naturally in the context of these new superconducting materials is how disorder, and thereby

doping, affects the diverse states of matter that have been observed in these materials, as well as their interplay.

While conventional superconductivity turned out to be quite robust against nonmagnetic disorder – known as the Anderson theorem [10–12] – unconventional superconductivity can already be destroyed by the presence of nonmagnetic impurities. On the other hand, also the ordered states competing with superconductivity can be weakened by impurity scattering. For example, magnetic order is often more vulnerable to the presence of impurities than unconventional superconductivity. In the case of iron-based superconductors, where the unconventional superconducting phase emerges from the magnetically ordered undoped compounds, the superconducting transition temperature has indeed been predicted to increase with disorder in this regime [13]. Moreover, these complicated materials might even provide new mechanisms for protection against certain types of disorder, as will be discussed in Chaps. 2 and 3 of the present thesis. Furthermore, even though disorder may be detrimental to the formation of ordered phases, it also provides the interesting opportunity to tune material properties by deliberately introducing disorder, e. g., by irradiation, or removing it via annealing. This idea has been put forward in the context of superconductivity [14, 15] and will also guide the discussion of magnetic order presented in Chap. 4 of this thesis.

The central theme of this dissertation is the investigation of disorder effects in the context of unconventional superconductors. This topic is approached from a theoretical point of view in the remainder of this thesis: We extend effective low-energy models for different types of order and in different systems to account for scattering processes of the conduction electrons off impurities. In doing so, we assume the disorder to be *weak* such that the mean-free path is sufficiently large and localization effects [16] can be neglected in our discussion. This thesis is structured as follows.

The introductory **Chapter 1** splits in three parts. Firstly, we present a description of the ordered state in terms of an order parameter (going back to Landau and Ginzburg [17, 18]) and establish the connection to microscopic theories. Secondly, we introduce two different systems probably hosting unconventional superconducting states that shall be discussed in more detail in the following chapters: the iron-based systems and the $LaAlO_3/SrTiO_3$ interface. The last part of this introduction is concerned with the weakening effects of competing phases, impurities, and fluctuations on a given ordered state. In particular, we provide details on the framework which is used for our investigation of impurity scattering in the remainder of this thesis.

Chapter 2 concentrates on the effect of disorder on the transition temperature for two different superconducting states suggested for the iron-based superconductors. Here, the focus of our discussion lies on the effect of orbital-magnetic impurities which are pairbreaking for conventional superconductivity but do not suppress the transition temperature of the proposed unconventional superconducting state. These results apply more generally, however, are of particular interest in the context of iron-based superconductors where orbital-magnetic impurities could arise from the nucleation of competing order around nonmagnetic impurities.

A similar analysis for superconductivity in the $LaAlO_3/SrTiO_3$ interface is presented in **Chapter 3**. Here, we consider the effect of the most general type of disorder due to magnetic impurities or nonmagnetic impurities, respectively. However, as the Fermi surface of this system is strongly polarized with respect to spin and orbital character, certain scattering processes are strongly suppressed. Most notably, this results in a relative protection of the proposed unconventional superconducting state (compared to the conventional one) against magnetic impurities.

In **Chapter 4**, we investigate the effect of disorder on three magnetic ground states conceivable for iron-based superconductors. We find that the consideration of disorder excludes neither type of magnetic ordering. Furthermore, our analysis demonstrates that disorder, in combination with basic

band structure parameters, can in principle be used to tune the nature of the magnetic ground state. In particular, weak disorder can quite naturally account for the formation of a nonuniform charge-spin density wave state, such as it has recently been observed experimentally in various of the hole-doped compounds.

Lastly, **Chapter 5** is not concerned with disorder but addresses a more fundamental question about the clean models we started with. Effective mean-field theories, such as those used throughout the previous chapters, are a useful tool in theoretical physics and can be applied to a variety of problems. They replace the interaction between particles (which leads to the formation of new states of matter) by the interaction of each particle with an effective 'mean field', and thus rely on the assumption that fluctuations of the mean field are negligible. In this chapter, we reassess the role of zero-temperature quantum fluctuation corrections to the gap equation for several mean-field theories.

For the sake of better readability, a list of the acronyms and the notation used throughout this thesis is provided on pages 143 and 145, respectively.

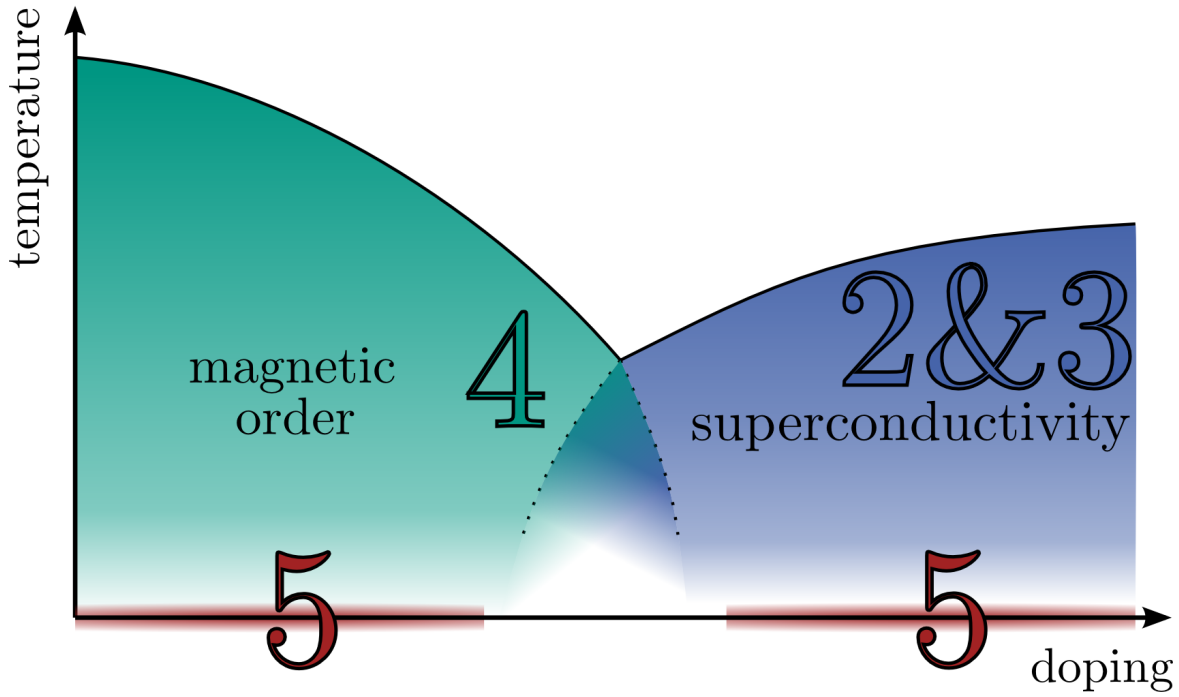

Schematic phase diagram of unconventional superconductors. We show magnetic order as one example of another ordered phase that competes with superconductivity. The numbers indicate the chapters of this thesis concentrating on the respective regions of the phase diagram.

Contents

Chapter 1

Fundamentals: Superconductivity

Superconductivity was first recognized as an exciting new state of matter by Heike Kamerlingh Onnes, who characterized superconductors as *perfect conductors* in 1911 [2–4]. This description, however, is not complete: Only the identification of superconductors as also being *perfect diamagnets* by Walther Meißner and Robert Ochsenfeld in 1933 [5] could fully account for their electrodynamics. This chapter is meant as a tailor-made introduction to the aspects of superconductivity advertised in the title of this thesis – unconventional superconductivity, and the effect of disorder on superconductivity.

As a preliminary, we summarize the theoretical description of conventional superconductivity by phenomenological as well as microscopic approaches which successfully reproduce the characteristics of the superconducting state as observed in a wide range of the conventional materials. These include the universal ratio $2\Delta(T=0)/k_{\mathrm{B}}T_{\mathrm{c}} = 3.528$ of the superconducting energy gap at zero temperature and the transition temperature, its characteristic square-root temperature dependence, as well as the jump in the specific heat at the phase transition.

In the second part, we turn towards unconventional superconductors. These systems can have unexpectedly high transition temperatures and arise in the vicinity of other types of order. They cannot be interpreted in terms of the phonon-mediated mechanism responsible for conventional superconductivity. However, analogous theories can be used to describe the more complicated unconventional superconducting states and their properties – even though the respective mechanisms have not been identified yet. We introduce two examples of materials hosting potentially unconventional superconductivity that will be investigated in more detail in the remainder of this thesis.

Lastly, we comment on the stability of the superconducting state. Many of the unconventional superconductors have particularly high transition temperatures, however, superconductivity is not per se more robust in these materials. On the contrary, it is a prevailing view that more complicated superconducting pairing states can be rather frail, for instance, in the presence of impurities. We postpone the discussion of these aspects to the following chapters and summarize the effect of weak disorder on conventional superconductivity here – both as a reference point for later discussions as well as to introduce the theoretical framework in which we will treat disorder throughout this thesis.

1.1 Theories of superconductivity: an introduction

After the discovery of superconductivity in 1911, it took a few decades until – after many attempts had failed [19] – a major step towards the microscopic understanding of superconductivity was finally provided by Bardeen, Cooper, and Schrieffer in 1957 [8, 9].

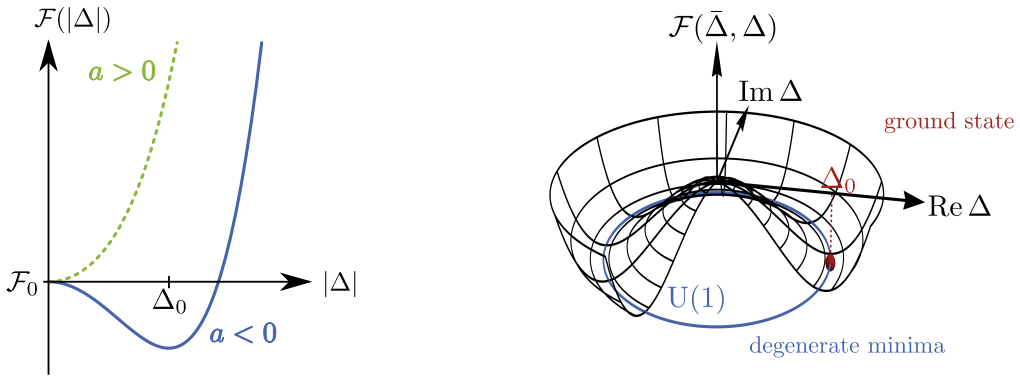

(a) free energy **(b)** 'Mexican hat' potential

Figure 1.1: Ginzburg-Landau expansion of the free energy up to quartic order. The sign of the quadratic coefficient $a(T)$ determines whether the minimum of the free energy occurs at $|\Delta| = 0$ or at a finite value Δ_0, as evident from the form of $\mathcal{F}(|\Delta|)$ shown in (a). In the ordered low-temperature phase, the free energy takes the characteristic 'Mexican hat' form depicted in (b), resulting in the U(1) manifold of possible ground states indicated in blue. Any given ground state (indicated by the red dot) corresponds to a specific choice for the phase of the complex order parameter Δ, and hence breaks the symmetry of the underlying Hamiltonian.

But even before the microscopic nature of the superconducting state was uncovered, at least phenomenological approaches had been successful: the London equations [20] describing the electrodynamics of superconductors, and the more general Ginzburg-Landau theory [18]. The latter was published in 1950, though the underlying Landau theory of phase transitions [17] dates back to 1937. It constitutes a very useful concept in the context of phase transitions and spontaneous symmetry breaking, and is applicable to other types of phase transition as well, e. g., magnetic phase transitions.

In the following sections, we summarize the concept of the phenomenological Ginzburg-Landau theory and its connection to the microscopic BCS theory of superconductivity. In the remainder of this thesis, we will then widely employ the Ginzburg-Landau free energy expansion, with coefficients derived from microscopic models.

1.1.1 Phenomenological Ginzburg-Landau theory

The Landau theory of phase transitions [17] provides a very useful phenomenological approach to second-order phase transitions, where the ordered low-temperature phase is characterized by an order parameter which vanishes continuously at the phase transition, and is zero in the high-temperature normal state. The application to superconductivity was achieved by Ginzburg and Landau [18], who introduced a complex pseudowavefunction $\psi(\boldsymbol{r})$ as the order parameter for the superconducting state, which is related to the local density of superconducting electrons as $n_s(\boldsymbol{r}) = |\psi(\boldsymbol{r})|^2$. Let us already note here that shortly after the publication of the microscopic BCS theory, Gor'kov succeeded in connecting these two theories in the regime close to the transition temperature [21], and identified $\psi(\boldsymbol{r})$ as the Cooper-pair wave function directly proportional to the gap function $\Delta(\boldsymbol{r})$ which we will use as an order parameter in the remainder.

Expansion of the free energy The cornerstone of Ginzburg-Landau theory is an expansion of the free energy in terms of the order parameter $\Delta \in \mathbb{C}$, valid in the vicinity of the phase transition where the order parameter is small. For a homogeneous superconductor in the absence of external fields,[1] the most general form of such an expansion is given by

$$\mathcal{F}(\Delta^*, \Delta) = \mathcal{F}_0 + a(T)|\Delta|^2 + \frac{b(T)}{2}|\Delta|^4 + \mathcal{O}(|\Delta|^6)\,, \tag{1.1}$$

reflecting the fact that a constant phase of the order parameter is of no physical significance and hence the free energy is invariant under the global U(1) transformation of the phase, $\Delta \to \Delta \mathrm{e}^{\mathrm{i}\varphi}$ ($\varphi \in \mathbb{R}$). We denote the free energy of the normal state by $\mathcal{F}_0$ and assume $b(T) \approx b > 0$ for the quartic coefficient to ensure the stability for $\Delta \to \infty$. The sign change of the quadratic coefficient then marks the phase transition, as sketched in Fig. 1.1 (a): While the free energy is minimized by $|\Delta_0| = 0$ as long as $a > 0$, a new minimum $|\Delta_0| = \sqrt{|a(T)|/b}$ arises in the low-temperature phase (characterized by $a < 0$) which lowers the free energy as compared to its normal-state value $\mathcal{F}_0$.

In principle, the Ginzburg-Landau coefficients contain the full knowledge about thermodynamic properties of the underlying system. However, within Ginzburg-Landau theory itself, they remain indeterminate; only the connection to microscopic theories allows to relate the coefficients to physically meaningful quantities. In App. A, we derive the corresponding coefficients for a neutral superconductor from a microscopic model. In particular, the transition temperature T_c can then be expressed in terms of parameters of this model: It follows from the condition that the quadratic coefficient change sign, $a(T_\mathrm{c}) = 0$, which we will exploit in Chaps. 2 and 3. Furthermore, in Chap. 4 we will use that the structure of the magnetic ground state can be inferred from an analogous expansion of the free energy in terms of the order parameter describing the magnetically ordered state.

Spontaneous symmetry breaking The superconducting ground state is characterized by a complex order parameter $\Delta_0 = |\Delta_0|\mathrm{e}^{\mathrm{i}\varphi_0}$, where $|\Delta_0|$ denotes the magnitude and φ_0 its fixed phase. (In the remainder, for the sake of convenience, we choose the value of the phase such that $\Delta_0 \in \mathbb{R}$.) Therefore, this ground state does not share the U(1) symmetry of the free energy (1.1), as visualized in Fig. 1.1 (b). This phenomenon of a ground state which is of lower symmetry than the underlying Hamiltonian of the system is referred to as *spontaneous symmetry breaking* and applies to a wide range of other phase transitions as well. A famous example is the ferromagnetic phase transition, where the magnetization $\boldsymbol{M} \in \mathbb{R}^{d_\mathrm{s}}$ can be used as an order parameter, and the $\mathrm{O}(d_\mathrm{s})$ spin-rotational symmetry is lowered to $\mathrm{O}(d_\mathrm{s} - 1)$ at the phase transition.

One immediate and interesting consequence of such a spontaneously broken continuous symmetry is the appearance of new massless modes [22, 23]. The number of these Nambu-Goldstone bosons corresponds to the number of generators of the symmetry that are broken. In the context of superconductivity, where U(1) is broken, this implies the existence of one Nambu-Goldstone mode which is readily identified with long-wavelength fluctuations of the phase of the order parameter. This is also illustrated in Fig. 1.1 (b), where the ground states characterized by different values of the phase are degenerate in energy whereas changes of the amplitude of the order parameter always lead to an increase in energy. For further discussion of fluctuations of the order parameter around its mean-field value, we refer to Sec. 1.3.3 and Chap. 5.

[1] The full Ginzburg-Landau equations contain gradient terms as well as the coupling to the electromagnetic field. Therefore, they also allow to determine spatial profiles of the order parameter, e. g., at interfaces or in the intermediate regime of type-II superconductors, and to describe the electrodynamics of superconductors.

1.1.2 Microscopic theory of superconductivity

One crucial preliminary for a microscopic understanding of the superconducting state was the notion that a Fermi gas is unstable towards the formation of a bound pair of electrons experiencing a net attractive interaction [24], no matter how weak. Such a net attractive interaction could for example arise from electron–phonon coupling [25]: Due to the huge mass difference of the itinerant electrons and the ions forming the lattice, the latter relax on much larger timescales, thereby allowing for a retarded effective interaction between electrons via the lattice which can be attractive. Indeed, pairs of electrons connected by time reversal – i. e., one characterized by momentum $\boldsymbol{k}$ and spin $\uparrow$ and the other by momentum $-\boldsymbol{k}$ and spin $\downarrow$ – turned out to form the superconducting condensate,[2] and are named Cooper pairs in honor of Leon Cooper who first proposed this concept in the context of superconductivity.

Mean-field theory Within the celebrated microscopic BCS theory of superconductivity [8, 9], the presence of Cooper pairs is reflected in a nonzero ground-state expectation value of the pair operator $\sum_{\boldsymbol{k}} \hat{\psi}_{-\boldsymbol{k},\downarrow}\hat{\psi}_{\boldsymbol{k},\uparrow}$. BCS theory then builds on the assumption that this operator deviates only little from its expectation value which is denoted Δ and corresponds to the order parameter as introduced in the context of Ginzburg-Landau theory. This assumption allows to reduce the original many-body problem of interacting electrons to the effective Hamiltonian

$$\hat{\mathcal{H}}_{\mathrm{BCS}} = \sum_{\boldsymbol{k},\sigma} \varepsilon_{\boldsymbol{k}} \hat{\psi}^\dagger_{\boldsymbol{k},\sigma}\hat{\psi}_{\boldsymbol{k},\sigma} + \sum_{\boldsymbol{k}} \left(\Delta \hat{\psi}^\dagger_{\boldsymbol{k}\uparrow}\hat{\psi}^\dagger_{-\boldsymbol{k},\downarrow} + \mathrm{H.\,c.}\right). \tag{1.2}$$

Since this Hamiltonian is bilinear in fermionic operators, it is readily diagonalized which results in a gapped spectrum that can indeed account for experimental characteristics of the superconducting state.

For pedagogical reviews of BCS theory, its derivation, and further implications, we refer to standard condensed matter textbooks. Let us however highlight two further aspects here. Firstly, BCS theory is a mean-field theory. Within such a mean-field description, the electron–electron interaction is replaced by the 'mean field' Δ to which the electrons couple instead, and which is generated by the interacting electrons themselves. This implies that its validity strongly builds on the assumption that deviations from the mean-field value – fluctuations – are negligible. We will continue the discussion of fluctuations in the context of mean-field theories in Secs. 1.3.3 and 5. Secondly, on a technical level, BCS theory readily follows from a decoupling of the quartic interaction term in the Cooper channel, which can be efficiently implemented in a field-integral approach to superconductivity.

Field-integral formulation One advantage of the field-integral approach over the canonical formulation of quantum-field theory is the straightforward application to problems which cannot be tackled by perturbation theory. Although we will not use its full capacity, we will formulate most calculations in the language of field integrals. The field integral for the partition function in terms of fermionic coherent states (represented by Grassmann fields $\bar{\psi}(\boldsymbol{r},\tau)$ and $\psi(\boldsymbol{r},\tau)$) reads $\mathcal{Z} = \int \mathcal{D}[\bar{\psi},\psi]\, \mathrm{e}^{-\mathcal{S}(\bar{\psi},\psi)}$, where

$$\mathcal{S}(\bar{\psi},\psi) = \int_0^\beta \mathrm{d}\tau\, \mathrm{d}\boldsymbol{r} \left[\sum_\sigma \bar{\psi}_\sigma(\boldsymbol{r},\tau)\Big(\partial_\tau - \frac{1}{2m}\boldsymbol{\nabla}^2 - \mu\Big)\psi_\sigma(\boldsymbol{r},\tau) + V_{\mathrm{SC}}\, \bar{\psi}_\uparrow(\boldsymbol{r},\tau)\bar{\psi}_\downarrow(\boldsymbol{r},\tau)\psi_\downarrow(\boldsymbol{r},\tau)\psi_\uparrow(\boldsymbol{r},\tau)\right] \tag{1.3}$$

[2] This is not true for the more exotic triplet superconducting states and the Fulde-Ferrell-Larkin-Ovchinnikov phase. However, these will not be included in our discussion of examples of unconventional superconductivity in the remainder of this thesis.

is the action for a (neutral) superconductor, stated in real space and imaginary-time representation. Here, $\beta = 1/T$, and μ denotes the chemical potential. Furthermore, this is a weak-coupling theory controlled by the small attractive coupling $V_{\mathrm{SC}} < 0$. The quartic interaction term can be decoupled by means of a Hubbard-Stratonovich transformation which artificially introduces an additional bosonic field. In the context of superconductivity, this auxiliary field is a complex scalar field usually denoted $\Delta \in \mathbb{C}$, already anticipating the connection to BCS theory. Indeed, the action at this step assumes a form analogous to the BCS Hamiltonian (1.2). On a technical level, this procedure transforms the fermionic field integral to Gaussian form and hence fermions can be 'integrated out'. This can be used to obtain an effective action for the new bosonic fields,

$$\mathcal{S}_{\mathrm{eff}}(\bar{\Delta}, \Delta) = \frac{1}{|V_{\mathrm{SC}}|} \int_q |\Delta_q|^2 - \mathrm{Tr} \ln(-\mathcal{G}^{-1}) \,. \tag{1.4}$$

Here, we denote the corresponding complex conjugate by $\bar{\Delta}$, and $\mathcal{G}$ is the matrix Green's function in Nambu space, see App. A.1.

At this point, we can use a saddle-point approximation to the field integral $\mathcal{Z} = \int \mathcal{D}[\bar{\Delta}, \Delta] \, \mathrm{e}^{-\mathcal{S}_{\mathrm{eff}}(\bar{\Delta}, \Delta)}$ to derive an effective low-energy description. In that, we utilize that the dominant contribution to the field integral stems from the saddle point and hence is determined by the condition $\delta \mathcal{S}_{\mathrm{eff}} / \delta \Delta_q = 0$. Then, by assumption of a static and spatially homogeneous mean field, one obtains the free energy in terms of the mean-field order parameter Δ_0 quite naturally from this alternative approach. The expansion takes the form of the Ginzburg-Landau free energy (1.1) and thus makes the connection between the phenomenological description and the microscopic model. Furthermore, the mean-field value Δ_0 is readily obtained from the saddle-point condition, which corresponds to the self-consistent gap equation within BCS theory.

1.2 Unconventional superconductivity

The term 'unconventional superconductor' is used to distinguish a variety of different materials with characteristics deviating from the well-studied 'conventional superconductors' whose properties are splendidly captured by BCS theory. The nature and mechanism of superconductivity in these materials, however, is not unique. Examples of unconventional superconductors include heavy-fermion compounds (such as $CeCu_2Si_2$ [26], UBe_{13} [27], and UPt_3 [28]), organic materials like the triplet superconductors $(TMTSF)_2PF_6$ [29] and $(TMTSF)_2ClO_4$ [30], and the d-wave cuprate superconductors [6] which still hold the record for highest T_c at ambient pressure. Many of these violate the so called 'Matthias' rules' – named after Bernd T. Matthias and established in the search for ever higher transition temperatures in conventional superconductors: Many of the unconventional and, more remarkably, the high-T_c compounds contain oxygen and are close to magnetism, which are both ingredients detrimental to conventional superconductivity.

In this section, we introduce the more recently discovered unconventional superconductors in detail on which we will focus in the remainder of this thesis: the class of iron-based superconductors and the heterointerface between $LaAlO_3$ and $SrTiO_3$. In both systems, impurities are inevitably present and we believe them to be important for the discussion of the unconventional superconducting states that have been proposed in these materials. In Chaps. 2, 3, and 4, we will investigate the role of disorder in these system and also highlight some unexpected effects of disorder.

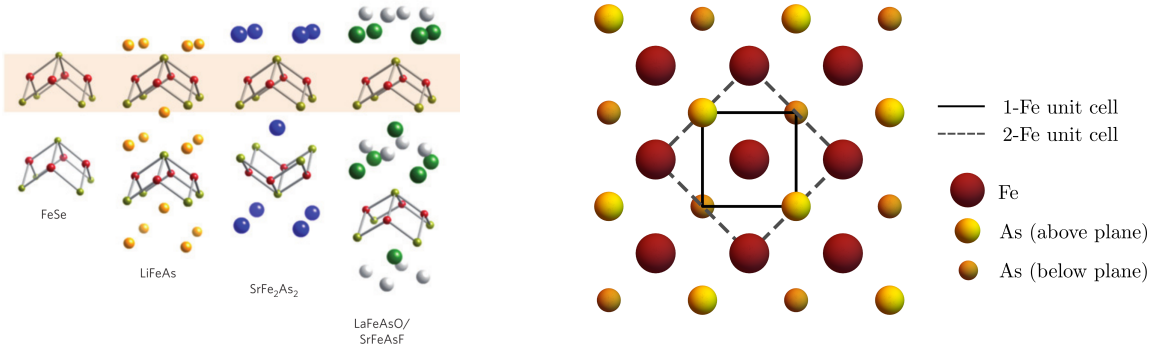

(a) crystal structures **(b)** top view of the FeAs plane

[Adapted by permission from Macmillan Publishers Ltd: Nature Physics **6**, 645, copyright 2010, cf. Ref. 33.]

Figure 1.2: Crystal structures of the best-studied families of iron-based superconductors. The characteristic FeAs-type planes – highlighted in light red in (a) and common to all representatives of the FeSCs – are responsible for their peculiar properties. Because of the staggered As atoms (indicated in yellow), the unit cell contains two iron atoms, yet minimalistic models often work with a 1-Fe unit cell instead. Both possibilities are shown in (b).

1.2.1 Iron-based superconductors

The 'iron age' of superconductivity began with the discovery of an unexpectedly high T_c of 26 K in the oxypnictide compound $La(O_{0.89}F_{0.11})FeAs$ in 2008 [7]. Electron-phonon coupling was soon shown to be too weak [31] to account for superconductivity (SC) with such a high transition temperature, implying the discovery of a new type of unconventional superconductors. The class of iron-based superconductors (FeSCs) includes iron pnictides (containing elements from the pnictogen group, in most cases As) and iron chalcogenides (containing an element from the chalcogen group, in most cases Se). The occurrence of bulk superconductivity with transition temperatures reaching up to 56 K (reported in $Sr_{0.5}Sm_{0.5}FeAsF$ [32]) in materials containing a considerable fraction of iron (which by itself is ferromagnetic) strengthened the new paradigm developed in the 'copper age' that magnetism could actually be beneficial for (unconventional) superconductivity. Thus, even though the transition temperatures in FeSCs might never reach the boiling point of liquid nitrogen, these materials provide another chance to get closer to a full understanding of the phenomenon of unconventional superconductivity. For a detailed overview on the research progress, we refer to the review articles provided by Refs. 33–36. More recently, also thin films of iron chalcogenides attracted considerable attention since the transition temperatures in FeSe layers on $SrTiO_3$ substrates have been found [37, 38] to be significantly higher than in the bulk material – but in the remainder, we concentrate on bulk FeSCs only. ($A = K, Rb, Cs$) or of the 11 type like FeSe.

Crystal structure There are several families of iron pnictides and iron chalcogenides which all share the same building blocks: the eponymous layers of iron atoms and pnictogens (e. g., As) or chalcogens (e. g., Se), respectively, separated by blocking layers consisting of alkali metals, alkaline earth metals, and rare-earth oxides or fluorides, for instance. These layers are only weakly coupled and the interesting physics takes place primarily in the quasi-2D FeAs layers. The best-known families, presented in Fig. 1.2 (a), are the 1111 iron pnictides of type RFeAsO (R = rare earth), the 122 iron pnictides with

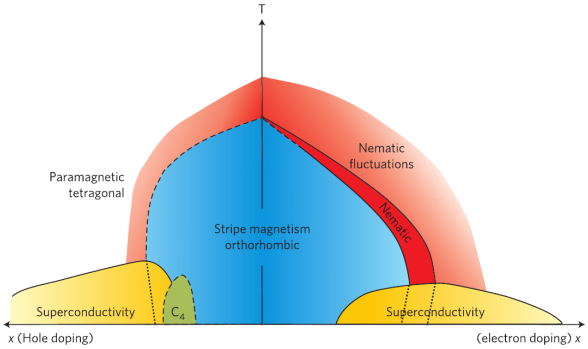

[Adapted by permission from Macmillan Publishers Ltd: Nature Physics **10**, 97, copyright 2014, cf. Ref. 39.]

Figure 1.3: Characteristic phase diagram of iron-based superconductors. This sketch summarizes the different types of order observed in FeSCs. As an example, doping is used as a tuning parameter here, however, similar phase diagrams are obtained by application of pressure, for instance. Quite generically, superconductivity emerges out of a magnetically ordered state of stripe type. The magnetic phase transition coincides with or is preceded by a structural phase transition, implying the possibility of an intermediate nematic state. Furthermore, in a small region of the phase diagram, another phase of tetragonal magnetic order has been observed in various materials.

molecular formula XFe_2As_2 (X = alkaline earth metal), the 111 iron pnictides like LiFeAs, and iron chalcogenides of structure $A_xFe_{2-y}Se$

In the paramagnetic ground state of the undoped parent compounds, the crystal structure is tetragonal and the iron atoms are arranged in a square lattice. The pnictogen or chalcogen atoms are located slightly below or above these planes, as indicated in Fig. 1.2 (b). However, since the electrons dominating the low-energy physics of the FeSCs stem from the Fe atoms, we can ignore the inequivalent pnictogen or chalcogen positions as long as we are concerned with minimal models rather than more realistic but potentially parameter-overloaded models. Therefore, in the remainder, we will work in the 1-Fe unit cell, reducing the number of orbitals (and thus bands) taken into account and ignoring a possible hybridization and splitting of these orbitals.

Phase diagrams Over the years, the family of FeSCs has grown considerably, and some representatives[3] exhibit interesting features that are nonuniversal. Most compounds, however, share the same characteristics, summarized in the rich phase diagram sketched in Fig. 1.3. In the following, we strive for simple models that can account for the most important properties the FeSCs have in common rather than for a multitude of theories accounting for particular features of individual compounds. One striking feature is the interplay of competing instabilities:

- The undoped (so-called parent) compounds are metallic and order antiferromagnetically at the Néel temperature T_N. This results in the characteristic *stripe-magnetic state*, which will be discussed in more detail in Sec. 4.1.1.

- Magnetic ordering is closely linked to a structural transition at T_s. In some compounds, the structural transition even occurs at temperatures $T_s > T_N$, implying an intermediate regime of

[3] For example, the stoichiometric compound LiFeAs is superconducting already at ambient pressure (without doping), and FeSe exhibits nematic order, yet no magnetic ordering occurs down to zero temperature.

nematic order where the tetragonal symmetry is broken while spin-rotational symmetry remains intact, cf. Sec. 4.1.1, or Ref. 39 for a review on nematicity.

- Upon doping, magnetism is suppressed and (unconventional) *superconductivity* with a critical temperature T_c emerges. More details concerning the nature of the superconducting state in FeSCs are provided in Sec. 2.1, or see Ref. 40 for a review on the pairing states.

- Hole doping can furthermore lead to a regime of *tetragonal magnetic order* before superconductivity sets in, as discussed in Sec. 4.1.2.

In some materials, such as $Ba(Fe_{1-x}Co_x)_2As_2$, magnetic order and superconductivity even coexist. Their competition, however, leads to a weakening of the ordered phase, reflected in the suppression of transition temperatures, see also Sec. 1.3.1. The importance of phase competition in FeSCs is further supported by theory, and model calculations [41–43] even predict a third instability: charge-density wave order (with imaginary order parameter, i. e., indicating static charge currents), that competes with superconductivity and spin-density wave order.

In most studies, the phase diagrams are tuned by doping, but pressure has a similar effect. However, the relation between changes of the lattice structure due to pressure and due to chemical substitution is not well understood. In addition to changes of the lattice parameters, chemical substitution is also associated with charge doping and, additionally, the dopants can act as impurities off which the electrons are scattered. The investigation of the latter effect will be a recurring theme of this thesis and is discussed in the context of FeSCs in Chaps. 2 and 4.

Models for iron-based superconductors Even though for some FeSC compounds correlations are clearly important [35, 44], we consider these materials from the viewpoint of itinerant electrons rather than local moments here. This approach is motivated by the fact that both magnetic order and superconductivity originate from the same electrons, and therefore should be treated on equal terms. Even more, the tetragonal magnetic phases observed in various hole-doped compounds arise quite naturally from itinerant models whereas the localized approaches used so far could not account for this type of order.

The electrons responsible for the low-energy physics in FeSCs stem from the orbitals of the $3d^6$ configuration of the Fe^{2+} ions. All five orbitals (d_{xz}, d_{yz}, d_{xy}, $d_{x^2-y^2}$, and $d_{3z^2-r^2}$) have to be considered in order to obtain the correct Fermi surface (FS) geometry, even though the electronic states at the Fermi energy all have t_{2g} character, i. e., involve only the d_{xz}, d_{yz}, and d_{xy} orbitals [45]. Therefore, due to the doubling of the unit cell resulting from the two inequivalent As positions, at least the ten orbitals from the Fe atoms contribute to a realistic description, resulting in a 10-band noninteracting Hamiltonian.

The orbital contribution of the electronic states close to the Fermi surface is however not essential to account for superconductivity or magnetic order in the iron-based materials as long as these orders are not merely a byproduct of orbital ordering. On the contrary, already two-band models (including both hole-like and electron-like bands) are sufficient for the description of superconductivity in FeSCs whereas a successful description of spin-density wave (SDW) order of the stripe type as in the FeSCs requires three bands. The advantage of these minimal models as opposed to a more realistic description is that it allows for a controlled study of the most important control parameters while avoiding obfuscating complexity from the interplay of too many parameters. A detailed overview and comparison of results obtained in orbital-basis models and band-basis models can be found in Ref. 45.

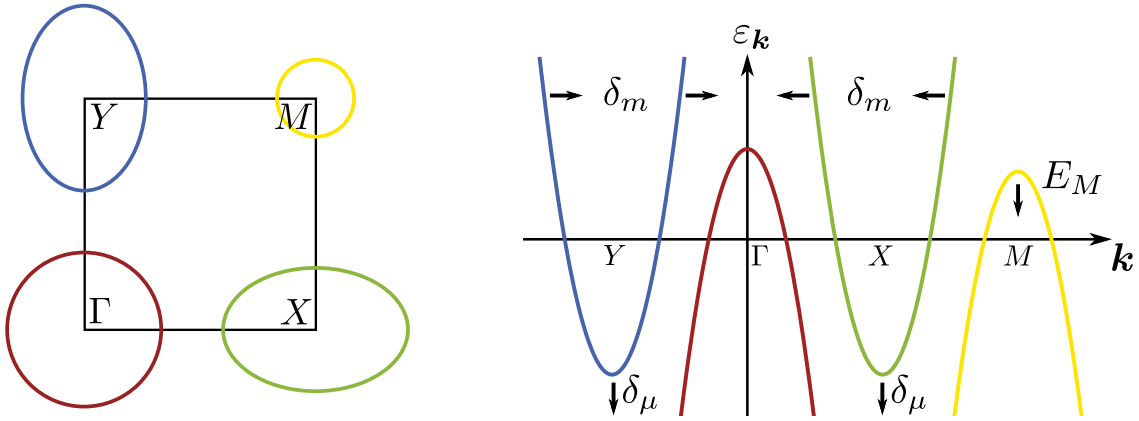

(a) Fermi surface **(b)** band structure

Figure 1.4: Toy model of iron-based superconductors. We show (a) the Fermi surface and (b) the band structure of the toy model of iron-based superconductors using the 1-Fe Brillouin zone. It consists of two circular hole pockets (red and yellow) and two elliptical electron pockets (green and blue) close to perfect nesting. Note that the hole pocket at the M point is not a generic feature of the materials. Furthermore, we introduce the parameters that will be used to tune the band structure in Chap. 4: The ellipticity of the electron pockets is reflected in δ_m, while δ_μ is associated with a relative shift of electron and hole bands. Lastly, increasing E_M pushes the second hole pocket to lower energies.

The Fermi surface and band structure of the toy model extracted from experimental data on many FeSCs are depicted in Fig. 1.4. Since the shape of the Fermi surface depends only weakly on k_z, using a two-dimensional Brillouin zone is a good approximation. In the 1-Fe unit cell, the minimal ingredients to model FeSCs are one hole pocket at the Γ point and two electron pockets at the X and Y points. Close to particle-hole symmetry, all FS pockets are approximately nested, meaning that large parts of the FS are connected by translation with an appropriate nesting vector $\boldsymbol{Q}$. The shape of the electron pockets *(ellipticity)* and the relative size of electron pockets to hole pockets *(doping)* can then be included as tuning parameters to study small deviations from perfect nesting. Another natural extension is the inclusion of a second circular hole pocket at the M point, however, this feature is not present in all the FeSCs and even if there is a hole band at M, it might not cross the Fermi level – hence often termed an *incipient band*. We will employ this toy model for our investigations of superconductivity and magnetic order in iron-based superconductors in Chaps. 2 and 4, respectively.

1.2.2 Oxide heterostructures

Another interesting example of a possibly unconventional superconducting state presents itself in the heterostructure fabricated from the two insulating and nonmagnetic oxides $LaAlO_3$ and $SrTiO_3$, often abbreviated LAO/STO. The 2D electron liquid that forms at the interface exhibits a high carrier mobility [46] and may undergo a superconducting transition [47] – though the transition temperatures of $100 \ldots 200\,\mathrm{mK}$ are comparably low. Theoretical studies propose an unconventional pairing state [48], even linked to nontrivial topology, as one possible candidate for the superconducting pairing state. Furthermore, superconductivity is expected to emerge in the proximity of magnetic order. Indeed, superconductivity has been found to coexist with magnetic order in the LAO/STO interface [49–51].

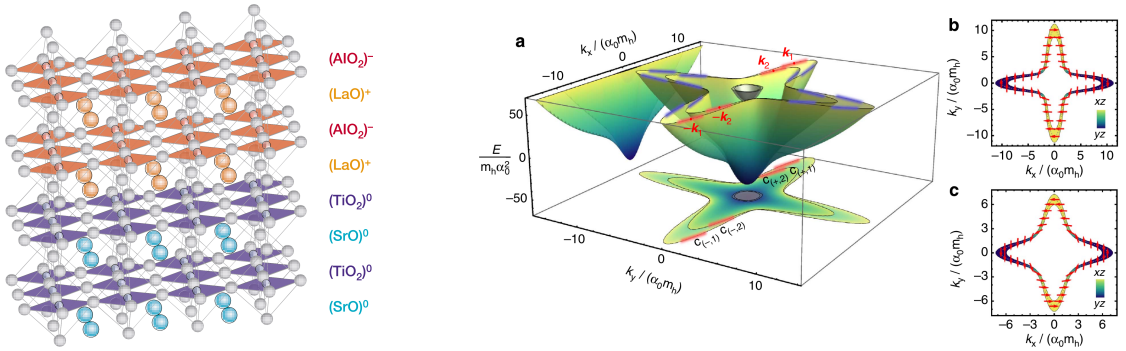

(a) crystal structure

[Reprinted by permission from Macmillan Publishers Ltd: Nature **427**, 423, copyright 2004, cf. Ref. 46.]

(b) dispersion

[Reprinted by permission from Macmillan Publishers Ltd: Nature Communications **6**, 6005, copyright 2015, cf. Ref. 48.]

Figure 1.5: The conducting $LaAlO_3/SrTiO_3$ interface. In the crystal structure, shown in (a), the different polarity of the layers is indicated. The strongly anisotropic dispersion obtained from a microscopic model building on the Ti $3d_{xz}$ and $3d_{yz}$ states is shown in (b), together with the resulting Fermi surface.

Conducting interface The explanation of the conducting properties of the interface between the (001)-oriented TiO_2-terminated STO substrate and (crystalline) LAO has stimulated a lot of interest. One intrinsic source of doping is certainly the polar discontinuity [46, 52] that develops at the interface since the layers forming the STO substrate are charge-neutral whereas LAO consists of alternately charged layers, as shown in Fig. 1.5 (a). In order to avoid the 'polar catastrophe',[4] above a critical thickness of the LAO layer of four unit cells [53], electrons are transferred to the Ti $3d$ states at the interface which thereby becomes conducting.

Another, extrinsic, source of doping that has been widely discussed in the community are oxygen vacancies that form at or near the surface of the STO substrate during the deposition process [54, 55]. The detailed analysis of Ref. 56 reveals that carrier doping in amorphous LAO layers on STO is mostly due to oxygen vacancies, whereas in the crystalline LAO/STO interface, both oxygen vacancies and the polar scenario contribute to conductivity.

Furthermore, superconducting properties such as the critical temperature and the superfluid density can conveniently be manipulated by application of electric fields [53, 57, 58], and the field effect can even be used to reversibly tune the interface from insulator to conductor. Hence, the conducting properties of the interface are not irrevocably fixed by growth conditions, but can be controlled by a gate voltage which is desirable for prospective applications.

Model for the LAO/STO interface Our calculations for the LAO/STO interface presented in Chap. 3 are based on the model for the interface introduced in Ref. 48. Here, we briefly summarize their ideas and refer to Ref. 48 and the references therein for further details.

The relevant states for the low-energy physics of the LAO/STO interface are the $3d$ Ti orbitals of the t_{2g} manifold. The $3d_{xy}$ electronic states mainly localize whereas the $3d_{xz}$ and $3d_{yz}$ states are delocalized. While the former are possibly related to magnetic order in the interface, the latter are the ones that are

[4] The term 'polar catastrophe' refers to the following scenario: The differently charged $(LaO)^+$ and $(AlO_2)^-$ layers result in a voltage built-up in the LAO side of the interface that diverges with the thickness of the LAO layer.

responsible for superconductivity. Therefore, the effective model in Ref. 48 concentrates on the $3d_{xz}$ and $3d_{yz}$ states, which results in the dispersion presented in Fig. 1.5 (b). These two orbitals have a different overlap in x and y directions, resulting in strongly anisotropic masses. Hence, the corresponding Fermi surfaces have a distinctive noncircular form which is also evident from Fig. 1.5 (b).

Furthermore, spin-orbit coupling lifts the spin-degeneracy of the Fermi surface and shifts two out of the four bands to higher energies which thus can be ignored in an effective low-energy description of the interface. The two remaining sheets of the Fermi surface exhibit strong orbital and spin polarization. Furthermore, large parts of the Fermi surface can be approximated by straight lines (indicated in Fig. 1.5 (b)) which are approximately nested in groups of four. This has been exploited in Ref. 48 to formulate a 'patch approximation' of the Fermi surface geometry which can account for both s^{++} and s^{+-} superconductivity as well as for magnetic ordering. In Chap. 3, we will extend their approach to disordered interfaces and study the effect of impurities on superconductivity.

1.3 Robustness of superconductivity

The discovery of superconductivity opened up a whole new field of possible technical applications: The vanishing resistance below T_c makes superconductors optimally suited materials for the construction of powerful electrical magnets and lossless transmission of electrical power, for instance. Unfortunately, complications arise because they have to be cooled below the respective T_c, which can also be costly and technologically challenging. Moreover, their range of application is restricted to magnetic fields below the respective critical field as well as critical currents below the respective critical current density. Even though after the discovery of the high-T_c cuprates, a lot of effort of both physicists and engineers has considerably put forward the research on superconductivity and superconducting materials, the ultimate goal of room-temperature superconductors is still a distant prospect.

In addition to the above-mentioned intrinsic limitations of superconductivity, especially in the newly discovered, more complex superconducting materials, further complications arise concerning both the fabrication and material properties of these new superconductors, and the sensitivity of the superconducting state to the proximity to magnetism or the presence of impurities. In this chapter, we summarize some of these effects which might weaken superconductivity and hence be reflected in characteristic properties like T_c. We will further discuss implications of fluctuations, which could even challenge the applicability of mean-field theory as introduced in Sec. 1.1.1.

1.3.1 Competing phases

Unconventional superconductivity usually appears close to other ordered phases. Sometimes, as for example in the cuprates and in the iron-based superconductors, superconductivity even emerges from a magnetically ordered state upon doping. This supports the notion of the importance of magnetism for unconventional superconductivity, however, the presence of a competing instability can also have detrimental effects for the SC state. We briefly discuss the implications of phase competition using the example of FeSCs – since both phases emerge from the same d electrons here, superconductivity and stripe-magnetic order compete for the same electrons, resulting in a complex interplay of these two orders.

On the one hand, in some iron-based compounds, superconductivity and antiferromagnetism coexist microscopically [59, 60] despite their competition, and their mutual influence is, for instance, reflected in a reduction of the static moment together with a suppression of the low-energy spin-wave excitations below T_c [61, 62]. Analogously, the superfluid density [63] and the transition temperature are

suppressed in the presence of antiferromagnetic order. Apart from this competition, SDW order does not destroy s^{+-} superconductivity, i. e., the nature of the superconducting state remains unaltered [64]. The resulting phase diagrams are complemented by theoretical studies [65–69], which also identify a regime of phase coexistence associated with suppression of T_c and a back bending of the antiferromagnetic transition line due to the presence of SC. What is more, theory also points towards a natural relation between these orders [41–43] owing to an enhanced SO(6) symmetry of the two-pocket model. Furthermore, this implies that also charge-density waves with an imaginary order parameter (iCDWs) are a potential instability of the model that could result in yet another competing state of order.

On the other hand, the presence of magnetic order restricts the possibilities for the superconducting state [68, 70]. What is more, even the mere proximity to a magnetic instability is suspected to affect superconductivity [71–73], and the optimal T_c is potentially related to an antiferromagnetic quantum-critical point [74–76] hidden below the SC dome. Consequently, spin fluctuations have been proposed to provide the 'pairing glue' for unconventional superconductivity in the iron-based superconductors as well as in the cuprates, but the discussion about the mechanism is ongoing.

1.3.2 Impurity scattering

Condensed matter theory usually uses the notion of a perfect crystal with a periodic structure as a starting point which provides tools such as Bloch's theorem or crystal symmetries to make life easier. Real materials, on the contrary, exhibit various imperfections in their structure even if they are crystals rather than amorphous materials: planar defects (such as grain boundaries and stacking faults), line defects (such as dislocations), and point defects (such as vacancies or interstitial atoms), for instance. The latter type of defect is of particular interest for compounds like the FeSC, in which doping (in form of chemical substitution, i. e., a replacement of the atoms at random positions) is used to tune material properties. Indeed, studies in the FeSCs find that some dopants [77] neither cause notable changes in the form of the Fermi surface nor do they add carriers and thereby change the chemical potential. In those compounds, impurity scattering might be the main effect caused by doping [78–80] and thus disorder would be another control parameter to tune material properties.

Substitutional disorder can be modeled by randomly distributed point defects off which the conduction electrons are scattered and thereby, the presence of impurities is expected to affect electronic properties of the respective materials. For example, the Drude conductivity decreases with the mean free time between collisions, which is inversely linked to impurity density. Other effects, however, can be much more dramatic such as the Anderson localization [16] resulting in insulating behavior. This possibility will however be excluded from our discussion of disorder in the remainder, which is permissible as long as the localization length R_{loc} is sufficiently large [81, 82],

$$R_{\mathrm{loc}} \gg (T_c \rho_F)^{-\frac{1}{d}} . \tag{1.5}$$

We furthermore omit the discussion of signatures of disorder in local probes – close to the impurity sites – but rather concentrate on the collective effect of disorder manifested in thermodynamic quantities. Lastly, the following introduction has a clear focus on the type of problems considered in the remainder of this thesis. For a broader introduction to disorder in the context of condensed matter, we refer to textbooks such as Refs. 83–85.

Anderson theorem Since the notion of phase coherence is important for an understanding of the superconducting state, the naive guess might be that even a minuscule amount of impurities will be

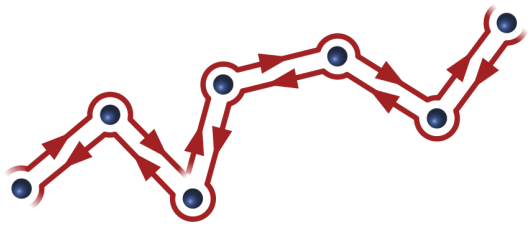

Figure 1.6: Visualization of the Anderson theorem in real space. Electrons are scattered off impurities, however, they can still be matched with another electron on a time-reversed path through the superconductor, hence forming a Cooper pair.

fatal for superconductivity since the electrons that are bound into Cooper pairs in the SC state are now scattered elastically off the impurities, involving a change in momentum. Indeed, the penetration depth of magnetic fields is found to increase with disorder, for instance. However, contrary to this expectation, s-wave BCS superconductivity is astonishingly robust against *nonmagnetic* isotropic, short-ranged impurities in the sense that the Fermi surface remains gapped, characterized by the order parameter Δ, and the transition temperature T_c remains approximately constant,

$$T_\mathrm{c}(\Gamma) \approx T_{\mathrm{c},0}\,. \tag{1.6}$$

Here, $T_{\mathrm{c},0}$ is the transition temperature following from BCS theory for a clean superconductor, and by Γ we denote the scattering rate as a measure comprising both impurity strength and impurity density, which will be introduced rigorously later in this section. This fact is usually referred to as the Anderson theorem since the underlying physical argument for the robustness of superconductivity in view of disorder was presented by Philip W. Anderson in Ref. 10: In the presence of impurities, it is still possible to find time-reversed pairs of electron states, i. e., Cooper pairs can also form in the presence of weak disorder. This argument is complemented by the rigorous calculation of Alexei A. Abrikosov and Lev P. Gor'kov [11, 12], who independently deduced the robustness of superconductivity against nonmagnetic scatterers.

A real-space visualization of the underlying physical argument can also be found in Fig. 1.6: The path of an electron through the superconductor is changed by the presence of disorder since impurity scattering changes the electron's momentum. Nevertheless, it is still possible to find an electron traversing the superconductor on a time-reversed path, and hence Cooper pairs can also form in the disordered superconductor. This argument, however, works only if the impurities preserve time-reversal symmetry (TRS), i. e., for nonmagnetic impurities, which is inferred most elegantly when formulated in the basis of time-reversed pairs, cf. Refs. 86 and 87.

Pair breaking If the impurities are *magnetic*, i. e., if the impurities break TRS, the situation is completely different: The transition temperature is suppressed quickly and as soon as the scattering rate reaches a critical value, superconductivity is destroyed completely. The relation between the transition temperature T_c and the scattering rate Γ due to magnetic point scatterers was established by Alexei A. Abrikosov and Lev P. Gor'kov in Ref. 88, and the corresponding functional dependence[5]

$$\ln\left(\frac{T_{\mathrm{c},0}}{T_\mathrm{c}}\right) = \psi_0\left(\frac{1}{2} + \frac{1}{4\mathrm{e}^\gamma}\frac{\Gamma/\Gamma_\mathrm{c}}{T_\mathrm{c}/T_{\mathrm{c},0}}\right) - \psi_0\left(\frac{1}{2}\right) \tag{1.7}$$

[5] To make the connection with the original publication [88], use $\Gamma = 1/(2\pi\rho_\mathrm{F}\tau_\mathrm{s})$, where $1/\tau_\mathrm{s}$ is directly related to the impurity concentration and the strength of the interaction between electron spin and the impurities' magnetic moment.

is often referred to as the Abrikosov-Gor'kov (AG) law in similar contexts. Here, $\psi_0(x)$ denotes the digamma function and γ is the Euler-Mascheroni constant. Furthermore, we defined

$$\Gamma_\mathrm{c} = \frac{T_{\mathrm{c},0}}{4\mathrm{e}^\gamma \rho_\mathrm{F}}\,, \tag{1.8}$$

where ρ_F is the density of states (DOS) at Fermi level. Since $\Gamma = \Gamma_\mathrm{c}$ implies $T_\mathrm{c} = 0$, we can conclude that superconductivity vanishes above a certain impurity concentration related to Γ_c. The above definition of Γ_c thus corresponds to a critical scattering rate at which magnetic scatterers destroy BCS superconductivity. At low impurity concentrations, the decrease of the transition temperature is linear,

$$T_\mathrm{c} = T_{\mathrm{c},0} - \frac{\pi^2}{2}\rho_\mathrm{F}\Gamma\,, \tag{1.9}$$

and the slope is a measure of pair-breaking strength of the impurities.

Let us already note here that pair breaking can also be caused by nonmagnetic disorder in multi-band superconductors with a more complicated pairing state. Hence pair breaking due to the presence of nonmagnetic impurities is usually related to unconventional superconductivity. This will be discussed in more detail in the context of iron-based superconductors (Chap. 2) and oxide interfaces (Chap. 3) in the remainder of this thesis.

Microscopic model Further consequences of disorder can be manifold and range from a mere smearing of experimental signatures to new effects (such as the above-mentioned Anderson localization) that cannot be understood as perturbations around the previous (clean) ground state. Most of these effects, however, have in common that they are macroscopically observable consequences of the underlying microscopic impurity distribution, yet do not depend on the specific distribution of the impurities but rather on characteristics[6] such as the density of the impurities n_imp and the strength of their scattering potential u_0. Such behavior is called *self-averaging* since the system behaves as averaged over subsystems of the size of the phase coherence length, which is much smaller than the system size in this case. Such an average is equivalent to an ensemble average over many systems with different disorder realizations (characterized by the same macroscopic parameters).

Since the time scales for the physical processes of interest are usually much smaller than the time scales on which a system containing randomly distributed impurities could equilibrate, it is usually justified to consider 'quenched' disorder, i. e., to add an additional static term to the Hamiltonian that represents the impurities. This could be straightforwardly implemented [83, 84, 89] by adding a term $\hat{\mathcal{H}}_\mathrm{dis}$ arising from N identical nonmagnetic impurities at random positions $\boldsymbol{R}_i$

$$\hat{\mathcal{H}}_\mathrm{dis} = \sum_{i=1}^{N} \hat{U}_{\boldsymbol{R}_i} \qquad \text{with} \qquad \hat{U}_{\boldsymbol{R}_i} = \int \mathrm{d}\boldsymbol{r}\,\mathrm{d}\boldsymbol{r}'\,\hat{\psi}^\dagger(\boldsymbol{r}) u(\boldsymbol{r}-\boldsymbol{R}_i, \boldsymbol{r}'-\boldsymbol{R}_i)\hat{\psi}(\boldsymbol{r}') \tag{1.10}$$

to the full Hamiltonian of the clean system. Here, we omitted the spin of the fermionic creation and annihilation operators, $\hat{\psi}^\dagger(\boldsymbol{r})$ and $\hat{\psi}(\boldsymbol{r})$, in position space since we consider nonmagnetic impurities here, which are insensitive to the electrons' spin. Note that we assume identical impurities, implying that the matrix elements $u(\boldsymbol{r}, \boldsymbol{r}')$ do not depend on the sites $\boldsymbol{R}_i$ of the respective impurities, however, in their

[6] This is different for 'mesoscopic' disorder effects which are manifestations of the microscopic disorder realization on a macroscopic scale in systems in which the phase coherence length at low temperatures grows large such that it becomes comparable to the system size. Such effects will not be discussed here.

most general form, they are not necessarily diagonal in real space since impurities could in principle have extended effects going beyond mere potential scattering. This representation of disorder readily allows for a perturbative analysis of disorder effects in orders of the impurity potential. An alternative formulation of the impurity Hamiltonian that is better suited for implementation in a field-integral approach is

$$\hat{\mathcal{H}}_{\text{dis}} = \int \mathrm{d}\boldsymbol{r}\, \mathrm{d}\boldsymbol{r}'\, \hat{\psi}^\dagger(\boldsymbol{r}) W(\boldsymbol{r},\boldsymbol{r}') \hat{\psi}(\boldsymbol{r}')\,, \tag{1.11}$$

where the focus is not on the single impurities but models disorder as a random matrix field characterized by a probability distribution $P[W]$ [85]. This version of the Hamiltonian is also better accessible for a symmetry analysis of the disorder. These two formulations of the disorder Hamiltonian, Eq. (1.10) and Eq. (1.11), are connected by

$$W(\boldsymbol{r},\boldsymbol{r}') = \sum_{i=1}^{N} u(\boldsymbol{r}-\boldsymbol{R}_i, \boldsymbol{r}'-\boldsymbol{R}_i)\,. \tag{1.12}$$

In the framework of Eq. (1.10), self-averaged quantities are obtained from averaging over all possible realizations of N randomly distributed impurities by taking the average over impurity positions,

$$\langle \ldots \rangle_{\text{dis}} \equiv V^{-N} \prod_{i=1}^{N} \int \mathrm{d}\boldsymbol{R}_i \ldots\,, \tag{1.13}$$

where V denotes the system volume, whereas in the field-integral formalism of Eq. (1.11), disorder averaging corresponds to

$$\langle \ldots \rangle_{\text{dis}} \equiv \int \mathcal{D}W\, P[W] \ldots\,. \tag{1.14}$$

A frequently used assumption for the disorder distribution is *Gaussian disorder*, which corresponds to the limit of infinitely weak and infinitely dense impurities [90], i. e., $u_0 \to 0$ and $n_{\text{imp}} \to \infty$ where $n_{\text{imp}} u_0^2 = \text{const.}$ is a measure of disorder strength. This is both a convenient choice and a reasonably good approximation for systems in which the length scales of other physical effects are much larger than the distance between impurities. Thereby, we treat impurity effects as collective effects rather than concentrating on local effects around a single impurity. Within this framework, the crucial information about the disorder is contained in the correlator

$$\Gamma(\boldsymbol{r}_1,\boldsymbol{r}_1';\boldsymbol{r}_2,\boldsymbol{r}_2') := \Big\langle W(\boldsymbol{r}_1,\boldsymbol{r}_1') W(\boldsymbol{r}_2,\boldsymbol{r}_2') \Big\rangle_{\text{dis}} \tag{1.15a}$$

$$= \sum_{i=1}^{N} \Big\langle u(\boldsymbol{r}_1-\boldsymbol{R}_i,\boldsymbol{r}_1'-\boldsymbol{R}_i) u(\boldsymbol{r}_2-\boldsymbol{R}_i,\boldsymbol{r}_2'-\boldsymbol{R}_i) \Big\rangle_{\text{dis}}\,. \tag{1.15b}$$

A technical complication that arises due to the presence of impurities is that not only the numerator but also the normalization in the field-integral technique depends on disorder, preventing a straightforward execution of the disorder average. To deal with this challenge, there are three methods at hand: the Keldysh technique [91, 92], the supersymmetry approach [93, 94], and the replica trick [85, 95]. Here, we follow the logic of the latter, meaning that we artificially introduce R copies of the system (replicas) in order to rewrite the disorder part of the action and subsequently perform the disorder average, see for example Ref. 85 for details. This results in an effective attractive interaction of the electrons induced

by the presence of disorder,

$$\mathcal{S}_{\mathrm{dis}}(\bar{\psi},\psi) = -\frac{1}{2}\sum_{r,r'=1}^{R}\int \mathrm{d}\tau\,\mathrm{d}\tau' \int \mathrm{d}\boldsymbol{r}_1\,\mathrm{d}\boldsymbol{r}_1'\,\mathrm{d}\boldsymbol{r}_2\,\mathrm{d}\boldsymbol{r}_2'\,\bar{\psi}^r(\boldsymbol{r}_1,\tau)\psi^r(\boldsymbol{r}_1',\tau) \times \Gamma(\boldsymbol{r}_1,\boldsymbol{r}_1';\boldsymbol{r}_2,\boldsymbol{r}_2')\bar{\psi}^{r'}(\boldsymbol{r}_2,\tau')\psi^{r'}(\boldsymbol{r}_2',\tau')\,, \tag{1.16}$$

where r and r' label replicas. Owing to the static nature of the impurities, energy and hence Matsubara frequencies are preserved even in single scattering events. Note that the effective interaction (1.16) in principle couples fermions from different replicas. As long as the replica-off-diagonal contributions are negligible, the limit $R \to 0$ can safely be taken at the end of the calculation of physical observables, resulting the disordered equivalent of the previous mean-field theory, which is the case that will be discussed in the remainder.

Diagrammatic technique From Eq. (1.16), it is evident that disorder can be implemented in a diagrammatic technique by introducing a new type of vertex. This is best done in momentum representation since the disorder averaging procedure turns out to restore translation invariance. Furthermore, before proceeding, we adopt further simplifications for the sake of readability. Firstly, another sensible assumption in the context of Gaussian disorder is the restriction to spatially *uncorrelated disorder*, meaning that

$$\Gamma(\boldsymbol{r}_1,\boldsymbol{r}_1';\boldsymbol{r}_2,\boldsymbol{r}_2') = \Gamma(\boldsymbol{r}_1,\boldsymbol{r}_1';\boldsymbol{r}_1,\boldsymbol{r}_1')\,\delta(\boldsymbol{r}_1-\boldsymbol{r}_2)\,\delta(\boldsymbol{r}_1'-\boldsymbol{r}_2')\,. \tag{1.17}$$

Secondly, we assume the disorder to be spatially local and homogeneous, i. e.,

$$u(\boldsymbol{r}-\boldsymbol{R}_i,\boldsymbol{r}'-\boldsymbol{R}_i) = u_0\,\delta(\boldsymbol{r}-\boldsymbol{R}_i)\,\delta(\boldsymbol{r}'-\boldsymbol{R}_i)\,, \tag{1.18}$$

implying that the disorder is constant in momentum space. Here, u_0 corresponds to the strength of the scattering potential of a single impurity. Note that it will become necessary to relax these assumptions to deal with spatially extended impurity effects or multi-band systems, as described in App. B.1. However, with these simplifications, the disorder correlator takes a very convenient form,

$$\Gamma(\boldsymbol{r}_1,\boldsymbol{r}_1';\boldsymbol{r}_2,\boldsymbol{r}_2') = \Gamma\,\delta(\boldsymbol{r}_1-\boldsymbol{r}_1')\,\delta(\boldsymbol{r}_2-\boldsymbol{r}_2')\,\delta(\boldsymbol{r}_1-\boldsymbol{r}_2)\,, \tag{1.19}$$

where $\Gamma = n_{\mathrm{imp}}u_0^2$ is a measure of the disorder strength that combines impurity density n_{imp} and impurity strength u_0. Finally, in momentum space, we can write the additional element (also referred to as the 'impurity line'[7]) representing disorder in a diagrammatic technique as

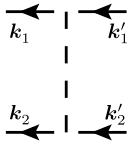

$$\equiv \Gamma_{\boldsymbol{k}_1\boldsymbol{k}_1',\boldsymbol{k}_2\boldsymbol{k}_2'} = \Gamma(2\pi)^d\,\delta(\boldsymbol{k}_1+\boldsymbol{k}_2-\boldsymbol{k}_1'-\boldsymbol{k}_2'+\boldsymbol{K})\,, \tag{1.20}$$

where the last equality is valid for δ-correlated, homogeneous potential disorder, though it can even be used as an approximation for sufficiently short-correlated disorder. Since we consider elastic scattering on static impurities, momentum is conserved at each vertex (up to a vector $\boldsymbol{K}$ from the reciprocal lattice) and Matsubara frequencies are not affected by scattering.

[7] The definition in Eq. (1.15a) refers to the impurity line, however the disconnected fermion lines in Eq. (1.20) have been added for the sake of clarity to represent the corresponding incoming and outgoing momenta.

To identify the physical meaning of the parameter Γ, we consider the disorder-averaged Green's function $G_{\boldsymbol{k}}(\nu_n)$, which is affected by disorder through a finite self energy $\Sigma_{\boldsymbol{k}}(\nu_n)$,


$$\equiv G_{\boldsymbol{k}}(\nu_n) = \frac{1}{\mathrm{i}\nu_n - \epsilon_{\boldsymbol{k}} - \Sigma_{\boldsymbol{k}}(\nu_n)}\,. \tag{1.21}$$

In the limit of weak disorder, which we already utilized when restricting ourselves to Gaussian disorder, it is sufficient to calculate the self energy in self-consistent Born approximation (SCBA), leading to


$$\equiv \Sigma_{\boldsymbol{k}}^{\mathrm{SCBA}}(\nu_n) = -\mathrm{i}\pi\rho_{\mathrm{F}}\Gamma\,\mathrm{sgn}(\nu_n) \tag{1.22a}$$

$$= -\frac{\mathrm{i}}{2\tau}\,\mathrm{sgn}(\nu_n)\,, \tag{1.22b}$$

where in the last line, we introduced the scattering time τ as the finite lifetime the quasiparticles acquire due to impurity scattering, i. e., the broadening due to $\mathrm{Im}\,\Sigma_{\boldsymbol{k}}(\nu_n)$. Consequently, we find that Γ plays the role of a (dimensionless) scattering rate,

$$\Gamma = \frac{1}{2\pi\rho_{\mathrm{F}}\tau}\,. \tag{1.23}$$

In real space, this corresponds to an exponential decay of the quasiparticle propagator, and the respective scale defines the mean-free path $l_{\mathrm{mfp}} = v_{\mathrm{F}}\tau$, where v_{F} is the Fermi velocity. The self-consistent Born approximation corresponds to the lowest order of an expansion in $1/k_{\mathrm{F}}l_{\mathrm{mfp}}$, since all diagrams with crossed impurity lines (see Fig. 1.7 (a) for an exemplary contribution to the self energy) are suppressed by a factor $1/k_{\mathrm{F}}l_{\mathrm{mfp}}$ compared to the respective non-crossed contributions to the self energy, where k_{F} denotes the Fermi momentum. This assumption is valid as long as the mean-free path l_{mfp} of the electrons is large compared to the range of the impurity potential. In the framework of Eq. (1.10), the SCBA further implies that we restrict ourselves to double-scattering processes of electrons off the same impurity – since single-scattering processes can be absorbed in a shift of the chemical potential and multiple-scattering processes are negligible compared to the double-scattering processes.[8] Within this approximation, the SC vertices are modified by the Cooperon-ladder corrections presented diagrammatically in Fig. 1.7 (b). Finally, it turns out that self-energy corrections and vertex corrections[9] due to nonmagnetic impurities cancel exactly in the quadratic coefficient $a(T)$ (cf. Fig. 1.7 (c)) of the disorder-averaged version of the Ginzburg-Landau expansion discussed in Sec. 1.1.1, leaving the transition temperature towards the superconducting state unchanged and hence resulting in the Anderson theorem.

Generalizations Many of the recently discovered superconductors are multi-band systems where pairing might involve electronic states from different bands. Then in addition to *intraband scattering* processes, whose effect can be readily inferred from the single-band consideration presented in this section, *interband scattering* processes have to be considered. The generalization of the diagrammatic technique to the multi-band case is straightforward and our notation is introduced in App. B.1.1. In particular, in systems hosting superconductivity with a more complicated structure of the order

[8] Multiple-scattering events could in principle be included easily by replacing the Born scattering amplitude by a total scattering amplitude which would lead to structurally identical diagrams.

[9] Note that in our notation, only one vertex of the quadratic coefficient should be renormalized to avoid double counting.

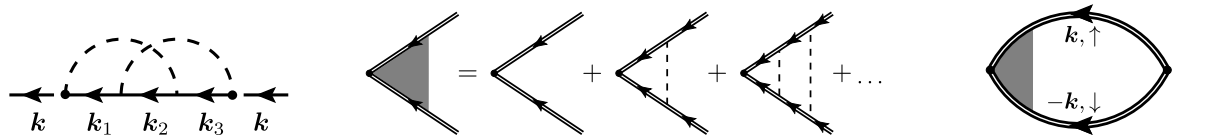

(a) example: crossed diagram **(b)** vertex corrections **(c)** quadratic coefficient

Figure 1.7: Self-consistent Born approximation for single-band s-wave superconductors. Within SCBA, crossed diagrams such as shown in (a) are suppressed by $1/k_\mathrm{F} l_\mathrm{mfp}$ and hence negligible. The corresponding vertex corrections are thus given by the 'Cooperon ladder' depicted in (b). The resulting quartic coefficient (c) is renormalized by self-energy and vertex corrections in the presence of disorder.

parameter than following from BCS theory, interband scattering can be crucial and the validity of the Anderson theorem and the AG law have to be reassessed, to which Chaps. 2 and 3 of this thesis are dedicated. Further possibilities for generalizations include magnetic impurities which are characterized by a local moment interacting with the electrons' spin, and anisotropic scattering potentials.

1.3.3 Fluctuations

Let us finally comment on fluctuations as an intrinsic effect that could destabilize superconductivity. Up to now, we considered static and homogeneous order parameters in our description of the superconducting state as a symmetry-broken low-temperature phase. In the regime close to the phase transition, however, thermal fluctuations become important and in fact drive the phase transition. In principle, such fluctuations of the order parameter around its mean-field value are also reflected in physical observables. However, the Ginzburg regime, where these effects are important, is usually restricted to the vicinity of the phase transition in three-dimensional conventional superconductors. This is due to the large coherence length in many superconducting materials and explains the remarkable success of the BCS theory in describing the superconducting state.

On the other hand, in lower-dimensional systems, such as superconducting films or granular materials, fluctuation effects can become quite important. They result in contributions to various thermodynamic and dynamic properties at the phase transition, see Ref. 96 for a review focusing on theoretical aspects. For instance, they lead to a smearing of the transition [97], and superconducting fluctuations can affect normal-state properties even above the transition temperature. Even more drastically, the Mermin-Wagner-Hohenberg theorem [98, 99] strictly excludes the possibility of a spontaneously broken continuous symmetry – associated with true long-range order – at finite temperatures in systems of dimensionality $d \leq 2$. At least, the possibility of quasi-long-range order (i. e., a low-temperature phase where correlations decay with a power law) persists in low-dimensional systems. All in all, the quickly expanding field of unconventional superconductivity also stimulated the interest in fluctuation effects.

In any case, at zero temperature, the order parameter is expected to be well developed and fluctuations should be less important as long as the system is deep inside the ordered phase and not close to a quantum-critical point. Indeed, it was shown by Kos, Millis, and Larkin [100] that Gaussian fluctuation corrections to the mean-field gap equation are indeed negligible in this regime, ensuring the stability of the BCS mean-field theory. Since their conclusion relies on the cancellation of individually large contributions resulting from amplitude and phase fluctuations, we will return to this peculiarity in Chap. 5, where we will also discuss the role of fluctuations in the context of other mean-field theories where no such cancellation is expected.

Chapter 2

2 Orbital-magnetic impurities in iron-based superconductors

Iron-based superconductors are multi-orbital materials that usually become superconducting upon doping. Hence the motivation to consider the effect of impurities is twofold: First, chemical substitution also introduces impurities into the system, and secondly, in a multi-band system the interband scattering processes might have quite substantial effects. In particular, single-band s-wave superconductors as described by BCS theory are robust against nonmagnetic scattering [10–12] whereas in multi-band superconductors, T_c can already be suppressed by nonmagnetic impurities, depending on the pairing symmetry. Therefore, the suppression of T_c in the presence of impurities has been employed in order to draw conclusions about the nature of the superconducting state in the iron-based superconductors [101–107], however, such studies can merely be an indication rather than proof for a certain pairing state. Furthermore, as we discuss here, the situation in the iron-based systems is considerably complicated by the proximity of superconductivity to competing phases of order.

We start this chapter with a discussion of experimental evidence concerning the nature of the superconducting state in iron-based superconductors, discuss the most likely candidates for the pairing state, and introduce the toy model which we will consider in the remainder of this chapter. Afterwards, we discuss impurity scattering in the framework of the proposed two-band model with a special focus on the role of time-reversal symmetry in the context of interband scattering processes. Finally, we discuss the implication of nonmagnetic and magnetic impurity scattering for both the s^{++} and the s^{+-} pairing state. The focus of this discussion lies on a scenario of orbital-magnetic impurities tailored to iron-based superconductors which could obstruct a straightforward interpretation of pair breaking in iron-based superconductors.

This chapter is based on my work in collaboration with Mathias S. Scheurer, Sergey V. Syzranov, and Jörg Schmalian, which has been published in Ref. 87.

2.1 Superconductivity in iron-based superconductors

At first glance, the recently discovered iron-based superconductors (FeSCs) and the cuprates, which have been studied for three decades now, seem to share many characteristics. Above all, the phase diagrams that are obtained by doping look rather similar. A closer look, however, reveals important differences. Most notably, the symmetry of the superconducting state of the cuprates has been identified to generically have d-wave character by phase-sensitive experiments [108] whereas the discussion

concerning the pairing state – and hence the mechanism for superconductivity – is still ongoing in the FeSCs. This section briefly summarizes the progress that has been made so far towards a characterization of the FeSC pairing state and, based thereon, introduces a minimal model for superconductivity in FeSCs which we will employ in the remainder of this chapter.

2.1.1 Candidate pairing states

A phonon-based mechanism for superconductivity has been ruled out [31] early after the discovery of superconductivity (SC) in the iron-based systems. However, the question of the pairing mechanism as well as the pairing state are still not finally settled. It might even be that the symmetry of the pairing state is not a universal feature in the class of FeSCs, and that some of the compounds elude a general description. In this work, however, we ignore such outliers and concentrate on candidate pairing states extracted from experimental data from a majority of the FeSC compounds. Detailed reviews which concentrate on the pairing symmetry in the FeSCs are provided in Refs. 36, 40, and 109, for instance.

Measurements of the Knight shift in nuclear magnetic resonance (NMR) on several materials [110–113] indicate that the spin symmetry of the SC state is singlet which suggests s-wave or d-wave pairing states as the most natural candidates for the iron-based systems. The gap amplitude and thus the presence of nodes can, in principle, be probed most directly by angle-resolved photoemission spectroscopy (ARPES) measurements, and while many compounds of the iron-based family show fully established gaps on all pockets of the Fermi surface, others have found to be nodal superconductors. However, the multi-orbital nature of the iron-based materials allows for more complicated variations of s and d-wave pairing states – so called extended states. This may implicate 'accidental' nodes not required by symmetry which may or may not be located on the Fermi surface. We summarize the most important candidates for the pairing state of FeSCs in Fig. 2.1. Besides the generalization of the BCS pairing state to the multi-band case, referred to as s^{++} and depicted in Fig. 2.1 (a), extended s-wave states are possible as suggested almost instantaneously after the discovery of superconductivity in FeSCs [114, 115]. Depending on the position of the associated accidental nodes, either the s^{+-} state as sketched in Fig. 2.1 (b) (with zeros of the gap between the Fermi pockets) is realized, or a more complicated nodal s^{+-} state, cf. the example in Fig. 2.1 (c). Even though d-wave symmetry of the order parameter (as depicted in Fig. 2.1 (d)) seems less likely, it has not been ruled out yet – a strong argument in favor being the near degeneracy [116] of sign-changing s-wave and the $d_{x^2-y^2}$-wave. Another possibility, however restricted to materials which lack the central hole pocket at the Γ point, is the nodeless d-wave pairing state sketched in Fig. 2.1 (e).

Especially the insufficient resolution of ARPES, the fact that effects such as impurity scattering can wash out the nodes [117], and the lack of phase sensitivity make it hard to discriminate between the suggested pairing states for FeSCs based on ARPES or signatures of nodes in other probes. In the cuprate high-T_c superconductors, phase-sensitive experiments [108] have proven to be most useful in determining the pairing state to be of d-wave symmetry. Unfortunately, in the iron-based compounds, it is not only hard to fabricate the samples needed for such experiments but also impossible to further discriminate between the s^{++} and s^{+-} state based on the setup used in the context of cuprate superconductors. Hence physicists have to resort to signatures of possible pairing states in other experimental probes. By now, a lot of evidence is pointing towards the s^{+-} pairing state for the FeSCs, including the spin resonance mode [118–120] found from inelastic neutron scattering in most of the FeSC materials (starting with Ref. 121) and in-gap bound states near nonmagnetic impurities [122–124] found from scanning tunneling microscopy (STM) [125, 126]. However, no ultimate 'smoking gun' experiment has been reported so far, leaving the question of the pairing state of the FeSCs still open.

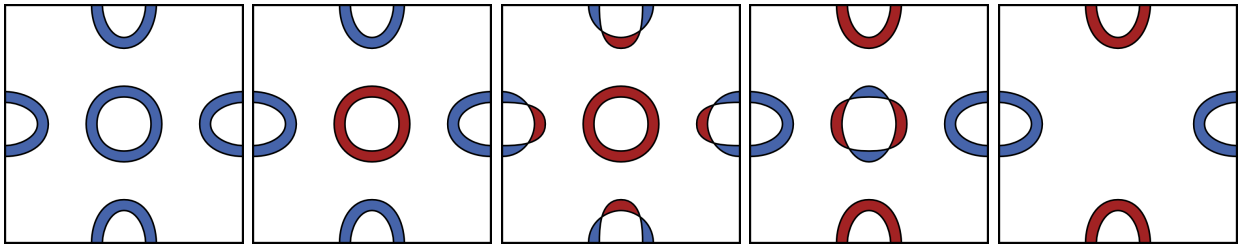

(a) s^{++} **(b)** s^{+-} **(c)** nodal s^{+-} **(d)** d **(e)** nodeless d

Figure 2.1: Candidate pairing states for iron-based superconductors. We summarize the most widely discussed pairing states suggested for iron-based superconductor here, represented in terms of the respective gaps on the Fermi surface, cf. Fig. 1.4 (a). Different colors correspond to different signs of the order parameter.

Furthermore, let us note that the possibility of a change of pairing symmetry with doping has been reported [15, 127–129]. However, we will neglect such peculiarities in our further discussion of disorder effects and consider the effect of weak disorder on a given pairing state instead. Since there is stronger evidence for an s-wave symmetry of the gap than for d-wave symmetry, we will concentrate on the distinction between s^{++} and s^{+-} pairing states in the following.

2.1.2 Minimal two-band model

As already discussed in Sec. 1.2.1, the orbital composition of the low-energy states is not crucial for a successful description of low-energy phenomena and their interplay in FeSCs. Consequently, band-basis models have proven very useful [45] to investigate phenomena such as superconductivity and magnetic order in these materials. By construction, such band-basis models cannot account for orbital order, and the minimal two-band model is too simple to cover anisotropic phenomena such as d-wave SC or nematic order. It is, however, a suitable playground for a comparative investigation of s^{++} and s^{+-} SC in FeSCs under the influence of disorder.

Two-band model As a minimal model for superconductivity in (disordered) FeSCs, we employ a two-band model taking into account one hole pocket, e. g. at the Γ point, and one of the two electron pockets centered around $\boldsymbol{Q}$ where it holds that $2\boldsymbol{Q}$ is a reciprocal primitive vector (derived from the 1-Fe unit cell), as it is suitable for the nesting vector in iron-based superconductors. The corresponding toy model [41] is defined by the noninteracting Hamiltonian

$$\hat{\mathcal{H}}_0 = \sum_{\lambda} \sum_{\boldsymbol{k},\sigma} \varepsilon_{\lambda,\boldsymbol{k}} \hat{\psi}^{\dagger}_{\lambda,\boldsymbol{k},\sigma} \hat{\psi}_{\lambda,\boldsymbol{k},\sigma} \,, \tag{2.1}$$

where $\lambda \in \{1, 2\}$ labels the bands, and $\hat{\psi}^{\dagger}_{\lambda,\boldsymbol{k},\sigma}$ and $\hat{\psi}_{\lambda,\boldsymbol{k},\sigma}$ are the creation and annihilation operators for quasiparticles of spin σ and crystal momentum $\boldsymbol{k}$ in band λ. Quasiparticles in the hole band, labeled by 1, have small momenta $\boldsymbol{k}$ near the center of the Brillouin zone (Γ point), while the momenta of the quasiparticles in the electron band, labeled by 2, are close to $\boldsymbol{Q}$. Furthermore, $\varepsilon_{\lambda,\boldsymbol{k}}$ is the dispersion of band λ, measured from the chemical potential μ. A good approximation for the FeSCs is the assumption of a circular hole pocket and elliptical electron pockets with parabolic dispersions. In this chapter, however, the concrete form of the dispersion relation is not important as long as $\varepsilon_{\lambda,\boldsymbol{k}} = \varepsilon_{\lambda,-\boldsymbol{k}}$

holds. In the following, we assume a constant density of states (DOS) at the Fermi level in each band, denoted ρ_λ, and as a consequence of this assumption, our results are independent of the shape of the two Fermi surfaces. In particular, the possibility of an elliptical electron Fermi surface, which is important in the context of magnetic order in iron-based superconductors, is thereby included in our considerations. Furthermore, for simplicity, we consider the system at particle-hole symmetry,

$$\varepsilon_{1,\boldsymbol{k}} = -\varepsilon_{2,\boldsymbol{k}}\,. \tag{2.2}$$

Thus, we assume the DOS near the Fermi level to have the same constant value ρ_F in both bands which will turn out useful in the context of superconductivity.

Superconductivity The two-band model for FeSCs allows for five different interaction terms – intra-band and interband density–density interactions, spin exchange, and pair hopping [41, 116]. The crucial process that distinguishes the extended s^{+-}-wave state from the conventional two-band s^{++} state is the pair-hopping term [41], hence we restrict ourselves to

$$\hat{\mathcal{H}}_\mathrm{int} = \sum_\lambda \sum_{\boldsymbol{k},\boldsymbol{k}'} V^{\lambda\bar{\lambda}}_{\boldsymbol{k}\boldsymbol{k}'} \hat{\psi}^\dagger_{\lambda,\boldsymbol{k},\uparrow} \hat{\psi}^\dagger_{\lambda,-\boldsymbol{k},\downarrow} \hat{\psi}_{\bar{\lambda},-\boldsymbol{k}',\downarrow} \hat{\psi}_{\bar{\lambda},\boldsymbol{k}',\uparrow}\,, \tag{2.3}$$

where $\bar{\lambda}$ labels the band other than λ. Here, we take the interaction to be constant for all states in the vicinity of the Fermi surface up to a cutoff Λ,

$$V^{\lambda\bar{\lambda}}_{\boldsymbol{k}\boldsymbol{k}'} = \begin{cases} V_\mathrm{SC} & \text{for } |\varepsilon_{\lambda,\boldsymbol{k}}|, |\varepsilon_{\bar{\lambda},\boldsymbol{k}'}| < \Lambda\,, \\ 0 & \text{otherwise}\,, \end{cases} \tag{2.4}$$

in analogy to the formulation of the BCS theory for conventional superconductivity.

We follow the usual route outlined in Sec. 1.1.2 to obtain an effective theory in terms of the low-energy degrees of freedom: We decouple the interaction by a Hubbard-Stratonovich transformation and trade the fermionic degrees of freedom for effective low-energy degrees of freedom. The action associated with the interacting Hamiltonian given in Eq. (2.3) can be decoupled [87] by introducing the bosonic fields

$$\Delta_\pm = \frac{1}{\sqrt{2}}(\Delta_1 \pm \Delta_2)\,, \tag{2.5}$$

where $\Delta_\lambda = \langle \int_{\boldsymbol{k}} \hat{\psi}_{\lambda,-\boldsymbol{k},\downarrow} \hat{\psi}_{\lambda,\boldsymbol{k},\uparrow} \rangle$ is the mean-field value of the SC order parameter on the respective Fermi surface pocket. The assumption of the same constant density of states ρ_F at the Fermi level in both bands guarantees gaps of equal magnitude $\Delta_1 = \pm\Delta_2$. Then, depending on whether the interaction is attractive ($V_\mathrm{SC} < 0$) or repulsive ($V_\mathrm{SC} > 0$), either the conventional s^{++} state or the extended s^{+-} state is realized, respectively. In either case, the SC transition in the clean system occurs at the same critical temperature $T_{\mathrm{c},0}$ as known from BCS theory [130],

$$T_{\mathrm{c},0} = \frac{2\Lambda \mathrm{e}^\gamma}{\pi} \mathrm{e}^{-\frac{1}{|V_\mathrm{SC}|\rho_\mathrm{F}}}\,, \tag{2.6}$$

where γ denotes the Euler-Mascheroni constant and ρ_F is the total DOS at the Fermi level per band.

In principle, the generalization of our results to different densities of states ρ_λ in the two bands is straightforward, however, the resulting pairing state is already a mixture of s^{++} and s^{+-} pairing states. The DOS mismatch thus provides an additional source of T_c suppression [131] which hinders the analysis of the role of different scattering processes in pair breaking. Therefore, this will not be considered in the remainder since our focus lies on the disorder effects.

2.2 Impurities in iron-based superconductors

Superconductivity in iron-based superconductors is realized by doping the so called 'parent compounds', and the transition temperature T_c depends on the dopant concentration x. This statement seems to be true no matter whether the dopants replace atoms from the active layer (FeAs or FeSe, respectively) or the intermediate layers, and whether they are isovalent or correspond to hole or electron doping. We introduced the prototypical phase diagram of FeSCs in Fig. 1.3: With few exceptions, the stripe-type magnetic order and the superconducting dome are found throughout all families of FeSCs, yet specifics of the phase diagrams (such as a split structural and magnetic transition or the tetragonal magnetic phase discussed in Chap. 4) do depend on the nature of the dopants. Furthermore, for example in $Ba(Fe_{1-x}Ru_x)_2As_2$, doping is not associated with changes of the Fermi surface [77], hence another mechanism must be at play which tunes the phase diagram. Indeed, theoretical studies [78–80] also emphasize the importance of effects beyond a rigid band shift, such as disorder scattering, and it has been demonstrated that changes of the band structure [65–68] as well as disorder [69] can reproduce the experimental phase diagrams of FeSCs.

In summary, the presence of dopant atoms manifests itself in many physical observables and can be accounted for in models by at least the two most noteworthy effects:

- a shift in the chemical potential ('carrier doping') and associated changes of the band structure
- as well as inclusion of scattering processes of the electrons off impurities ('disorder').

The former effect is readily included in the minimal two-band model for the FeSCs introduced in Sec. 2.1.2 by adjusting the band-structure parameters, see also Chap. 4. This section provides details on how to include the latter effect in the minimal two-band model of FeSCs. We further emphasize the differing consequences of intraband and interband scattering processes and discuss the relationship between time-reversal symmetry (TRS)-breaking impurities and pair-breaking scattering processes.

2.2.1 Classification of scattering processes in a two-band model

A single nonmagnetic impurity basically acts as an additional local potential for the conduction electrons. Consequently, we can account for disorder in the two-band model of FeSCs by adding a potential term

$$\hat{\mathcal{H}}_{\text{dis}} = \sum_{\lambda,\lambda'} \sum_{\sigma} \int \mathrm{d}\boldsymbol{r}\, \mathrm{d}\boldsymbol{r}'\, \hat{\psi}^\dagger_{\lambda,\sigma}(\boldsymbol{r}) \Big[\sum_{i=1}^{N} u_{\lambda\lambda'}(\boldsymbol{r}-\boldsymbol{R}_i, \boldsymbol{r}'-\boldsymbol{R}_i) \Big] \hat{\psi}_{\lambda',\sigma}(\boldsymbol{r}') \tag{2.7}$$

to the clean Hamiltonian $\hat{\mathcal{H}}_0 + \hat{\mathcal{H}}_{\text{int}}$ (introduced in Eqs. (2.1) and (2.3)), generated by randomly distributed impurities of a certain strength. Here, $\lambda \in \{1,2\}$ is a band index, meaning that, in momentum representation, states from band 1 are close to $\boldsymbol{0}$ and states from band 2 are close to $\boldsymbol{Q}$. $u_{\lambda\lambda'}$ is the corresponding matrix element of the perturbation due to a single impurity at $\boldsymbol{R} = \boldsymbol{0}$. This idea and its implications for single-band s-wave superconductors have been discussed in Sec. 1.3.2 and the technical details of the generalization to multi-band materials are presented in Apps. B.1.1 and B.1.2.

For Gaussian disorder, which we will consider in the remainder, the crucial information about disorder is encoded in the disorder correlator $\Gamma_{\lambda_1\lambda_1',\lambda_2\lambda_2'}(\boldsymbol{r}_1,\boldsymbol{r}_1';\boldsymbol{r}_2,\boldsymbol{r}_2')$ as long as disorder-averaged quantities are concerned.[1] Scattering processes in a two-band model can thus be characterized by the respective

[1] For the connection of the disorder correlators to the impurity potentials, we refer to (B.8).

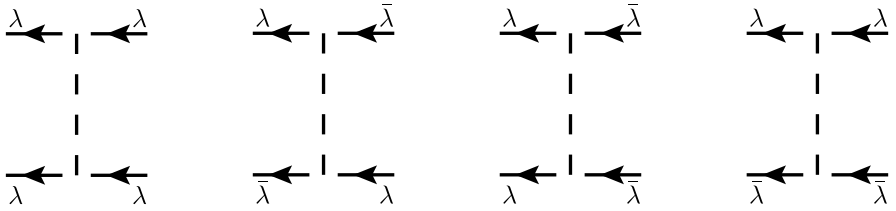

(a) $\Gamma_{\lambda\lambda,\lambda\lambda}$ **(b)** $\Gamma_{\lambda\bar{\lambda},\bar{\lambda}\lambda}$ **(c)** $\Gamma_{\lambda\bar{\lambda},\lambda\bar{\lambda}}$ **(d)** $\Gamma_{\lambda\lambda,\bar{\lambda},\bar{\lambda}}$

Figure 2.2: Non-spin-magnetic scattering processes in the two-band model of iron-based superconductors. Momentum conservation allows for the intraband scattering process depicted in (a) as well as several interband scattering processes. The latter can be categorized into processes that contribute to (b) the self energy, (c) SC vertices, or (d) magnetic properties.

scattering rates

$$\Gamma_{\lambda_1\lambda_1',\lambda_2\lambda_2'} = n_{\mathrm{imp}} u_{\lambda_1\lambda_1'} u_{\lambda_2\lambda_2'} \tag{2.8}$$

provided that the momentum dependence is sufficiently weak, cf. App. B.1.2. Quasi-momentum conservation imposes restrictions on the possible combinations of band indices, and the scattering processes allowed within the two-band model of the iron-based superconductors are summarized in Fig. 2.2. These scattering processes can be classified into intraband scattering and interband scattering processes, where the latter are responsible for qualitatively new effects in multi-band materials as compared to single-band superconductors.

Intraband scattering The *intraband scattering* process within band λ is depicted in Fig. 2.2 (a) and can be characterized by the scattering rate

$$\Gamma_\lambda := \Gamma_{\lambda\lambda,\lambda\lambda}\,. \tag{2.9}$$

We emphasize that, in general, the intraband scattering rates within the two bands,

$$\Gamma_1 = n_{\mathrm{imp}} |u_{11}|^2 \tag{2.10a}$$

$$\text{and} \quad \Gamma_2 = n_{\mathrm{imp}} |u_{22}|^2\,, \tag{2.10b}$$

can be different ($\Gamma_1 \neq \Gamma_2$) because the momentum states in the two bands may have different structure and thus may be scattered differently by impurities. We further note that such nonmagnetic intraband scattering processes are pair-breaking neither for conventional nor for unconventional superconductivity as also results explicitly from our calculations discussed in Sec. 2.3.

Interband scattering The various types of *interband scattering* processes are depicted in Figs. 2.2 (b), 2.2 (c), and 2.2 (d). The process depicted in Fig. 2.2 (b) affects the quasiparticle self-energy part, see App. C.2 for details. The respective correlator is a real number, $\Gamma_{\lambda\bar{\lambda},\bar{\lambda}\lambda} \equiv n_{\mathrm{imp}} |u_{\lambda\bar{\lambda}}|^2 \in \mathbb{R}$, and we term it the interband scattering rate

$$\Gamma_{12} := \Gamma_{12,21} = \Gamma_{21,12} \equiv n_{\mathrm{imp}} |u_{12}|^2\,, \tag{2.11}$$

as it will contribute to the disorder-averaged electron propagator in self-consistent Born approximation (SCBA)

$$G_{\lambda,\boldsymbol{k}}(\nu_n) = \frac{1}{\mathrm{i}\nu_n - \varepsilon_{\lambda,\boldsymbol{k}} + \frac{\mathrm{i}}{2\tau_\lambda}\,\mathrm{sgn}(\nu_n)} \tag{2.12}$$

via the full elastic scattering time τ_λ for quasiparticles in band λ,

$$\tau_\lambda = [2\pi\rho_\mathrm{F}(\Gamma_\lambda + \Gamma_{12})]^{-1}\,, \tag{2.13}$$

where ρ_F is the total DOS per band at the Fermi level.

On the contrary, the correlator associated with the scattering process shown in Fig. 2.2 (c) in general comes with a phase,

$$\Gamma_{\lambda\bar{\lambda},\lambda\bar{\lambda}} \equiv n_\mathrm{imp}(u_{\lambda\bar{\lambda}})^2 = n_\mathrm{imp}|u_{\lambda\bar{\lambda}}|^2 \mathrm{e}^{\mathrm{i}\phi_\lambda}\,, \tag{2.14}$$

where $\phi_\lambda \neq 0$ (modulo 2π) if $\mathrm{Im}\, u_{\lambda\bar{\lambda}} \neq 0$. This process describes the scattering of a pair of momentum states in one band into a pair of momentum states in the other band which is possible since $2\boldsymbol{Q}$ is a reciprocal lattice vector in the FeSCs.[2] Since $|\Gamma_{\lambda\bar{\lambda},\lambda\bar{\lambda}}| = \Gamma_{\lambda\bar{\lambda},\bar{\lambda}\lambda}$ and $\Gamma_{12,12} = \Gamma^*_{21,21}$, we introduce the phase ϕ as

$$\Gamma_{12,12} = \Gamma_{12}\mathrm{e}^{\mathrm{i}\phi}\,. \tag{2.15}$$

Note that this phase is defined relative to a similar phase of the BCS coupling matrix element $V^{\lambda\bar{\lambda}}_{\boldsymbol{k}\boldsymbol{k}'}$ contained in Eq. (2.3), which couples pairs of momentum states in different bands. Thus, it seems likely that the interplay of the scattering process in Fig. 2.2 (c) and the SC coupling affects the superconducting properties of the system. The fact that ϕ must be understood as a relative phase will become more evident in our discussion in Sec. 2.3.3.

Finally, the process in Fig. 2.2 (d) affects neither the quasiparticle self-energy part nor the superconducting properties but can be important, e. g., for the magnetic properties of the material. In our discussion in Chap. 4, however, this process will not be of importance.

2.2.2 The role of time-reversal symmetry

The robustness of different superconducting pairing states against certain types of disorder can be inferred[3] from a symmetry analysis [86, 87], and it turns out that for s^{++} and s^{+-} superconductors, the behavior of the disorder Hamiltonian under time reversal is crucial [87]. Namely, the following generalizations of the Anderson theorem for the two-band model at particle-hole symmetry have been deduced from symmetry in Ref. 87:

- The s^{++} pairing state is protected against any form of time-reversal-symmetric scattering, i. e., against nonmagnetic impurities. This means, the Anderson theorem can be generalized straightforwardly to the case of a two-band superconductor.
- The s^{+-} pairing state is protected against
  - purely band-diagonal time-reversal-symmetric scattering, i. e., against nonmagnetic intraband scattering,
  - as well as purely band-off-diagonal time-reversal-antisymmetric scattering, i. e., against magnetic interband scattering.

[2] In materials where $2\boldsymbol{Q}$ is not a vector of the reciprocal lattice, such Umklapp scattering processes are suppressed along with electron–electron pair hopping interactions. Examples include the quasi-one-dimensional conductors of the Bechgaard salt family [132] and two-dimensional models for rare-earth or actinide heavy-fermion compounds [133].

[3] By looking at the spectrum of the mean-field Hamiltonian in the presence of a given disorder realization, it can be shown that the gap is not reduced in the presence of disorder with certain symmetries.

The explicit derivation of T_c is summarized in App. C, and it turns out that the phase in the interband scattering correlator $\Gamma_{\lambda\bar{\lambda},\lambda\bar{\lambda}}$ as introduced in Eq. (2.15) can be directly related to pair breaking. Hence in this section, we elucidate the role of time-reversal symmetry (TRS) in the context of disorder in iron-based superconductors and its relation to such a nontrivial phase ϕ.

Since $\Gamma_{12,12} = \Gamma_{12}\mathrm{e}^{\mathrm{i}\phi} \propto (u_{12})^2$, in order to have a nontrivial phase in the impurity line, we need

$$u_{12} = \sum_{s,s'} \mathrm{e}^{\mathrm{i}\boldsymbol{R}_{s'}\cdot\boldsymbol{Q}} u_{12}(\boldsymbol{R}_s, \boldsymbol{R}_{s'}) = u_{21}^* \tag{2.16}$$

to have a nonzero imaginary part. Here, $u_{\lambda\bar{\lambda}}$ denotes the matrix element of a single impurity at $\boldsymbol{R} = \boldsymbol{0}$ in momentum space, assuming that it depends only weakly on momentum. Then, $u_{\lambda\bar{\lambda}}(\boldsymbol{R}_s, \boldsymbol{R}_{s'})$ is the respective matrix element in real space and we label lattice sites by s and s' here. Since $2\boldsymbol{Q}$ is a reciprocal lattice vector, and thus $\exp(-\mathrm{i}\boldsymbol{R}\cdot\boldsymbol{Q}) = \pm 1$ for any lattice vector $\boldsymbol{R}$, this requirement can only be met if the matrix element

$$u_{\lambda\bar{\lambda}}(\boldsymbol{R}_s, \boldsymbol{R}_{s'}) = \int \mathrm{d}\boldsymbol{r}\, (\varphi^{\lambda}_{\boldsymbol{R}_s}(\boldsymbol{r}))^* \hat{U}_{\boldsymbol{R}=\boldsymbol{0}} \varphi^{\bar{\lambda}}_{\boldsymbol{R}_{s'}}(\boldsymbol{r}) \tag{2.17}$$

itself has a nonzero imaginary part. Here, $\varphi^{\lambda}_{\boldsymbol{R}_s}(\boldsymbol{r})$ denotes the Wannier function of band λ centered around site $\boldsymbol{R}_s$. The Wannier functions in band space are related to the tight-binding wave functions in orbital space by an orthogonal, i. e., real, transformation matrix, since the dispersion in band space is symmetric. Furthermore, in the FeSCs, electrons from d orbitals [45, 116, 134] are forming the superconducting condensate. Since the wavefunctions of electrons from d orbitals can be chosen real, a possible imaginary part of $u_{\lambda\bar{\lambda}}(\boldsymbol{R}_s, \boldsymbol{R}_{s'})$ must be due to the phases in the impurity Hamiltonian $\hat{\mathcal{H}}_{\mathrm{dis}}$.

In the absence of spin-orbit coupling, the Hamiltonian can be split into an orbital part and a spin part, $\hat{U}_{\boldsymbol{R}=\boldsymbol{0}} = \hat{U}^{\mathrm{orb}}_{\boldsymbol{R}=\boldsymbol{0}} \otimes \hat{U}^{\mathrm{spin}}_{\boldsymbol{R}=\boldsymbol{0}}$. We consider the transformation properties under time reversal, described by the anti-unitary operator

$$\hat{\Theta} = (\hat{\mathcal{T}}^{\mathrm{orb}} \otimes \hat{\mathcal{T}}^{\mathrm{spin}})\hat{\mathcal{K}}\,, \tag{2.18}$$

where $\hat{\mathcal{K}}$ denotes complex conjugation and $\hat{\mathcal{T}}$ is a unitary operator. For spin-$\frac{1}{2}$, the spin part $\hat{\mathcal{T}}^{\mathrm{spin}}$ is given by the Pauli matrix $\mathrm{i}\hat{\sigma}_2$, and in real space, the orbital part $\hat{\mathcal{T}}^{\mathrm{orb}}$ corresponds to the identity, $\hat{\mathcal{T}}^{\mathrm{orb}} = \hat{\mathbb{1}}^{\mathrm{orb}}$.

Let us consider the most generic TRS impurity Hamiltonian, meaning that $\hat{U}_{\boldsymbol{R}=\boldsymbol{0}} = \hat{\Theta}\hat{U}_{\boldsymbol{R}=\boldsymbol{0}}\hat{\Theta}^{-1}$. If $\hat{U}_{\boldsymbol{R}=\boldsymbol{0}}$ is invariant under time reversal, the matrix element $u_{\lambda\bar{\lambda}}(\boldsymbol{R}_s, \boldsymbol{R}_{s'})$ is invariant as well. If we restrict ourselves to non-spin-magnetic disorder, i. e., scattering processes that are insensitive to spin ($\hat{U}^{\mathrm{spin}}_{\boldsymbol{R}=\boldsymbol{0}} \propto \hat{\sigma}_0$), then the spin part is also invariant under time reversal. As a consequence, the orbital part of the Hamiltonian is real, yielding $u_{\lambda\bar{\lambda}} \in \mathbb{R}$. In conclusion, impurities that are invariant under time-reversal and insensitive to spin are not able to generate nontrivial phases in the scattering matrix elements. Consequently, no such nontrivial phase can arise in $\Gamma_{\lambda\bar{\lambda},\lambda\bar{\lambda}}$ either.

Furthermore, as long as we assume impurity scattering to be insensitive to the conduction electrons' spin, TRS breaking can only be due to orbital magnetism. Therefore, a possible nontrivial phase in the pair-hopping interband scattering process can only be due to orbital-magnetic impurities in the two-band model of the FeSCs. This concept will be picked up in Sec. 2.3.2 where we discuss an example of orbital-magnetic impurities in the context of FeSCs.

2.3 The effect of weak disorder in iron-based superconductors

In order to tune the properties of FeSCs, these materials are doped, see also Sec. 2.2. Theoretically, doping can be included in the model of FeSC introduced in Sec. 2.1.2 by a modification of band structure

parameters such as a shift of the chemical potential and the ellipticity of the electron pockets as well as by including scattering of the conduction electrons off impurities. Indeed, it has been shown that both aspects of doping can account for the experimentally observed phase diagram of FeSC [66, 69]. The question, however, which of these points of view is the more appropriate one is not settled yet, though studies indicate that effects beyond mere carrier doping are important [77–80].

Disorder can also be introduced deliberately by irradiation with electrons, neutrons, and protons, for instance, and diminished again by annealing. Such studies complement those where doping is used to control material properties since they allow to control the amount of disorder without substantial changes of the band structure. Hence they provide a useful tool to assess which effects of doping are primarily due to impurity scattering.

For lack of a smoking gun experiment for the pairing state of the FeSCs, various indirect clues for or against certain scenarios have been collected. Among these, the relation between the transition temperature and the scattering rate has been used as a tool [101–107] to discriminate between pairing states. In this section, we reassess the ramifications of impurity scattering for different pairing states while neglecting other effects of doping by considering the model at particle-hole symmetry, as already indicated in Sec. 2.1.2. We start with a summary of the classic results from Anderson and Abrikosov and Gor'kov, on which the above-mentioned studies are based, before discussing the implication of phase competition in the FeSCs for disorder effects and their interpretation. We concentrate on the s^{++} and s^{+-} pairing states since they are among the most widely discussed candidates and cannot be told apart by experiments relying on the symmetry of the order parameter.

2.3.1 Weak disorder and the pairing symmetry of iron-based superconductors

Here, we consider the effect of weak disorder on the transition temperature T_c towards s^{+-} SC which at present seems to be the most likely scenario for the pairing state of FeSCs. Before discussing the implications of orbital-magnetic impurities in a multi-band superconductor, we briefly review the expected dependence of T_c on scattering due to nonmagnetic as well as spin-magnetic impurities in s^{+-} superconductors. We contrast the respective results to those obtained for the s^{++} pairing state since the behavior of T_c in the presence of nonmagnetic disorder has been brought forward as an argument for both s^{+-} [101, 107] and s^{++} superconductivity [103, 104, 106] to be realized in FeSCs.

Results for s^{++} pairing The transition temperature T_c of conventional BCS superconductors is not notably affected by the presence of nonmagnetic impurities [10–12], implying that single-band s-wave SC is not destroyed by nonmagnetic scattering. This is usually referred to as the Anderson theorem in literature. The extension of BCS theory to multi-band systems [135, 136] has been achieved soon after the formulation of the single-band case. Also in the presence of interband scattering, the Anderson theorem can be adopted for the s^{++} pairing state, i. e., nonmagnetic impurities do not suppress the SC transition temperature T_c of the s^{++} pairing state either [137–139]. In contrast, if the impurities are magnetic, the transition temperature of the s^{++} state is suppressed by disorder according to the Abrikosov-Gor'kov (AG) law [88, 137, 139, 140] as stated in Eq. (1.7), where both intraband and interband scattering contribute to the suppression.

Results for s^{+-} pairing In the case of the s^{+-} pairing state and other more complex pairing states, the presence of nonmagnetic impurities is sufficient to reduce T_c in an AG-like fashion [137–139, 141] as long as these impurities cause interband scattering. Since in the absence of interband scattering, s^{++} and s^{+-} pairing states are affected by disorder in the exact same manner, magnetic intraband scattering

must be pair breaking for s^{+-} SC as well. Magnetic disorder with a pure interband component however does not affect T_c [128, 137, 140] in the s^{+-} pairing state, meaning that the roles of magnetic and nonmagnetic impurities for pair breaking due to interband scattering are reversed by the sign reversal of the order parameter when considering s^{+-} instead of s^{++}. This can be generalized even further to an analogue of the Anderson theorem for the s^{+-} superconductor as derived by Ref. 87: The s^{+-} state is stable against time-reversal-symmetric intraband disorder and time-reversal-antisymmetric interband disorder. We emphasize that this conclusion holds irrespective of whether the TRS breaking of the interband scattering occurs due to spin or orbital magnetism which will be utilized further in our discussion of Sec. 2.3.2.

Disorder and the pairing state Nonmagnetic impurities can only destroy the s^{+-} state, whereas spin-magnetic interband scattering is pair breaking for the s^{++} state while leaving the s^{+-} state unharmed. Hence experiments relating the superconducting transition temperature T_c to disorder have been utilized to draw conclusions about the pairing state [101–107, 142]. In those studies, the amount of impurities is either controlled by irradiation and annealing of the samples, or by the dopant content x.

All studies report a suppression of T_c with increasing scattering rate obtained from transport measurements, however, since the suppression is weaker than the typical AG-type suppression, the conclusions drawn from these measurements differ: While some groups (Refs. 101 and 107, for instance) consider the evident suppression as a perfect agreement with the s^{+-} suggestion, others (such as Refs. 103, 104 and 106) argue that the relatively weak suppression rather points towards a conventional pairing state.

One explanation for this contradiction might be that intraband and interband scattering are not equally strong in the FeSCs, and transport properties are mainly determined by intraband scattering whereas the suppression of T_c is due to interband scattering. Moreover, we will argue in Secs. 2.3.2 and 2.3.3 that the interpretation of such experiments might be even more hindered in the case of materials with competing states of order.

Further generalizations Finally, the clarity of the above-discussed results originates from the idealized superconducting state we were considering. In particular, the exact protection of SC against disorder of a certain type only applies to pure s^{++} and s^{+-} superconductors, where either $\Delta_1 = \Delta_2$ or $\Delta_1 = -\Delta_2$ holds, respectively. This assumption can be relaxed by allowing for a mismatch in the DOS of the two bands. Such a DOS mismatch provides an additional source of pair breaking [131], resulting in a suppression of T_c in s^{+-} superconductors even in the absence of interband scattering. Moreover, the derivation of the above generalizations of the Anderson theorem uses the Born approximation, i. e., applies to the limit of sufficiently weak disorder. However, investigations of the unitary limit [128, 140, 143], i. e., of strong impurities, even find that both s^{++} and s^{+-} SC are protected against nonmagnetic as well as magnetic disorder.

Furthermore, many of the above studies allude to disorder effects beyond T_c suppression with the typical AG law. For example, after the initial drop of T_c reflecting pair breaking, nonmagnetic disorder can induce an $s^{+-} \rightarrow s^{++}$ transition [127, 129] since interband scattering tends to adjust the order parameter on both Fermi surface (FS) pockets to the same value. Vice versa, magnetic disorder can possibly induce a transition from s^{++} to s^{+-} [128]. Such effects naturally result in a T_c suppression that is not of AG-type. Adding to this, correlations [144] and the presence of competing phases such as the spin-density wave (SDW) state in the FeSCs also contribute to deviations from the standard AG law for T_c suppression. The latter might even lead to an increase of T_c [13] owing to a weakening

of the phase competition in the underdoped regime of the FeSCs since the SDW state is affected more strongly by impurities than SC.

2.3.2 Orbital-magnetic impurities from nucleation of competing order

Competing states of order are a characteristic of FeSCs, and model calculations [41–43] even suggest the proximity to charge-density wave (CDW) formation – throwing in another possible competitor for SC and SDW order. Even though the formation of CDW order has not been observed in experiment yet, considering this possible ordered state in the context of disordered materials is worthwhile: Since the presence of an impurity locally changes the environment for electrons in the crystal, a competing state of order could become locally favorable. Indeed, the nucleation of SDW around a single impurity has been demonstrated theoretically [145–148]. Analogously, the nucleation of CDW order around impurities is a conceivable scenario for the FeSCs which shall be discussed further in the remainder of this chapter.

Phase competition The renormalization group analysis [41] of the two-band model for iron-based superconductors at particle-hole symmetry revealed the existence of a fixed point, where the Hamiltonian exhibits an SO(6) symmetry and three different states of order compete [41–43]. For repulsive interband pair hopping, these states are

- spin-density wave (SDW) order with a real order parameter (three components)

$$\boldsymbol{M} = \sum_{\boldsymbol{k},\sigma,\sigma'} \left\langle \hat{\psi}^\dagger_{1,\boldsymbol{k},\sigma} \boldsymbol{\sigma}_{\sigma\sigma'} \hat{\psi}_{2,\boldsymbol{k},\sigma'} + \hat{\psi}^\dagger_{2,\boldsymbol{k},\sigma} \boldsymbol{\sigma}_{\sigma\sigma'} \hat{\psi}_{1,\boldsymbol{k},\sigma'} \right\rangle , \tag{2.19}$$

- s^{+-} superconductivity (SC) with order parameter (two components)

$$\Delta = \sum_{\boldsymbol{k}} \left\langle \hat{\psi}^\dagger_{1,\boldsymbol{k},\uparrow} \hat{\psi}^\dagger_{1,-\boldsymbol{k},\downarrow} - \hat{\psi}^\dagger_{2,\boldsymbol{k},\uparrow} \hat{\psi}^\dagger_{2,-\boldsymbol{k},\downarrow} \right\rangle , \tag{2.20}$$

- and charge-density wave with an imaginary order parameter (iCDW) (one component)

$$\rho = \mathrm{i} \sum_{\boldsymbol{k},\sigma} \left\langle \hat{\psi}^\dagger_{1,\boldsymbol{k},\sigma} \hat{\psi}_{2,\boldsymbol{k},\sigma} - \hat{\psi}^\dagger_{2,\boldsymbol{k},\sigma} \hat{\psi}_{1,\boldsymbol{k},\sigma} \right\rangle . \tag{2.21}$$

At this fixed point, the free energy $\mathcal{F}$ is a function of the combined order parameter, $\mathcal{F} = \mathcal{F}(|\boldsymbol{M}|^2 + |\Delta|^2 + |\rho|^2)$. FeSCs are only close to this SO(6)-symmetric fixed point, and the SDW or SC instabilities occur first. This explains why iCDW order has not been observed in any FeSC so far, although being close in energy. It is, however, a conceivable scenario that such order could nucleate around impurities in these materials, similar to SDW order [147, 148], even if the bulk is still in the superconducting state. Such iCDW-type impurities break time-reversal symmetry and thereby would be associated with *orbital magnetism*. Note that ρ is an Ising order parameter, and hence can nucleate with either sign around a given impurity site.

iCDW impurities We consider iCDW impurities as an example to demonstrate the emergence of a nontrivial phase in the impurity line in FeSC. Such an impurity at site $\boldsymbol{R}_i$ is described by

$$\hat{U}^{\mathrm{iCDW}}_{\boldsymbol{R}_i} = \mathrm{i}\frac{U_0}{2}\sum_{s,\sigma} \mathrm{e}^{\mathrm{i}\boldsymbol{Q}\cdot(\boldsymbol{R}_i+\boldsymbol{R}_s)} \left[\hat{\psi}^\dagger_{1,\sigma}(\boldsymbol{R}_i+\boldsymbol{R}_s)\hat{\psi}_{2,\sigma}(\boldsymbol{R}_i+\boldsymbol{R}_s) - \hat{\psi}^\dagger_{2,\sigma}(\boldsymbol{R}_i+\boldsymbol{R}_s)\hat{\psi}_{1,\sigma}(\boldsymbol{R}_i+\boldsymbol{R}_s)\right] , \quad (2.22)$$

and therefore, each impurity breaks time-reversal symmetry. Here, U_0 is proportional to the iCDW order parameter ρ and an appropriate electron–electron interaction matrix element. Furthermore, each impurity is associated with an orbital loop current, which can be described by an Ising order parameter. Hence the sign of U_0 might be different for impurities at different sites whereas the impurity line would remain unaffected since it only depends on the square of the order parameter,

$$\Gamma^{\mathrm{iCDW}}_{(\lambda_1\boldsymbol{k}_1)(\lambda_1'\boldsymbol{k}_1'),(\lambda_2\boldsymbol{k}_2)(\lambda_2'\boldsymbol{k}_2')} = -n_{\mathrm{imp}}U_0^2\sum_{s,s'} \mathrm{e}^{\mathrm{i}(\boldsymbol{k}_1-\boldsymbol{k}_1'+\boldsymbol{Q})\cdot\boldsymbol{R}_s+\mathrm{i}(\boldsymbol{k}_2-\boldsymbol{k}_2'+\boldsymbol{Q})\cdot\boldsymbol{R}_{s'}}\, \delta^{\mathrm{iCDW}}_{\lambda_1\lambda_1',\lambda_2\lambda_2'} . \quad (2.23)$$

Also, the crystal momentum is conserved as $(2\pi)^2\,\delta(\boldsymbol{k}_1+\boldsymbol{k}_2-\boldsymbol{k}_1'-\boldsymbol{k}_2'+\boldsymbol{K})$ is implied in each scattering process. For details of the derivation, we refer to App. B.2. For the interband scattering process corresponding to the exchange of two electrons between the bands, characterized by $\Gamma^{\mathrm{iCDW}}_{\lambda\bar{\lambda},\bar{\lambda}\lambda}$, it holds that $\delta^{\mathrm{iCDW}}_{\lambda\bar{\lambda},\bar{\lambda}\lambda} = -1$. The interband scattering process $\Gamma^{\mathrm{iCDW}}_{\lambda\bar{\lambda},\lambda\bar{\lambda}}$ from which a phase in the impurity line might arise is associated with $\delta^{\mathrm{iCDW}}_{\lambda\bar{\lambda},\lambda\bar{\lambda}} = +1$ and corresponds to a Cooper pair being scattered to the other band. Note that other scattering processes cannot be generated by pure iCDW impurities since $\delta^{\mathrm{iCDW}}_{\lambda\lambda,\lambda\lambda} = 0 = \delta^{\mathrm{iCDW}}_{\lambda\lambda,\bar{\lambda}\bar{\lambda}}$.

Finally, the impurity lines for the respective interband scattering processes can be evaluated assuming a lattice possessing certain symmetries and a finite range of the impurities. For short-ranged iCDW impurities, the sums over lattice sites could be restricted to nearest neighbors, for instance. It turns out that, as long as inversion symmetry is present in the crystal, the imaginary part of the impurity line $\Gamma^{\mathrm{iCDW}}_{12,12}$ is zero. Still, a nontrivial phase of $\phi = \pi$ is possible even in the case of an inversion-symmetric lattice since a global prefactor of -1 in the impurity line $\Gamma^{\mathrm{iCDW}}_{12,12}$ would correspond to a phase of $\phi = \pi$. Indeed, assuming an inversion-symmetric lattice and short-ranged impurities that only affect neighboring sites results in

$$\Gamma^{\mathrm{iCDW}}_{12,12} = -n_{\mathrm{imp}}U_0^2N_{\mathrm{NN}}^2 = \mathrm{e}^{\mathrm{i}\pi}n_{\mathrm{imp}}U_0^2N_{\mathrm{NN}}^2 , \quad (2.24)$$

where N_{NN} is the number of nearest-neighbor sites and again, we neglected the weak momentum dependence resulting in an impurity line that only depends on band indices. When, additionally, the lattice breaks inversion symmetry, even arbitrary phases are conceivable. This also leads to suppression of T_{c}, but with a different functional behavior, which will also be part of the discussion in the next chapter.

2.3.3 Effect of orbital-magnetic impurities on the transition temperature

In the previous section, we justified the importance of orbital-magnetic impurities for the FeSCs by considering the nucleation of competing iCDW order around nonmagnetic impurities, manifesting itself in a phase $\phi = \pi$ in the pair-hopping interband scattering process (2.15). To keep the discussion as general as possible, we revert to the effect of generic orbital-magnetic impurities here, characterized by an arbitrary phase but insensitive to the electrons' spin.

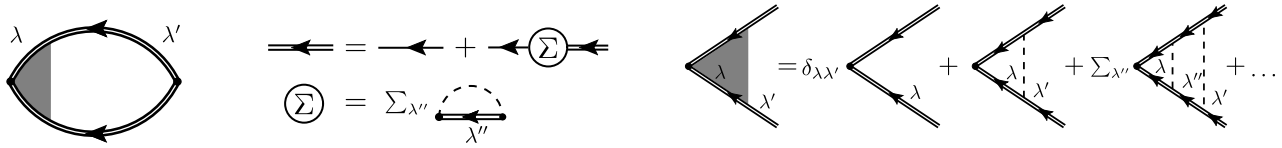

(a) diagram $d_{\lambda\lambda'}$ **(b)** self energy **(c)** vertex corrections

Figure 2.3: Self-consistent Born approximation in the two-band model of iron-based superconductors. Here, both intraband and interband scattering renormalize the quadratic coefficients a associated with the diagrams depicted in (a). The structure of (b) self energy and (c) vertex corrections is however of the same form as in single-band superconductors, cf. Fig. 1.7.

We consider the minimal model for superconductivity in the FeSCs, which is the two-band model with one hole band and one electron band as introduced in Eqs. (2.1) and (2.3). Depending on whether the interaction leading to superconductivity is attractive or repulsive, the resulting pairing state is either the conventional s^{++} state or the unconventional s^{+-} state, respectively, which are known to react differently to the presence of impurities. The derivation of the free energy

$$\mathcal{F}(\bar{\Delta},\Delta) = a_{++}|\Delta_+|^2 + a_{--}|\Delta_-|^2 + a_{+-}\bar{\Delta}_+\Delta_- + a_{-+}\bar{\Delta}_-\Delta_+ \tag{2.25}$$

in the presence of weak disorder is presented in App. C, where we employ the self-consistent Born approximation (SCBA) to derive analytic expressions for the quadratic coefficients a in the presence of disorder. The SCBA is valid as long as the mean-free path l_{mfp} satisfies $k_{\mathrm{F}} l_{\mathrm{mfp}} \gg 1$ and hence single-particle interference effects are subleading. This means that diagrams with crossed impurity lines can be neglected since they are suppressed by a factor $1/(k_{\mathrm{F}} l_{\mathrm{mfp}})$. The diagrammatic elements of our approach are depicted in Fig. 2.3 and technical details concerning the application of our formalism to FeSCs can be found in App. C.3. It turns out that, since the intraband scattering processes in our model preserve TRS, only interband scattering can cause pair breaking. In principle, our results allow to determine the transition temperature as a function of interband scattering rate Γ_{12} for arbitrary phases ϕ numerically, but it is most instructive to highlight three important limits for which analytic solutions can be obtained: nonmagnetic impurities ($\phi = 0$) as a reference, orbital-magnetic impurities with $\phi = \pi$ such as the example of iCDW impurities presented in the previous section, and the intermediate case $\phi = \frac{\pi}{2}$. Our results for both the s^{++} and the s^{+-} pairing state are summarized in Fig. 2.4 and discussed in detail in the remainder of this section.

$\boldsymbol{\phi = 0}$ Let us first note here that our results for a dirty superconductor with truly nonmagnetic impurities ($\phi = 0$) are consistent with previous works. In particular, the limit $\Gamma_{12} = 0$ recovers the results obtained in the clean case. In the case of an attractive interaction ($V_{\mathrm{SC}} < 0$), s^{++} superconductivity occurs at a transition temperature T_{c} which is unaffected by the presence of weak disorder,

$$T_{\mathrm{c}}(\Gamma_{12}) = T_{\mathrm{c},0} = \frac{2\Lambda \mathrm{e}^{\gamma}}{\pi} \mathrm{e}^{-\frac{1}{|V_{\mathrm{SC}}|\rho_{\mathrm{F}}}} . \tag{2.26}$$

This result is consistent with the extension of the usual Anderson theorem for BCS superconductivity to the two-band case.

For repulsive interaction ($V_{\mathrm{SC}} > 0$), we find a transition towards the (unconventional) s^{+-} pairing state at a critical temperature which is affected by the presence of nonmagnetic impurities: The transition temperature is suppressed with increasing interband scattering rate, and s^{+-} superconductivity

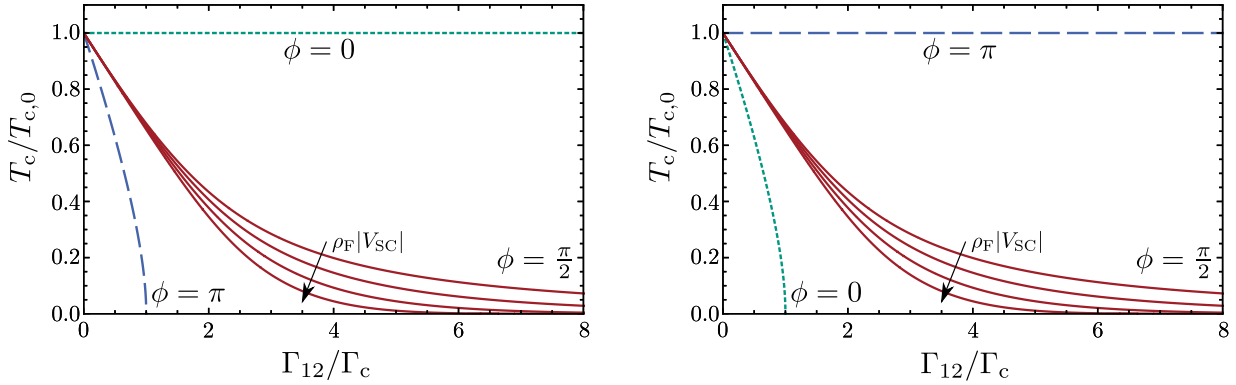

(a) attractive interaction ($V_{SC} < 0$) **(b)** repulsive interaction ($V_{SC} > 0$)

Figure 2.4: Suppression of the transition temperature due to interband scattering. We show the transition temperature T_c as a function of interband scattering rate Γ_{12} for the examples discussed in the text: The fate of the SC state due to (a) attractive and (b) repulsive interaction in the presence of impurities leading to interband scattering with phases $\phi = 0$ (green dotted line), $\phi = \frac{\pi}{2}$ (red lines), and $\phi = \pi$ (blue dashed line). The transition temperature is measured in terms of the transition temperature of a clean system $T_{c,0}$, and the scattering rate is expressed in terms of the critical scattering rate Γ_c. For $\phi = \frac{\pi}{2}$, the transition temperature depends on the dimensionless coupling constant, and we plotted our results for $\rho_F|V_{SC}| \in \{0.1, 0.2, 0.3, 0.4\}$ here.

even vanishes completely at the critical scattering rate

$$\Gamma_c = \frac{T_{c,0}}{4e^{\gamma}\rho_F}\,. \tag{2.27}$$

The functional behavior of T_c on the interband scattering rate Γ_{12} corresponds to the functional behavior originally only associated with paramagnetic impurities by Abrikosov and Gor'kov [88]. In particular, in the regime of small interband scattering rate, the T_c suppression is linear,

$$T_c(\Gamma_{12}) = T_{c,0} - \frac{\pi^2}{2}\rho_F\Gamma_{12} \qquad \text{for} \qquad \frac{\rho_F\Gamma_{12}}{T_c} \ll 1\,. \tag{2.28}$$

In order to get a qualitative understanding, we can employ the same type of visualization in real space that we already discussed in Sec. 1.3.2 for the BCS case, cf. Fig. 1.6. For the effect of nonmagnetic impurities in s^{++} superconductors, we refer to Fig. 2.5 (a): Impurity scattering can result in interband scattering processes which convey a time-reversed pair of electrons from one band to another, cf. Fig. 2.2 (c), however, phase coherence is not destroyed by this process. Analogously, in Fig. 2.5 (c), we illustrate the results for the s^{+-} pairing state in real space. The sign reversal of the order parameter, $\Delta_1 = -\Delta_2$, can also be expressed as a relative phase π of the order parameter in different bands. This means that, effectively, the SC interaction matrix element accumulates a random phase factor (a multiple of π) which destroys superconductivity if the mean-free path becomes smaller than the superconducting coherence length, see also our discussion in the subsequent paragraph.

$\phi = \pi$ For a phase $\phi = \pi$, we find the reversed situation. Then, impurities are pair breaking for conventional s^{++} superconductors with the same AG-type suppression of T_c that we found for the

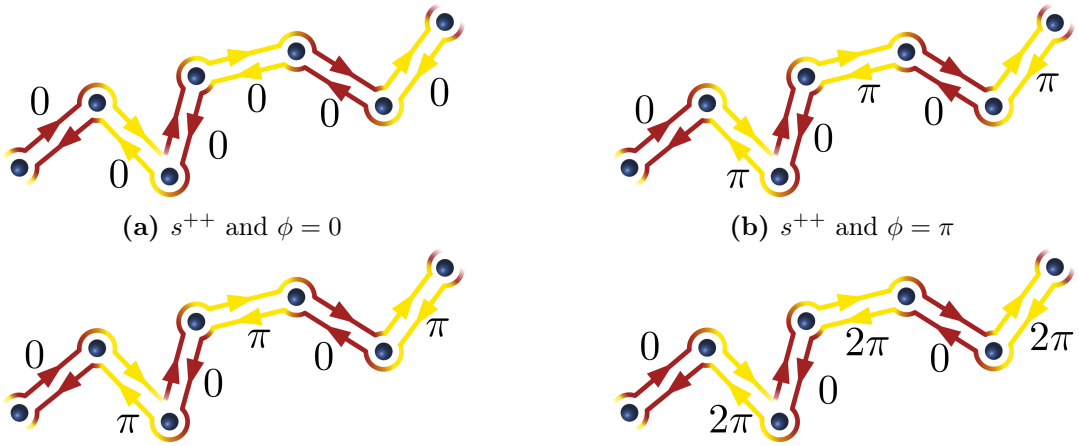

(a) s^{++} and $\phi = 0$ **(b)** s^{++} and $\phi = \pi$

(c) s^{+-} and $\phi = 0$ **(d)** s^{+-} and $\phi = \pi$

Figure 2.5: Visualization of the generalized Anderson theorem and pair breaking in a two-band model. In analogy to Fig. 1.6, we show a real-space illustration of two electrons on time-reversed paths, scattered off impurities. We indicate different bands by different colors and concentrate on the interband scattering process characterized by $\Gamma_{\lambda\bar{\lambda},\lambda\bar{\lambda}} \in \mathbb{C}$ in our comparison of the effect of nonmagnetic ($\phi = 0$) and orbital-magnetic ($\phi = \pi$) impurities. The first row shows the effect on the s^{++} pairing state whereas the second row illustrates the situation for s^{+-} superconductivity.

s^{+-} state in the presence of nonmagnetic impurities. Even more interestingly, there exists an analog of the Anderson theorem for s^{+-} superconductivity. More specifically, s^{+-} superconductivity is protected against impurities with purely time-reversal-symmetric intraband scattering and purely time-reversal-antisymmetric interband scattering as revealed by the symmetry analysis of Ref. 87 and confirmed by our explicit calculation of T_c. Let us note that one example for orbital-magnetic impurities with a phase $\phi = \pi$ is the scenario previously discussed in Sec. 2.3.2: originally nonmagnetic impurities around which the iCDW state discussed in Refs. 41–43 condenses.

Since the phase ϕ in the impurity line $\Gamma_{12,12}$ as introduced in Eq. (2.15) is only defined relative to a similar phase in the BCS coupling matrix element $V_{\boldsymbol{k}\boldsymbol{k}'}^{\lambda\bar{\lambda}}$ in Eq. (2.3), these results can also be understood in terms of a redefinition of the electron operators in order to absorb the phase of the impurity line of the respective interband scattering process,

$$\begin{aligned} \hat{\psi}_{1,\boldsymbol{k},\sigma} &\to \hat{\psi}'_{1,\boldsymbol{k},\sigma} = \mathrm{e}^{\mathrm{i}\frac{\phi}{2}} \hat{\psi}_{1,\boldsymbol{k},\sigma} \,, \\ \hat{\psi}_{2,\boldsymbol{k},\sigma} &\to \hat{\psi}'_{2,\boldsymbol{k},\sigma} = \hat{\psi}_{2,\boldsymbol{k},\sigma} \,. \end{aligned} \tag{2.29}$$

This leaves the intraband scattering processes (associated with Γ_1 and Γ_2) as well as the interband scattering process entering the self energy (characterized by $\Gamma_{\lambda\bar{\lambda},\bar{\lambda}\lambda}$) unaffected, but entails a simultaneous rescaling of the BCS coupling matrix element, which had been chosen real in Eq. (2.4),

$$V \to V' = \mathrm{e}^{-\mathrm{i}\phi} V \,. \tag{2.30}$$

In the case of $\phi = \pi$, such a redefinition corresponds to $V \to V' = -V$, and thus an attractive interaction under this transformation becomes effectively repulsive, and vice versa. From this consideration, it is obvious that for $\phi = \pi$, an Anderson theorem for the s^{+-} pairing state is to be expected, as well as a suppression of the transition temperature of the s^{++} pairing state with AG law.

An illustration of our results for $\phi = \pi$ can be found in Figs. 2.5 (b) and 2.5 (d). The relative phase $\phi = \pi$ in the interband scattering process of a Cooper pair off an impurity considered here leads to pair breaking[4] for s^{++} for the same reason as nonmagnetic impurities destroy s^{+-} superconductivity. However, in the latter case, the phase ϕ was due to the relative sign. In the case of orbital-magnetic interband scattering, the sign reversal of the order parameter and the phase of π conveyed by the impurity scattering process combine to a trivial phase of 2π associated with each interband scattering process, leading to the protection of s^{+-} against orbital-magnetic impurities of this type.

$\boldsymbol{\phi = \frac{\pi}{2}}$ In the case of $\phi = \frac{\pi}{2}$, we find that the transition temperature is suppressed in the same fashion for attractive and repulsive interaction. For small scattering rates, the transition temperature is suppressed linearly as in the AG case, however, with the slope doubled. Furthermore, neither for attractive, nor for repulsive interaction, a critical scattering rate at which superconductivity vanishes exists, but the transition temperature is suppressed as

$$T_{\mathrm{c}}(\Gamma_{12}) = \begin{cases} T_{\mathrm{c},0} - \frac{\pi^2}{2}\frac{\rho_{\mathrm{F}}\Gamma_{12}}{2}\,, & \frac{\rho_{\mathrm{F}}\Gamma_{12}}{T_{\mathrm{c}}} \ll 1\,, \\ \frac{2\Lambda \mathrm{e}^{\gamma}}{\pi}\mathrm{e}^{-\frac{1}{\rho_{\mathrm{F}}V_{\mathrm{eff}}(\Gamma_{12})}}\,, & \frac{\rho_{\mathrm{F}}\Gamma_{12}}{T_{\mathrm{c}}} \gg 1\,, \end{cases} \tag{2.31}$$

where $V_{\mathrm{eff}}(\Gamma_{12}) = \rho_{\mathrm{F}}|V|^2 \ln(\frac{\Lambda}{2\pi\rho_{\mathrm{F}}\Gamma_{12}})$. Furthermore, the pairing state in case of such an intermediate phase ϕ is a superposition of s^{++} and s^{+-}.

Implications for the pairing state In conclusion, in the presence of impurities associated with orbital magnetism, pair breaking due to interband scattering does not only occur in unconventional superconductors. It is a rather generic result of the accumulation of a random phase in the course of successive interband scattering events of pairs of electrons related by time-reversal on orbital-magnetic impurities. Furthermore, the robustness of T_{c} against impurities does not necessarily imply conventional superconductivity since there is an analog of the Anderson theorem for s^{+-}. It holds for impurities with a purely time-reversal-symmetric intraband component and a purely time-reversal-antisymmetric interband component, and one example would be the effectively orbital-magnetic impurities that arise from nucleation of iCDW order around nonmagnetic impurities – a conceivable scenario for FeSCs where iCDW is a hidden state of order competing with superconductivity.

Let us furthermore note that the symmetry analysis of Ref. 87 finds that also SDW order is stable against such iCDW impurities, for instance, but prone to intraband scattering breaking particle-hole symmetry. Hence, SDW order is affected more severely by impurity scattering than s^{+-} superconductivity, meaning that in a coexistence state of SDW and superconductivity T_{c} may even increase with adding impurities, as demonstrated in Refs. 13 and 102.

Therefore, we find that conclusions concerning the pairing state of the FeSC are hard to draw based solely on the suppression of the transition temperature T_{c} in the presence of disorder. Even if the exact nature of the impurities and their surroundings were known, the interpretation might be clouded by the effects of phase competition.

[4] This is consistent with previous results for spin-magnetic impurities but, in contrast, the orbital-magnetic impurities described here only affect interband scattering processes whereas pair breaking due to spin-magnetic impurities is associated with the intraband scattering processes as well.

2.4 Summary of Chapter 2

In this chapter, we considered a minimal model for superconductivity in the iron-based superconductors – stated in Eqs. (2.1), (2.3), and (2.4) – that can be used to study two of the most widely discussed candidates for the pairing state in these materials: conventional s^{++} superconductivity and the unconventional extended s^{+-} SC state. Since these two possibilities cannot be told apart by experimental probes relying on the symmetry of the order parameter, other tools are needed to uncover the pairing state of the FeSCs.

One example is the response of the superconducting state to nonmagnetic disorder: As known from previous work, the transition temperature T_c of an s^{++} superconductors is expected to remain robust in the presence of nonmagnetic impurities (in line with the Anderson theorem), whereas the unconventional s^{+-} state is expected to be destroyed already by nonmagnetic interband scattering, reflected in a AG-like suppression of T_c with increasing interband scattering rate. Consequently, comparison of the experimentally determined transition temperatures with measurements of the Hall coefficient (or simply with dopant concentration) in various materials has been used to draw conclusions about the pairing state [101–107]. Here, we point out two main problems with this approach:

- Intraband and interband scattering are not equally strong in the iron-based systems, hence transport measurements (determined by the much stronger intraband scattering rate) might overestimate the scattering rate Γ contributing to pair breaking.
- Phase competition is an important characteristic of FeSCs and potentially leads to nucleation of competing orders in the close vicinity of nonmagnetic impurities. This might well render originally nonmagnetic impurities effectively magnetic, requiring caution in the interpretation of experimental data.

Theoretically, the relation $T_c(\Gamma)$ has been well established for both pairing states discussed here in the presence of nonmagnetic and spin-magnetic impurities [88, 137–141]. What this thesis adds to the discussion is the consideration of *orbital-magnetic* impurities which are insensitive to spin, however might break time-reversal symmetry because the pair-hopping interband scattering process (Fig. 2.2 (c)) could be associated with a phase ϕ. Furthermore, we present a concrete example how such a phase could be realized in the context of iron-based superconductors, where iCDW order is a competing state of order. Nucleation of this order around nonmagnetic impurities would then give rise to a phase $\phi = \pi$. Our results, presented in Fig. 2.4, however, are more general and could further be generalized to arbitrary phases. Let us briefly summarize our findings here. Firstly, $\phi = 0$ recovers the results previously obtained in the context of nonmagnetic disorder. Secondly, iCDW impurities ($\phi = \pi$) change the role of impurities for the two pairing states under consideration (compared to nonmagnetic disorder):

- Orbital-magnetic impurities with $\phi = \pi$ act as pair breakers for s^{++} superconductivity, resulting in the well-known AG law.
- The s^{+-} pairing state is robust against such impurities which is a manifestation of the generalized Anderson theorem described in Ref. 87.

Thirdly, arbitrary orbital-magnetic phases lead to a superposition of the two pairing states under consideration here, and are expected to always suppress the transition temperature.

Chapter 3

3 Partial protection against disorder from spin-orbit locking in $LaAlO_3/SrTiO_3$

Superconductivity in the heterointerface of $LaAlO_3$ deposited on a (001)-oriented $SrTiO_3$ substrate emerges at the interface between two nonmagnetic insulators. Two major mechanisms for carrier doping into the interface (as a prerequisite for interface superconductivity) have been identified: The polar discontinuity as a direct result of the differently charged layers of the material, and oxygen vacancies created during the deposition process. The latter is of particular interest in view of a possibly unconventional pairing state that has been suggested as one of the candidates for superconductivity in the $LaAlO_3/SrTiO_3$ interface since, usually, unconventional superconducting states are already suppressed by nonmagnetic impurities and thus only expected in sufficiently clean systems. In particular, in the $LaAlO_3/SrTiO_3$ interface, the coherence length and the mean-free path are estimated to be of the same order. On the other hand, spin-orbit locking can provide [149] a mechanism for protection of unconventional superconductivity against disorder. Therefore, it is imperative for an understanding of superconductivity in $LaAlO_3/SrTiO_3$ to take all characteristics – the multi-orbital nature as well as anisotropic effective masses and spin-orbit coupling – into account.

The first part of this chapter provides some details on the microscopic model for $LaAlO_3/SrTiO_3$ interfaces and the patch approximation as introduced in Ref. 48. One immediate consequence of this model and the resulting nondegenerate and anisotropic nature of the Fermi surface of $LaAlO_3/SrTiO_3$ is a reduction of phase space for certain scattering processes. Hence in the remainder, we extend this model to disordered systems and assess the effect of weak magnetic and nonmagnetic impurities on the transition temperature in both conventional and unconventional candidates for the pairing state.

This chapter is based on a joint project with Mathias S. Scheurer and Jörg Schmalian, which has been published in Ref. 150. It has also been partially included in Ref. 151, where Mathias presented his contribution to the project.

3.1 Model for the $LaAlO_3/SrTiO_3$ interface

The electron gas that forms at the heterointerface of crystalline $LaAlO_3$ (LAO) on $SrTiO_3$ (STO) may undergo a superconducting transition. While the emergence of an electron gas of highly mobile carriers at the interface of two insulators seems to be well understood in terms of the polar scenario in combination with oxygen vacancies, the nature of the superconducting state remains an unsolved problem up to now – as it is also the case with many other newly discovered superconductors. Depending

on the pairing mechanism, both conventional s^{++} and unconventional s^{+-} superconductivity[1] are conceivable [48]. More complicated pairing states such as the finite-momentum Fulde-Ferrell-Larkin-Ovchinnikov state, discussed as a competing state for ferromagnetic order, e. g., in Ref. 152, result only as subleading instabilities from the above-mentioned effective low-energy approach.

The s^{++} state arises from conventional electron-phonon pairing, i. e., an attractive interaction, whereas unconventional s^{+-} superconductivity arises when Coulomb repulsion is dominant. Even though electron-phonon coupling is important in LAO/STO [153], a recent study found the effective interaction to be repulsive for all frequencies [154]. This strengthens the possibility of unconventional superconductivity in LAO/STO while still allowing for a conventional state owing to the strong frequency dependence of the interaction kernel.

In this section, we briefly summarize the ingredients for the effective low-energy model as suggested for the 2D electron liquid in the LAO/STO interface by Ref. 48, supplemented by nonmagnetic or magnetic impurities. Furthermore, we introduce the patch approximation [48] of the Fermi surface (FS) which we will employ for our consideration of disorder effects. The derivation of the disorder vertex in patch approximation combines knowledge about the form of the FS and the eigenstates of the electrons with that about the nature of the impurities present in the material. Yet, the result for the superconducting transition temperature T_c will be independent of these microscopic details and solely depend on the pairing state and on whether the disorder is symmetric or antisymmetric with respect to time reversal, as further discussed in Sec. 3.2.

3.1.1 Effective low-energy theory for clean $LaAlO_3/SrTiO_3$

This section gives an overview of the effective low-energy model for the 2D electron liquid in the LAO/STO interface suggested by Scheurer and Schmalian in Ref. 48. As discussed in Sec. 1.2.2, the model of the LAO/STO interface devised to study superconductivity and magnetic instabilities is focused on the $3d_{xz}$ and $3d_{yz}$ states of titanium. The noninteracting part of the Hamiltonian,

$$\hat{\mathcal{H}}_0 = \sum_{\boldsymbol{k}} \hat{\psi}^\dagger_{\alpha,\boldsymbol{k}} \left(h(\boldsymbol{k})\right)_{\alpha\alpha'} \hat{\psi}_{\alpha',\boldsymbol{k}} \,, \tag{3.1}$$

consists of two parts, $h(\boldsymbol{k}) = h_\mathrm{m}(\boldsymbol{k}) + h_\mathrm{SO}(\boldsymbol{k})$. Here, $\hat{\psi}^\dagger_{\alpha,\boldsymbol{k}}$ and $\hat{\psi}_{\alpha,\boldsymbol{k}}$ denote creation and annihilation operators for quasiparticle states characterized by crystal momentum $\boldsymbol{k}$ and the index α comprising orbital and spin.

The dispersion is characterized by a large mass anisotropy [155] resulting from the different overlap of the two orbitals in x and y direction,

$$h_\mathrm{m}(\boldsymbol{k}) = \begin{pmatrix} \frac{k_1^2}{2m_\mathrm{l}} + \frac{k_2^2}{2m_\mathrm{h}} - \mu & \delta k_1 k_2 \\ \delta k_1 k_2 & \frac{k_1^2}{2m_\mathrm{h}} + \frac{k_2^2}{2m_\mathrm{l}} - \mu \end{pmatrix} \otimes \sigma_0 \,, \tag{3.2}$$

where the orbital mixing term δ is due to interorbital second-nearest-neighbor hopping, and by σ_i we denote Pauli matrices in spin space.

The second crucial ingredient of the model is spin-orbit coupling. The most general expression up to linear order in $\boldsymbol{k}$ which is consistent with time-reversal symmetry and the C_{4v} point group of the

[1] In the s^{++} (s^{+-}) superconducting state, the order parameter has the same (opposite) sign on the two Fermi-surface sheets, in complete analogy to the notation for iron-based superconductors.

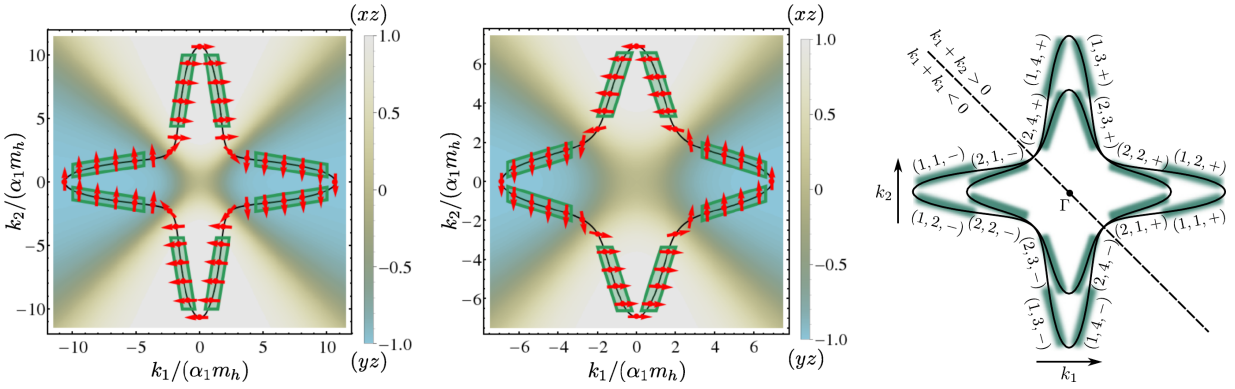

(a) outer Fermi surface **(b)** inner Fermi surface **(c)** patch approximation

[Reprinted figure with permission from M. S. Scheurer, M. Hoyer, and J. Schmalian, Phys. Rev. B **92**, 014518 (2015), cf. Ref. 150. Copyright 2015 by the American Physical Society.]

Figure 3.1: Fermi surface of $LaAlO_3/SrTiO_3$. The form of the outer and inner Fermi surface (obtained from the model (3.1) using realistic values of the parameters as deduced in Ref. 150) are shown in (a) and (b), respectively. Red arrows indicate the spin polarization and the background color corresponds to the respective orbital character. Within the patches indicated in green, the wave functions are approximately constant, allowing to use a 'patch approximation' of the Fermi surface. The corresponding notation that we use throughout the remainder of this chapter is introduced in (c).

system reads as

$$h_{\mathrm{SO}}(\boldsymbol{k}) = \frac{1}{2}\beta\tau_2\sigma_3 + \alpha_1\tau_0(k_1\sigma_2 - k_2\sigma_1) + \alpha_2\tau_1(k_1\sigma_1 - k_2\sigma_2) + \alpha_3\tau_3(k_1\sigma_2 + k_2\sigma_1)\,, \tag{3.3}$$

where we adopted the notation of Ref. 150, i. e., α_i and β are real constants and by τ_i we denote Pauli matrices in orbital space. The spin orbit-coupling term breaks inversion symmetry, and furthermore lifts the degeneracy of the FS with respect to spin. The corresponding dispersion is shown in Fig. 1.5 (b) and the resulting FS sheets are depicted in Fig. 3.1 (a) and 3.1 (b), emphasizing the striking anisotropy of orbital and spin textures. Furthermore, the approximately nested parts of the FS are highlighted in green.

The renormalization group analysis of Ref. 48 revealed two superconducting instabilities of the above model: The conventional s^{++} pairing state with the same sign of the order parameter on both sheets of the FS, and the unconventional s^{+-} pairing state with opposite signs of the order parameter on the two FS sheets. Furthermore, pair hopping[2] between the approximately nested patches of different bands has been identified as the relevant interaction channel for the formation of superconductivity, and depending on the respective coupling constant, either the conventional or the unconventional pairing state will be favored. Interestingly, the nature of the superconducting instability is intimately linked to its topological properties [48]: the conventional state is topologically trivial and adiabatically connected to the BCS superconductor whereas the unconventional state is topologically nontrivial. This opens

[2] The pair hopping term describes the annihilation of a state and its time-reversed partner in band λ, and the creation of another such Kramers pair in the other band $\bar{\lambda}$. For a detailed discussion of other interaction terms that are allowed in the model and their implications for the interplay of the superconducting instabilities we are concerned with in this thesis and the magnetic instabilities also resulting from the model, we refer to Refs. 48 and 151.

new possibilities to study the pairing state in the LAO/STO interface, though will not be discussed further here since the focus of this thesis lies on disorder effects.

3.1.2 Disorder in the $LaAlO_3/SrTiO_3$ interface

As in every real material, imperfections of the crystal structure might be present in the interface and thus influence its properties. Oxygen vacancies created in the deposition process are of particular interest for LAO/STO interfaces, but also other vacancies or other types of impurities are likely to be present and should be considered in the context of unconventional superconductivity. Here, we discuss both nonmagnetic and magnetic impurities and start from the most general quadratic Hamiltonian describing static quenched disorder,

$$\hat{\mathcal{H}}_{\mathrm{dis}} = \int \mathrm{d}\boldsymbol{r}\, \mathrm{d}\boldsymbol{r}'\, \hat{\psi}^\dagger_\alpha(\boldsymbol{r}) W_{\alpha\alpha'}(\boldsymbol{r},\boldsymbol{r}') \hat{\psi}_{\alpha'}(\boldsymbol{r}')\,. \tag{3.4}$$

As discussed in Sec. 1.3.2, we are primarily interested in disorder-averaged quantities. Again, we assume Gaussian disorder in our calculations. The crucial information about disorder is then encoded in the disorder correlator

$$\Gamma_{\alpha_1\alpha_1',\alpha_2\alpha_2'}(\boldsymbol{r}_1,\boldsymbol{r}_1';\boldsymbol{r}_2,\boldsymbol{r}_2') = \left\langle W_{\alpha_1\alpha_1'}(\boldsymbol{r}_1,\boldsymbol{r}_1') W_{\alpha_2\alpha_2'}(\boldsymbol{r}_2,\boldsymbol{r}_2') \right\rangle_{\mathrm{dis}}\,. \tag{3.5}$$

It corresponds to the bare disorder vertex function in the diagrammatic technique discussed for the calculation of T_c in a two-band model in App. C. For simplicity, we assume homogeneous, spatially local disorder governed by δ-correlated statistics, resulting in

$$\Gamma_{\alpha_1\alpha_1',\alpha_2\alpha_2'}(\boldsymbol{r}_1,\boldsymbol{r}_1';\boldsymbol{r}_2,\boldsymbol{r}_2') = \Gamma_{\alpha_1\alpha_1',\alpha_2\alpha_2'}\, \delta(\boldsymbol{r}_1-\boldsymbol{r}_1')\, \delta(\boldsymbol{r}_2-\boldsymbol{r}_2')\, \delta(\boldsymbol{r}_1-\boldsymbol{r}_2)\,, \tag{3.6}$$

where the disorder averaging procedure restores translation invariance. Hence the disorder-induced effective action resulting from the replica approach will conserve crystal momentum.

Furthermore, we assume that the correlator has the full point symmetry of the clean system, i. e., the point symmetries of the system are preserved on average. Regardless, a given disorder configuration is not necessarily consistent with the point group of the system since each single impurity may locally break certain point symmetries. This is discussed in detail in Refs. 150 and 151, and illustrated in Fig. 3.2. For example, an oxygen vacancy at position 3 locally breaks all point symmetries of the lattice except for one mirror symmetry (with respect to the yz plane), and analogously, for a vacancy at position $3'$, only the mirror symmetry with respect to the xz plane remains intact. The requirement that the full C_{4v} point symmetry be preserved on average means that vacancies at positions 3 and $3'$ are included with equal probability.

The crucial criterion which determines the influence of a certain term in the disorder vertex on the transition temperature of the LAO/STO interface turns out to be the transformation behavior of the respective term under time reversal $\hat{\Theta} = \hat{\mathcal{T}}\hat{\mathcal{K}}$. Here, $\hat{\mathcal{K}}$ denotes complex conjugation, and the unitary transformation $\hat{\mathcal{T}}$ is given by $\hat{\mathcal{T}} = \mathrm{i}\tau_0\sigma_2$ in the basis chosen here. Hence, we distinguish between time-reversal symmetric and time-reversal antisymmetric disorder realizations in the remainder, which we interchangeably refer to by 'nonmagnetic' and 'magnetic' disorder, respectively.

The corresponding constraints for the correlator have been used in Refs. 150 and 151 to construct the most general time-reversal symmetric and time-reversal antisymmetric disorder vertices for the LAO/STO interface, which we utilize in Sec. 3.2 to assess the effect of nonmagnetic and magnetic disorder on the two pairing states suggested for LAO/STO.

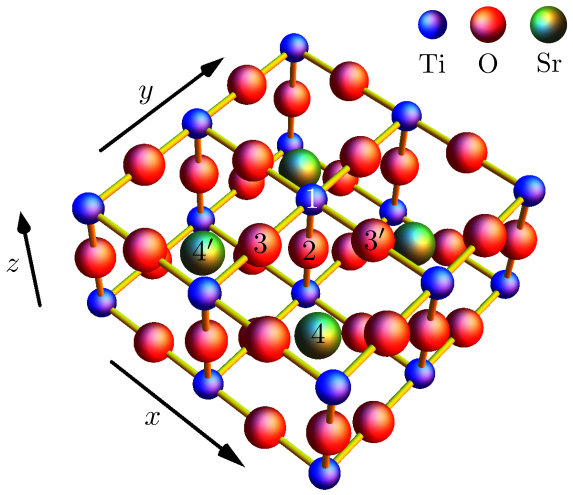

[Reprinted figure with permission from M. S. Scheurer, M. Hoyer, and J. Schmalian, Phys. Rev. B **92**, 014518 (2015), cf. Ref. 150. Copyright 2015 by the American Physical Society.]

Figure 3.2: Impurities in $LaAlO_3/SrTiO_3$. Different impurity positions break different point symmetries, as illustrated here in a close-up view of the conducting STO region of the interface.

3.1.3 Patch approximation

Huge parts of the Fermi surface can be approximated by introducing 16 patches in the form of straight lines as indicated in Figs. 3.1 (a) and 3.1 (b) – this is the heart of the patch approximation as introduced by Ref. 48 and adopted for the disordered interface in Ref. 150. Here, it is convenient to switch to the band basis where the normal-state Hamiltonian (3.1) is diagonal. Owing to the strong anisotropy and spin-orbit coupling, these patches are strongly polarized with respect to spin and orbital character. Accordingly, the wave functions are approximately constant within each patch. This can be utilized to reduce the interacting Hamiltonian in the presence of disorder to a simplistic form within the patch approximation.

In the remainder, we denote the respective patches by the multi-index $\tau \equiv (\lambda, j, \eta)$. Here, $\lambda \in \{1, 2\}$ refers to the two sheets of the FS, $\eta \in \{+, -\}$ specifies whether $k_1 + k_2 > 0$ or $k_1 + k_2 < 0$, and $j \in \{1, \ldots, 4\}$ labels the four distinct patches of a FS sheet in each half space, as introduced in Fig. 3.1 (c). These patches are, in groups of four, approximately parallel, hence nested, and thus host the electronic states that are essential for superconducting pairing and magnetic ordering. The above choice of notation will prove very convenient in the context of superconductivity, since the states $\tau \equiv (\lambda, j, +)$ and $\tau_{\mathrm{K}} \equiv (\lambda, j, -)$ are Kramers partners, i. e., related by time reversal. Furthermore, in the remainder, momentum $\boldsymbol{k}$ will be measured from the center of the respective patch and cut off in a way that prevents overlap of the patches.[3]

Within the patch approximation, the fermionic degrees of freedom are characterized by constant spin and orbital polarization in each patch (according to Fig. 3.1 (a) and 3.1 (b)), implying that the

[3] In the explicit calculation of the diagrams according to App. C, the momentum component perpendicular to the FS is restricted by the energetic cut-off Λ, whereas the integration over momentum components parallel to the FS is absorbed by introducing a constant density of states at the Fermi level in each patch, ρ_τ.

scattering vertices

$$\Gamma^{\mathrm{PA}}_{\tau_1\tau_1',\tau_2\tau_2'} \equiv$$ 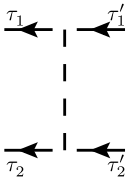

(3.7)

reduce to simple analytic expressions within the patch approximation as briefly summarized in App. C.4. Details on the calculation of the elements of the tensor Γ^{PA}, and in particular on the phase convention used for the eigenstates, can be found in Ref. 150. Let us only note here that scattering processes between certain patches are forbidden as a result of the orbital and spin polarization, i. e., the respective elements of the disorder correlator tensor in patch approximation vanish exactly. Furthermore, in the effective action induced by disorder, this vertex is complemented by the constraint that total momentum is conserved.

Moreover, the disorder vertex enters only in two distinct combinations of patch indices in the calculation of the free energy close to the phase transition, meaning that the calculation of diagrams contributing to T_{c} can be conveniently formulated in terms of a matrix approach as outlined in App. C. This reduces the complexity of the problem considerably, since only the 16×16 matrices summarizing the processes entering the self energy in self-consistent Born approximation (SCBA)

$$\mathcal{S}_{\tau\tau'} := \Gamma^{\mathrm{PA}}_{\tau\tau',\tau'\tau} \equiv$$ 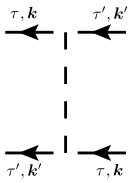

(3.8)

and the corresponding corrections

$$\mathcal{V}_{\tau\tau'} := \Gamma^{\mathrm{PA}}_{\tau\tau',\tau_{\mathrm{K}}\tau_{\mathrm{K}}'} \equiv$$ 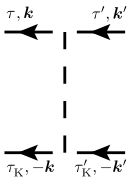

(3.9)

to the superconducting vertex at zero total momentum have to be calculated rather than the full tensor $\Gamma^{\mathrm{PA}}_{\tau_1\tau_1',\tau_2\tau_2'}$ with its 16^4 index combinations. Note that the structure of these scattering vertices automatically guarantees momentum conservation in the diagrams contributing to T_{c}, meaning that the momentum summation within the patches is not constrained further.

3.2 The effect of weak disorder in the $LaAlO_3/SrTiO_3$ interface

The pair-hopping interaction, formulated in the patch approximation introduced in the previous section and using the notation and phase convention of Ref. 150 as summarized in App. B.3, is given by

$$\hat{\mathcal{H}}_{\mathrm{int}} = V_{\mathrm{SC}} \sum_{j,j'=1}^{4} \sum_{\boldsymbol{k},\boldsymbol{k}'} \left[\hat{f}^{\dagger}_{(1,j,+),\boldsymbol{k}} \hat{f}^{\dagger}_{(1,j,-),-\boldsymbol{k}} \hat{f}_{(2,j',-),-\boldsymbol{k}'} \hat{f}_{(2,j',+),\boldsymbol{k}'} + \mathrm{H.\,c.} \right]. \tag{3.10}$$

It leads to conventional s^{++} superconductivity if the interaction V_{SC} is attractive ($V_{\mathrm{SC}} < 0$), while in the case of repulsive pair hopping ($V_{\mathrm{SC}} > 0$), unconventional s^{+-} superconductivity develops. In the clean system, the transition temperature coincides with the result obtained for the usual BCS superconductor

$$T_{\mathrm{c},0} = \frac{2\Lambda \mathrm{e}^{\gamma}}{\pi} \mathrm{e}^{-\frac{1}{\rho_{\mathrm{F}}|V_{\mathrm{SC}}|}} \tag{3.11}$$

in case of both conventional and unconventional superconductivity.

In this section, we finally discuss the implications of nonmagnetic and magnetic disorder for the superconducting transition temperature T_{c} of the two candidate pairing states for the LAO/STO interface. The logic and formalism is in complete analogy with Chap. 2, but the focus here is a different one. As outlined in App. C, the transition temperature is found from the quadratic coefficients of the disorder-averaged Ginzburg-Landau expansion by demanding that the corresponding eigenvalue change sign. In the calculation of the coefficients, we exploit that the scattering rates between different patches are constant and hence the momentum integrals decouple. Specifics on how the formalism is tailored to the LAO/STO interface are summarized in App. C.4.

3.2.1 Nonmagnetic impurities

We start with the discussion of nonmagnetic disorder. The most general disorder vertex that is symmetric under time reversal has been derived in Refs. 150 and 151:

$$\begin{aligned}\Gamma_{\alpha_1\alpha_1',\alpha_2\alpha_2'} = {}& \gamma_{A_1}^{\mathrm{I}} (\tau_0\sigma_0)_{\alpha_1\alpha_1'} (\tau_0\sigma_0)_{\alpha_2\alpha_2'} + \gamma_{A_1}^{\mathrm{II}} (\tau_2\sigma_3)_{\alpha_1\alpha_1'} (\tau_2\sigma_3)_{\alpha_2\alpha_2'} \\ & + \frac{\gamma_{A_1}^{\mathrm{III}}}{2} \Big[(\tau_0\sigma_0)_{\alpha_1\alpha_1'} (\tau_2\sigma_3)_{\alpha_2\alpha_2'} + (\tau_2\sigma_3)_{\alpha_1\alpha_1'} (\tau_0\sigma_0)_{\alpha_2\alpha_2'} \Big] \\ & + \gamma_{B_1} (\tau_3\sigma_0)_{\alpha_1\alpha_1'} (\tau_3\sigma_0)_{\alpha_2\alpha_2'} + \gamma_{B_2} (\tau_1\sigma_0)_{\alpha_1\alpha_1'} (\tau_1\sigma_0)_{\alpha_2\alpha_2'} \\ & + \frac{\gamma_E}{2} \Big[(\tau_2\sigma_1)_{\alpha_1\alpha_1'} (\tau_2\sigma_1)_{\alpha_2\alpha_2'} + (\tau_2\sigma_2)_{\alpha_1\alpha_1'} (\tau_2\sigma_2)_{\alpha_2\alpha_2'} \Big] .\end{aligned} \tag{3.12}$$

It consists of various contributions corresponding to different spin and orbital character of the underlying disorder configuration,[4] characterized by six independent coupling constants $\gamma_{A_1}^{\mathrm{I}}, \gamma_{A_1}^{\mathrm{II}}, \gamma_{A_1}^{\mathrm{III}}, \gamma_{B_1}, \gamma_{B_2}, \gamma_E \in \mathbb{R}$. These coupling constants are proportional to the density of impurities, however, also depend on the microscopic nature of the impurities considered since they are proportional to the square of the matrix element of a single impurity as discussed in Sec. 1.3.2.

The analysis of the effect of each of these terms on the transition temperature of LAO/STO within the above-discussed patch approximation however reveals that the different contributions enter the calculation only as the sum

$$\Gamma = \gamma_{A_1}^{\mathrm{I}} + \gamma_{A_1}^{\mathrm{II}} + \gamma_{B_1} + \gamma_{B_2} + \gamma_E \,, \tag{3.13}$$

which is a measure of the scattering strength of the disorder configuration as a whole, implying that the transition temperature does not depend on specifics of the impurity scattering other than the transformation behavior of the disorder under time reversal. Note that the term associated with $\gamma_{A_1}^{\mathrm{III}}$ does not contribute to pair breaking within the patch approximation since the strong spin and orbital polarization prevents contributions from this term to enter the vertices $\mathcal{S}$ and $\mathcal{V}$.

Our results for the transition temperature in the presence of nonmagnetic disorder are summarized in Fig. 3.3 (a) and details concerning the derivation are presented in App. C. Attractive interaction ($V_{\mathrm{SC}} < 0$) leads to conventional s^{++} superconductivity as in the clean case, and we find that T_{c} remains

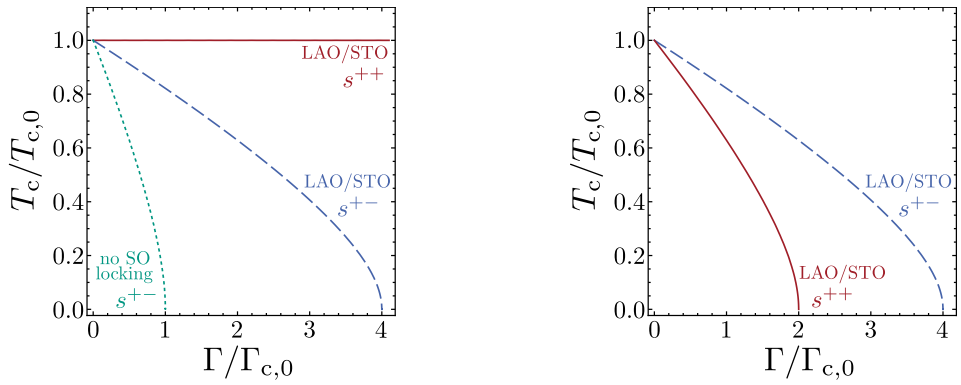

(a) nonmagnetic scattering **(b)** magnetic scattering

Figure 3.3: Pair breaking in $LaAlO_3/SrTiO_3$. We show the critical temperature T_c for s^{++} and s^{+-} superconductivity as a function of scattering rate Γ_c due to (a) nonmagnetic and (b) magnetic impurities. Here, $T_{c,0}$ refers to the SC transition temperature of the clean system, and $\Gamma_{c,0}$ is the critical scattering rate of the reference model described in the text after Eq. (3.16).

robust in the presence of nonmagnetic impurities: $T_c(\Gamma) = T_{c,0}$. This is consistent with the Anderson theorem [10–12] and its generalization to the s^{++} pairing state, as previously discussed in the context of iron-based superconductors in Sec. 2.3.3.

Repulsive interaction ($V_{SC} > 0$) again results in the unconventional s^{+-} pairing state which is already vulnerable to nonmagnetic scattering. For the relation between the transition temperature T_c and the scattering rate Γ, we recover the usual Abrikosov-Gor'kov (AG) behavior [88] originally found for the suppression of T_c due to spin-magnetic impurities in single-band s-wave superconductors,

$$\ln\left(\frac{T_{c,0}}{T_c}\right) = \psi_0\left(\frac{1}{2} + \frac{1}{4e^\gamma}\frac{\Gamma/\Gamma_c}{T_c/T_{c,0}}\right) - \psi_0\left(\frac{1}{2}\right), \tag{3.14}$$

where ψ_0 denotes the digamma function and γ is the Euler-Mascheroni constant. For convenience, we measure scattering rates in units of

$$\Gamma_c = \frac{T_{c,0}}{e^\gamma \rho_F}, \tag{3.15}$$

where ρ_F denotes the total density of states (DOS) at the Fermi level per FS sheet. The quantity Γ_c plays the role of a critical scattering rate at which s^{+-} superconductivity in LAO/STO is fully destroyed by nonmagnetic disorder, since $\Gamma = \Gamma_c$ implies $T_c = 0$. Remarkably, the critical scattering rate Γ_c is by a factor of 4 higher than the critical scattering rate

$$\Gamma_{c,0} = \frac{T_{c,0}}{4e^\gamma \rho_F} \tag{3.16}$$

of a reference model of fermions with the same band structure but without any spin and orbital degrees of freedom, corresponding to $\mathcal{S}_{\tau\tau'} = \Gamma$ for all patches. As already insinuated in the beginning of this chapter, this enhancement of the critical scattering rate is an immediate consequence of the orbital and spin polarization of the FS patches which reduces the available phase space for scattering: States from patch $(1, 1, +)$, for instance, can only be scattered into states in patches $(1, 2, +)$, $(2, 1, -)$, and $(2, 2, -)$

[4] The meaning of each of these terms along with examples for a microscopic realization is discussed in Refs. 150 and 151.

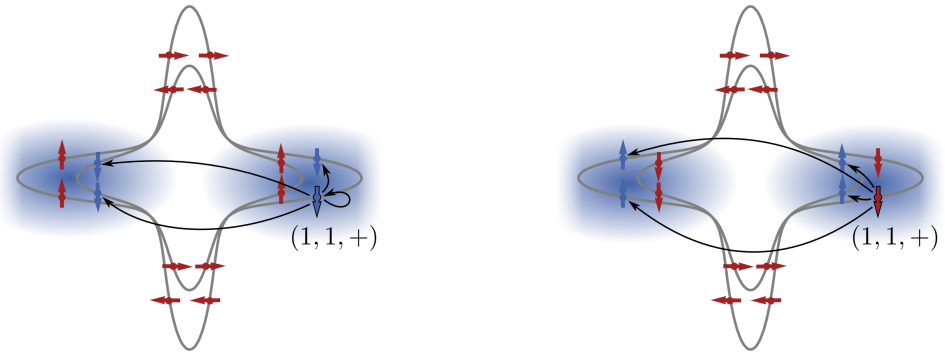

(a) $\tau_0\sigma_0$ (nonmagnetic disorder) **(b)** $\tau_0\sigma_1$ (magnetic disorder)

Figure 3.4: Visualization of the relative protection against disorder. Owing to the spin and orbital polarization of the Fermi surface, certain scattering processes are suppressed, depending on the structure of the respective impurities in spin and orbital space. We show the allowed scattering processes for electrons starting in patch $(1, 1, +)$ for two examples: (a) nonmagnetic potential impurities ($\tau_0\sigma_0$) and (b) in-plane magnetic impurities ($\tau_0\sigma_1$). The regions shaded in blue mark the final states of compatible orbital polarization for electrons starting in patch $(1, 1, +)$ under scattering by these two types of impurities. The arrows indicate the spin polarization of the respective FS patches and their color is chosen analogously: For each type of disorder, we show accessible patches in blue while the others are marked in red.

by the spin-trivial s-wave impurities ($\tau_0\sigma_0$) associated with $\gamma^{\mathrm{I}}_{A_1}$ because these impurities affect neither spin nor orbital character of the scattered quasiparticles. We visualize the allowed scattering processes for this example in Fig. 3.4 (a). Analogous restrictions hold for the other patches and contributions to the disorder vertex. Accordingly, the suppression rate of T_c in the limit of $\Gamma/\Gamma_\mathrm{c} \to 0$,

$$T_\mathrm{c}(\Gamma) = T_{\mathrm{c},0} - \frac{\pi^2}{2}\frac{\Gamma_{\mathrm{c},0}}{\Gamma_\mathrm{c}}\rho_\mathrm{F}\Gamma \tag{3.17}$$

is by the same factor smaller than in the reference model. Spin-orbit locking as a mechanism of protection against disorder is not exclusive to superconductivity in the LAO/STO interface. Ref. 149 provides an example for a system where spin-orbit coupling can even rule out all pair-breaking scattering processes.

Finally, the different roles of intraband and interband scattering processes for nonmagnetic and magnetic disorder can be investigated by artificially discriminating intraband ($\lambda = \lambda'$) and interband ($\lambda \neq \lambda'$) scattering processes by rescaling

$$\mathcal{S}_{(\lambda,j,\eta)(\lambda',j',\eta')} \to \begin{cases} \chi_\mathrm{intra}\mathcal{S}_{(\lambda,j,\eta)(\lambda',j',\eta')}\,, & \lambda = \lambda'\,, \\ \chi_\mathrm{inter}\mathcal{S}_{(\lambda,j,\eta)(\lambda',j',\eta')}\,, & \lambda \neq \lambda'\,, \end{cases} \tag{3.18a}$$

$$\mathcal{V}_{(\lambda,j,\eta)(\lambda',j',\eta')} \to \begin{cases} \chi_\mathrm{intra}\mathcal{V}_{(\lambda,j,\eta)(\lambda',j',\eta')}\,, & \lambda = \lambda'\,, \\ \chi_\mathrm{inter}\mathcal{V}_{(\lambda,j,\eta)(\lambda',j',\eta')}\,, & \lambda \neq \lambda'\,. \end{cases} \tag{3.18b}$$

Then, the above-discussed results correspond to the limit $\chi_\mathrm{intra} = \chi_\mathrm{inter} = 1$. Furthermore, in the absence of interband scattering ($\chi_\mathrm{inter} = 0$), the s^{++} and s^{+-} pairing states are indistinguishable and

thus both should be protected against nonmagnetic impurities. Indeed, we find from the rescaling procedure that, as expected, only interband scattering processes are pair breaking for the s^{+-} pairing state and are responsible for the well-known AG suppression of the transition temperature.

3.2.2 Magnetic impurities

Magnetic impurities are of particular interest in LAO/STO because superconductivity occurs in the proximity of a magnetic instability. Indeed, numerical calculations [156, 157] suggest that oxygen vacancies could lead to the formation of magnetic moments.

For the derivation of the most general disorder vertex being antisymmetric under time reversal, we refer to Refs. 150 and 151 once more, where also the meaning of each term and suggestions for microscopic realizations are discussed. The resulting vertex consists of a part due to impurities with in-plane magnetic moments, and another part due to impurities with magnetic moments aligned perpendicular to the plane. There are three independent contributions to the former,

$$\begin{aligned}\Gamma^{\parallel}_{\alpha_1\alpha_1',\alpha_2\alpha_2'} = {}& \frac{\gamma_E^{\mathrm{I}}}{2}\Big[(\tau_0\sigma_1)_{\alpha_1\alpha_1'}(\tau_0\sigma_1)_{\alpha_2\alpha_2'} + (\tau_0\sigma_2)_{\alpha_1\alpha_1'}(\tau_0\sigma_2)_{\alpha_2\alpha_2'}\Big] \\ & + \frac{\gamma_E^{\mathrm{II}}}{2}\Big[(\tau_1\sigma_1)_{\alpha_1\alpha_1'}(\tau_1\sigma_1)_{\alpha_2\alpha_2'} + (\tau_1\sigma_2)_{\alpha_1\alpha_1'}(\tau_1\sigma_2)_{\alpha_2\alpha_2'}\Big] \\ & + \frac{\gamma_E^{\mathrm{III}}}{2}\Big[(\tau_3\sigma_1)_{\alpha_1\alpha_1'}(\tau_3\sigma_1)_{\alpha_2\alpha_2'} + (\tau_3\sigma_2)_{\alpha_1\alpha_1'}(\tau_3\sigma_2)_{\alpha_2\alpha_2'}\Big],\end{aligned} \tag{3.19}$$

and the five independent contributions to the latter are given by

$$\begin{aligned}\Gamma^{\perp}_{\alpha_1\alpha_1',\alpha_2\alpha_2'} = {}& \gamma_{A_2}^{\mathrm{I}}(\tau_0\sigma_3)_{\alpha_1\alpha_1'}(\tau_0\sigma_3)_{\alpha_2\alpha_2'} + \gamma_{A_2}^{\mathrm{II}}(\tau_2\sigma_0)_{\alpha_1\alpha_1'}(\tau_2\sigma_0)_{\alpha_2\alpha_2'} \\ & + \frac{\gamma_{A_2}^{\mathrm{III}}}{2}\Big[(\tau_2\sigma_0)_{\alpha_1\alpha_1'}(\tau_0\sigma_3)_{\alpha_2\alpha_2'} + (\tau_0\sigma_3)_{\alpha_1\alpha_1'}(\tau_2\sigma_0)_{\alpha_2\alpha_2'}\Big] \\ & + \gamma_{B_1}(\tau_1\sigma_3)_{\alpha_1\alpha_1'}(\tau_1\sigma_3)_{\alpha_2\alpha_2'} + \gamma_{B_2}(\tau_3\sigma_3)_{\alpha_1\alpha_1'}(\tau_3\sigma_3)_{\alpha_2\alpha_2'},\end{aligned} \tag{3.20}$$

where all couplings γ are real numbers. Again, the analysis of these contributions reveals that they enter the disorder-averaged free energy only as the sum

$$\Gamma = \gamma_E^{\mathrm{I}} + \gamma_E^{\mathrm{II}} + \gamma_E^{\mathrm{III}} + \gamma_{A_2}^{\mathrm{I}} + \gamma_{A_2}^{\mathrm{II}} + \gamma_{B_1} + \gamma_{B_2}, \tag{3.21}$$

making our results independent of microscopic details of the disorder realization such as the weight of the different terms. In particular, both types of magnetic impurities – those with magnetic moments lying within the plane as well as those with magnetic moments aligned perpendicular to the plane – contribute to T_c suppression in the same way. Only the term associated with $\gamma_{A_2}^{\mathrm{III}}$ does not result in pair breaking since, in analogy to $\gamma_{A_1}^{\mathrm{III}}$ for nonmagnetic disorder, it does not contribute to the vertices $\mathcal{S}$ and $\mathcal{V}$. Let us furthermore note that the disorder vertex as stated in Eqs. (3.19) and (3.20) also contains terms which would classify as 'orbital magnetic' since they are associated with σ_0. Hence, in its most general form, the vertex is not restricted to spin-magnetic disorder.

In the presence of magnetic disorder, both the conventional s^{++} pairing state (arising from attractive pair hopping $V < 0$) and the unconventional s^{+-} pairing state (associated with $V > 0$) are affected by scattering as represented in Fig. 3.3 (b). However, as in the case of nonmagnetic impurities, the phase space for certain scattering processes is strongly reduced as a consequence of the spin and orbital polarization of the Fermi surface, and hence not all scattering processes contribute, as illustrated in

Fig. 3.4 (b). The transition temperature is again suppressed according to the AG law as formulated in Eq. (3.14), where the critical scattering rate for magnetic disorder in LAO/STO is given by $\Gamma_c = 2\Gamma_{c,0}$ in case of s^{++} superconductivity, and by $\Gamma_c = 4\Gamma_{c,0}$ for s^{+-} superconductivity. Hence, s^{+-} superconductivity is, by a factor 2, more robust against magnetic disorder than s^{++} superconductivity which can be understood by analyzing the roles of intraband and interband scattering processes for the two pairing states according to the rescaling procedure (3.18). It turns out that conventional s^{++} superconductivity is affected by both intra- and interband scattering whereas s^{+-} superconductivity is only suppressed by the intraband scattering processes arising from magnetic impurities. This is in line with our results for the iron-based superconductors discussed in Sec. 2.3 and Ref. 87, where an analog of the Anderson theorem is discussed for the s^{+-} pairing state in the presence of magnetic interband scattering.

3.3 Summary of Chapter 3

Here, we considered the model proposed for the LAO/STO interface in Ref. 48 in the presence of disorder. In particular, we compared the robustness of both candidate pairing states proposed for LAO/STO by Ref. 48: conventional s^{++} superconductivity and unconventional s^{+-} superconductivity. A striking characteristic of the system is the strongly anisotropic Fermi surface which results from anisotropic masses as well as strong spin-orbit coupling. It can be modeled by introducing 16 patches which are assumed to be fully polarized with respect to spin and orbital character (Fig. 3.1).

In our consideration, we allowed for the most general type of disorder – which might even locally break point symmetries as long as they are preserved 'on average'. The most general form of the disorder vertex consistent with the symmetries of the system has been deduced in Ref. 150 for impurities being either symmetric or antisymmetric w. r. t. time reversal. Even though the respective vertices include several terms associated with different types of impurities, all terms that are symmetric (antisymmetric) w. r. t. time reversal contribute in the same manner to the nonmagnetic (magnetic) scattering rates ultimately resulting in pair breaking. Furthermore, the scattering rates between different FS patches are constant within the patch approximation, and owing to the polarization of the Fermi surface, many scattering processes are strongly suppressed. Based on these assumptions, we analyzed the effect of disorder on the SC transition temperature in LAO/STO, and our findings are:

- Not surprisingly, nonmagnetic impurities are only pair breaking for s^{+-} superconductivity, following the usual AG suppression of T_c, whereas the Anderson theorem for the s^{++} pairing state can be adopted for the LAO/STO interface.
- While magnetic impurities suppress both s^{++} and s^{+-} according to the AG law, the unconventional pairing state is found to be more robust – with a critical scattering rate twice as large as for the conventional one.

Therefore, the possibility of an unconventional superconducting state for LAO/STO is not per se ruled out by the presence of disorder in the heterointerface since the strong orbital and spin polarization of the Fermi surface in fact leads to a *relative protection* of superconductivity. In particular, in the presence of magnetic impurities, the unconventional s^{+-} state is more robust than the conventional one, going back to the fact that only intraband scattering is pair breaking for the former, whereas the latter is affected by both intraband and interband scattering here.

Chapter 4

4 Disorder-promoted tetragonal magnetic order in iron-based superconductors

In the iron-based superconductors, superconductivity emerges close to a magnetically ordered state, which has been identified to be of stripe type in most of these compounds. This type of magnetic ordering further implies a structural phase transition reducing the symmetry of the lattice from tetragonal to orthorhombic. However, more recently, another type of magnetic order preserving the tetragonal symmetry of the lattice has been reported in a certain doping regime for several hole-doped compounds. Experimentally, this state has been uniquely identified as a charge-spin density wave whereas theoretical models quite generically predict either stripe-magnetic order or yet another type of tetragonal magnetic order. It is therefore desirable to find extensions to the respective effective low-energy models which naturally account for the observed charge-spin density wave, and as we show here, the inclusion of disorder effects constitutes one possibility.

We commence this chapter with a discussion of the characteristic stripe-ordered magnetic phase, followed by a summary of other possible ground states for the free energy compatible with the symmetry of the system. We introduce a minimal model to study magnetic order in iron-based superconductors and in particular comment on the implications of an incipient hole band as well as impurity scattering. As a result, we can extract a phase diagram of magnetic ground states from the interplay of disorder effects and band structure parameters, which indeed shows that charge-spin density wave is favored by disorder close to particle-hole symmetry.

This chapter is based on my work in collaboration with Rafael M. Fernandes, Alex Levchenko, and Jörg Schmalian, which has been published in Ref. 158.

4.1 Magnetic order in iron-based superconductors

The most general expansion of the free energy in terms of the magnetic order parameters $\boldsymbol{M}_1$ and $\boldsymbol{M}_2$ close to $T = T_\mathrm{N}$ that is compatible with the tetragonal lattice symmetry of the iron-based superconductors (FeSCs) is given by [159–161]

$$\mathcal{F}(\boldsymbol{M}_1, \boldsymbol{M}_2) = a(\boldsymbol{M}_1^2 + \boldsymbol{M}_2^2) + \frac{u}{2}(\boldsymbol{M}_1^2 + \boldsymbol{M}_2^2)^2 - \frac{g}{2}(\boldsymbol{M}_1^2 - \boldsymbol{M}_2^2)^2 + 2w(\boldsymbol{M}_1 \cdot \boldsymbol{M}_2)^2 \,. \tag{4.1}$$

The sign change of the quadratic coefficient a determines the transition temperature T_N. This is in complete analogy to the Ginzburg-Landau expansion of the free energy in terms of the superconducting order parameter Δ close to $T = T_\mathrm{c}$ which we employed in Chaps. 2 and 3. As discussed in

		order parameter orientation	parameter regime	
single-$\boldsymbol{Q}$	stripe magnetism	$\boldsymbol{M}_1 = 0$ or $\boldsymbol{M}_2 = 0$	$g > \max(0, -w)$	
double-$\boldsymbol{Q}$	charge-spin density wave	$\boldsymbol{M}_1 = \pm\boldsymbol{M}_2$	$g < \max(0, -w)$	$w < 0$
	spin-vortex crystal	$\boldsymbol{M}_1 \perp \boldsymbol{M}_2$		$w > 0$

Table 4.1: The three possible magnetic ground states which minimize the Ginzburg-Landau free energy (4.1), and their characteristics.

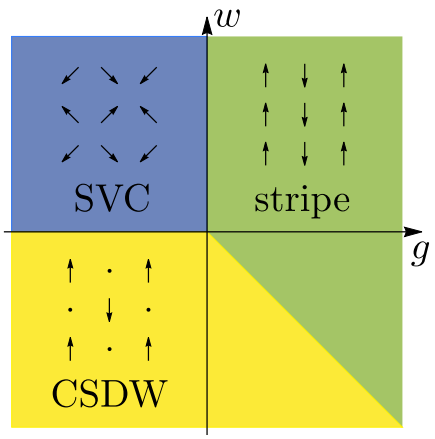

Figure 4.1: Magnetic phase diagram of the Ginzburg-Landau free energy. We show the magnetically ordered states minimizing the free energy (4.1), depending on the nematic coupling g and the planar coupling w.

Refs. 13, 70, and 162, for instance, disorder of course also suppresses the magnetic transition temperature. Here, however, we are concerned with the nature of the magnetic ground state which depends on the relative orientation of the two order parameters $\boldsymbol{M}_1$ and $\boldsymbol{M}_2$, which is determined by the quartic part of the free energy: Depending on the coefficients u, g, and w, the free energy is minimized by one of the three magnetic ground states summarized in Tab. 4.1, provided that $u > \max(0, g, -w)$. The corresponding phase diagram for the coefficients is shown in Fig. 4.1. We term g the 'nematic coupling', since it favors the stripe-ordered state, whereas the 'planar coupling' w determines the relative orientation of $\boldsymbol{M}_1$ and $\boldsymbol{M}_2$, and thereby distinguishes between charge-spin density wave (CSDW) order and spin-vortex crystal (SVC) order. These three possibilities for magnetic order are depicted in Figs. 4.2 and 4.4 and will be discussed in more detail in the context of iron-based superconductors in Secs. 4.1.1 and 4.1.2. Furthermore, the quartic coefficients in the Ginzburg-Landau expansion can be derived from a microscopic model which will be the subject of Sec. 4.2. However, let us note here that our discussion concentrates on the regime $T \approx T_\mathrm{N}$, since further away from the magnetic phase transition, higher-order terms that favor the stripe-magnetic state might become relevant.[1]

[1] Indeed, the experimentally observed re-entrance of the C_2-magnetic phase upon lowering the temperature can be explained in terms of a Ginzburg-Landau expansion of the clean three-band model if sixth-order terms are taken into account [163].

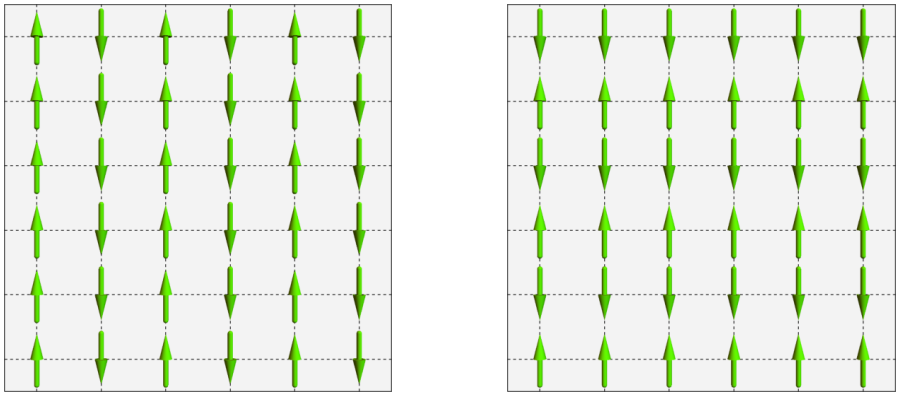

(a) $\boldsymbol{Q} = (\pi, 0)$ **(b)** $\boldsymbol{Q} = (0, \pi)$

Figure 4.2: Illustration of the stripe-magnetic state in the iron-based superconductors. We show the top view of the two different patterns on the lattice in the FeAs-type planes, originating from the two possibilities for the ordering vector $\boldsymbol{Q}$.

4.1.1 Stripe-magnetic order and the structural transition

It is experimentally well established that most of the compounds of the FeSC family exhibit magnetic stripe order with the spins on the iron sites lying in the planes and being aligned ferromagnetically along one crystallographic axis and antiferromagnetically along the other. In particular, the undoped compounds exhibit this type of magnetic order, but stripe magnetism persists up to higher doping and even coexists with superconductivity in many compounds. The scenario of a stripe-ordered C_2-magnetic phase as the magnetic ground state of FeSCs is further supported by itinerant as well as by localized theoretical approaches to magnetism.

Single-Q spin-density wave order The above-described stripe order corresponds to either $\boldsymbol{M}_1 = 0$ or $\boldsymbol{M}_2 = 0$ in the Ginzburg-Landau expansion of the free energy (4.1). Correspondingly, the stripe-type modulation

$$\boldsymbol{M} \mathrm{e}^{\mathrm{i}\boldsymbol{Q}\cdot\boldsymbol{r}} \tag{4.2}$$

in real space is characterized by a single ordering vector $\boldsymbol{Q}$ in momentum space, hence this is termed a single-$\boldsymbol{Q}$ spin-density wave (SDW). In the context of FeSCs, there are two possibilities for the ordering vector, $\boldsymbol{Q} = (\pi, 0)$ or $\boldsymbol{Q} = (0, \pi)$. The resulting stripe-magnetic states are illustrated in Fig. 4.2. Therefore, in addition to the continuous O(3) spin-rotational symmetry broken in the magnetically ordered state, this stripe-magnetic state also breaks a $\mathbb{Z}_2$ Ising-like symmetry, meaning that the symmetry between a and b lattice directions is broken. The spin-rotational symmetry breaking happens at the Néel temperature T_N whereas the additional $\mathbb{Z}_2$-symmetry breaking can occur at transition temperatures $T_\mathrm{s} \geq T_\mathrm{N}$. Moreover, the latter entails a structural transition from tetragonal (C_4) to orthorhombic (C_2) lattice symmetry.

Nematic order Interestingly, if the two transitions are split ($T_\mathrm{s} > T_\mathrm{N}$), this allows for an intermediate phase with broken $\mathbb{Z}_2$ symmetry but no magnetic long-range order. This intermediate phase has been dubbed *nematic order* [164, 165] – in analogy with the preferred direction existing in the nematic phase of liquid crystals. The nematic state in the FeSCs attracted attention since its origin is possibly

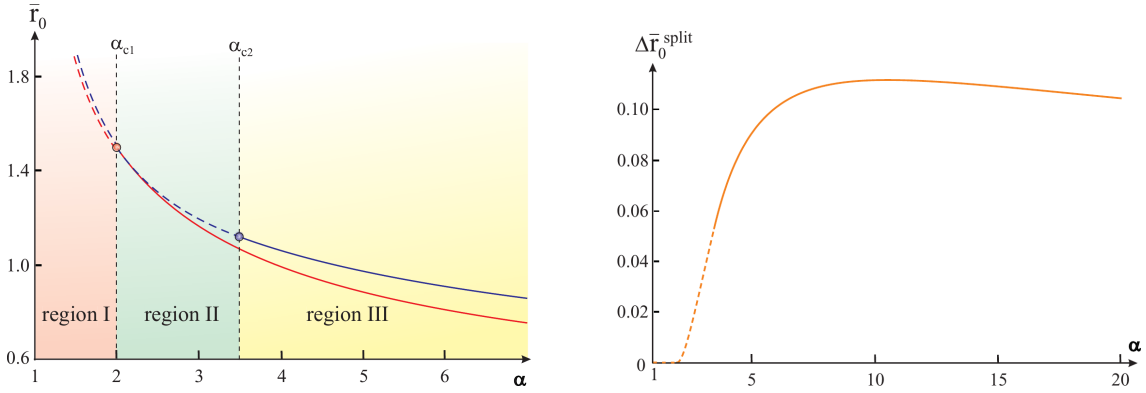

(a) phase diagram of nematic/magnetic transition **(b)** splitting

[Reprinted figure with permission from R. M. Fernandes, A. V. Chubukov, J. Knolle, I. Eremin, and J. Schmalian, Phys. Rev. B **85**, 024534 (2012), cf. Ref. 159. Copyright 2012 by the American Physical Society.]

Figure 4.3: Splitting between nematic and magnetic transition. The phase diagram presented in (a) shows regions of simultaneous (I) and split (II and III) first-order (second-order) nematic and magnetic transitions for a system of dimensionality $d = 2.5$, indicated by dashed (solid) lines. Here, $\bar{r}_0$ is, up to a constant, equal to the quadratic term $a(T - T_{\mathrm{N},0})$ of the respective Ginzburg-Landau expansion. The corresponding splitting of the transition temperatures as a function of the inverse dimensionless nematic coupling constant $\alpha = u/g$ is shown in (b).

of electronic nature and not driven by the lattice degrees of freedom as in ordinary structural transitions: Electronic properties exhibit anisotropies in the nematic state which are much larger than the orthorhombic distortion of the lattice would suggest. Most noteworthy in this context is the resistivity anisotropy [166, 167] which is associated with a susceptibility diverging close to the nematic transition [168]. However, at the structural phase transition, three types of order develop simultaneously – the structural distortion along with orbital order and spin order – and the appropriate order parameter, i. e., which of these fluctuations drive the nematic instability, remains yet to be determined. A review on the nematic state with a special focus on its origin can be found in Ref. 39. Furthermore, the origin of nematicity in the FeSCs is also linked to superconductivity: If the nematic instability is driven by orbital (i. e., charge) fluctuations, the conventional s^{++} superconducting state is expected, whereas the spin-nematic scenario favors s^{+-} or d-wave superconductivity. Consequently, uncovering the origin of the nematic phase may also elucidate the mechanism for superconductivity.

Another interesting aspect is the character of the nematic and magnetic transitions which could each be first-order or second-order, also implying the possibility of tricritical points. In Fig. 4.3 (a), we show an exemplary phase diagram of nematic and magnetic transitions resulting from the theoretical analysis of Ref. 159. The resulting splitting $\Delta T = T_{\mathrm{s}} - T_{\mathrm{N}}$ between the two transitions is controlled by the inverse dimensionless nematic coupling constant u/g and the dimensionality d of the system. In particular, for $2 < d < 3$, the two transitions turn out to be simultaneous and first order for $(u/g) < (u/g)_{c_1} = 1/(3-d)$. For $(u/g)_{c_1} < (u/g) < (u/g)_{c_2}$, the transitions are split and one of them remains first-order whereas the other transition is second-order. In this regime, an increase in u/g results in an enhanced splitting ΔT. On the other hand, deep in the regime of two split second-order phase transitions, $(u/g) \gg (u/g)_{c_2} = (6-d)/(6-2d)$, increasing the ratio u/g reduces the splitting ΔT. In Fig. 4.3 (b), these results are shown for a system of dimensionality $d = 2.5$, i. e.,

a system mimicking a strongly anisotropic three-dimensional system as it seems appropriate for the description of FeSCs. As many properties of the FeSCs, this splitting, and thereby the stabilization of an intermediate nematic phase, depends on disorder [162, 169, 170]. We will briefly comment on our results in this context in Sec. 4.3.1. However, before investigating the influence of disorder, we discuss further candidates for the magnetic ground state in FeSCs.

4.1.2 Tetragonal magnetic phases

In addition to the orthorhombic stripe-magnetic phase that extends over a wide range of doping in the majority of the FeSCs, also a tetragonal magnetic phase has been discovered in a small temperature and doping regime in various hole-doped compounds, including $Ba(Fe_{1-x}Mn_x)_2As_2$ [171], $Ba_{1-x}Na_xFe_2As_2$ [172, 173], $Ba_{1-x}K_xFe_2As_2$ [174–177], and $Sr_{1-x}K_xFe_2As_2$ [178]. This suggests that also C_4-magnetic phases might be a general feature in the phase diagram of hole-doped FeSCs [179].

Double-Q spin-density wave order In contrast to the stripe-magnetically ordered phase, no structural distortion has been found in this newly discovered magnetic phase from X-ray diffraction, implying that it preserves the tetragonal symmetry of the paramagnetic phase. The magnetic Bragg peaks of the C_4-magnetic phases occur at the same momenta $\boldsymbol{Q}_1 = (\pi, 0)$ and $\boldsymbol{Q}_2 = (0, \pi)$ as in the stripe-ordered state. Consequently, such a state can be understood as the superposition of two single-$\boldsymbol{Q}$ stripe-magnetic states,

$$\boldsymbol{M}_1 \mathrm{e}^{\mathrm{i}\boldsymbol{Q}_1\cdot\boldsymbol{r}} + \boldsymbol{M}_2 \mathrm{e}^{\mathrm{i}\boldsymbol{Q}_2\cdot\boldsymbol{r}}\,, \tag{4.3}$$

hence termed a double-$\boldsymbol{Q}$ SDW. Depending on the relative orientation of the two order parameters $\boldsymbol{M}_1$ and $\boldsymbol{M}_2$, the properties of the resulting state are different. The two additional tetragonal ground states that minimize the free energy (4.1) are summarized in Tab. 4.1 and illustrated in Fig. 4.4.

The *charge-spin density wave* that arises from aligning $\boldsymbol{M}_1$ and $\boldsymbol{M}_2$ either parallel or antiparallel, $\boldsymbol{M}_1 = \pm\boldsymbol{M}_2$, is shown in Fig. 4.4 (a). It results in a nonuniform magnetization with vanishing average magnetic moment at even lattice sites and staggered-like order at odd lattice sites, or vice versa. This magnetic state is accompanied by charge-density wave order since it couples to a modulation of the density [161]: The charge couples to the square of the magnetization, thus magnetic sites acquire a charge that is different from nonmagnetic sites. If, on the other hand, $\boldsymbol{M}_1$ and $\boldsymbol{M}_2$ are orthogonal, $\boldsymbol{M}_1 \perp \boldsymbol{M}_2$, the resulting *spin-vortex crystal* is characterized by a noncollinear magnetization pattern that is illustrated in Fig. 4.4 (b).

Furthermore, as in the case of stripe antiferromagnetism, which is preceded by nematic order, these two double-$\boldsymbol{Q}$ magnetic states can in principle be melted in two stages, passing through an intermediate state of vestigial charge or chiral order [161].

Experimental characterization Experimentally, a reorientation of the spins has been found from neutron diffraction [180], implying that the magnetic moments within the C_4-magnetic phase are oriented parallel to the c-axis, i. e., perpendicular to the FeAs planes. In order to further characterize the nature of the tetragonal magnetic phase, local probes are best suited. In particular, ^{57}Fe-Mössbauer spectroscopy on $Sr_{1-x}Na_xFe_2As_2$ [178] and muon spin rotation on $Ba_{1-x}K_xFe_2As_2$ [181] concordantly found that the magnetic moment vanishes at every second lattice site while it is doubled at the others. Furthermore, the data is also consistent with the spin reorientation.

Therefore, these experiments uniquely identify the C_4-magnetic phase as a realization of the charge-spin density wave depicted in Fig. 4.4 (a). Within the free-energy expansion (4.1), a negative planar

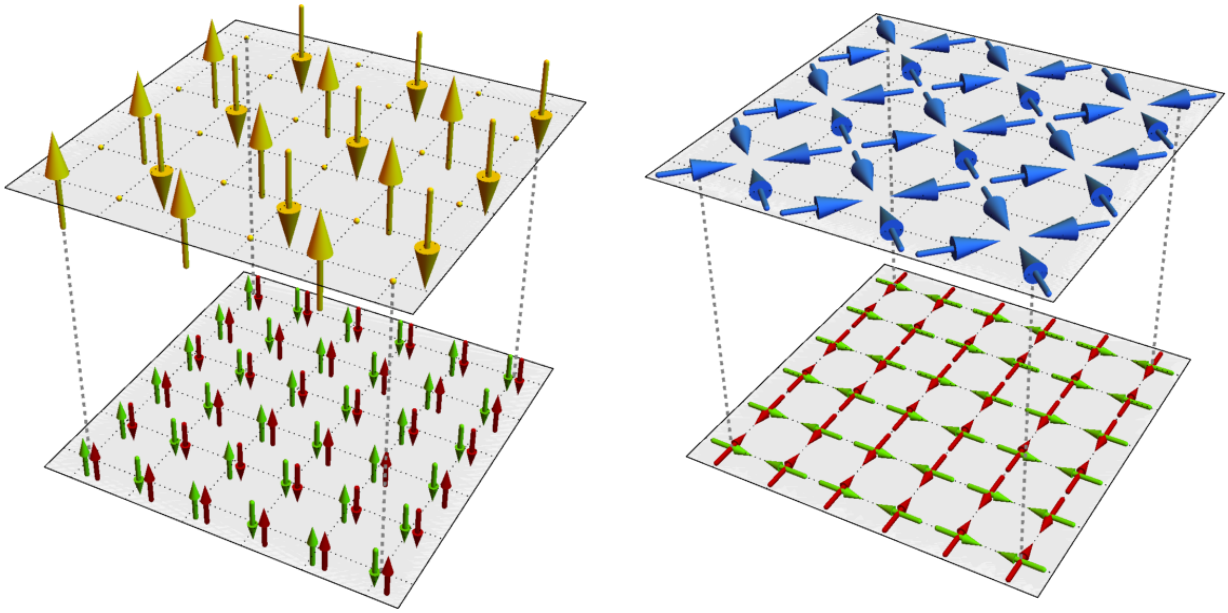

(a) charge-spin density wave **(b)** spin-vortex crystal

Figure 4.4: Illustration of the two double-$\boldsymbol{Q}$ magnetic states. We present the double-$\boldsymbol{Q}$ (a) charge-spin density wave order and (b) spin-vortex crystal order in the upper panels as a superposition of two single-$\boldsymbol{Q}$ stripe-magnetic states (lower panels).

coupling $w < 0$ is a necessary condition for CSDW. Therefore, it is important to elucidate theoretically which generic features of low-energy models yield $w < 0$ (and $g < |w|$).

Theoretical perspective The existence of double-$\boldsymbol{Q}$ magnetic states as additional ground states for the FeSCs has also been established by different theoretical approaches based on itinerant models [43, 159, 163, 182–187], all of which suggest the two double-$\boldsymbol{Q}$ ground states visualized in Fig. 4.4 in addition to the single-$\boldsymbol{Q}$ stripe-magnetic order (Fig. 4.2). Localized approaches based on the J_1-J_2 Heisenberg model, on the other hand, favor the single-$\boldsymbol{Q}$ stripe-ordered state [164, 165, 188–190].

Focusing on the three-band itinerant low-energy model previously employed in the literature [159, 179, 183], one finds a band-structure-driven transition, since the single-$\boldsymbol{Q}$ state is favored near perfect nesting, whereas the double-$\boldsymbol{Q}$ state is expected away from perfect nesting. This transition from single-$\boldsymbol{Q}$ to double-$\boldsymbol{Q}$ coincides with a decrease of the magnitude of the nematic coupling constant g [163], indicating that the overall weakening of magnetic order allows for the formation of the C_4 phase. However, this same model generically leaves the noncollinear SVC and the nonuniform CSDW order degenerate since $w = 0$ due to phase space restrictions, as explained in Sec. 4.2.2.

Extensions of this model tend to favor the spin-vortex crystal – in disagreement with the recent experiments. This is, for instance, obtained by including residual electronic interactions [179, 183] or, as we will show in Sec. 4.2.3, an incipient fourth pocket. We note that although Ref. 160 proposes that the proximity to a Néel-like state can favor CSDW order, this scenario is only applicable to $Ba(Fe_{1-x}Mn_x)_2As_2$, since the compound $BaMn_2As_2$ displays Néel order – which is not the case for $Ba_{1-x}Na_xFe_2As_2$ or $Ba_{1-x}K_xFe_2As_2$. Note also that Ref. 191 showed that the spin-orbit coupling leads to anisotropic quadratic terms in the free energy (4.1) that favor the CSDW order, even though

$w = 0$. This however only works near the magnetic transition, since at low temperatures the quartic terms (or possibly even higher-order terms) are the ones that determine the ground state.

4.2 Minimal three-band model

As in our discussion of superconductivity, we aim to understand the interplay of magnetic order and superconductivity by means of a minimal model in band basis. To account for the double-$\boldsymbol{Q}$ states as well as for stripe order, we have to consider the two nesting vectors $\boldsymbol{Q}_1 = (\pi, 0)$ and $\boldsymbol{Q}_2 = (0, \pi)$. Thus the minimal model to consider magnetic order in FeSCs includes two (elliptical) electron pockets at the X and Y points in addition to the hole pocket at the Γ point. However, in order to keep our discussion clear, we already include the second hole pocket at the M point from the beginning, but in a way that allows us to easily discard this pocket when discussing only the minimal three-band model.

4.2.1 Four-band model of iron-based superconductors

We consider a multi-band model [159, 183] for FeSCs, consisting of two circular hole pockets centered at the Γ and M points of the 1-Fe Brillouin zone, respectively, and two elliptical electron pockets centered at X and Y. The corresponding Fermi surface is depicted in Fig. 1.4 (a). The pocket at the M point however is not a generic feature of this class of materials, since it exists only in some of the iron-based compounds. Moreover, even in the compounds in which the pocket at the M point exists, this band is not guaranteed to cross the Fermi level for all values of k_z. Furthermore, our analysis in Sec. 4.2.3 will show that the presence of such an incipient hole pocket at the M point cannot explain the formation of a charge-spin density wave and hence can be neglected in the remainder of this chapter.

Four-band model The noninteracting part of the model is described by the Hamiltonian

$$\hat{\mathcal{H}}_0 = \sum_{\lambda,\boldsymbol{k},\sigma} \varepsilon_{\lambda,\boldsymbol{k}} \hat{\psi}^\dagger_{\lambda,\boldsymbol{k},\sigma} \hat{\psi}_{\lambda,\boldsymbol{k},\sigma} \,, \tag{4.4}$$

where the fact that the bands are centered around different momenta is reflected in the band index $\lambda \in \{\mathrm{h}_1, \mathrm{h}_2, \mathrm{e}_1, \mathrm{e}_2\}$. In the following, the hole bands are labeled interchangeably by $\mathrm{h}_1 \equiv \mathrm{h}_\Gamma$ and $\mathrm{h}_2 \equiv \mathrm{h}_M$, and the electron bands by $\mathrm{e}_1 \equiv \mathrm{e}_X$ and $\mathrm{e}_2 \equiv \mathrm{e}_Y$. Thus, $\hat{\psi}^\dagger_{\lambda,\boldsymbol{k},\sigma}$ creates an electron in band λ with spin σ and crystal momentum $\boldsymbol{k}$. The respective dispersions near the Fermi energy can, for simplicity, be parametrized by

$$\varepsilon_{\mathrm{h}_1,\boldsymbol{k}} = -\varepsilon_{\boldsymbol{k}} \,, \tag{4.5a}$$
$$\varepsilon_{\mathrm{e}_1,\boldsymbol{k}} = \varepsilon_{\boldsymbol{k}} - \delta_\mu + \delta_m \cos(2\theta) \,, \tag{4.5b}$$
$$\varepsilon_{\mathrm{e}_2,\boldsymbol{k}} = \varepsilon_{\boldsymbol{k}} - \delta_\mu - \delta_m \cos(2\theta) \,, \tag{4.5c}$$
$$\varepsilon_{\mathrm{h}_2,\boldsymbol{k}} = -\varepsilon_{\boldsymbol{k}} - E_M \,, \tag{4.5d}$$

close to the parameter regime of perfectly nested electron and hole bands. The respective band structure is shown in Fig. 1.4 (b). Perfect nesting corresponds to $E_M = \delta_\mu = \delta_m = 0$ and leads to a degeneracy of all three magnetic ground states in the clean limit, as we will see later. Here, we introduced $\varepsilon_{\boldsymbol{k}} = \frac{k^2}{2m} - \varepsilon_0$ and $\theta = \arctan(k_2/k_1)$. Note that changes of δ_μ involve changes of the chemical potential, and can therefore be associated with doping. On the other hand, δ_m is a measure of the ellipticity of the electron bands. The top of the hole band at the M point is lower in energy than the top of the hole band at the

Γ point, i.e. $E_M > 0$, such that it is not guaranteed to cross the Fermi surface even if it does exist. In the limit $E_M \to \infty$, the incipient band is pushed far below the Fermi level where it cannot contribute to any observables, meaning that we effectively recover the minimal three-band model.

Magnetic order The four-band model of the iron-based superconductors as introduced above allows for eleven fermionic interactions connecting the different pockets of the Fermi surface, as discussed in Ref. 192. These interactions can be decomposed into different density-wave and pairing channels. Since in this chapter, we are only concerned with magnetic ordering in these systems, we restrict ourselves to the contributions in the SDW channel,

$$\hat{\mathcal{H}}_{\text{int}} = -\frac{V_{\text{SDW}}}{2} \sum_{i=1}^{2} \sum_{\boldsymbol{q}} \hat{\boldsymbol{S}}_{i,\boldsymbol{q}} \cdot \hat{\boldsymbol{S}}_{i,-\boldsymbol{q}} \,, \tag{4.6a}$$

$$\text{where} \quad \hat{\boldsymbol{S}}_{1,\boldsymbol{q}} = \sum_{\boldsymbol{k}} \sum_{\sigma,\sigma'} \left(\hat{\psi}^{\dagger}_{\text{h}_1,\boldsymbol{k},\sigma} \boldsymbol{\sigma}_{\sigma,\sigma'} \hat{\psi}_{\text{e}_1,\boldsymbol{k}+\boldsymbol{q},\sigma'} + \hat{\psi}^{\dagger}_{\text{e}_2,\boldsymbol{k},\sigma} \boldsymbol{\sigma}_{\sigma,\sigma'} \hat{\psi}_{\text{h}_2,\boldsymbol{k}+\boldsymbol{q},\sigma'} + \text{H. c.} \right) \tag{4.6b}$$

$$\text{and} \quad \hat{\boldsymbol{S}}_{2,\boldsymbol{q}} = \sum_{\boldsymbol{k}} \sum_{\sigma,\sigma'} \left(\hat{\psi}^{\dagger}_{\text{h}_1,\boldsymbol{k},\sigma} \boldsymbol{\sigma}_{\sigma,\sigma'} \hat{\psi}_{\text{e}_2,\boldsymbol{k}+\boldsymbol{q},\sigma'} + \hat{\psi}^{\dagger}_{\text{e}_1,\boldsymbol{k},\sigma} \boldsymbol{\sigma}_{\sigma,\sigma'} \hat{\psi}_{\text{h}_2,\boldsymbol{k}+\boldsymbol{q},\sigma'} + \text{H. c.} \right) \tag{4.6c}$$

are associated with the two nesting vectors $\boldsymbol{Q}_1 = (\pi, 0)$ and $\boldsymbol{Q}_2 = (0, \pi)$, respectively. Here, $V_{\text{SDW}} > 0$ denotes the attractive coupling in the SDW channel and $\boldsymbol{\sigma} = (\sigma_1, \sigma_2, \sigma_3)$ denotes the vector of spin-space Pauli matrices.

This interaction can be decoupled by means of a Hubbard-Stratonovich transformation upon which two magnetic order parameters $\boldsymbol{M}_1$ and $\boldsymbol{M}_2$ arise, which are associated with the two ordering vectors $\boldsymbol{Q}_1$ and $\boldsymbol{Q}_2$, respectively. Their coupling to the electronic degrees of freedom on mean-field level is given by

$$\begin{aligned} \hat{\mathcal{H}}^{\text{MF}}_{\text{int}} = &- \sum_{\boldsymbol{k}} \sum_{\sigma,\sigma'} \left(\hat{\psi}^{\dagger}_{\text{h}_1,\boldsymbol{k},\sigma} \boldsymbol{\sigma}_{\sigma,\sigma'} \hat{\psi}_{\text{e}_1,\boldsymbol{k},\sigma'} + \hat{\psi}^{\dagger}_{\text{e}_2,\boldsymbol{k},\sigma} \boldsymbol{\sigma}_{\sigma,\sigma'} \hat{\psi}_{\text{h}_2,\boldsymbol{k},\sigma'} + \text{H. c.} \right) \cdot \boldsymbol{M}_1 \\ &- \sum_{\boldsymbol{k}} \sum_{\sigma,\sigma'} \left(\hat{\psi}^{\dagger}_{\text{h}_1,\boldsymbol{k},\sigma} \boldsymbol{\sigma}_{\sigma,\sigma'} \hat{\psi}_{\text{e}_2,\boldsymbol{k},\sigma'} + \hat{\psi}^{\dagger}_{\text{e}_2,\boldsymbol{k},\sigma} \boldsymbol{\sigma}_{\sigma,\sigma'} \hat{\psi}_{\text{h}_1,\boldsymbol{k},\sigma'} + \text{H. c.} \right) \cdot \boldsymbol{M}_2 \,. \end{aligned} \tag{4.7}$$

For details on the Hubbard-Stratonovich decoupling and the further derivation of the Ginzburg-Landau expansion, we refer to App. D.2: Following the usual procedure, in the vicinity of the magnetic phase transition, we integrate out the electronic degrees of freedom and derive the free energy expansion of the system

$$\mathcal{F}(\boldsymbol{M}_1, \boldsymbol{M}_2) = \sum_i a_i |\boldsymbol{M}_i|^2 + \sum_{i,j} u_{ij} |\boldsymbol{M}_i|^2 |\boldsymbol{M}_j|^2 + 2w (\boldsymbol{M}_1 \cdot \boldsymbol{M}_2)^2 \,, \tag{4.8}$$

where the coefficients a_i, u_{ij}, and w can be calculated from the microscopic model introduced above. Due to the rotational symmetry connecting the electron bands, it holds that $a := a_1 = a_2$, $u_{11} = u_{22}$, and $u_{12} = u_{21}$. The free energy (4.8) can thus be brought to the form of Eq. (4.1) using

$$u = u_{12} + u_{11} \qquad \text{and} \qquad g = u_{12} - u_{11} \,. \tag{4.9}$$

The transition temperature T_{N} is determined by the quadratic coefficient of the free energy. In principle, we expect a kink in the transition temperature, reflecting the tricritical point associated with the $C_2 \leftrightarrow C_4$ transition. Furthermore, disorder is also expected to suppress the transition temperature [70].

Here, however, we focus on the nature of the magnetic ground state, which is solely determined by the interplay of the quartic coefficients g and w in the expansion (4.1) provided that $u > \max(0, g, -w)$. Therefore, we will not discuss the quadratic coefficients further here.

4.2.2 Results of the minimal model

We start our considerations with the clean three-band model, i. e., disregarding the second hole pocket at the M point which is not present in all FeSC compounds. The coefficients in the expansion of the free energy (4.1), previously defined in Ref. 159, are given by

$$a_i = \frac{1}{4V_{\mathrm{SDW}}} + 2\int_k G_{\mathrm{h}\Gamma,\boldsymbol{k}}(\nu_n) G_{\mathrm{e}_i,\boldsymbol{k}}(\nu_n)\,, \tag{4.10a}$$

$$u = \frac{1}{2}\int_k G^2_{\mathrm{h}\Gamma,\boldsymbol{k}}(\nu_n)[G_{\mathrm{e}_1,\boldsymbol{k}}(\nu_n) + G_{\mathrm{e}_2,\boldsymbol{k}}(\nu_n)]^2\,, \tag{4.10b}$$

$$g = -\frac{1}{2}\int_k G^2_{\mathrm{h}\Gamma,\boldsymbol{k}}(\nu_n)[G_{\mathrm{e}_1,\boldsymbol{k}}(\nu_n) - G_{\mathrm{e}_2,\boldsymbol{k}}(\nu_n)]^2\,, \tag{4.10c}$$

$$w = 0\,. \tag{4.10d}$$

For convenience, we write u and g in the symmetrized form, namely $u = \frac{1}{2}(u_{11} + u_{12} + u_{21} + u_{22})$ and $g = -\frac{1}{2}(u_{11} - u_{12} - u_{21} + u_{22})$. Furthermore, we abbreviated $\int_k \ldots \equiv T\sum_n \int \frac{\mathrm{d}\boldsymbol{k}}{(2\pi)^2} \ldots$ and the fermionic Green's function is defined as $G_{\lambda,\boldsymbol{k}}(\nu_n) = [\mathrm{i}\nu_n - \varepsilon_{\lambda,\boldsymbol{k}} + \frac{\mathrm{i}}{2\tau_\lambda}\,\mathrm{sgn}(\nu_n)]^{-1}$ in analogy to our notation in Chap. 2, cf. Eq. (2.12) .

At perfect nesting, where $\delta_\mu = \delta_m = 0$, the nematic coupling constant g vanishes since $G_{\mathrm{e}_1,\boldsymbol{k}}(\nu_n) = G_{\mathrm{e}_2,\boldsymbol{k}}(\nu_n)$. Therefore, in the clean system at particle-hole symmetry, all three candidates for the magnetic ground state are degenerate, cf. Fig. 4.1. The dispersion (4.5) readily implies that finite ellipticity $\delta_m \neq 0$ is crucial in order to obtain a finite nematic coupling g, i. e., to lift the degeneracy of stripe magnetism and tetragonal magnetism if $w = 0$. The finite chemical potential $\delta_\mu \neq 0$ partially accounts for the presence of impurities by including doping effects. However, neither effect renders the coefficient w finite.

Degeneracy of the tetragonal states The planar coupling w vanishes in the clean model as a consequence of the trace in spin space [191]. This is illustrated in Fig. 4.5 (a), where we show the most generic quartic diagram before performing the spin trace. The disconnected propagators indicate that, depending on the model, such a diagram could be decorated by further diagrammatical elements originating, for instance, from additional interactions or impurity scattering. The corresponding quartic diagram, after performing the spin trace, results in a contribution proportional to

$$\begin{aligned}\mathrm{tr}\Big[\sum_{i,j,k,l} M^{(i)}_{\lambda_1}\sigma_i M^{(j)}_{\lambda_2}\sigma_j M^{(k)}_{\lambda_3}\sigma_k M^{(l)}_{\lambda_4}\sigma_l\Big] &= \sum_{i,j,k,l} M^{(i)}_{\lambda_1} M^{(j)}_{\lambda_2} M^{(k)}_{\lambda_3} M^{(l)}_{\lambda_4}\,\mathrm{tr}(\sigma_i\sigma_j\sigma_k\sigma_l)\\ &= 2\Big[(\boldsymbol{M}_{\lambda_1}\cdot\boldsymbol{M}_{\lambda_2})(\boldsymbol{M}_{\lambda_3}\cdot\boldsymbol{M}_{\lambda_4}) - (\boldsymbol{M}_{\lambda_1}\cdot\boldsymbol{M}_{\lambda_3})(\boldsymbol{M}_{\lambda_2}\cdot\boldsymbol{M}_{\lambda_4}) + (\boldsymbol{M}_{\lambda_1}\cdot\boldsymbol{M}_{\lambda_4})(\boldsymbol{M}_{\lambda_2}\cdot\boldsymbol{M}_{\lambda_3})\Big]\,, \end{aligned}\tag{4.11}$$

where we used the identity $\mathrm{tr}(\sigma_i\sigma_j\sigma_k\sigma_l) = 2(\delta_{ij}\,\delta_{kl} - \delta_{ik}\,\delta_{jl} + \delta_{il}\,\delta_{jk})$. Within the minimal model, introduced in Eqs. (4.4) and (4.6), and with the additional simplification of neglecting the pocket at the M point, the absence of scattering as well as interactions between the electron bands requires that either $\lambda_1 = \lambda_2$ and $\lambda_3 = \lambda_4$, or $\lambda_1 = \lambda_4$ and $\lambda_2 = \lambda_3$ holds, as can be seen from Fig. 4.5 (a). Both conditions result in $\mathrm{tr}[(\boldsymbol{M}_{\lambda_1}\cdot\boldsymbol{\sigma})(\boldsymbol{M}_{\lambda_2}\cdot\boldsymbol{\sigma})(\boldsymbol{M}_{\lambda_3}\cdot\boldsymbol{\sigma})(\boldsymbol{M}_{\lambda_4}\cdot\boldsymbol{\sigma})] \equiv 2|\boldsymbol{M}_{\lambda_1}|^2|\boldsymbol{M}_{\lambda_3}|^2$ and thus imply $w = 0$

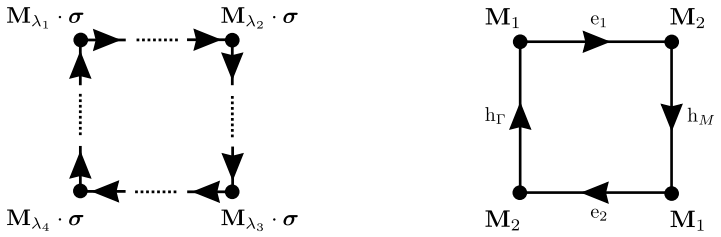

(a) generic quartic diagram **(b)** w in a four-band model

Figure 4.5: Quartic diagrams in the absence of disorder. (a) Sketch of a generic quartic diagram before performing the spin trace: Each vertex couples the hole band to one of the electron bands, and the dashed lines indicate that scattering or additional interactions could alter the diagram. (b) The additional contribution from taking the incipient hole pocket at M into account indeed renders the planar coupling w finite.

in the clean case. On the contrary, the inclusion of interband scattering or interactions between the two electron pockets at $\boldsymbol{Q}_1$ and $\boldsymbol{Q}_2$ allows for contributions where $\lambda_1 = \lambda_3$ and $\lambda_2 = \lambda_4$, rendering w finite since $\mathrm{tr}[(\boldsymbol{M}_{\lambda_1}\cdot\boldsymbol{\sigma})(\boldsymbol{M}_{\lambda_2}\cdot\boldsymbol{\sigma})(\boldsymbol{M}_{\lambda_3}\cdot\boldsymbol{\sigma})(\boldsymbol{M}_{\lambda_4}\cdot\boldsymbol{\sigma})] \equiv 2[2(\boldsymbol{M}_{\lambda_1}\cdot\boldsymbol{M}_{\lambda_2})^2 - |\boldsymbol{M}_{\lambda_1}|^2|\boldsymbol{M}_{\lambda_2}|^2]$.

The main advantage of the minimal three-band model in this context is that it allows for a well-defined perturbative expansion near the perfect-nesting limit ($\delta_\mu = \delta_m = 0$) and the clean limit, since in this case $g = w = 0$, and the degeneracy of the magnetic ground state is maximal (i.e. the stripe-magnetic, CSDW, and SVC phases are all degenerate). Therefore, one can assess qualitatively how different types of perturbations favor distinct ground states.

4.2.3 Incipient hole pocket

The inclusion of an incipient hole pocket at $M = (\pi, \pi)$ as anticipated in Eqs. (4.4) and (4.5d) also allows for contributions that render w finite. The contribution to the planar coupling w that survives the spin trace as a consequence of the presence of the second hole pocket is depicted diagrammatically in Fig. 4.5 (b). We consider the simplest case where $\delta_\mu = \delta_m = 0$, i. e., perfect nesting of the hole band at the Γ point and the two electron bands, since this already yields a finite value for the planar coupling,

$$\begin{aligned} w &= 4\int_k G_{\mathrm{h}_\Gamma,\boldsymbol{k}}(\nu_n) G_{\mathrm{h}_M,\boldsymbol{k}}(\nu_n) G_{\mathrm{e}_X,\boldsymbol{k}}(\nu_n) G_{\mathrm{e}_Y,\boldsymbol{k}}(\nu_n) \\ &= \frac{\mathrm{i}\rho_\mathrm{F}}{2E_M\pi T}\Big[\psi_1\Big(\frac{1}{2}+\frac{\mathrm{i}E_M}{4\pi T}\Big) - \psi_1\Big(\frac{1}{2}-\frac{\mathrm{i}E_M}{4\pi T}\Big)\Big] = \begin{cases} \frac{7\rho_\mathrm{F}\zeta(3)}{2\pi^2T^2} \approx 0.43\frac{\rho_\mathrm{F}}{T^2} & , \quad E_M \ll T\,, \\ \frac{4\rho_\mathrm{F}}{E_M^2} & , \quad E_M \gg T\,. \end{cases} \end{aligned} \tag{4.12}$$

Here $\psi_n(x)$ is the n^{th} derivative of the digamma function, $\zeta(z)$ is the Riemann zeta function, and we assumed the density of states at the Fermi level to be given by the same constant ρ_F in all bands. The diagrams can be evaluated in full analogy to the case of superconductivity, see Apps. C and D.2 for details.

From Eq. (4.12), we find indeed that the degeneracy of the two double-$\mathbf{Q}$ magnetically ordered states is lifted since $w \neq 0$. Close to particle-hole symmetry, the planar coupling w is even of the same order as the other quartic couplings. Furthermore, the coefficient w vanishes in the limit $E_M \to \infty$. That is, if the pocket at M is shifted to energies far below the Fermi level, we reproduce the results of the

previously discussed three-band model, which is the relevant limit for many of the FeSC compounds. However, the planar coupling remains positive for all values of E_M, and therefore, the inclusion of the second hole pocket can only account for the formation of an SVC phase, but not for the experimentally observed CSDW order. Since it is not a generic feature of the FeSC family and its inclusion is not able to explain why the nonuniform CSDW state is favored over the noncollinear SVC state in the hole-doped compounds, we discard the second hole pocket at the M in our further discussion.

Let us further mention that a positive planar coupling $w > 0$ has also been obtained in previous studies of other extensions of the clean three-band model such as the perturbative inclusion of additional interactions [179, 183]. This suggests a different route is needed in order to explain the formation of the collinear CSDW state within the low-energy model. Consequently, in the remainder of this chapter, we investigate the effect of disorder on the magnetic ground state.

4.3 Impurity scattering in the three-band model of iron-based superconductors

In the remainder, we investigate the impact of disorder that is induced by doping the FeSC compounds, and concentrate on effects beyond mere changes of the band structure. For instance, charged potential impurities can locally stabilize charge-spin density wave order [182, 187], thus suggesting that the inclusion of disorder for the itinerant electrons participating in the formation of the magnetically ordered state is an important ingredient for the investigation of the CSDW state. In analogy to our analysis of disorder effects on the superconducting state in previous chapters, we consider an arbitrary realization of nonmagnetic impurities. Thus we add the term

$$\hat{\mathcal{H}}_{\text{dis}} = \sum_{\lambda,\lambda'} \sum_{\boldsymbol{k},\boldsymbol{k}'} \sum_{\sigma} \hat{\psi}^{\dagger}_{\lambda,\boldsymbol{k},\sigma} W_{(\lambda\boldsymbol{k})(\lambda'\boldsymbol{k}')} \hat{\psi}_{\lambda',\boldsymbol{k}',\sigma} \tag{4.13}$$

to the Hamiltonian. The only difference to our discussion of disorder in iron-based superconductors in Sec. 2.2 is the additional band that increases the number of allowed scattering processes. In particular, the three-band model entails an interband scattering process between electron pockets.

As usual, we are not interested in quantities that depend on the microscopic disorder realization, but rather in self-averaged physical observables. Therefore, we are interested in disorder-averaged quantities. In the case of Gaussian disorder, all information about the impurities is encoded in the correlation function

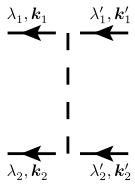

$$\equiv \left\langle W_{(\lambda_1\boldsymbol{k}_1)(\lambda_1'\boldsymbol{k}_1')} W_{(\lambda_2\boldsymbol{k}_2)(\lambda_2'\boldsymbol{k}_2')} \right\rangle_{\text{dis}} = \Gamma_{\lambda_1\lambda_1',\lambda_2\lambda_2'} (2\pi)^2 \, \delta(\boldsymbol{k}_1 + \boldsymbol{k}_2 - \boldsymbol{k}_1' - \boldsymbol{k}_2' + \boldsymbol{K}) \,, \tag{4.14}$$

which constitutes a measure of impurity strength and is proportional to the scattering rate Γ characterizing the respective scattering processes. These scattering rates depend on the impurity concentration as well as on the strength of the disorder potential itself. In Eq. (4.14), we concentrated on the simplest type of impurities and assumed the disorder to be sufficiently smooth on the individual sheets of the Fermi surface such that the momentum dependence of the scattering rates can be neglected for momenta from the same pocket of the Fermi surface. Note that in a multi-band model, the effect of

impurity scattering can have subtle consequences [87] which we avoid here by requiring that all scattering processes be characterized by real numbers, $\Gamma_{\lambda_1\lambda_1',\lambda_2\lambda_2'} \in \mathbb{R}$, i. e., the impurities do not break time-reversal invariance locally.

Furthermore, we assume the impurity potential to be sufficiently weak such that single-particle interference effects can be neglected. Then it is justified to work within self-consistent Born approximation (SCBA) when calculating the self energy and vertex corrections, since diagrams with crossed impurity lines are suppressed by the small factor $1/k_\mathrm{F} l_\mathrm{mfp}$, where l_mfp is the mean-free path and k_F is the Fermi momentum.

In the remainder, we assume that both electron bands are affected by impurities in the same way, and thus the respective scattering rates are equal – consistent with the tetragonal symmetry of the system. Scattering within one band or between two bands is then characterized by four, in principle different, constant scattering rates:

$$\Gamma_\mathrm{h}^\mathrm{intra} \equiv \Gamma_1 \qquad \text{intraband scattering within the hole band,} \tag{4.15a}$$

$$\Gamma_\mathrm{e}^\mathrm{intra} \equiv \Gamma_2 \qquad \text{intraband scattering within one of the electron bands,} \tag{4.15b}$$

$$\Gamma_\mathrm{e-h}^\mathrm{inter} \equiv \Gamma_{12} \qquad \text{interband scattering between hole band and one of the electron bands,} \tag{4.15c}$$

$$\Gamma_\mathrm{e-e}^\mathrm{inter} \qquad \text{and interband scattering between the two electron bands.} \tag{4.15d}$$

In Eq. (4.15), we also related these scattering rates to those introduced earlier in the context of the two-band model, cf. Eqs. (2.10) and (2.11), to point out the connection to our discussion of superconductivity in the presence of disorder in Chap. 2. The novel feature of the three-band model in terms of scattering is the presence of a scattering process (4.15d) between the two electron pockets at X and Y, which leads to additional, structurally nonequivalent diagrams as compared to those resulting from a two-band model.

Hierarchy of scattering rates In multi-band systems, the interplay of a multitude of different intraband and interband scattering processes can affect physical properties. Fortunately, in the iron-based systems, experiments as well as ab-initio calculations reveal that not all of them are equally important [79, 80, 101, 103, 105, 193–195]. This permits us to devise models of impurity scattering that concentrate on the dominant scattering processes [70] relevant for the calculation of the quantities of interest. Such a simplification allows us to draw conclusions about the dominant effects that are to be expected due to impurity scattering, but of course limits exact quantitative predictions.

For many aspects, it is sufficient to discriminate between intraband and interband scattering processes, and thus it is important to note that interband scattering (which for example causes pair breaking in the s^{+-} superconducting state as discussed in Sec. 2.3.3) is much weaker than the dominant intraband scattering process affecting transport properties [101, 103, 105]. Furthermore, as demonstrated by transport measurements [193, 194], scanning tunneling microscopy [195], and first-principles density functional theory calculations [79, 80], the intraband scattering rate in the hole band exceeds the intraband scattering rate in the electron bands. For these reasons, we consider the following hierarchy of scattering rates in the remainder of this chapter:

$$\Gamma_\mathrm{e-e}^\mathrm{inter}, \Gamma_\mathrm{e-h}^\mathrm{inter}, \Gamma_\mathrm{e}^\mathrm{intra} \ll \Gamma_\mathrm{h}^\mathrm{intra}. \tag{4.16}$$

Let us however note that $\Gamma_\mathrm{e-e}^\mathrm{inter}$ will also be important in our discussion of magnetic order, since it leads to structurally new contributions to the planar coupling, as discussed in Sec. 4.3.2, whereas the respective contributions to the other couplings are subleading.

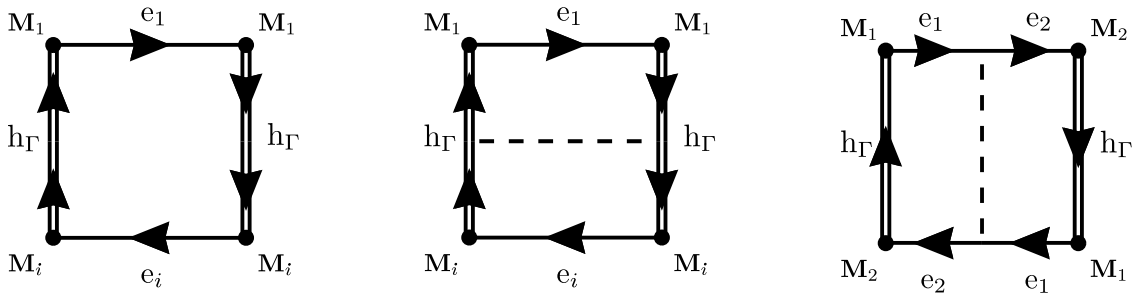

(a) $\mathfrak{g}_i^{(1)}$ **(b)** $\mathfrak{g}_i^{(2)}$ **(c)** $\mathfrak{w}$

Figure 4.6: Leading-order contributions to the quartic coefficients. Double lines indicate that the respective propagators acquire a finite lifetime due to impurity scattering whereas single lines are used for propagators in bands that, within our model, are not affected by impurity scattering. Additional scattering processes in (b) and (c) are indicated by a dashed line corresponding to the scattering rates $\Gamma_{\mathrm{h}}^{\mathrm{intra}}$ and $\Gamma_{\mathrm{e-e}}^{\mathrm{inter}}$, respectively. $\mathfrak{g}_i^{(1)}$ and $\mathfrak{g}_i^{(2)}$ ($i \in \{1,2\}$) are the contributions to g (as well as to u) in the presence of intraband scattering in the hole band which is the dominant scattering mechanism in FeSCs. $\mathfrak{w}$ is the contribution to w, which is finite owing to interband scattering between the two electron bands.

4.3.1 Nematic coupling

We first analyze how disorder affects g, since it is the coupling constant which determines whether the system condenses into a single-$\boldsymbol{Q}$ or double-$\boldsymbol{Q}$ state. While $g = 0$ at perfect nesting, the nematic coupling constant takes a finite value within the three-band model as a consequence of the ellipticity of the electron bands; although orbital dressing effects can make it nonzero even at perfect nesting [196]. We focus on the contribution from the dominant scattering rate $\Gamma_{\mathrm{h}}^{\mathrm{intra}}$, see the hierarchy of scattering rates in Eq. (4.16). Near perfect nesting, we can expand in the band structure parameters accounting for ellipticity of the electron bands $\delta_m \ll 2\pi T$ and the shift in energy $\delta_\mu \ll 2\pi T$, which results in

$$g = -\frac{\rho_{\mathrm{F}}\delta_m^2}{1536\pi^4 T^4}\left[\psi_4\left(\frac{1}{2}+\frac{\rho_{\mathrm{F}}\Gamma_{\mathrm{h}}^{\mathrm{intra}}}{4T}\right) - \frac{\delta_\mu^2}{32\pi^2T^2}\,\psi_6\left(\frac{1}{2}+\frac{\rho_{\mathrm{F}}\Gamma_{\mathrm{h}}^{\mathrm{intra}}}{4T}\right)\right]. \tag{4.17}$$

The respective diagrammatic contributions to the nematic coupling constant, $\mathfrak{g}_i^{(1)}$ and $\mathfrak{g}_i^{(2)}$, are depicted in Figs. 4.6 (a) and 4.6 (b), respectively. In our calculation of the coefficient, we used that $\mathfrak{g}_2^{(2)} - \mathfrak{g}_1^{(2)} \propto \int \frac{\mathrm{d}\theta}{2\pi}\cos(2\theta) = 0$. Further details on our calculation can be found in App. D.2.

In the clean limit, where $\Gamma_{\mathrm{h}}^{\mathrm{intra}} = 0$, $g \propto \delta_m^2$ changes sign from positive to negative for sufficiently large $\delta_\mu/(2\pi T)$, as shown in Fig. 4.7 (a) and in agreement with previous results [179]. This describes the transition from a single-$\boldsymbol{Q}$ to a double-$\boldsymbol{Q}$ magnetic ground state as the carrier concentration increases. We note that the resulting coefficient is dependent on δ_μ^2 rather than on δ_μ, thus yielding the same results for electron and hole doping. However, a more realistic band structure indeed results in an electron-hole asymmetry of the coupling constant g, see Ref. 197, in accordance with experiments where the C_4-magnetic phase has only been observed for hole-doped compounds so far.

The resulting coupling constant g as a function of the scattering rate $\Gamma_{\mathrm{h}}^{\mathrm{intra}}$, plotted for different values of detuning δ_μ and ellipticity δ_m, is shown in Fig. 4.7 (a). In the particle-hole symmetric case, $g = 0$ as a consequence of $\delta_m = 0$, regardless of whether the system is in the clean or dirty limit. Interestingly, if g is finite in the clean limit, the addition of disorder suppresses g and can even induce

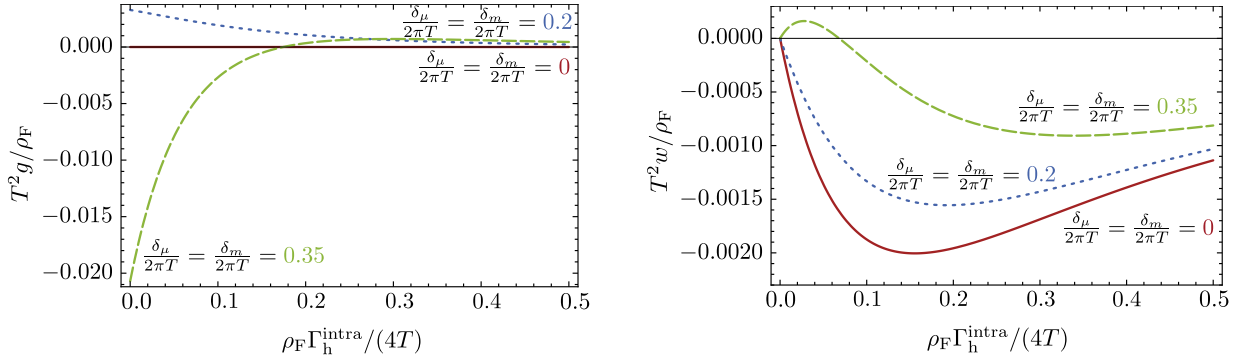

(a) nematic coupling g **(b)** planar coupling w

Figure 4.7: Quartic couplings in the presence of disorder. We show (a) the nematic and (b) the planar coupling as a function of the intraband scattering rate in the hole band, Γ_h^{intra}, and in the presence of weak scattering between the two electron pockets. For these plots, we set $\Gamma_{e-e}^{inter} = 0.1\Gamma_h^{intra}$. We chose $\delta_\mu/(2\pi T) = \delta_m/(2\pi T) = 0.2$ (blue, dotted line) as an example of small ellipticity and detuning which guarantees $w < 0$ and $g > 0$, and $\delta_\mu/(2\pi T) = \delta_m/(2\pi T) = 0.35$ (green, dashed line) as an example where disorder can tune g and w to be either positive or negative. The red line represents the result at particle-hole symmetry, $\delta_\mu/(2\pi T) = \delta_m/(2\pi T) = 0$.

a sign-change. Therefore, the transition from a single-$\boldsymbol{Q}$ to a double-$\boldsymbol{Q}$ state can be controlled not only by carrier concentration, but also by the disorder potential.

Even when the suppression of g by disorder does not induce a sign-change, it has interesting consequences for the phase diagram. In particular, as shown in Ref. 159, the splitting $\Delta T = T_s - T_N$ between the nematic/structural and the magnetic transitions is controlled by the inverse dimensionless nematic coupling constant u/g, see Fig. 4.3 (b) for the result in a 2.5-dimensional system. To compute the dimensionless parameter u/g, we compute u using the same assumptions as in the calculation of g, resulting in

$$\begin{aligned} u = &-\frac{\rho_F}{8\pi^2 T^2}\left[\psi_2\left(\frac{1}{2}+\frac{\rho_F\Gamma_h^{intra}}{4T}\right)+\frac{\rho_F\Gamma_h^{intra}}{12T}\psi_3\left(\frac{1}{2}+\frac{\rho_F\Gamma_h^{intra}}{4T}\right)\right] \\ &+\frac{\rho_F}{768\pi^4 T^4}\psi_4\left(\frac{1}{2}+\frac{\rho_F\Gamma}{4T}\right)[3\delta_\mu^2+\delta_m^2]+\frac{\rho_F^2\Gamma_h^{intra}}{30720\pi^4 T^5}\psi_5\left(\frac{1}{2}+\frac{\rho_F\Gamma}{4T}\right)[10\delta_\mu^2+3\delta_m^2] \end{aligned} \tag{4.18}$$

in accordance with previous work [70]. Furthermore, we used that $u_{11} = u_{22}$ and $u_{12} = u_{21}$ holds for the quartic coefficients in the expansion (4.8) also in the presence of disorder.

Near particle-hole symmetry, where $\delta_\mu/(2\pi T)$ and $\delta_m/(2\pi T)$ are sufficiently small, and the magnetic ground state is the stripe one, g/u decreases monotonically with increasing scattering rate as shown in Fig. 4.8 (a). Thus, if the system initially is near the regime of first-order simultaneous transitions, as it is the case in undoped $BaFe_2As_2$, the addition of disorder is expected to cause (or enhance) a splitting between the magnetic transition and the structural transition. This agrees with recent experiments in $BaFe_2As_2$, which observed enhanced splitting of the transitions upon electron irradiation [170]. This result is also consistent with the theoretical finding of Ref. 162 that disorder stabilizes the nematic phase. We note, however, that the dependence of the ratio g/u on disorder is nonuniversal, as illustrated in Figs. 4.8 (b) and 4.8 (c). In particular, farther away from particle-hole symmetry, the dependence of g/u on disorder is no longer monotonic: g/u first increases with increasing scattering rate, and above a critical value starts decreasing again.

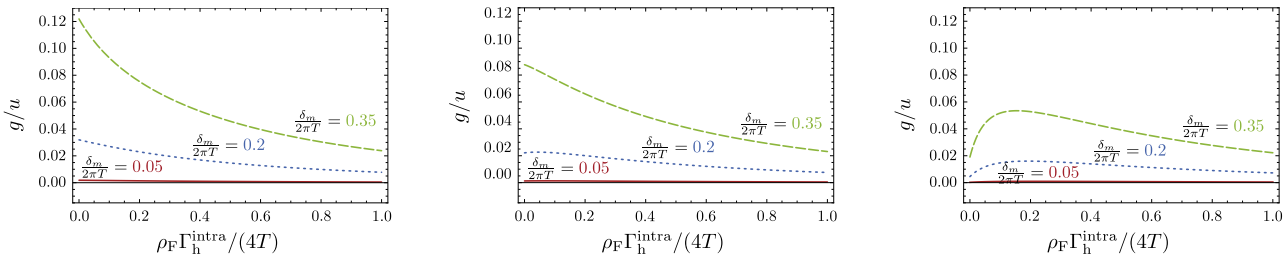

(a) $\delta_\mu/(2\pi T) = 0.15$ **(b)** $\delta_\mu/(2\pi T) = 0.20$ **(c)** $\delta_\mu/(2\pi T) = 0.25$

Figure 4.8: Dependence of the dimensionless nematic coupling constant g/u on disorder. (a) Close to particle-hole symmetry, the ratio g/u decreases monotonically with increasing scattering rate. (b) and (c) With increasing distance to particle-hole symmetry, an initial increase of the dimensionless nematic coupling constant is found for small scattering rates, but for stronger disorder, g/u decreases again.

4.3.2 Planar coupling

Having established that the nematic coupling g can become either positive or negative in both clean and dirty systems, we now analyze the planar coupling w associated with the angle between the two order parameters $\boldsymbol{M}_1$ and $\boldsymbol{M}_2$. Hence, a finite planar coupling lifts the degeneracy of the two tetragonal magnetic states – charge-spin density wave and spin-vortex crystal.

As discussed in Sec. 4.2.2 and illustrated in Fig. 4.5 (a), the planar coupling vanishes exactly in the clean three-band model. Following the analysis of the generic fourth-order diagram after performing the spin trace in Eq. (4.11), the only scattering processes that gives rise to a nonzero contribution to w is the one that couples the electron pocket at $\boldsymbol{Q}_1$ and the electron pocket at $\boldsymbol{Q}_2$, characterized by the scattering rate $\Gamma_{\mathrm{e-e}}^{\mathrm{inter}}$. For the sake of clarity, we neglect all other interband scattering processes, since they only give subleading contributions to the planar coupling, i. e., $w = 0$ always as long as $\Gamma_{\mathrm{e-e}}^{\mathrm{inter}} = 0$. Then, in the presence of the dominant scattering process, intraband scattering in the hole band and, additionally, interband scattering between the electron bands, we find

$$w = -\frac{\rho_{\mathrm{F}}^2 \Gamma_{\mathrm{e-e}}^{\mathrm{inter}}}{96\pi^2 T^3}\left[\psi_3\left(\frac{1}{2}+\frac{\rho_{\mathrm{F}}(\Gamma_{\mathrm{h}}^{\mathrm{intra}}+\Gamma_{\mathrm{e-e}}^{\mathrm{inter}})}{4T}\right) - \frac{10\delta_\mu^2+\delta_m^2}{320\pi^2T^2}\,\psi_5\left(\frac{1}{2}+\frac{\rho_{\mathrm{F}}(\Gamma_{\mathrm{h}}^{\mathrm{intra}}+\Gamma_{\mathrm{e-e}}^{\mathrm{inter}})}{4T}\right)\right], \qquad (4.19)$$

with the same assumptions made as in the calculation of the coefficients g and u. In particular, we expanded for small ellipticity $\delta_m \ll 2\pi T$ and small detuning $\delta_\mu \ll 2\pi T$ to obtain the above expression. The respective diagram, denoted by $\mathfrak{w}$, is depicted in Fig. 4.6 (c). Note that contributions with more than one scattering process between electron bands vanish upon momentum integration and thus the above result already includes contributions up to infinite order in $\Gamma_{\mathrm{e-e}}^{\mathrm{inter}}$.

We show the coefficient w as a function of the scattering rate for different values of detuning δ_μ and ellipticity δ_m in Fig. 4.7 (b). In the absence of impurity scattering, we recover $w = 0$ irrespective of the value of the band structure parameters. At particle-hole symmetry, $\delta_\mu = \delta_m = 0$, disorder leads to $w < 0$, thus naturally favoring the formation of a charge-spin density wave (illustrated in Fig. 4.4 (a)) as long as $g < |w|$. In contrast, finite detuning and ellipticity yield a contribution of opposite sign and thus, depending on the scattering rate and the distance from particle-hole symmetry, w can be either positive or negative, allowing for both proposed double-$\boldsymbol{Q}$ states – CSDW and SVC.[2]

[2] Let us note that these conclusions holds also in the presence of magnetic impurities. In this case, however, the global

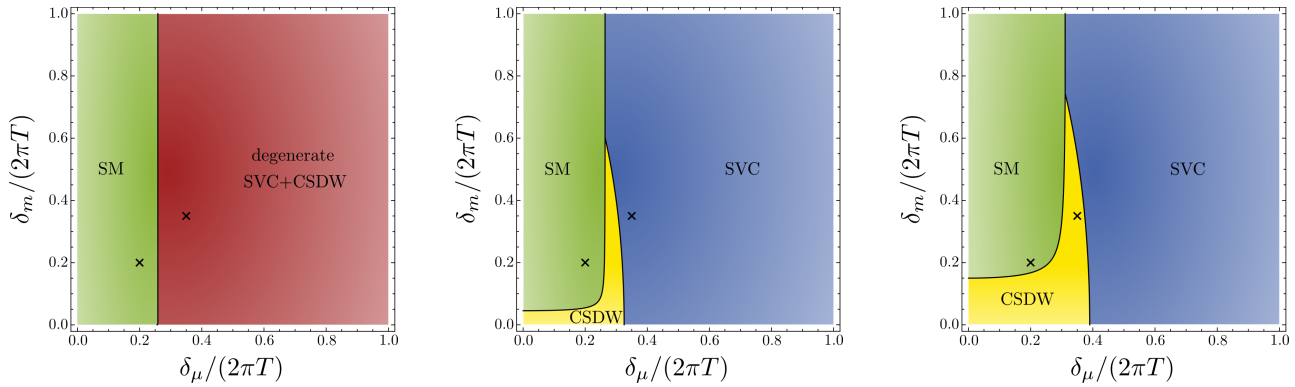

(a) $\rho_F\Gamma_h^{\text{intra}}/(4T) = 0$ **(b)** $\rho_F\Gamma_h^{\text{intra}}/(4T) = 0.01$ **(c)** $\rho_F\Gamma_h^{\text{intra}}/(4T) = 0.1$

[Reprinted figure with permission from M. Hoyer, R. M. Fernandes, A. Levchenko, and J. Schmalian, Phys. Rev. B **93**, 144414 (2016), cf. Ref. 158. Copyright 2016 by the American Physical Society.]

Figure 4.9: Evolution of the magnetic phase diagram with disorder. We show the phase diagram (in terms of band structure parameters) of the possible magnetic ground states of the three-band model upon increasing scattering rate. Here, we used $\Gamma_{e-e}^{\text{inter}} = 0.1\Gamma_h^{\text{intra}}$, and the phase diagrams are obtained close to perfect nesting where $\delta_\mu \ll 2\pi T$ and $\delta_m \ll 2\pi T$. The regime of single-$\boldsymbol{Q}$ stripe order is shown in green, the double-$\boldsymbol{Q}$ spin-vortex crystal order is indicated by blue, and the yellow region represents the double-$\boldsymbol{Q}$ charge-spin density wave state. In the clean regime, shown in (a), SVC and CSDW order are degenerate and we indicated this region with $w = 0$ in red. The crosses mark the points in the phase diagram at which we plotted g and w as a function of scattering rate in Figs. 4.7 (a) and 4.7 (b), respectively.

4.3.3 Magnetic phase diagram in the presence of disorder

The magnetic phase diagram is governed by the interplay of nematic and planar couplings, g and w, respectively. If $g > \max(0, -w)$, stripe-magnetic order with either $\boldsymbol{M}_1 = 0$ or $\boldsymbol{M}_2 = 0$ is favored, as it has been observed in many compounds of the iron pnictide and iron chalcogenide families. If $g < \max(0, -w)$, a double-$\boldsymbol{Q}$ state with $|\boldsymbol{M}_1| = |\boldsymbol{M}_2|$ minimizes the free energy, and the sign of w determines whether $\boldsymbol{M}_1 \perp \boldsymbol{M}_2$ (spin-vortex crystal, for $w > 0$) or $\boldsymbol{M}_1 = \pm\boldsymbol{M}_2$ (charge-spin density wave, for $w < 0$) is more favorable. So far, only the CSDW state has been observed experimentally [178, 180, 181], in contrast to theoretical models [179, 183, 189].

Our investigation of impurity scattering, in contrast, provides a natural explanation for the formation of CSDW order in doped FeSCs. Since the three-band model under consideration yields $w = 0$ in the absence of impurity scattering, we concentrated on the interband scattering process between the two electron bands that can render w finite. In addition, we included intraband scattering within the hole band into our calculation, since it is the dominant impurity scattering process in FeSCs. We find $w < 0$ at particle-hole symmetry, suggesting that disorder can promote charge-spin density wave order. The CSDW state even persists to finite ellipticity δ_m and detuning δ_μ, however, sufficiently large ellipticity and detuning in combination with impurity scattering also allow for $w > 0$, i. e., the formation of a spin-vortex crystal. Our findings are visualized in the phase diagrams depicted in Fig. 4.9, where we show the

prefactor and the total scattering rate are altered as compared to the case of nonmagnetic impurities, since for magnetic impurities, the evaluation of the trace $\text{tr}[\sigma_i\sigma_j\sigma_k\sigma_l\sigma_j\sigma_m]$ allows for additional contributions including other interband scattering processes between the electron pockets at the X point and the Y point.

magnetic ground states that are favored in different regimes of detuning δ_μ and ellipticity δ_m. Close to particle-hole symmetry ($\delta_m = \delta_\mu = 0$), disorder favors the double-$\boldsymbol{Q}$ charge-spin density wave state over the single-$\boldsymbol{Q}$ stripe-magnetic SDW order, as obvious from Fig. 4.9 (b). Increasing disorder, measured in terms of the intraband scattering rate $\Gamma_\mathrm{h}^\mathrm{intra}$ in the hole band, even increases the parameter regime in which CSDW order is expected to occur, as shown in Fig. 4.9 (c).

Previously, controlled disorder has been proposed as a way to tune the properties of the superconducting state in the iron-based materials [14, 15]. Analogously, our findings provide a promising control knob to tune their magnetic ground state as well. In particular, addition of impurities via electron irradiation in hole-doped compounds near the composition where the single-$\boldsymbol{Q}$ to double-$\boldsymbol{Q}$ magnetic transition is observed could stabilize a C_4-magnetic phase as the leading instability of the system – currently, the C_4-magnetic phase has been mostly observed inside the C_2-magnetic phase boundary. Similarly, removal of impurities via annealing in samples that display the double-$\boldsymbol{Q}$ magnetic order could change the nature of the C_4 phase from charge-spin density wave to spin-vortex crystal.

4.4 Summary of Chapter 4

In this chapter, we discussed possible magnetic ground states for iron-based superconductors, starting from the minimal three-band model introduced in Eqs. (4.4) and (4.6). This allows for the stripe-magnetic state observed in most of the FeSC compounds in the underdoped regime, as well as for two different magnetically ordered states which preserve the tetragonal symmetry of the high-temperature state: spin-vortex crystal and charge-spin density wave order. The latter has been found in a certain regime of the phase diagram of several hole-doped compounds, yet does not arise naturally from effective low-energy models and their extensions discussed to date. Consequently, our focus here was on extensions to the three-band model which could render the CSDW state favorable.

- We included an *incipient hole pocket* at the M point and found that it does lift the degeneracy of CSDW and SVC, however, also favors the latter and thus cannot explain the experimental findings.
- Furthermore, we considered the effect of *weak disorder*, concentrating on the dominant scattering process (intraband scattering in the hole band), complemented by an interband scattering process between the two electron pockets at X and Y which is responsible for an additional contribution (cf. Fig. 4.6 (c)) to the free energy that naturally favors CSDW order.

Besides, our analysis of the interplay of disorder and band structure parameters (summarized in the phase diagrams in Fig. 4.9) revealed that the weakly disordered three-band model in fact allows for all three magnetic ground states considered in this chapter – opening the interesting possibility to tune the magnetic ground state of iron-based superconductors with controlled disorder, i. e., by irradiation or annealing.

Chapter 5

5 Gaussian fluctuation corrections to mean-field theories

Mean-field theories have proven incredibly useful in reducing complex many-body problems to simpler effective models: The effect of interactions between particles on an individual particle is simulated by the coupling to a 'mean field' resulting from this interaction. In previous chapters, we greatly benefited from this tool when studying quite diverse types of order in different materials. However, the applicability of such theories relies strongly on the existence and stability of the respective mean field. If, for example, fluctuations around the mean-field value lead to sizable corrections to the gap equation, the mean-field assumption is unjustified. The analysis of Kos, Millis, and Larkin [100] in the context of superconductivity revealed an interesting technical aspect: the cancellation of amplitude and phase fluctuations is crucial in ensuring the validity of BCS theory.

Hence, we start this chapter with a review of fluctuation corrections to the BCS mean-field gap equation and briefly comment on generalizations. The main part of this chapter is dedicated to the analysis of the corresponding fluctuation corrections in the context of commensurate density-wave instabilities arising from nesting of the Fermi surface where longitudinal and transversal fluctuations of the mean field do not necessarily cancel.

This chapter is based on a joint project with Sonja Fischer, Matthias Hecker, and Jörg Schmalian, which originated from Sonja's Master's thesis (Ref. 198) and will be published in Ref. 199. Here, my additional work in this context is presented, which is to be published in Ref. 200.

5.1 Fluctuation corrections to the mean-field gap equation

Taking up our discussion of fluctuations as a detrimental factor for superconducting order started in Sec. 1.3.3, we concentrate on the effect of quantum fluctuations on the gap equation deep inside the ordered regime (at $T = 0$) here. The role of fluctuation corrections to the mean-field gap for various types of order, mostly motivated by superconductivity and magnetic order arising from models used to study the cuprate high-T_c superconductors, has been approached from different perspectives [100, 201–206]. Most of these studies came to the conclusion that, even though they tend to reduce the gap, fluctuation corrections are controlled by a small parameter and hence mean-field theory should apply.

Here, we review the logic used by Kos, Millis, and Larkin [100] when assessing the role of fluctuation corrections in the context of BCS theory and upon neglecting long-range Coulomb interaction.

Throughout this section, we will use the notation introduced in the context of superconductivity, however, the logic applies to other mean-field theories as well:

> The description in terms of a mean-field theory relies on the existence of a stable minimum of the free energy characterized by an order parameter whose value is determined by the gap equation. Let us assume mean-field theory to be valid and calculate fluctuation corrections to the gap equation. Only if we self-consistently find them to be negligible, the mean-field assumption was justified.

Within the field-integral formalism introduced in Sec. 1.1.2 and App. A in the context of superconductivity, the fluctuations are readily included by considering small deviations from the saddle point, i. e., the mean field configuration Δ_0. The action can then be expanded in terms of these fluctuations. If we restrict ourselves to leading order – Gaussian fluctuations – the field integral for the fluctuation part can be performed straightforwardly, which results in an additional contribution E_{fluct} to the ground-state energy,

$$E(\Delta_0) = E_{\text{MF}}(\Delta_0) + E_{\text{fluct}}(\Delta_0) = E_0 + V\rho_{\text{F}}\Delta_0^2\Big[\frac{1}{\rho_{\text{F}}V_{\text{SC}}} - \ln\Big(\frac{2v_{\text{F}}\Lambda}{\Delta_0}\Big) + \mathcal{O}(1)\Big] + E_{\text{fluct}}(\Delta_0)\,, \tag{5.1}$$

where E_0 is the ground-state energy of the normal state, V denotes the volume of the system, ρ_{F} is the density of states (DOS) at the Fermi level, V_{SC} denotes the coupling constant, and $v_{\text{F}}\Lambda$ is the energy cutoff (which corresponds to the Debye energy in the context of BCS superconductivity). Depending on the sign of the fluctuation contribution, this could either enhance or reduce the ground-state energy further.

The consequences for the justification of mean-field theory are best checked self-consistently. We assume that the new superconducting ground state, which minimizes the energy in the absence of fluctuations, is characterized by a static and homogeneous order parameter $\Delta_0 > 0$. As discussed in App. A.2 for the superconductor, its value is fixed by the gap equation

$$0 = \frac{1}{\rho_{\text{F}}V_{\text{SC}}} - \ln\Big(\frac{2v_{\text{F}}\Lambda}{\Delta_0}\Big)\,, \tag{5.2}$$

which is derived from minimizing the ground state energy, or, equivalently, from the saddle-point condition for the action, see App. A.2. Hence the mean-field value of the gap is given by $\Delta_0 = 2v_{\text{F}}\Lambda\exp(-1/\rho_{\text{F}}V_{\text{SC}})$. Taking fluctuations around the mean-field value of the gap into account amounts to additional contributions to the ground state energy, and minimization with respect to $\tilde{\Delta}_0$ results in a new condition for the ground state,[1]

$$0 = 2\tilde{\Delta}_0 V\rho_{\text{F}}\Big[\frac{1}{\rho_{\text{F}}V_{\text{SC}}} - \ln\Big(\frac{2v_{\text{F}}\Lambda}{\tilde{\Delta}_0}\Big) + \frac{1}{V\rho_{\text{F}}}\frac{\mathrm{d}E_{\text{fluct}}(\tilde{\Delta}_0)}{\mathrm{d}\tilde{\Delta}_0^2}\Big]\,. \tag{5.3}$$

However, as long as fluctuation corrections amount only to contributions of $\mathcal{O}(1)$ or smaller in the gap equation, they are negligible and the new ground state remains stable against fluctuations since it is indeed justified to characterize the superconducting ground state by the mean-field value Δ_0. If, on the other hand, terms of the same order as the mean-field contributions (i. e., $\mathcal{O}(1/\rho_{\text{F}}V_{\text{SC}})$) occur in the gap equation as a result of taking fluctuations into account, the value of the gap is considerably

[1] Note that we use $\frac{\mathrm{d}}{\mathrm{d}\tilde{\Delta}_0}\ldots \equiv 2\tilde{\Delta}_0\frac{\mathrm{d}}{\mathrm{d}\tilde{\Delta}_0^2}\ldots$ here. This is a convenient choice here, and furthermore, the fluctuation correction to the energy does not contain terms of linear order in $\tilde{\Delta}_0$.

altered by the presence of fluctuations. This means that the assumption of a static and homogeneous gap cannot reveal the dominant contribution to the energy, and hence the mean-field approximation is not justified in this case.

In order to assess the role of fluctuation corrections qualitatively, let us assume that they indeed give rise to a contribution of order $\mathcal{O}(1/\rho_{\mathrm{F}}V_{\mathrm{SC}})$. Hence, we write

$$\frac{1}{V\rho_{\mathrm{F}}}\frac{\mathrm{d}E_{\mathrm{fluct}}(\tilde{\Delta}_0)}{\mathrm{d}\tilde{\Delta}_0^2} =: \frac{c}{\rho_{\mathrm{F}}V_{\mathrm{SC}}} \qquad \text{where} \qquad c \in \mathbb{R} \quad \text{and} \quad c \neq 0\,. \tag{5.4}$$

Then, Eq. (5.3) results in

$$\tilde{\Delta}_0 = 2v_{\mathrm{F}}\Lambda \mathrm{e}^{-\frac{1+c}{\rho_{\mathrm{F}}V_{\mathrm{SC}}}}\,, \tag{5.5}$$

meaning that negative fluctuation contributions further enhance the gap as compared to its mean-field value, whereas positive fluctuation contributions result in a reduction. Hence, in the latter case, we can conclude that fluctuations weaken the ordered state. However, in both cases, fluctuation corrections of order $\mathcal{O}(1/\rho_{\mathrm{F}}V_{\mathrm{SC}})$ or the logarithmically divergent term in Eq. (5.1) imply that the respective mean-field theory cannot capture all relevant contributions, and a homogeneous and static mean-field was not a good assumption to start with.

5.2 Superconductivity

Probably the best example for the value of results obtained from a mean-field approach is provided by the BCS theory of superconductivity. In Sec. 5.1, we reviewed one approach that could be used to assess the importance of fluctuation corrections in the context of a given mean-field theory, and commented on how large fluctuation corrections can call the mean-field approximation into question. The analysis of fluctuations on Gaussian level in the context of BCS theory was provided by Kos, Millis, and Larkin [100], who arrived at the result that indeed, fluctuation corrections are negligible, and mean-field theory is justified. Strikingly, their conclusion is based on a cancellation of large terms originating from phase and amplitude fluctuations which would, if taken separately, each lead to fluctuation corrections that would call the mean-field results into question. In this section, we briefly review the approach of Kos, Millis, and Larkin with a focus on this peculiar cancellation, also drawing on findings from Ref. 198, and slightly generalize their result. In Sec. 5.3, the same logic will be applied to mean-field theories for density-wave instabilities, where we will also build on the results presented here in the context of superconductivity.

5.2.1 Fluctuation corrections to the BCS mean-field gap

Building on App. A, where we summarize the derivation of the BCS mean-field theory as a saddle-point approximation to the field integral, it is straightforward to include fluctuations up to Gaussian order around the mean-field value of the order parameter Δ_0. The latter can be chosen real, $\Delta_0 \in \mathbb{R}$, and following the notation of Ref. 100, we introduce deviations from the mean-field value as

$$\Delta(\boldsymbol{r},\tau) = \Delta_0 + \eta(\boldsymbol{r},\tau) \tag{5.6}$$

where $\eta \in \mathbb{C}$. We denote real and imaginary part of the fluctuations as η_1 and η_2, respectively. These can approximately be identified with amplitude and phase fluctuations and will be referred to as such

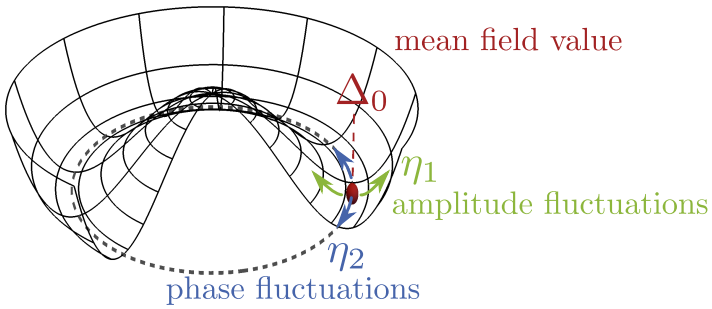

Figure 5.1: Amplitude and phase fluctuations of the order parameter for superconductivity. Fluctuations of the phase are indicated in blue and their location in the minimum of the 'Mexican hat' potential emphasizes the role of the collective phase mode as the Goldstone boson of the theory. The amplitude fluctuations are labeled in green and the corresponding collective mode is massive.

interchangeably in the remainder.[2] This is illustrated in Fig. 5.1, which shows the 'Mexican hat' form of the free energy in the SC state. In Matsubara frequency and momentum space, this amounts to

$$\Delta_q = \Delta_0\,\delta_{0,q} + \eta_{1,q} + \mathrm{i}\eta_{2,q}\,, \tag{5.7}$$

where we comprised incoming momentum and frequency into one variable as $(\boldsymbol{q}, \omega_n) \equiv q$, and $\eta_{i,q}$ are complex numbers satisfying $\eta_{i,q} = \bar{\eta}_{i,-q}$ owing to $\eta_i(\boldsymbol{r}, \tau) \in \mathbb{R}$.

Fluctuations in the field integral Going back to the effective action $\mathcal{S}_{\mathrm{eff}}(\bar{\Delta}, \Delta) = V_{\mathrm{SC}}^{-1} \int_q |\Delta_q|^2 - \mathrm{Tr}\ln \mathcal{G}^{-1}$ introduced in Eq. (1.4), we separate the mean-field contribution to the action from the fluctuation part by rewriting

$$\mathcal{G}^{-1}_{kk'} = \mathcal{G}^{-1}_{\mathrm{MF};k}\,\delta_{kk'} + H_{k-k'}\,, \tag{5.8a}$$

$$\text{where} \qquad \mathcal{G}^{-1}_{\mathrm{MF};k} = \mathrm{i}\nu_n\tau_0 + \Delta_0\tau_1 - \varepsilon_{\boldsymbol{k}}\tau_3 \tag{5.8b}$$

$$\text{and} \qquad H_{k-k'} = \eta_{1,k-k'}\tau_1 - \eta_{2,k-k'}\tau_2\,. \tag{5.8c}$$

As usual, this allows for a convenient expansion of the Tr ln-term in the action, here in terms of fluctuations of the order parameter, see App. A.3 for more details. We restrict ourselves to quadratic order and note that terms linear in phase and amplitude fluctuations vanish as a result of the saddle-point condition $\mathrm{d}\mathcal{S}/\mathrm{d}\Delta|_{\Delta=\Delta_0} = 0$. The remaining field integral over fluctuations is a Gaussian integral, which can be evaluated straightforwardly as

$$\mathcal{Z} = \mathrm{e}^{-\mathcal{S}_{\mathrm{MF}}} \int \mathcal{D}\boldsymbol{\eta}\, \mathrm{e}^{-\frac{1}{2}\int_q \boldsymbol{\eta}_q \boldsymbol{\mathcal{D}}_q^{-1} \boldsymbol{\eta}_{-q}} = \mathrm{e}^{-(\mathcal{S}_{\mathrm{MF}} + \mathcal{S}_{\mathrm{fluct}})}\,, \tag{5.9}$$

where we introduced the inverse fluctuation propagator $\boldsymbol{\mathcal{D}}_q^{-1}$ with matrix elements

$$(\mathcal{D}_q^{-1})_{ij} = \frac{2}{V_{\mathrm{SC}}}\,\delta_{ij} + (-1)^{i+j} \int_k \mathrm{tr}(\mathcal{G}_{\mathrm{MF};k-\frac{q}{2}}\tau_i \mathcal{G}_{\mathrm{MF};k+\frac{q}{2}}\tau_j)\,, \tag{5.10}$$

[2] Admittedly, it would seem more appropriate to use polar coordinates here, however, the corresponding Jacobian renders the evaluation of the resulting field integral an intricate problem. Hence the representation introduced in Eq. (5.7) is better suited for our calculations.

where $i,j \in \{1,2\}$ refer to amplitude and phase sector. The Gaussian fluctuation correction to the action is thus given by $\mathcal{S}_{\text{fluct}}(\Delta_0) = \int_q \ln\det(\boldsymbol{\mathcal{D}}_q^{-1})$, and we need to evaluate

$$\frac{\mathrm{d}\mathcal{S}_{\text{fluct}}(\Delta_0)}{\mathrm{d}\Delta_0^2} = \int_q \frac{\frac{\mathrm{d}}{\mathrm{d}\Delta_0^2}\det(\boldsymbol{\mathcal{D}}_q^{-1})}{\det(\boldsymbol{\mathcal{D}}_q^{-1})} \tag{5.11}$$

in order to judge the importance of fluctuations in the context of the BCS mean-field theory, as outlined in Sec. 5.1.[3] The technical challenge lies in the evaluation of the integral (5.11) which includes the whole Matsubara axis and momenta up to the energy cutoff $v_\mathrm{F}\Lambda$. This implies that an expansion of the fluctuation propagator for small incoming frequency and momentum is not sufficient in the context of fluctuation corrections, which renders the angular integration impractical even at $T = 0$. Fortunately, the integrals depend on external frequency and momentum only via the combination

$$r = \sqrt{\Big(\frac{\omega}{2\Delta_0}\Big)^2 + \Big(\frac{v_\mathrm{F} q\cos\theta}{2\Delta_0}\Big)^2}\,, \tag{5.12}$$

where θ is the angle between internal and external momenta $\boldsymbol{k}$ and $\boldsymbol{q}$. Therefore, we can resort to the two regimes of $r \ll 1$ and $r \gg 1$, where approximate analytical expressions can be obtained for the inverse fluctuation propagator.

Evaluation of the fluctuation propagator Using the explicit form of the fermionic mean-field matrix Green's function (5.8b), the inverse fluctuation propagator (5.10) is readily stated in the form

$$(\mathcal{D}_q^{-1})_{ij} = \frac{2}{V_{\text{SC}}}\,\delta_{ij} + (-1)^{i+j}\int_k \frac{(\mathrm{i}\nu_+\tau_0 + \varepsilon_+\tau_3 - \Delta_0\tau_1)\tau_i(\mathrm{i}\nu_-\tau_0 + \varepsilon_-\tau_3 - \Delta_0\tau_1)\tau_j}{(\nu_+^2 + \varepsilon_+^2 + \Delta_0^2)(\nu_-^2 + \varepsilon_-^2 + \Delta_0^2)} \tag{5.13}$$

where we adopted the notation of Ref. 100, $\nu_\pm = \nu \pm \frac{\omega}{2}$ and $\varepsilon_\pm = \varepsilon_{\boldsymbol{k}\pm\frac{\boldsymbol{q}}{2}}$. To make this expression more informative, let us introduce normal and anomalous contributions to the fermionic matrix Green's function,

$$g_k = -\frac{\mathrm{i}\nu_n + \varepsilon_{\boldsymbol{k}}}{\nu_n^2 + \varepsilon_{\boldsymbol{k}}^2 + \Delta_0^2} \qquad \text{and} \qquad f_k = \frac{\Delta_0}{\nu_n^2 + \varepsilon_{\boldsymbol{k}}^2 + \Delta_0^2}\,, \tag{5.14}$$

respectively. In the normal state, where $\Delta_0 = 0$, the former reduces to the usual form of the free electron propagator, whereas the latter vanishes. Furthermore, in the analysis of the fluctuation propagator, we assume particle-hole symmetry, i. e., we evaluate the integrals assuming a constant DOS at the Fermi level. This assumption immediately implies that $(\mathcal{D}_q^{-1})_{12} = (\mathcal{D}_q^{-1})_{21} = 0$, and hence phase and amplitude fluctuations decouple. For more details on the evaluation of the integrals and a summary of the results in the two regimes, we refer to App. E. The inverse propagators of amplitude and phase fluctuations can be expressed as

$$(\mathcal{D}_q^{-1})_{ii} = \frac{2}{V_{\text{SC}}} + 2\Pi_q^{\text{n}} - (-1)^i 2\Pi_q^{\text{a}}\,, \tag{5.15}$$

in terms of the normal and anomalous contributions

$$\Pi_q^{\text{n}} = -\frac{1}{2}\int_k (g_{k+q}g_{-k} + g_{k-q}g_{-k}) \qquad \text{and} \qquad \Pi_q^{\text{a}} = \int_k f_{k+q}f_{-k}\,. \tag{5.16}$$

[3] Note that in Sec. 5.1, we considered the ground-state energy E which at $T = 0$ corresponds to the free energy readily obtained from the action in Eq. (5.9), and hence we will use both interchangeably here.

Obviously, amplitude and phase fluctuations differ only in the sign with which the anomalous contribution enters. Let us note here that this sign originates from the trace of Pauli matrices in Eq. (5.13) and therefore is inevitably linked to the structure of Eq. (5.8).

Finally, the fluctuation corrections to the gap equation amount to

$$\frac{\mathrm{d}\mathcal{S}_{\mathrm{fluct}}(\Delta_0)}{\mathrm{d}\Delta_0^2} = \int_q \frac{\frac{\mathrm{d}\Pi_q^{\mathrm{n}}}{\mathrm{d}\Delta_0^2} + \frac{\mathrm{d}\Pi_q^{\mathrm{a}}}{\mathrm{d}\Delta_0^2}}{\frac{1}{V_{\mathrm{SC}}} + \Pi_q^{\mathrm{n}} + \Pi_q^{\mathrm{a}}} + \int_q \frac{\frac{\mathrm{d}\Pi_q^{\mathrm{n}}}{\mathrm{d}\Delta_0^2} - \frac{\mathrm{d}\Pi_q^{\mathrm{a}}}{\mathrm{d}\Delta_0^2}}{\frac{1}{V_{\mathrm{SC}}} + \Pi_q^{\mathrm{n}} - \Pi_q^{\mathrm{a}}} \tag{5.17}$$

and the remaining task is the evaluation of the integrand in the regimes $r \ll 1$ and $r \gg 1$, and the subsequent integration over external frequency and momentum.

Regime $r \ll 1$ The structure of the fluctuation propagator in the regime of $\omega^2 + (v_{\mathrm{F}} q \cos\theta)^2 \ll (2\Delta_0)^2$ determines the nature of the long-wavelength collective modes of the neutral superfluid. Indeed, as demonstrated by Ref. 207, analytic continuation of the results presented here for the fluctuation propagator in the regime of $r \ll 1$ recovers well-known results [208, 209]: the energy gap of $2\Delta_0$ for the massive amplitude mode, as well as the dispersion $\omega = v_{\mathrm{F}} q/\sqrt{d}$ of the phase mode, which is the Goldstone mode of the model.

Furthermore, the analysis of Refs. 100 and 198 shows that fluctuation corrections to the mean-field gap equation originating from the regime $r \ll 1$ are associated with the small factor $\Delta_0/v_{\mathrm{F}}\Lambda$, but already the individual contributions of amplitude and phase fluctuations are negligible.

Regime $r \gg 1$ In the opposite regime $\omega^2 + (v_{\mathrm{F}} q \cos\theta)^2 \gg (2\Delta_0)^2$, the justification for a mean-field treatment is only provided by the cancellation of two individually large contributions stemming from amplitude and phase fluctuations. The mathematical reason as revealed by Ref. 100 is that, to leading order, the two eigenvalues of the inverse fluctuation propagator have the same absolute value, but opposite signs. Furthermore, the analysis of Ref. 198 finds that the divergent contributions originate from the regime where $v_{\mathrm{F}} q > \omega$.

In addition, our notation in Eqs. (5.15) and (5.17) clarifies that the cancellation effect is only due to the anomalous part. Reverting to our definition of normal and anomalous contributions, cf. Eq. (5.16), we find that the anomalous contribution in the denominator of Eq. (5.17) vanishes in the limit $\Delta_0 \to 0$. The derivative of the anomalous part, on the other hand, diverges in this regime, leading to large fluctuation corrections associated with each amplitude and phase fluctuations. However, the different sign of the anomalous part (5.15) which originates from the Pauli-matrix trace ensures the cancellation of the divergent terms. Overall, the resulting fluctuation corrections to the BCS gap equation are negligible, justifying the mean-field approach in this context.

5.2.2 Generalizations

The observation that fluctuation corrections to the BCS mean-field gap equations are small owing to the peculiar cancellation of individually large terms from amplitude and phase fluctuations opens up further questions. Unfortunately, the most obvious and interesting ones – whether it is possible to observe direct consequences of amplitude and phase fluctuations separately in experiment, and what the underlying reason for the cancellation is – remain unsolved so far. Nevertheless, we can comment on two other interesting aspects here.

Fluctuation corrections in charged superconductors In charged superconductors, the long-range Coulomb interaction shifts the phase mode to the plasma frequency $\omega_\mathrm{p} \gg 2\Delta_0$ [210] whereas the amplitude mode remains unchanged. (This is the condensed-matter analogue of the famous 'Higgs mechanism' in particle physics.) This might pose a challenge for the cancellation effect providing the justification for a mean-field approach to superconductivity, since a naive guess suggests that fluctuation corrections due to amplitude and phase should be affected differently by the presence of the Coulomb interaction. The thorough analysis of Ref. 198 however shows that this conjecture is only partly true. The derivation can be performed in complete analogy with the case of a neutral superfluid as sketched in the previous section. Including the plasmon mode arising from the long-range Coulomb interaction using the same assumptions as in Sec. 5.2.1 results in a block-diagonal form of the fluctuation propagator

$$\boldsymbol{\mathcal{D}}_q^{-1} = \begin{pmatrix} (\mathcal{D}_q^{-1})_{11} & 0 & 0 \\ 0 & (\mathcal{D}_q^{-1})_{22} & (\mathcal{D}_q^{-1})_{23} \\ 0 & -(\mathcal{D}_q^{-1})_{23} & (\mathcal{D}_q^{-1})_{33} \end{pmatrix} \tag{5.18}$$

since the plasmon couples only to the phase mode, and the amplitude–phase subspace remains unaffected by the presence of long-range Coulomb interaction.

In the regime $r \ll 1$, the phase mode indeed couples to the plasmon mode arising from the long-range Coulomb interaction, and the corresponding matrix elements $(\mathcal{D}_q^{-1})_{23} \neq 0$ are even of the same order as the other matrix elements. As a result, the fluctuation corrections to the gap equation from this regime are indeed changed by the presence of long-range Coulomb interaction, however, remain negligible as long as $\Delta_0 \ll E_\mathrm{C} \ll E_\mathrm{F}$ holds, where E_C is the Coulomb energy at the Fermi momentum.

As the amplitude–phase subspace is not altered by inclusion of the plasmon mode, the cancellation of large terms originating from amplitude and phase fluctuations persists in charged superconductors. However, as the Coulomb interaction is momentum-dependent, we have to differentiate between $v_\mathrm{F} q \cos\theta < \omega$ and $v_\mathrm{F} q \cos\theta > \omega$ in order to assess the role of the plasmon in the regime $r \gg 1$. For large frequencies, an additional cancellation between the plasmon term and its coupling to the phase mode ensures the smallness of fluctuation corrections. For large momenta, the fluctuation corrections are negligible as well, but here as a result of a vanishing coupling of the plasmon to the phase mode. This implies that, astonishingly, the Higgs mechanism is not effective in this regime.

In conclusion, contrary to naive expectations, fluctuation corrections to the mean-field gap equation are negligible for charged superconductors as well, though for different reasons in the three different regimes.

Fluctuation corrections for anisotropic pairing Another interesting aspect is the generalization to superconductivity arising from an interaction which is anisotropic in momentum space. Probably the most obvious and best-studied example is d-wave superconductivity as found in the cuprate high-T_c superconductors. In real space, the d-wave state can be described by an order parameter that lives on the bonds of a square lattice, and hence is associated with two amplitude modes and two phase modes [211]. The latter two, however, are not equivalent, since one is the Goldstone mode whereas the other constitutes a relative phase between x and y bonds.

Still, in momentum representation, the structure of the action in Nambu space is the same as for the constant interaction leading to BCS theory: The inverse Green's function in Nambu space is given by

$$\mathcal{G}_{kk'}^{-1} = \begin{pmatrix} (\mathrm{i}\nu_n - \varepsilon_{\boldsymbol{k}})\,\delta_{kk'} & \Delta_{k-k'}\varphi_d(\frac{\boldsymbol{k}+\boldsymbol{k}'}{2}) \\ \bar{\Delta}_{k'-k}\varphi_d(\frac{\boldsymbol{k}+\boldsymbol{k}'}{2}) & (\mathrm{i}\nu_n + \varepsilon_{\boldsymbol{k}})\,\delta_{kk'} \end{pmatrix}, \tag{5.19}$$

see App. A.4 for more details. Therefore, we can conclude already at this level that the structure of the fluctuation propagators should be the same as in the context of BCS theory, and therefore, the anomalous part enters again with opposite signs for amplitude and phase modes. The only difference to Eq. (5.8) is in fact the appearance of a form factor, $\varphi_d(\boldsymbol{k}) = \cos k_1 - \cos k_2$ in our example of d-wave superconductivity. This form factor of course modifies the results of the integrals contributing to the gap equation as well as the fluctuation propagators. However, it is evident from the limit $\Delta_0 \to 0$ (which corresponds to the regime $r \gg 1$) that the anomalous contribution still vanishes whereas its derivative w. r. t. Δ_0^2 yields a divergent contribution to the numerator of the fluctuation corrections to the gap equation, suggesting that, again, the fluctuation corrections are negligible only owing to a cancellation of the contributions from amplitude and phase modes, however a proper analysis requires evaluation of these integrals.

Let us furthermore note that, due to Hermiticity of the Hamiltonian, the most general Nambu Green's function for a superconducting system is of the same structure,

$$\mathcal{G}^{-1}_{kk'} = \mathrm{i}\nu_n\,\delta_{kk'}\,\tau_0 - \varepsilon_{\boldsymbol{k}}\,\delta_{kk'}\,\tau_3 + \Delta_{kk'}\tau_+ + \bar{\Delta}_{kk'}\tau_- = \mathrm{i}\nu_n\tau_0 - \varepsilon_{\boldsymbol{k}}\tau_3 + \Delta_{1,kk'}\tau_1 - \Delta_{2,kk'}\tau_2\,, \tag{5.20}$$

where $\tau_\pm = \frac{1}{2}(\tau_1 \pm \mathrm{i}\tau_2)$ and $\Delta_{1,kk'}$ and $\Delta_{2,kk'}$ denote real and imaginary part of the order parameter, respectively. In conclusion, as long as we allow for both amplitude and phase fluctuations, the conclusions from Sec. 5.2.1 should not change. As a result, we expect the stability of mean-field theory for superconductivity even in a more general context.

5.3 Density-wave instabilities

Another type of long-known and well-studied emerging order are (commensurate) density-wave instabilities, already discussed in the context of iron-based superconductors in previous sections. However, charge-density waves (CDWs) [212] and spin-density waves (SDWs) [213] manifested as periodic spatial modulations of the electrons' charge and spin, respectively, are much more general. They generically result from a (partial) nesting of the Fermi surface, i. e., the fact that large parts of the Fermi surface are connected by the nesting vector $\boldsymbol{Q}$. As such, they occur most naturally in one-dimensional models, but indeed have been observed in many anisotropic low-dimensional systems as well. Furthermore, unconventional superconductivity often arises in the vicinity of an SDW phase (for example in the iron-based superconductors) or CDW order (as in the cuprate superconductors).

From a theoretical point of view, mean-field theories have often proven useful to describe CDW and SDW order. They can be derived in full analogy to BCS theory as outlined in App. A – by decoupling the interaction either in the charge channel or in the spin channel. The resulting CDW state is characterized by a scalar order parameter $\rho \in \mathbb{R}$, whereas SDW order is associated with $\boldsymbol{M} \in \mathbb{R}^3$. Recalling the fact that fluctuation corrections in the context of BCS theory were only small because divergent terms stemming from amplitude and phase fluctuations occurred with opposite sign and hence canceled, it is interesting to consider fluctuation corrections to the mean-field theories for CDW and SDW order for the following reason. In case of CDW order, there is only a single fluctuating mode which renders a cancellation impossible. The order parameter of an SDW state, on the other hand, allows for longitudinal and transverse fluctuations which could at least partially cancel. Hence in this section, we apply the framework outlined for the BCS mean-field theory of superconductivity in Sec. 5.2.1 and App. A to density-wave instabilities due to nesting.

For the sake of simplicity, we adopt the notation of the two-band model of iron-based superconductors once more, which provides an excellent example of a system with nested parts of the Fermi surface.

The resulting mean-field theory and the discussion of fluctuation corrections does however not rely on any details specific to the iron-based superconductors.[4] As discussed in previous chapters, the simplest model of these materials consists of one hole pocket at the Γ point and one electron pocket shifted by a vector $\boldsymbol{Q}$, which at particle-hole symmetry results in two perfectly nested Fermi surface pockets, as reflected in the nesting condition

$$\varepsilon_{\boldsymbol{k}} = -\varepsilon_{\boldsymbol{k}+\boldsymbol{Q}}\,, \tag{5.21}$$

or $\varepsilon_{\lambda,\boldsymbol{k}} = -\varepsilon_{\bar{\lambda},\boldsymbol{k}}$ using the band index λ and its 'opposite' $\bar{\lambda}$. As discussed in Sec. 2.1.2, the corresponding two-band model is the minimal model to study superconductivity in these materials. It is, however, not sufficient for a thorough discussion of the more complicated magnetic ground state in the iron-based superconductors (cf. the discussion of the structural phase transition and tetragonal magnetism in Chap. 4). Nevertheless, it provides a simple model for studying density-wave instabilities and their interplay with superconductivity, see for example the analysis of Ref. 41.

5.3.1 Charge-density wave order

We start with the consideration of fluctuation corrections in the context of a nesting-induced charge-density instability with momentum $\boldsymbol{Q}$. Details of our derivation can be found in App. D.1.1. In addition to the usual noninteracting action $\mathcal{S}_0 = \sum_\lambda \sum_\sigma \int_k \bar{\psi}_{\lambda,k,\sigma}(-\mathrm{i}\nu_n + \varepsilon_{\lambda,\boldsymbol{k}})\psi_{\lambda,k,\sigma}$, we consider an interaction in the charge channel

$$\mathcal{S}_{\mathrm{int}} = -\frac{V_{\mathrm{CDW}}}{2}\sum_{\sigma,\sigma'}\int_{k,k',q}(\bar{\psi}_{1,k,\sigma}\psi_{2,k+q,\sigma} + \bar{\psi}_{2,k,\sigma}\psi_{1,k+q,\sigma})(\bar{\psi}_{1,k',\sigma'}\psi_{2,k'-q,\sigma'} + \bar{\psi}_{2,k',\sigma'}\psi_{1,k'-q,\sigma'})\,. \tag{5.22}$$

Here, $\psi_{\lambda,k,\sigma}$ denote fermionic fields characterized by band index λ, crystal momentum $\boldsymbol{k}$, Matsubara frequency ν_n, and spin σ, consistent with the notation used in previous chapters. If the coupling $V_{\mathrm{CDW}} > 0$ is attractive, this interaction can lead to the formation of CDW order characterized by the real scalar order parameter $\rho(\boldsymbol{r}) \in \mathbb{R}$. In momentum representation, this amounts to the finite expectation value

$$\rho_q = \sum_\sigma \int_k \left\langle \bar{\psi}_{1,k,\sigma}\psi_{2,k+q,\sigma} + \bar{\psi}_{2,k,\sigma}\psi_{1,k+q,\sigma} \right\rangle . \tag{5.23}$$

Let us note here that there is a second possibility for charge-density wave formation, namely if we consider not the sum but the difference $\sum_\sigma \int_k (\bar{\psi}_{1,k,\sigma}\psi_{2,k+q,\sigma} - \bar{\psi}_{2,k,\sigma}\psi_{1,k+q,\sigma})$ in Eq. (5.22). This instability, termed charge-density wave with an imaginary order parameter (iCDW), is discussed in App. D.1.1 as well. However, for the sake of clarity, we will not elaborate on this possibility here, since the structure of the fluctuation corrections turns out to be the same in both cases.

Mean-field theory The mean-field theory of charge-density wave order due to nesting is then stated by the action

$$\mathcal{S}_{\mathrm{MF}}^{\mathrm{CDW}}(\rho_0) = \frac{\rho_0^2}{2V_{\mathrm{CDW}}} - \mathrm{Tr}\ln[-(\mathrm{i}\nu_n\tau_0 + \rho_0\tau_1 - \varepsilon_{\boldsymbol{k}}\tau_3)]\,, \tag{5.24}$$

where ρ_0 denotes the mean-field value of the CDW order parameter, and τ_i are Pauli matrices in band space. This action is of the same structure as the BCS mean-field action (cf. Eqs. (A.12) and (5.8b)), yet differs in that the order parameter is a real number, and hence only the amplitude of the CDW order

[4] The only assumption that we make is in fact that the couplings can be assumed to be only weakly momentum-dependent insofar as they depend only on band indices but not on small deviations from Γ or $\boldsymbol{Q}$.

parameter fluctuates. The expansion in terms of the mean-field order parameter up to second order yields

$$T_{\mathrm{CDW}} = \frac{2\mathrm{e}^{\gamma}\Lambda}{\pi}\mathrm{e}^{-\frac{1}{2\rho_{\mathrm{F}}V_{\mathrm{CDW}}}} \tag{5.25}$$

as the temperature at which the transition towards CDW order occurs. Finally, the mean-field gap equation for the CDW state at $T = 0$, deep in the ordered regime, amounts to

$$0 = \frac{1}{2V_{\mathrm{CDW}}} - \rho_{\mathrm{F}} \ln\Big(\frac{2v_{\mathrm{F}}\Lambda}{\rho_0}\Big)\,, \tag{5.26}$$

which is again of the same structure as the BCS result.

Fluctuation corrections Having established the mean-field theory for CDW order, we turn to the evaluation of fluctuation corrections up to Gaussian order. We split the order parameter into its mean-field value and the fluctuation part according to

$$\rho_q = \rho_0 + \varrho_q\,. \tag{5.27}$$

The contribution to the action from Gaussian fluctuations then amounts to $\mathcal{S}^{\mathrm{CDW}}_{\mathrm{fluct}}(\rho_0) = \frac{1}{2}\int_q \ln(\mathcal{D}^{-1}_{\mathrm{CDW};q})$ where the fluctuation propagator for the fluctuations around the CDW mean-field configuration is given by

$$\mathcal{D}^{-1}_{\mathrm{CDW};q} = \frac{1}{V_{\mathrm{CDW}}} + 2\Pi^{\mathrm{n}}_q + 2\Pi^{\mathrm{a}}_q \tag{5.28}$$

where of course the normal and anomalous contribution Π^{n}_q and Π^{a}_q (as defined in Eqs. (E.1) and (E.2), or Eq. (5.16)) have to be understood as functions of the CDW order parameter here. Therefore, as conjectured, we find that the fluctuation contributions to the ground state energy and thus the mean-field gap equation are not negligible, since

$$\frac{\mathrm{d}\mathcal{S}^{\mathrm{CDW}}_{\mathrm{fluct}}(\rho_0)}{\mathrm{d}\rho_0^2} = \frac{1}{2}\int_q \frac{\frac{\mathrm{d}\Pi^{\mathrm{n}}_q}{\mathrm{d}\rho_0^2} + \frac{\mathrm{d}\Pi^{\mathrm{a}}_q}{\mathrm{d}\rho_0^2}}{\frac{1}{2V_{\mathrm{CDW}}} + \Pi^{\mathrm{n}}_q + \Pi^{\mathrm{a}}_q} > 0 \tag{5.29}$$

has the same form as the contribution from amplitude fluctuations in BCS theory, where the divergent nature $\sim \ln(v_{\mathrm{F}}\Lambda/\Delta_0)$ of this integral in the regime of large momenta, $\sqrt{\omega^2 + (v_{\mathrm{F}}q\cos\theta)^2} \gg 2\Delta_0$ and $v_{\mathrm{F}}q > \omega$, was observed by Refs. 100 and 198.

In conclusion, the mean-field theory for the charge-density wave instability as presented above is not justified since fluctuation corrections alter the gap equation drastically and as a result, fluctuation corrections lead to a decrease of the gap compared to the mean-field value.

5.3.2 Spin-density wave order

We continue our discussion of density-wave instabilities due to nesting by considering the following interaction in the spin-channel,

$$\begin{aligned}\mathcal{S}_{\mathrm{int}} = -\frac{V_{\mathrm{SDW}}}{2}\sum_{\sigma_1,\sigma_2}\sum_{\sigma_1',\sigma_2'}\int_{k,k',q}&(\bar\psi_{1,k,\sigma_1}\boldsymbol{\sigma}_{\sigma_1\sigma_2}\psi_{2,k+q,\sigma_2} + \bar\psi_{2,k,\sigma_1}\boldsymbol{\sigma}_{\sigma_1\sigma_2}\psi_{1,k+q,\sigma_2})\\ &\cdot(\bar\psi_{1,k',\sigma_1'}\boldsymbol{\sigma}_{\sigma_1'\sigma_2'}\psi_{2,k'-q,\sigma_2'} + \bar\psi_{2,k',\sigma_1'}\boldsymbol{\sigma}_{\sigma_1'\sigma_2'}\psi_{1,k'-q,\sigma_2'})\,,\end{aligned} \tag{5.30}$$

where $\boldsymbol{\sigma} = (\sigma_1, \sigma_2, \sigma_3)$ denotes the vector of spin Pauli matrices and therefore Eq. (5.30) corresponds to a model of *Heisenberg spins*. In Sec. 5.3.3, we will discuss our findings also in the context of lower-dimensional spin models. Furthermore, we note that the analogous decoupling in the flavor channel of an SU(N)-invariant action leads to essentially the same conclusions, where the $N^2 - 1$ generators λ^i of SU(N) supersede the Pauli matrices generating SU(2).

If the interaction in Eq. (5.30) is attractive ($V_{\mathrm{SDW}} > 0$), this opens up the possibility of SDW formation characterized by the order parameter $\boldsymbol{M}(\boldsymbol{r}) \in \mathbb{R}^3$, or

$$\boldsymbol{M}_q = \sum_{\sigma\sigma'} \int_k \left\langle \bar{\psi}_{1,k,\sigma_1} \boldsymbol{\sigma}_{\sigma_1\sigma_2} \psi_{2,k+q,\sigma_2} + \bar{\psi}_{2,k,\sigma_1} \boldsymbol{\sigma}_{\sigma_1\sigma_2} \psi_{1,k+q,\sigma_2} \right\rangle \tag{5.31}$$

in momentum representation. Again, we note the possibility of a second SDW instability here: If we consider the difference $\sum_{\sigma\sigma'} \int_k (\bar{\psi}_{1,k,\sigma_1} \boldsymbol{\sigma}_{\sigma_1\sigma_2} \psi_{2,k+q,\sigma_2} - \bar{\psi}_{2,k,\sigma_1} \boldsymbol{\sigma}_{\sigma_1\sigma_2} \psi_{1,k+q,\sigma_2})$ instead of the sum in Eq. (5.30), this results in an SDW state with purely imaginary order parameter. Here, we only discuss the SDW state with real order parameter since the results for both types of SDW instabilities turn out to be the same, see App. D.1.2 where more details are provided.

Mean-field theory Again, we start from the mean-field theory for SDW order in this model, as obtained from a saddle-point approximation to the field integral. We can choose the coordinate system such that the mean-field value of the order parameter is aligned with the z-axis, i. e., $\boldsymbol{M}_0 = M_0 \boldsymbol{e}_z$, resulting in

$$\mathcal{S}_{\mathrm{MF}}^{\mathrm{SDW}}(M_0) = \frac{M_0^2}{2V_{\mathrm{SDW}}} - \mathrm{Tr}\ln[-(\mathrm{i}\nu_n \sigma_0\tau_0 + M_0\sigma_3\tau_1 - \varepsilon_{\boldsymbol{k}}\sigma_0\tau_3)]\,, \tag{5.32}$$

where again, τ_i denote Pauli matrices in band space whereas σ_i are the Pauli matrices in spin space.[5] Again, we can obtain the SDW transition temperature

$$T_{\mathrm{SDW}} = \frac{2\mathrm{e}^{\gamma}\Lambda}{\pi} \mathrm{e}^{-\frac{1}{4\rho_{\mathrm{F}} V_{\mathrm{SDW}}}} \tag{5.33}$$

from an expansion of the action up to quadratic order, and the mean-field gap equation determining the nontrivial solution at $T = 0$ assumes BCS form as well:

$$0 = \frac{1}{2V_{\mathrm{SDW}}} - 2\rho_{\mathrm{F}} \ln\left(\frac{v_{\mathrm{F}}\Lambda}{M_0}\right). \tag{5.34}$$

Fluctuation corrections The fluctuation corrections to the above-presented mean-field theory of SDW order can be obtained from splitting the order parameter into its mean-field part and a fluctuating contribution as

$$\boldsymbol{M}_q = M_0 \boldsymbol{e}_z + \boldsymbol{m}_q\,. \tag{5.35}$$

Owing to the vectorial nature of the order parameter, we can identify one mode fluctuating longitudinal to the mean-field order parameter (corresponding to amplitude fluctuations in the BCS theory), and two fluctuating modes transverse to the mean-field order parameter. The latter are the two Goldstone modes of the system, corresponding to fluctuations of the phase of the order parameter in the context

[5] If we started with an SU(N)-invariant interaction, the $N^2 - 1$ generators λ^i of SU(N) would appear here instead of the three Pauli matrices. Let us note further that our conclusions can be generalized straightforwardly to such an interaction in the flavor channel of the corresponding N-component Grassmann fields.

of superconductivity. Our detailed analysis presented in App. D.1.2 reveals that the three fluctuating modes do not couple to each other, and the two transverse modes are equivalent, leading to

$$\boldsymbol{\mathcal{D}}^{-1}_{\mathrm{SDW};q} = \begin{pmatrix} \frac{1}{V_{\mathrm{SDW}}} + \Pi_q^{\perp} & 0 & 0 \\ 0 & \frac{1}{V_{\mathrm{SDW}}} + \Pi_q^{\perp} & 0 \\ 0 & 0 & \frac{1}{V_{\mathrm{SDW}}} + \Pi_q^{\parallel} \end{pmatrix} . \tag{5.36}$$

This structure of the inverse matrix fluctuations propagator is in fact quite general and also occurs in other $\mathrm{O}(d_{\mathrm{s}})$ models. Furthermore, the inverse fluctuation propagators of longitudinal and transverse modes differ only in how the anomalous part Π_q^{a} (cf. Eq. (E.2), but as a function of M_0 here) enters,

$$\Pi_q^{\perp} = 4\Pi_q^{\mathrm{n}} - 4\Pi_q^{\mathrm{a}} , \tag{5.37}$$

$$\Pi_q^{\parallel} = 4\Pi_q^{\mathrm{n}} + 4\Pi_q^{\mathrm{a}} . \tag{5.38}$$

Building on our discussion of Sec. 5.2.1, we can investigate the contribution to the zero-temperature gap equation in two regimes of the quantity $r = \sqrt{\omega^2 + (v_{\mathrm{F}} q \cos\theta)^2}/2M_0$,

$$\frac{\mathrm{d}\mathcal{S}^{\mathrm{SDW}}_{\mathrm{fluct}}(M_0)}{\mathrm{d}M_0^2} = \frac{1}{2}\int_q \left[2\frac{\frac{\mathrm{d}\Pi_q^{\perp}}{\mathrm{d}M_0^2}}{\frac{1}{V_{\mathrm{SDW}}} + \Pi_q^{\perp}} + \frac{\frac{\mathrm{d}\Pi_q^{\parallel}}{\mathrm{d}M_0^2}}{\frac{1}{V_{\mathrm{SDW}}} + \Pi_q^{\parallel}} \right] \approx \left.\frac{\mathrm{d}\mathcal{S}^{\mathrm{SDW}}_{\mathrm{fluct}}}{\mathrm{d}M_0^2}\right|_{r\ll 1} + \left.\frac{\mathrm{d}\mathcal{S}^{\mathrm{SDW}}_{\mathrm{fluct}}}{\mathrm{d}M_0^2}\right|_{r\gg 1} . \tag{5.39}$$

The latter ($r \gg 1$) is the regime that potentially leads to a divergent contribution. Using the results summarized in App. E.2, we can identify the leading terms to numerator and denominator, and we find that

$$\left.\frac{\mathrm{d}\mathcal{S}^{\mathrm{SDW}}_{\mathrm{fluct}}}{\mathrm{d}M_0^2}\right|_{r\gg 1} \approx -\frac{1}{2}\int_q \frac{(2-1)\frac{\mathrm{d}\Pi_q^{\mathrm{a}}}{\mathrm{d}M_0^2}}{\frac{1}{4V_{\mathrm{SDW}}} + \Pi_q^{\mathrm{n}}} < 0 . \tag{5.40}$$

In contrast to amplitude and phase fluctuation corrections to the BCS mean-field gap equation, longitudinal and transverse fluctuations only partially cancel here, and the (negative) contribution of one transverse mode survives, resulting in a nonnegligible correction that enhances the gap compared to its mean-field value, cf. Sec. 5.1. Nevertheless, it renders the mean-field theory as presented in the beginning of this section unjustified.

5.3.3 Generalization to lower spin dimensionality

Our discussion of mean-field theories for spin-density wave instabilities in the previous section concentrated on the interaction (5.30) of Heisenberg spins, i. e., an O(3) model. Here, we generalize our results to models of lower spin dimensionality d_{s}: Considering Eq. (5.30) for spins oriented in the xy plane corresponds to the *XY model*, and restricting the spins to one spatial dimension leads to an *Ising model*. The matrix fluctuation propagator (5.36) is readily generalized to these $\mathrm{O}(d_{\mathrm{s}})$ models with $d_{\mathrm{s}} \leq 3$. Since the order parameter is $\boldsymbol{M}(\boldsymbol{r}) \in \mathbb{R}^{d_{\mathrm{s}}}$, fluctuations around the mean-field value can be categorized into one longitudinal mode and $d_{\mathrm{s}} - 1$ transverse modes.

Consequently, the Gaussian fluctuation corrections to the mean-field action amount to

$$\mathcal{S}^{\mathrm{SDW}}_{\mathrm{fluct}}(d_{\mathrm{s}}; M_0) = \frac{1}{2}\int_q \ln\left[\left(\frac{1}{V_{\mathrm{SDW}}} + \Pi_q^{\perp}\right)^{d_{\mathrm{s}}-1} \left(\frac{1}{V_{\mathrm{SDW}}} + \Pi_q^{\parallel}\right) \right] , \tag{5.41}$$

spin dimensionality		fluctuation corrections
Heisenberg model	($d_\mathrm{s}=3$)	increase the gap compared to its mean-field value
XY model	($d_\mathrm{s}=2$)	are negligible
Ising model	($d_\mathrm{s}=1$)	decrease the gap compared to its mean-field value

Table 5.1: Gaussian fluctuation corrections in O(d_s) models. Except for the XY model, we find a diverging contribution from the regime of large momenta, and depending on the spin dimensionality, fluctuations either increase or decrease the gap value.

implying that the potentially divergent contributions to the gap equation from the regime of large momenta, $\sqrt{\omega^2+(v_\mathrm{F}q\cos\theta)^2}\gg 2M_0$ and $v_\mathrm{F}q>\omega$, only cancel for $d_\mathrm{s}=2$,

$$\left.\frac{\mathrm{d}\mathcal{S}^{\mathrm{SDW}}_{\mathrm{fluct}}(d_\mathrm{s})}{\mathrm{d}M_0^2}\right|_{r\gg 1}\approx -\frac{1}{2}\int_q \frac{[(d_\mathrm{s}-1)-1]\frac{\mathrm{d}\Pi^\mathrm{a}_q}{\mathrm{d}M_0^2}}{\frac{1}{4V_\mathrm{SDW}}+\Pi^\mathrm{n}_q}\,. \tag{5.42}$$

In all other cases, large corrections call the mean-field approach into question. However, depending on the spin dimensionality d_s, they can either increase or decrease the gap compared to its mean-field value. Our findings are summarized in Tab. 5.1.

XY model For XY spins, fluctuation corrections to the SDW mean-field gap are negligible since contributions due to longitudinal and transverse fluctuations cancel exactly, making the mean-field analysis of the problem controlled. This observation is consistent with the results obtained in the context of BCS theory [100], which is reasonable since SO(2) and U(1) are isomorphic.

Ising model In the context of the Ising model, fluctuation corrections amount to a large contribution $\sim\ln(v_\mathrm{F}\Lambda/M_0)$ to the gap equation, decreasing the gap compared to its mean-field value. This is in line with our findings for charge-density wave order, where longitudinal fluctuations also suppress the gap.

5.3.4 Comparison to a renormalization group analysis

Our analysis of fluctuation corrections shows that the above-described mean-field theories for CDW and SDW instabilities are not justified, although they often provide an adequate phenomenological description of the respective ordered states. However, by construction, we restrict our consideration to the instability in a certain channel, neglecting logarithmically diverging susceptibilities in other channels. As discussed in previous chapters, the presence of competing phases of order is a characteristic of systems like the iron-based superconductors.

An alternative approach, which is suited to consider several competing instabilities on equal footing, is a renormalization group (RG) analysis of the coupling constants. The RG analysis of the model of two perfectly nested electron and hole Fermi surface (FS) pockets that we considered in Secs. D.1.1 and D.1.2 was performed by Ref. 41 to one-loop level. For a brief summary of their results and the connection to our work, see App. D.1.3. Taking into account all couplings and their mutual influence shows that not necessarily the channel with the largest bare interaction is the instability with highest transition temperature, since the couplings in all channels flow under renormalization.

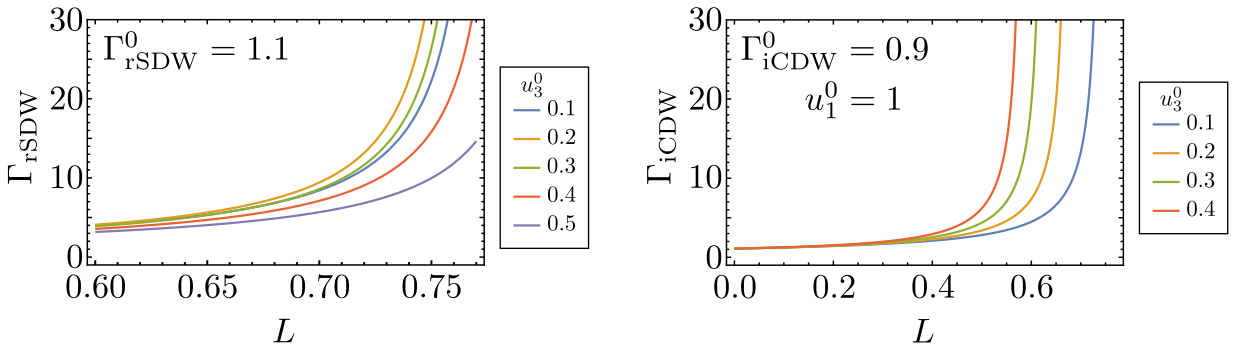

(a) rSDW channel **(b)** iCDW channel

Figure 5.2: Manifestation of channel interference effects in the RG analysis. The plots show the RG flows of exemplary effective couplings (measured in units of u^0) as a function of $L = u^0 \ln(W/E)$ for fixed bare values.

In the model of two perfectly nested electron and hole FS pockets analyzed by Ref. 41, the full interactions Γ in density-wave and pairing channels[6] are determined by the interplay of five coupling constants u_i, see App. D for details. Up to a factor 2, the bare interactions Γ^0_{rSDW} and Γ^0_{rCDW} in the density-wave channels correspond to the coupling constants in our discussion of the respective mean-field theories (V_{CDW} and V_{SDW}) in Secs. 5.3.1 and 5.3.2, respectively. They can be related to the coupling constants u_i by

$$\Gamma_{\mathrm{rSDW}} = u_1 + u_3\,, \qquad \Gamma_{\mathrm{iCDW}} = u_1 + u_3 - 2u_2\,, \tag{5.43a}$$

$$\Gamma_{\mathrm{iSDW}} = u_1 - u_3\,, \qquad \Gamma_{\mathrm{rCDW}} = u_1 - u_3 - 2u_2\,, \tag{5.43b}$$

and as expected, channel interference occurs quite naturally: The flow of the coupling constants u_i is given in Eq. (D.66) and implies that

$$\frac{\mathrm{d}}{\mathrm{d}t}(u_1 \mp u_3 - 2u_2) = (u_1 \mp u_3 - 2u_2)^2 \mp 2u_3(u_1 + u_2 - u_4)\,, \tag{5.44a}$$

$$\frac{\mathrm{d}}{\mathrm{d}t}(u_1 \pm u_3) = (u_1 \pm u_3)^2 \pm 2u_3(u_1 - u_2 - u_4)\,, \tag{5.44b}$$

where the derivatives are with respect to $t = \ln(W/E)$ with the bandwidth W and the running energy scale E. If the second term in Eqs. (5.44a) and (5.44b) were not present, the solution would be $\Gamma(t) = \Gamma_0/(1 - t\Gamma_0)$. Then the divergence at t_{c} would mark the energy scale at which the transition to the ordered state occurs. However, the fact that all other couplings contribute to the flow of the interactions in the density-wave channels as well means that each density-wave instability is also influenced by the flow of couplings in other channels – the other density-wave channels as well as superconductivity. Depending on the structure of these terms, channel interference might then change the energy scale at which the divergence in the respective channel occurs. However, already within the two-band model, the effect of a specific channel on another channel is not obvious and further complicated by the intricate dependence on bare couplings.

To illustrate interference effects in a certain channel, let us consider a fixed value of the bare interaction in the respective channel and examine how the flow of this interaction changes for different bare

[6] Note that, in consistency with the notation in Ref. 41, Γ refers to the interaction here, while in all other chapters, it denotes the scattering rate.

values of the original couplings u_i. In Fig. 5.2, we show exemplary RG flows for the two density-wave instabilities favored by repulsive pair hopping $u_3^0 > 0$ – rSDW and iCDW – starting from the bare couplings used in Ref. 41. Most importantly, the relation between the ratio of u_1^0 and u_3^0 and the SDW instability is nonuniversal, as apparent from Fig. 5.2 (a). The same is true when considering the CDW at fixed u_2^0, which results in qualitatively the same flows. On the other hand, when keeping u_1^0 fixed, increasing u_2^0 and u_3^0 (while $\Gamma_{\mathrm{iCDW}}^0 = \text{const.}$) implies that the energy scale at which the instability occurs decreases, as illustrated in Fig. 5.2 (b). In conclusion, we find that – depending on bare parameters – channel interference effects can be both advantageous and detrimental to charge and spin-density wave order, whereas the effect of fluctuation corrections (discussed in Secs. 5.3.1 and 5.3.2) does not depend on bare couplings.

5.4 Summary of Chapter 5

This chapter is devoted to a careful analysis of fluctuation contributions to various mean-field theories in order to assess their justification. We use the approach put forward by Kos, Millis and Larkin in the context of neutral superconductors: Assuming the validity of the mean-field approximation, we include fluctuations up to Gaussian order and calculate the corresponding corrections to the gap equation self-consistently.

In the context of *superconductivity*, we can infer that potentially large contributions stemming from amplitude and phase fluctuations cancel generically, since the relative sign associated with the anomalous part of the corresponding fluctuation propagators is deeply rooted in the Nambu-space structure of the action, cf. Eqs. (5.8) and (5.19). In conclusion, the result of Kos, Millis, and Larkin that mean-field theory is indeed justified, is quite generic in the context of superconductivity.

This is different for *commensurate density-wave instabilities* resulting from nesting of the Fermi surface: Only for the spin-density wave state arising from interacting XY spins, we recover the exact cancellation of longitudinal and transverse fluctuation contributions. In contrast, for charge-density wave order as well as for spin-density wave order of Heisenberg or Ising spins, sizable corrections to the gap equation arise from Gaussian fluctuations, as demonstrated by this thesis. Consequently, the respective mean-field theories are not controlled.

Conclusion

The main part of this thesis presents various interesting aspects of disorder in two systems probably hosting unconventional superconductivity: iron-based superconductors and the $LaAlO_3/SrTiO_3$ interface. Ultimately, we aim at a deeper understanding of the ordered phases that can potentially form in such systems, as well as their mutual interplay. As doping is used to manipulate the properties of these materials, disorder is intrinsic, however could also be introduced deliberately by irradiation to use it as an additional tuning parameter for these systems.

Iron-based superconductors In Chaps. 2 and 4, we discuss several implications of disorder for the iron-based superconductors (FeSCs). These materials attracted attention due to their relatively high transition temperatures despite the fact that they contain iron, as well as their complex phase diagram (including magnetic order) and the vast number of compounds available to study this class of materials. An introduction summarizing common properties of most FeSCs, and the ingredients for minimal models to study them, is provided in Sec. 1.2.1. Here, we want to highlight two aspects that result from our investigation of weak disorder in these materials.

Firstly, in Chap. 2, we complemented the discussion of the robustness of unconventional and conventional candidate pairing states for superconductivity in FeSCs [88, 128, 137–141] by the investigation of *orbital-magnetic impurities*. Such orbital-magnetic impurities break time-reversal symmetry, however, do not interact with the spin of the scattered electrons. While these are generally pair breaking for superconductivity, we found one important exception: If such orbital-magnetic impurities arise from charge-density waves with an imaginary order parameter (iCDWs), nucleated around originally nonmagnetic impurities, the unconventional s^{+-} pairing state suggested for FeSCs is not affected. This is indeed a conceivable scenario for iron-based superconductors, where iCDW order and spin-density wave order compete with unconventional superconductivity [41]. Furthermore, this can be understood in terms of a generalization of the Anderson theorem, as presented in Ref. 87.

Naturally, this calls for a further investigation of the proposed iCDW impurities and their role in FeSCs. One important task in this direction would be the calculation of experimental signatures of such impurities in local probes that could be used to detect them. Subsequently, it would be interesting to systematically study nonmagnetic disorder, preferably introduced by, e. g., electron irradiation, rather than as an immanent consequence of doping. Furthermore, even though our discussion of orbital-magnetic impurities has been tailored to FeSCs, our results apply in a broader sense. On this note, it would be interesting to investigate which other systems lead to analogous interband scattering processes, characterized by a nontrivial phase, as they would also be expected to give rise to a generalized Anderson theorem for unconventional superconductivity.

Secondly, in Chap. 4, we demonstrated that the magnetic ground state of iron-based superconductors can be tuned not only by basic band structure parameters, but also by disorder. In particular, our detailed analysis shows that in addition to the stripe-ordered magnetic state, which has been observed in many compounds in the underdoped regime, also magnetically ordered states that preserve the tetragonal lattice symmetry arise naturally from weakly disordered effective models. These have been discovered more recently in various hole-doped compounds [171–178] and were uniquely characterized

as a *charge-spin density wave state* [178, 180, 181]. Even more importantly, our analysis shows that disorder lifts the degeneracy between the two possible tetragonal magnetic states – spin-vortex crystal (SVC) and charge-spin density wave (CSDW) – and even promotes the formation of CSDW order in a growing regime of band structure parameters close to the limit of perfectly nested Fermi surface pockets. Thereby, we provide a possible explanation for why the CSDW order seems generically favored over SVC order in FeSCs – a question that previously lacked a theoretical description universally applicable to all compounds in which the alternative magnetic ground state was observed.

To further scrutinize our conclusions, successional studies of the predicted disorder-controlled transitions – either between stripe-magnetic order and tetragonal magnetism, or between the two different tetragonal magnetically ordered states – are desirable. In this context, numerical studies could prove useful to single out candidate materials for a subsequent experimental analysis using controlled disorder via irradiation and annealing. Another interesting aspect is the possibility of phase coexistence. For example, theoretical studies have shown that s^{+-} superconductivity can coexist with single-$\boldsymbol{Q}$ magnetic order, whereas s^{++} superconductivity and stripe-magnetism mutually exclude each other [68, 70]. Furthermore, the interplay of superconductivity and tetragonal as well as stripe-magnetic order has been investigated in Ref. 163. It would therefore be interesting to combine these ideas and check whether analogous constraints apply to the tetragonal magnetic states in the presence of disorder as well and if they have implications for possible superconducting pairing states.

$LaAlO_3/SrTiO_3$ interface Chap. 3 concentrates on potentially unconventional superconductivity in the $LaAlO_3/SrTiO_3$ interface. Such oxide heterostructures are promising materials for application since their (super)conducting properties can be tuned not only by material parameters such as composition, but also by application of electric fields. However, the nature of the superconducting pairing state still requires excessive research. So far, two candidates for the pairing state have been put forward [48]: a conventional superconducting state and, as an exciting alternative, an unconventional topologically nontrivial state. The realization of the latter, however, is particularly challenged by the fact that the superconducting coherence length and the mean-free path are of the same order in $LaAlO_3/SrTiO_3$, which calls for a thorough investigation of the effect of disorder in these materials. This thesis contributes an analysis of the two suggested pairing states with regard to their robustness against disorder.

We find that the strongly polarized nature of the Fermi surface provides an effective protection mechanism against impurity scattering, as the phase space for certain scattering processes becomes strongly suppressed. Most interestingly, the unconventional pairing state is more robust against magnetic disorder than the conventional one, however, no analogue of the Anderson theorem is found here. The underlying physical reason for the relative protection is the combination of anisotropic masses and spin-orbit coupling. In conclusion, the presence of disorder resulting in mean-free paths of the same order as the superconducting coherence length does not rule out unconventional superconductivity in the $LaAlO_3/SrTiO_3$ interface.

On the technical side, we introduced a formalism to investigate pair breaking that could readily be applied to other systems for which a corresponding patch approximation of the Fermi surface can be found. Hence, it would certainly be interesting to explore the possibility of such protection mechanisms also for other materials possibly hosting unconventional superconductivity, since a similar mechanism involving spin-orbit coupling has previously been found for odd-parity superconductivity [149].

Fluctuation corrections The last part of this thesis is concerned with the consequences of quantum fluctuations for mean-field theories. The description of ordered states by mean-field theories relies on

the assumption that the low-energy physics can be fully captured by an effective mean field. This could also serve as an order parameter within a Ginzburg-Landau approach, which proved very useful in the phenomenological description of different types of ordered states. However, this approach relies on the assumption that fluctuations around the mean-field value can be neglected as they do not lead to sizable corrections to observables calculated from mean-field theory. Of course, close to the classical phase transition, thermal fluctuations become important and drive the phase transition. Here, in contrast, we concentrate on corrections at zero temperature, deep in the ordered phase, where thermal fluctuation corrections are negligible.

One interesting approach to assess the role of quantum fluctuation corrections was put forward by Ref. 100 in the context of superconductivity. It is based on corrections to the BCS mean-field gap equation resulting from the inclusion of fluctuations up to Gaussian order. The anomalous contribution, which is nonzero only in the the ordered phase, in principle gives rise to logarithmically divergent contributions that would significantly alter the gap equation. In the case of superconductivity, however, the applicability of mean-field theory is ensured by canceling contributions due to fluctuations of both amplitude and phase of the order parameter.

In Chap. 5, we employ this approach to mean-field theories for commensurate charge-density wave (CDW) order and spin-density wave (SDW) order generically arising from nesting of the Fermi surface. As CDW order is described by a scalar order parameter and the number of spatial components for the SDW order parameter depends on spin dimensionality, one might suspect that the cancellation observed in the context of BCS theory does not generally translate to mean-field theories for density-wave instabilities. Indeed, we show here that the fluctuation corrections to the gap equation turn out to be negligible only for XY spins. As a result, the mean-field theories for commensurate density-wave order are strictly spoken not justified.

Nevertheless, mean-field theories are regularly used for a phenomenological description of density-wave order in itinerant electron systems with a nested Fermi surface. One example are the FeSCs, which have also been discussed in this thesis. Since the crucial contribution to quantum fluctuation corrections is due to the anomalous part, these are expected to be less relevant at finite temperature. An extension of our calculation to finite temperature could be a first step towards a better understanding of the validity of mean-field theory with respect to fluctuations. This is an issue that certainly calls for further investigation and constitutes ongoing work. In our comparison to a renormalization group analysis of the two-band model with perfectly nested Fermi surface pockets, we could observe interference effects due to potential instabilities in other channels. However, there are no clear trends in whether these promote density-wave instabilities or are detrimental. Additionally, as the origin of potentially large corrections from anomalous terms arises from the regime of large momenta (corresponding to length scales smaller than the coherence length), it would be interesting to pinpoint why, and whether this is reflected in experimental observables. A related question concerns the actual reason for the cancellation effect observed in superconductors that might further help in interpreting our results in the context of density-wave order.

In conclusion, not only can some of the ordered phases observed in unconventional superconducting materials be astonishingly robust against disorder, but the presence of impurities could even promote new types of order. This is of particular interest for unconventional superconducting states which are naively expected to be more vulnerable to impurity scattering and hence less likely to appear in disordered systems than conventional superconductivity. Furthermore, the aspects highlighted in this thesis are all related to interband scattering processes and hence characteristic for multi-band

materials. Finally, this thesis can by no means provide an exhaustive analysis of disorder effects in unconventional superconductors. It rather advocates the huge potential of systematic studies of controlled disorder in such systems: By combining general trends obtained from minimal models (such as the present work) with quantitative predictions from numerical calculations, promising compounds for experimental studies could be identified in order to get a deeper insight in these complex materials.

Appendix A

A Field theory for the neutral superconductor

This appendix introduces the formalism used throughout this thesis and, in particular, complements our presentation of Secs. 1.1.2 and 5.2. We use the field-integral formalism to derive BCS mean-field theory from the saddle-point condition and consider fluctuations around this saddle point. More details on the field-integral formalism for superconductors can be found in modern textbooks on condensed matter theory such as Ref. 85.

We start from the path integral for the partition function $\mathcal{Z} = \int \mathcal{D}[\bar{\psi}, \psi] \exp[-\mathcal{S}(\bar{\psi}, \psi)]$ in terms of the fermionic fields ψ. For a neutral superconductor, i. e., in the absence of long-range Coulomb interaction, the action is given by $\mathcal{S} = \mathcal{S}_0 + \mathcal{S}_{\text{int}}$, where the noninteracting part is given by

$$\mathcal{S}_0(\bar{\psi}, \psi) = \sum_\sigma \int_0^\beta \mathrm{d}\tau \int \mathrm{d}\boldsymbol{r}\, \bar{\psi}_\sigma(\boldsymbol{r}, \tau)\Big(\partial_\tau - \frac{\hbar^2\nabla^2}{2m}\Big)\psi_\sigma(\boldsymbol{r}, \tau) \tag{A.1a}$$

$$= \sum_\sigma \int_k \bar{\psi}_{k,\sigma}(-\mathrm{i}\nu_n + \varepsilon_{\boldsymbol{k}})\psi_{k,\sigma}\,, \tag{A.1b}$$

where for convenience, we conflate fermionic Matsubara frequencies $\nu_n = (2n+1)\pi T$ and momenta into $k := (\mathrm{i}\nu_n, \boldsymbol{k})$ and abbreviate $\int_k \ldots \equiv T\sum_n \int \frac{\mathrm{d}\boldsymbol{k}}{(2\pi)^d} \ldots$. Furthermore, the quasi-particle energy $\varepsilon_{\boldsymbol{k}}$ is measured from the chemical potential. The attractive ($V_{\text{SC}} < 0$) quartic interaction leading to superconductivity is given by

$$\mathcal{S}_{\text{int}}(\bar{\psi}, \psi) = V_{\text{SC}} \int_0^\beta \mathrm{d}\tau \int \mathrm{d}\boldsymbol{r}\, \bar{\psi}_\uparrow(\boldsymbol{r}, \tau)\bar{\psi}_\downarrow(\boldsymbol{r}, \tau)\psi_\downarrow(\boldsymbol{r}, \tau)\psi_\uparrow(\boldsymbol{r}, \tau) \tag{A.2a}$$

$$= V_{\text{SC}} \int_{k,k',q} \bar{\psi}_{k,\uparrow}\bar{\psi}_{-k+q,\downarrow}\psi_{-k'+q,\downarrow}\psi_{k',\uparrow}\,, \tag{A.2b}$$

and is considered to be local and instantaneous.

A.1 Effective action

We use the standard procedure and decouple the quartic interaction by introducing an auxiliary bosonic field via a Hubbard-Stratonovich transformation. In the case of superconductivity, we use the identity $\int \mathrm{d}\bar{x}\,\mathrm{d}x\, \exp(-\bar{x}ax + \bar{b}x + b\bar{x}) = \frac{1}{a}\exp(\bar{b}a^{-1}b)$, which holds for $x \in \mathbb{C}$ and positive $a \in \mathbb{R}$, to rewrite

$$\mathrm{e}^{-[\mathcal{S}_0(\bar{\psi},\psi)+\mathcal{S}_{\text{int}}(\bar{\psi},\psi)]} = \int \mathcal{D}[\bar{\Delta}, \Delta]\, \mathrm{e}^{-\mathcal{S}(\bar{\psi},\psi,\bar{\Delta},\Delta)}\,, \tag{A.3}$$

where we abbreviated

$$\mathcal{S}(\bar{\psi},\psi,\bar{\Delta},\Delta) = \mathcal{S}_0(\bar{\psi},\psi) + \int_0^\beta \mathrm{d}\tau \int \mathrm{d}\boldsymbol{r} \left[\frac{1}{|V_{\mathrm{SC}}|} |\Delta(\boldsymbol{r},\tau)|^2 - \Delta(\boldsymbol{r},\tau)\bar{\psi}_\uparrow(\boldsymbol{r},\tau)\bar{\psi}_\downarrow(\boldsymbol{r},\tau) - \bar{\Delta}(\boldsymbol{r},\tau)\psi_\downarrow(\boldsymbol{r},\tau)\psi_\uparrow(\boldsymbol{r},\tau) \right] \tag{A.4a}$$

$$= \mathcal{S}_0(\bar{\psi},\psi) + \int_q \left[\frac{1}{|V_{\mathrm{SC}}|} |\Delta_q|^2 - \Delta_q \int_k \bar{\psi}_{k+q,\uparrow}\bar{\psi}_{-k,\downarrow} - \bar{\Delta}_q \int_k \psi_{-k,\downarrow}\psi_{k+q,\uparrow} \right]. \tag{A.4b}$$

The resulting expression for the action is bilinear in the fermionic fields and can be restated in matrix form as

$$\mathcal{S}(\bar{\Psi},\Psi,\bar{\Delta},\Delta) = \mathcal{S}_0(\bar{\psi},\psi) + \frac{1}{|V_{\mathrm{SC}}|}\int_q |\Delta_q|^2 + \int_{k,k'} \bar{\Psi}_k(-\mathcal{G}^{-1}_{kk'})\Psi_{k'}\,, \tag{A.5}$$

where we introduced the spinors

$$\bar{\Psi}_k = \begin{pmatrix} \bar{\psi}_{k,\uparrow} & \psi_{-k,\downarrow} \end{pmatrix} \qquad \text{and} \qquad \Psi_k = \begin{pmatrix} \psi_{k,\uparrow} \\ \bar{\psi}_{-k,\downarrow} \end{pmatrix} \tag{A.6}$$

in Nambu space together with the corresponding inverse matrix Green's function

$$\mathcal{G}^{-1}_{kk'} = \begin{pmatrix} (G_{0;\boldsymbol{k}}(\nu_n))^{-1}\,\delta_{kk'} & \Delta_{k-k'} \\ \bar{\Delta}_{k'-k} & -(G_{0;-\boldsymbol{k}}(-\nu_n))^{-1}\,\delta_{kk'} \end{pmatrix}. \tag{A.7}$$

Here, we introduced $G_{0;\boldsymbol{k}}(\nu_n) = (\mathrm{i}\nu_n - \varepsilon_{\boldsymbol{k}})^{-1}$, which is the Green's function of noninteracting electrons. For a quadratic dispersion, we can use that $\varepsilon_{\boldsymbol{k}} = \varepsilon_{-\boldsymbol{k}}$, implying $G_{0;-\boldsymbol{k}}(-\nu_n) = G_{0;\boldsymbol{k}}(-\nu_n)$.

The fermionic integral is now of Gaussian form and can thus be performed straightforwardly. Hence we can express the partition function in terms of the auxiliary fields Δ as

$$\mathcal{Z} = \int \mathcal{D}[\bar{\Delta},\Delta] \int \mathcal{D}[\bar{\Psi},\Psi]\, \mathrm{e}^{-\mathcal{S}(\bar{\Psi},\Psi,\bar{\Delta},\Delta)} = \int \mathcal{D}[\bar{\Delta},\Delta]\, \mathrm{e}^{-\frac{1}{|V_{\mathrm{SC}}|}|\Delta_q|^2} \int \mathcal{D}[\bar{\Psi},\Psi]\, \mathrm{e}^{-\int_k \bar{\Psi}_k(-\mathcal{G}^{-1}_{kk'})\Psi_{k'}} \tag{A.8}$$

$$= \int \mathcal{D}[\bar{\Delta},\Delta]\, \mathrm{e}^{-\frac{1}{|V_{\mathrm{SC}}|}\int_q |\Delta_q|^2 + \mathrm{Tr}\ln(-\mathcal{G}^{-1})} = \int \mathcal{D}[\bar{\Delta},\Delta]\, \mathrm{e}^{-\mathcal{S}_{\mathrm{eff}}(\bar{\Delta},\Delta)}\,, \tag{A.9}$$

where we used the relation $\ln\det(-\mathcal{G}^{-1}) = \mathrm{tr}\ln(-\mathcal{G}^{-1})$ and defined the trace Tr as a trace in both momentum and Nambu space. In the last step, we introduced the effective action in terms of the bosonic fields Δ,

$$\mathcal{S}_{\mathrm{eff}}(\bar{\Delta},\Delta) = \frac{1}{|V_{\mathrm{SC}}|}\int_q |\Delta_q|^2 - \mathrm{Tr}\ln(-\mathcal{G}^{-1})\,. \tag{A.10}$$

A.2 Mean-field theory

The dominant contribution to the field integral stems from the saddle point, where the action has an extremum,

$$\frac{\mathrm{d}\mathcal{S}_{\mathrm{eff}}}{\mathrm{d}\Delta} = 0 \qquad \text{and} \qquad \frac{\mathrm{d}\mathcal{S}_{\mathrm{eff}}}{\mathrm{d}\bar{\Delta}} = 0\,. \tag{A.11}$$

Such a saddle-point approximation to the field integral results in a mean-field theory where the value of Δ at the saddle point corresponds to the mean-field value of the order parameter which we assume

to be static and homogeneous here. We denote the mean-field value of the order parameter by Δ_0, and furthermore assume that $\Delta_0 \in \mathbb{R}$. The mean-field action then reads

$$\mathcal{S}_{\mathrm{MF}}(\Delta_0) = \frac{1}{|V_{\mathrm{SC}}|}\Delta_0^2 - \operatorname{Tr}\ln(-\mathcal{G}_{\mathrm{MF}}^{-1})\,, \tag{A.12}$$

and hence the difference in free energy between the ordered state and the high-temperature ground state in mean-field theory can be expressed as

$$\mathcal{F} - \mathcal{F}_0 = -T\ln\left(\frac{\mathcal{Z}}{\mathcal{Z}_0}\right) \approx -T\ln \mathrm{e}^{-[\mathcal{S}_{\mathrm{MF}}(\Delta_0)-\mathcal{S}_{\mathrm{MF}}(\Delta_0=0)]} = T\mathcal{S}_{\mathrm{MF}}(\Delta_0) - T\mathcal{S}_{\mathrm{MF}}(\Delta_0=0)\,. \tag{A.13}$$

Ginzburg-Landau expansion We could further split the mean-field matrix Green's function into the bare part and a contribution due to the interaction,

$$\mathcal{G}^{-1}_{\mathrm{MF};kk'} = \delta_{kk'}\begin{pmatrix}(G_{0;\boldsymbol{k}}(\nu_n))^{-1} & 0\\ 0 & -(G_{0;-\boldsymbol{k}}(-\nu_n))^{-1}\end{pmatrix} + \delta_{kk'}\begin{pmatrix}0 & \Delta_0\\ \Delta_0 & 0\end{pmatrix} \tag{A.14}$$

$$= \delta_{kk'}\,\mathcal{G}_0^{-1} + \delta_{kk'}\,\mathcal{U}\,. \tag{A.15}$$

This allows for an expansion of the Tr ln-term according to

$$\operatorname{Tr}\ln(-\mathcal{G}_{\mathrm{MF}}^{-1}) = \operatorname{Tr}\ln(-\mathcal{G}_0^{-1}) + \operatorname{Tr}\ln(\mathbb{1} + \mathcal{G}_0\mathcal{U}) \tag{A.16}$$

$$= \operatorname{Tr}\ln(-\mathcal{G}_0^{-1}) - \frac{1}{2}\operatorname{Tr}(\mathcal{G}_0\mathcal{U}\mathcal{G}_0\mathcal{U}) - \frac{1}{4}\operatorname{Tr}(\mathcal{G}_0\mathcal{U}\mathcal{G}_0\mathcal{U}\mathcal{G}_0\mathcal{U}\mathcal{G}_0\mathcal{U}) + \mathcal{O}(\Delta_0^6)\,, \tag{A.17}$$

where we already exploited that terms of odd order in Δ_0 vanish. Furthermore, this expansion is based on the smallness of Δ_0 and thus works best close to the phase transition where the order parameter is small. For our discussion in the main text of this thesis, it is sufficient to keep terms up to quartic order,

$$\mathcal{S}_{\mathrm{MF}}(\Delta_0) = \mathcal{S}_{\mathrm{MF}}(\Delta_0=0) + \frac{1}{|V_{\mathrm{SC}}|}\Delta_0^2 + \frac{1}{2}\operatorname{Tr}(\mathcal{G}_0\mathcal{U}\mathcal{G}_0\mathcal{U}) + \frac{1}{4}\operatorname{Tr}(\mathcal{G}_0\mathcal{U}\mathcal{G}_0\mathcal{U}\mathcal{G}_0\mathcal{U}\mathcal{G}_0\mathcal{U})\,, \tag{A.18}$$

although in principle, higher-order terms could be included easily at this step. Hence, the corresponding expansion of the free energy in terms of the mean-field gap Δ_0 takes the form of Eq. (1.1),

$$\mathcal{F} = \mathcal{F}_0 + T\Big[\frac{1}{|V_{\mathrm{SC}}|}\Delta_0^2 + \frac{1}{2}\operatorname{Tr}(\mathcal{G}_0\mathcal{U}\mathcal{G}_0\mathcal{U}) + \frac{1}{4}\operatorname{Tr}(\mathcal{G}_0\mathcal{U}\mathcal{G}_0\mathcal{U}\mathcal{G}_0\mathcal{U}\mathcal{G}_0\mathcal{U})\Big]\,, \tag{A.19}$$

which makes the connection to the Ginzburg-Landau theory of Sec. 1.1.1 obvious. Furthermore, the explicit evaluation of the traces allows to determine the quadratic and quartic coefficients of this expansion from the microscopic model (A.1) and (A.2). For the quadratic coefficient, the evaluation of the trace leads to

$$a(T)\Delta_0^2 = \frac{\Delta_0^2}{|V_{\mathrm{SC}}|} + \frac{1}{2}\operatorname{Tr}(\mathcal{G}_0\mathcal{U}\mathcal{G}_0\mathcal{U}) = \Big[\frac{1}{|V_{\mathrm{SC}}|} + \int_k \frac{1}{(\mathrm{i}\nu_n - \varepsilon_{\boldsymbol{k}})(\mathrm{i}\nu_n + \varepsilon_{\boldsymbol{k}})}\Big]\Delta_0^2\,. \tag{A.20}$$

This integral is divergent, but since the effective interaction within BCS theory vanishes above the Debye frequency, we may introduce a momentum cut-off Λ here. Since frequency and momentum

appear on an equal footing, the momentum cut-off could also be transformed into a cut-off for the Matsubara frequencies as

$$\int_k \frac{1}{\varepsilon_{\boldsymbol{k}}^2+\nu_n^2} = T\sum_n \rho_{\mathrm{F}} \int_{-\Lambda}^{\Lambda} \mathrm{d}\varepsilon\, \frac{1}{\varepsilon^2+\nu_n^2} = T\sum_{\nu_n} \frac{\pi\rho_{\mathrm{F}}}{|\nu_n|}\frac{2}{\pi}\arctan\Big(\frac{\Lambda}{|\nu_n|}\Big) \simeq T\sum_{\nu_n}\frac{\pi\rho_{\mathrm{F}}}{|\nu_n|}\frac{2}{\pi}\frac{\Lambda}{\Lambda+|\nu_n|} \tag{A.21}$$

$$= \rho_{\mathrm{F}} \ln\Big(\frac{2\Lambda \mathrm{e}^{\gamma}}{\pi T}\Big) \tag{A.22}$$

$$= T\sum_{|\nu_n|\leq\Lambda}\frac{\pi\rho_{\mathrm{F}}}{|\nu_n|} = T\sum_{|\nu_n|\leq\Lambda}\rho_{\mathrm{F}}\int_{-\infty}^{\infty}\mathrm{d}\varepsilon\,\frac{1}{\varepsilon^2+\nu_n^2}\,, \tag{A.23}$$

which we will use in the remainder. The BCS transition temperature $T_{\mathrm{c},0}$ is determined by the condition $a(T_{\mathrm{c},0})=0$, resulting in

$$T_{\mathrm{c},0} = \frac{2\Lambda \mathrm{e}^{\gamma}}{\pi}\mathrm{e}^{-\frac{1}{\rho_{\mathrm{F}}|V_{\mathrm{SC}}|}}\,. \tag{A.24}$$

Furthermore, the evaluation of the quartic term results in the expression

$$b\Delta_0^4 = \frac{1}{2}\,\mathrm{Tr}(\mathcal{G}_0\mathcal{U}\mathcal{G}_0\mathcal{U}\mathcal{G}_0\mathcal{U}\mathcal{G}_0\mathcal{U}) = \int_k \frac{1}{(\mathrm{i}\nu_n-\varepsilon_{\boldsymbol{k}})^2(\mathrm{i}\nu_n+\varepsilon_{\boldsymbol{k}})^2}\Delta_0^4 = \frac{7\zeta(3)\rho_{\mathrm{F}}}{8\pi^2T^2}\Delta_0^4\,. \tag{A.25}$$

Gap equation In addition, we can easily obtain a self-consistent equation for the mean-field value of the order parameter from the field integral approach. We start from the saddle-point condition (A.11) in terms of the mean-field order parameter,

$$0 = \frac{\mathrm{d}\mathcal{S}_{\mathrm{MF}}}{\mathrm{d}\Delta_0} = \frac{\mathrm{d}}{\mathrm{d}\Delta_0}\Big[\frac{1}{|V_{\mathrm{SC}}|}\Delta_0^2 - \int_k \ln\det(-\mathcal{G}^{-1}_{\mathrm{MF};k})\Big] = 2\Delta_0\Big[\frac{1}{|V_{\mathrm{SC}}|} - \int_k \frac{1}{\nu_n^2+\varepsilon_{\boldsymbol{k}}^2+\Delta_0^2}\Big]\,, \tag{A.26}$$

implying that the nontrivial solution $\Delta_0\neq 0$ can be obtained from solving the gap equation

$$\frac{1}{|V_{\mathrm{SC}}|} = \int_k \frac{1}{\nu_n^2+\varepsilon_{\boldsymbol{k}}+\Delta_0^2}\,. \tag{A.27}$$

Assuming a constant DOS ρ_{F} at the Fermi level, the momentum integration can be replaced by an energy integration as $\int \frac{\mathrm{d}\boldsymbol{k}}{(2\pi)^d}\ldots \equiv \rho_{\mathrm{F}}\int \mathrm{d}\varepsilon\ldots$. Furthermore, at zero temperature, the Matsubara sum reduces to a frequency integration, $T\sum_n \ldots \equiv \int_{-\infty}^{\infty}\frac{\mathrm{d}\nu}{2\pi}\ldots$. Introducing the energy cut-off $v_{\mathrm{F}}\Lambda$, these two integrals can be straightforwardly evaluated,

$$\frac{1}{|V_{\mathrm{SC}}|} = \rho_{\mathrm{F}}\int_{-v_{\mathrm{F}}\Lambda}^{v_{\mathrm{F}}\Lambda}\mathrm{d}\varepsilon\int_{-\infty}^{\infty}\frac{\mathrm{d}\nu}{2\pi}\frac{1}{\nu^2+\varepsilon^2+\Delta_0^2} = \rho_{\mathrm{F}}\ln\Big(\frac{2v_{\mathrm{F}}\Lambda}{\Delta_0}\Big)\,, \tag{A.28}$$

resulting in a mean-field gap value of

$$\Delta_0(T=0) = 2v_{\mathrm{F}}\Lambda \mathrm{e}^{-\frac{1}{\rho_{\mathrm{F}}|V_{\mathrm{SC}}|}}\,. \tag{A.29}$$

A.3 Gaussian fluctuations around the saddle-point configuration

Let us now introduce fluctuations around the mean-field value as $\Delta(\boldsymbol{r},\tau)=\Delta_0+\eta_1(\boldsymbol{r},\tau)+\mathrm{i}\eta_2(\boldsymbol{r},\tau)$, where the real part η_1 and the imaginary part η_2 can be identified with phase and amplitude fluctuations.

The inverse matrix Green's function can be split into the mean-field contribution and the fluctuation part according to $\mathcal{G}^{-1} = \mathcal{G}_{\mathrm{MF}}^{-1} + H$, or explicitly as

$$\mathcal{G}^{-1}_{kk'} = \begin{pmatrix} (G_{0;\boldsymbol{k}}(\nu_n))^{-1}\,\delta_{kk'} & \Delta_{k-k'} \\ \bar{\Delta}_{k'-k} & -(G_{0;\boldsymbol{k}}(-\nu_n))^{-1}\,\delta_{kk'} \end{pmatrix} \tag{A.30}$$

$$= \begin{pmatrix} (G_{0;\boldsymbol{k}}(\nu_n))^{-1} & \Delta_0 \\ \Delta_0 & -(G_{0;\boldsymbol{k}}(-\nu_n))^{-1} \end{pmatrix} \delta_{kk'} + \begin{pmatrix} 0 & \eta_{1,k-k'} + \mathrm{i}\eta_{2,k-k'} \\ \bar{\eta}_{1,k'-k} - \mathrm{i}\bar{\eta}_{2,k'-k} & 0 \end{pmatrix} \tag{A.31}$$

$$= (\mathrm{i}\nu_n\tau_0 + \Delta_0\tau_1 - \varepsilon_{\boldsymbol{k}}\tau_3)\,\delta_{kk'} + \eta_{1,k-k'}\tau_1 - \eta_{2,k-k'}\tau_2\,, \tag{A.32}$$

where we exploited that $\eta_i(\boldsymbol{r},\tau) \in \mathbb{R}$, implying $\bar{\eta}_{i,q} = \eta_{i,-q}$. As usual, this allows for a convenient expansion of the Tr ln-term in the effective action,

$$\begin{aligned} \mathrm{Tr}\ln(-\mathcal{G}^{-1}) &= \mathrm{Tr}\ln[-(\mathcal{G}_{\mathrm{MF}}^{-1} + H)] = \mathrm{Tr}\ln[-\mathcal{G}_{\mathrm{MF}}^{-1}(\mathbb{1} + \mathcal{G}_{\mathrm{MF}}H)] \\ &= \mathrm{Tr}\ln(-\mathcal{G}_{\mathrm{MF}}^{-1}) + \mathrm{Tr}(\mathcal{G}_{\mathrm{MF}}H) - \frac{1}{2}\,\mathrm{Tr}(\mathcal{G}_{\mathrm{MF}}H\mathcal{G}_{\mathrm{MF}}H) + \mathcal{O}(\eta^3) \end{aligned} \tag{A.33}$$

up to Gaussian order. Then, the partition function also separates into a mean-field part and the fluctuation contribution as

$$\mathcal{Z} = \int \mathcal{D}[\bar{\Delta},\Delta]\,\mathrm{e}^{-\frac{1}{|V_{\mathrm{SC}}|}\int_q |\Delta_q|^2 + \mathrm{Tr}\ln(-\mathcal{G}^{-1})} \tag{A.34}$$

$$\simeq \int \mathcal{D}[\bar{\eta},\eta]\,\mathrm{e}^{-\frac{1}{|V_{\mathrm{SC}}|}[\Delta_0^2 + 2\Delta_0\int_q \mathrm{Re}\,\eta_q + \int_q |\eta_q|^2] + \mathrm{Tr}\ln(-\mathcal{G}_{\mathrm{MF}}^{-1}) + \mathrm{Tr}(\mathcal{G}_{\mathrm{MF}}H) - \frac{1}{2}\mathrm{Tr}(\mathcal{G}_{\mathrm{MF}}H\mathcal{G}_{\mathrm{MF}}H)} \tag{A.35}$$

$$= \mathrm{e}^{-\mathcal{S}_{\mathrm{MF}}} \int \mathcal{D}[\bar{\eta},\eta]\,\mathrm{e}^{-\frac{1}{|V_{\mathrm{SC}}|}\int_q |\eta_q|^2 - \frac{1}{2}\mathrm{Tr}(\mathcal{G}_{\mathrm{MF}}H\mathcal{G}_{\mathrm{MF}}H)} \tag{A.36}$$

where the last line follows from the fact that contributions linear in η and $\bar{\eta}$ vanish as a consequence of the saddle point condition

$$\left.\frac{\mathrm{d}\mathcal{S}}{\mathrm{d}\Delta}\right|_{\Delta=\Delta_0=\bar{\Delta}} = \left.\frac{\mathrm{d}\mathcal{S}}{\mathrm{d}\Delta}\right|_{\eta=0=\bar{\eta}} = 0\,. \tag{A.37}$$

Using $H = \eta_1\tau_1 - \eta_2\tau_2$, we can write the remaining field integral over fluctuations as a Gaussian integral which can be readily evaluated, leading to an additional contribution $\mathcal{S}_{\mathrm{fluct}}$ to the action coming from Gaussian fluctuations,

$$\mathrm{e}^{-\mathcal{S}_{\mathrm{fluct}}(\Delta_0)} = \int \mathcal{D}[\bar{\eta},\eta]\,\mathrm{e}^{-\frac{1}{|V_{\mathrm{SC}}|}\int_q |\eta_q|^2 - \frac{1}{2}\mathrm{Tr}(\mathcal{G}_{\mathrm{MF}}H\mathcal{G}_{\mathrm{MF}}H)} \tag{A.38}$$

$$= \int \mathcal{D}[\bar{\eta},\eta]\,\mathrm{e}^{-\frac{1}{|V_{\mathrm{SC}}|}\int_q \sum_i |\eta_{i,q}|^2 - \frac{1}{2}\int_{k,k'}\mathrm{tr}[\mathcal{G}_{\mathrm{MF};k}(\eta_{1,k-k'}\tau_1 - \eta_{2,k-k'}\tau_2)\mathcal{G}_{\mathrm{MF};k'}(\eta_{1,k'-k}\tau_1 - \eta_{2,k'-k}\tau_2)]} \tag{A.39}$$

$$= \int \mathcal{D}[\bar{\eta},\eta]\,\mathrm{e}^{-\frac{1}{2}\int_q \sum_{i,j}\eta_{i,q}\left[\frac{2}{|V_{\mathrm{SC}}|}\delta_{ij} + (-1)^{i+j}\int_k \mathrm{tr}(\mathcal{G}_{\mathrm{MF};k+\frac{q}{2}}\tau_i\mathcal{G}_{\mathrm{MF};k-\frac{q}{2}}\tau_j)\right]\eta_{j,-q}} \tag{A.40}$$

$$= \int \mathcal{D}\boldsymbol{\eta}\,\mathrm{e}^{-\frac{1}{2}\int_q \boldsymbol{\eta}_q(\frac{2}{|V_{\mathrm{SC}}|}\mathbb{1} + 2\boldsymbol{\Pi}_q)\boldsymbol{\eta}_{-q}} \tag{A.41}$$

$$= \mathrm{e}^{-\frac{1}{2}\int_q \ln\det(\frac{2}{|V_{\mathrm{SC}}|}\mathbb{1} + 2\boldsymbol{\Pi}_q)}\,, \tag{A.42}$$

where we defined $\boldsymbol{\eta}_q = (\eta_{1,q}, \eta_{2,q})$ and introduced the polarization matrix $\boldsymbol{\Pi}_q$ as

$$(\Pi_q)_{ij} = \frac{(-1)^{i+j}}{2}\int_k \mathrm{tr}(\mathcal{G}_{\mathrm{MF};k+\frac{q}{2}}\tau_i\mathcal{G}_{\mathrm{MF};k-\frac{q}{2}}\tau_j)\,. \tag{A.43}$$

The relative sign of the anomalous part in amplitude and phase fluctuation contributions follows inevitably from the Pauli matrix structure of the polarization matrix which is due to the fact that SC fluctuations are off-diagonal in Nambu space. The fluctuation correction to the action could alternatively be stated as

$$\mathcal{S}_{\text{fluct}}(\Delta_0) = \frac{1}{2}\int_q \ln\det(\boldsymbol{\mathcal{D}}_q^{-1}) = \frac{1}{2}\operatorname{Tr}\ln(\boldsymbol{\mathcal{D}}_q^{-1})\,, \tag{A.44}$$

where we introduced the inverse fluctuation propagator

$$\boldsymbol{\mathcal{D}}_q^{-1} = \frac{2}{|V_{\text{SC}}|}\mathbb{1} + 2\boldsymbol{\Pi}_q\,. \tag{A.45}$$

For further details on the evaluation of the corresponding fluctuation corrections, we refer to Sec. 5.2.1 and App. E.

A.4 Generalization to anisotropic superconductors

Let us now generalize the results for fluctuation corrections to the BCS mean-field gap equation to the case of superconductivity due to an anisotropic pairing interaction $V_{\boldsymbol{k}\boldsymbol{k}'}$. The structure of the inverse Green's function matrix in Nambu space is again given by

$$\mathcal{G}_{kk'}^{-1} = \mathrm{i}\nu_n\,\delta_{kk'}\,\tau_0 - \varepsilon_{\boldsymbol{k}}\,\delta_{kk'}\,\tau_3 + \Delta_{kk'}\tau_+ + \bar{\Delta}_{kk'}\tau_- = \mathrm{i}\nu_n\tau_0 - \varepsilon_{\boldsymbol{k}}\tau_3 + \Delta_{1,kk'}\tau_1 - \Delta_{2,kk'}\tau_2\,, \tag{A.46}$$

where we defined $\tau_\pm = \frac{1}{2}(\tau_1 \pm \mathrm{i}\tau_2)$. Alternatively, we could use $\Delta_{1,kk'}$ and $\Delta_{2,kk'}$, which denote real and imaginary part of the order parameter, respectively. Using the same notation as in the previous section, we separate mean-field propagator and fluctuation part as

$$\mathcal{G}_{\text{MF};k} = \frac{-\mathrm{i}\nu_n\tau_0 - \varepsilon_{\boldsymbol{k}}\tau_3 + \Delta_{1,k}\tau_1 - \Delta_{2,k}\tau_2}{\nu_n^2 + \varepsilon_{\boldsymbol{k}}^2 + |\Delta_k|^2} \qquad \text{and} \qquad H = \eta_{1,kk'}\tau_1 - \eta_{2,kk'}\tau_2\,. \tag{A.47}$$

Again, we introduce amplitude and phase fluctuations of the order parameter by writing $|\Delta_{kk'}|^2 = |\Delta_k|^2\,\delta_{kk'} + |\eta_{1,kk'}|^2 + |\eta_{2,kk'}|^2$. As in the analysis of fluctuations in neutral superconductors, we can consider fluctuations up to Gaussian order, leaving us with

$$\frac{1}{2}\operatorname{Tr}(\mathcal{G}_{\text{MF}}H\mathcal{G}_{\text{MF}}H) = \sum_{i,j}\int_{k,k'}\eta_{i,kk'}\underbrace{\frac{(-1)^{i+j}}{2}\operatorname{tr}(\mathcal{G}_{\text{MF};k}\tau_i\mathcal{G}_{\text{MF};k'}\tau_j)}_{=(\tilde{\Pi}_{kk'})_{ij}}\eta_{j,k'k}\,, \tag{A.48}$$

where, again, we introduce the polarization bubble $\tilde{\boldsymbol{\Pi}}$. The resulting integrals have the same structure as those obtained in the context of BCS theory (see App. E),

$$\tilde{\Pi}_{11} = -\int\frac{\nu\nu' + \varepsilon\varepsilon'}{NN'} + \int\frac{\Delta_1\Delta_1' - \Delta_2\Delta_2'}{NN'} =: \tilde{\Pi}^{\text{n}} + \tilde{\Pi}^{\text{a}_1}\,, \tag{A.49a}$$

$$\tilde{\Pi}_{22} = -\int\frac{\nu\nu' + \varepsilon\varepsilon'}{NN'} - \int\frac{\Delta_1\Delta_1' - \Delta_2\Delta_2'}{NN'} =: \tilde{\Pi}^{\text{n}} - \tilde{\Pi}^{\text{a}_1}\,, \tag{A.49b}$$

$$\tilde{\Pi}_{12} = \underbrace{\int\frac{\nu\varepsilon' - \varepsilon\nu'}{NN'}}_{\to 0} + \int\frac{\Delta_1\Delta_2' + \Delta_2\Delta_1'}{NN'} =: \tilde{\Pi}^{\text{a}_2}\,, \tag{A.49c}$$

$$\tilde{\Pi}_{21} = \underbrace{-\int\frac{\nu\varepsilon' - \varepsilon\nu'}{NN'}}_{\to 0} + \int\frac{\Delta_1\Delta_2' + \Delta_2\Delta_1'}{NN'} =: \tilde{\Pi}^{\text{a}_2}\,, \tag{A.49d}$$

where we introduced $N = \nu^2 + \varepsilon^2 + |\Delta_k|^2$. Here, however, also the off-diagonal matrix elements contain anomalous contributions. In order to judge the importance of fluctuation corrections, we need to evaluate the determinant of the inverse fluctuation propagator,

$$\det \boldsymbol{\mathcal{D}}^{-1} = \Big(\frac{1}{|V_{\mathrm{SC}}|} + \tilde{\Pi}^{\mathrm{n}} + \tilde{\Pi}^{\mathrm{a}_1}\Big)\Big(\frac{1}{|V_{\mathrm{SC}}|} + \tilde{\Pi}^{\mathrm{n}} - \tilde{\Pi}^{\mathrm{a}_1}\Big) - \tilde{\Pi}^{\mathrm{a}_2}\tilde{\Pi}^{\mathrm{a}_2} \tag{A.50}$$

$$= \Big(\frac{1}{|V_{\mathrm{SC}}|} + \tilde{\Pi}^{\mathrm{n}}\Big)\Big(\frac{1}{|V_{\mathrm{SC}}|} + \tilde{\Pi}^{\mathrm{n}}\Big) - \Big(\tilde{\Pi}^{\mathrm{a}_1}\tilde{\Pi}^{\mathrm{a}_1} + \tilde{\Pi}^{\mathrm{a}_2}\tilde{\Pi}^{\mathrm{a}_2}\Big) \tag{A.51}$$

which is of the same structure as before, only the numerator of the anomalous term is more complicated. However, the second line makes obvious that the eigenvalues are of structure

$$\frac{1}{|V_{\mathrm{SC}}|} + \tilde{\Pi}^{\mathrm{n}} \pm \sqrt{\tilde{\Pi}^{\mathrm{a}_1}\tilde{\Pi}^{\mathrm{a}_1} + \tilde{\Pi}^{\mathrm{a}_2}\tilde{\Pi}^{\mathrm{a}_2}}\,, \tag{A.52}$$

already implying the cancellation.

Application to d-wave superconductivity In order to be more specific, let us consider the case of d-wave superconductivity here. We assume the momentum-dependent coupling to be separable and normalized, e. g., $V_{\boldsymbol{k}\boldsymbol{k}'} = V_{\mathrm{SC}}\varphi_d(\boldsymbol{k})\varphi_d(\boldsymbol{k}')$ and $\sum_{\boldsymbol{k}} \varphi_d^2(\boldsymbol{k}) = 1$. Furthermore, for d-wave pairing we could choose $\varphi_d(\boldsymbol{k}) = \cos k_1 - \cos k_2$. The appropriate quartic interaction term in the action hence reads

$$\mathcal{S}_{\mathrm{int}} = V_{\mathrm{SC}} \int_{k,k',q} \varphi_d(\boldsymbol{k})\varphi_d(\boldsymbol{k}')\bar{\psi}_{k+\frac{q}{2},\uparrow}\bar{\psi}_{-k+\frac{q}{2},\downarrow}\psi_{-k'+\frac{q}{2},\downarrow}\psi_{k'+\frac{q}{2},\uparrow} \tag{A.53}$$

The Hubbard-Stratonovich decoupling can be performed in complete analogy to the case of s-wave BCS superconductivity discussed previously. The crucial difference is the form factor $\varphi_d(\boldsymbol{k})$ that is now associated with the order parameter (and hence the fluctuations). We obtain

$$\mathcal{G}^{-1}_{kk'} = \begin{pmatrix} (\mathrm{i}\nu_n - \varepsilon_{\boldsymbol{k}})\,\delta_{kk'} & \Delta_{k-k'}\varphi_d(\frac{\boldsymbol{k}+\boldsymbol{k}'}{2}) \\ \bar{\Delta}_{k'-k}\varphi_d(\frac{\boldsymbol{k}+\boldsymbol{k}'}{2}) & (\mathrm{i}\nu_n + \varepsilon_{\boldsymbol{k}})\,\delta_{kk'} \end{pmatrix} \tag{A.54}$$

such that we can introduce mean-field part and fluctuations as

$$\mathcal{G}^{-1}_{\mathrm{MF};k} = \mathrm{i}\nu_n\tau_0 - \varepsilon_{\boldsymbol{k}}\tau_3 + \Delta_d\varphi_d(\boldsymbol{k})\tau_1 \tag{A.55}$$

$$\text{and} \qquad H_{kk'} = \varphi_d\Big(\tfrac{\boldsymbol{k}+\boldsymbol{k}'}{2}\Big)[\eta_{1,k-k'}\tau_1 - \eta_{2,k-k'}\tau_2]\,. \tag{A.56}$$

Finally, the polarization bubble is introduced as

$$\frac{1}{2}\,\mathrm{Tr}(\mathcal{G}_{\mathrm{MF};k}H_{kk'}\mathcal{G}_{\mathrm{MF};k'}H_{k'k}) = \sum_{i,j}\int_q \eta_{i,q}(\tilde{\Pi}_q)_{ij}\eta_{j,-q} \tag{A.57a}$$

$$\text{where} \qquad (\tilde{\Pi}_q)_{ij} = \frac{(-1)^{i+j}}{2}\int_k \varphi_d^2(\boldsymbol{k})\,\mathrm{tr}[\mathcal{G}_{\mathrm{MF};k+\frac{q}{2}}\tau_i\mathcal{G}_{\mathrm{MF};k-\frac{q}{2}}\tau_j]\,. \tag{A.57b}$$

This is of the same structure in Nambu space as the BCS result. Consequently, potentially large contributions always come with opposite signs.

B Appendix B

Disorder in multi-band systems

This appendix provides technical details on the inclusion of disorder in a multi-band system, mainly focusing on the generalization of the disorder correlator introduced for single-band superconductors in Eq. (1.15) in Sec. 1.3.2. Thereby, this appendix provides details on our discussion of Chaps. 2, 3, and 4. Specifics on our discussion in the context of iCDW impurities in iron-based superconductors are provided in Sec. B.2 whereas details on the disorder correlator within the patch approximation of $LaAlO_3/SrTiO_3$ can be found in Sec. B.3. The notation used throughout this appendix has been introduced in App. A and the main text.

B.1 Generalization of the disorder correlator

This section provides various generalizations of quantities introduced in Sec. 1.3.2 to more complicated systems. For instance, impurities could have a magnetic moment that interacts with the scattered electrons, or the fermionic states could be characterized by further quantum numbers such as their orbital character. Furthermore, scattering effects could be spatially extended, i. e., nonlocal. In its most general form, the quadratic Hamiltonian for impurity scattering in real space reads as

$$\hat{\mathcal{H}}_{\text{dis}} = \sum_{\alpha,\alpha'} \sum_{\sigma,\sigma'} \int_{\boldsymbol{r},\boldsymbol{r}'} \hat{\psi}^\dagger_{\alpha,\sigma}(\boldsymbol{r}) W^{\sigma\sigma'}_{\alpha\alpha'}(\boldsymbol{r},\boldsymbol{r}') \hat{\psi}_{\alpha',\sigma'}(\boldsymbol{r}') \,, \tag{B.1}$$

where σ denotes spin and we use a multi-index α to comprise all further quantum numbers into one additional index for fermionic creation and annihilation operators $\hat{\psi}^\dagger_{\alpha,\sigma}(\boldsymbol{r})$ and $\hat{\psi}_{\alpha,\sigma}(\boldsymbol{r})$.

B.1.1 Multi-orbital and multi-band systems

Diagonalization of the quadratic part of a clean system with additional orbital degrees of freedom leads to a band-basis formulation where electronic states are characterized by an additional band index λ. We consider non-spin-magnetic disorder here, and thus, for the sake of clarity, suppress the spin indices in the remainder. To keep the discussion as general as possible, we proceed using the multi-index α which could refer to orbitals and bands as well as to patches of the Fermi surface as introduced in Sec. 3.1.3. Again, for simplicity, we restrict our discussion to spatially local, uncorrelated Gaussian disorder,

$$\hat{\mathcal{H}}_{\text{dis}} = \sum_{\alpha,\alpha'} \int_{\boldsymbol{r}} \hat{\psi}^\dagger_{\alpha}(\boldsymbol{r}) W_{\alpha\alpha'}(\boldsymbol{r}) \hat{\psi}_{\alpha'}(\boldsymbol{r}) \tag{B.2}$$

and

$$\Gamma_{\alpha_1\alpha_1',\alpha_2\alpha_2'}(\boldsymbol{r}_1;\boldsymbol{r}_2) := \Big\langle W_{\alpha_1\alpha_1'}(\boldsymbol{r}_1) W_{\alpha_2\alpha_2'}(\boldsymbol{r}_2)\Big\rangle_{\text{dis}} = \Gamma_{\alpha_1\alpha_1',\alpha_2\alpha_2'}(\boldsymbol{r}_1;\boldsymbol{r}_1)\,\delta(\boldsymbol{r}_1-\boldsymbol{r}_2)\,, \tag{B.3}$$

where the last equality reflects the assumption of uncorrelated disorder. If the disorder is furthermore homogeneous[1] but the potential depends on further degrees of freedom of the scattered electrons, we can introduce several constant scattering rates $\Gamma_{\alpha_1\alpha_1',\alpha_2\alpha_2'}$ labeled by the respective quantum numbers α_i. For example, if the Fermi surface can be partitioned into several patches such that scattering processes within and between such patches can be characterized by constant scattering rates, these scattering rates are solely characterized by the respective patch indices.

Another important example arises when we allow for a variation of the potential on length scales $\ll 1/k_\text{F}$, inflicting a weak momentum dependence on the correlator. In the case of a disconnected Fermi surface where the individual pockets of the Fermi surface are small and separated by a large momentum $|\boldsymbol{Q}| \gg k_\text{F}$ this implies that the correlator in momentum space can be characterized by band indices only[2] and small deviations of the momentum from the Γ point and $\boldsymbol{Q}$ can be neglected,

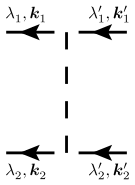

$$\equiv \Gamma_{(\lambda_1\boldsymbol{k}_1)(\lambda_1'\boldsymbol{k}_1'),(\lambda_2\boldsymbol{k}_2)(\lambda_2'\boldsymbol{k}_2')} = \Gamma_{\lambda_1\lambda_1',\lambda_2\lambda_2'}(2\pi)^d\,\delta(\boldsymbol{k}_1+\boldsymbol{k}_2-\boldsymbol{k}_1'-\boldsymbol{k}_2'+\boldsymbol{K})\,, \tag{B.4}$$

where $\boldsymbol{K}$ is a vector from the reciprocal lattice. The conservation of quasi-momentum also imposes restrictions on the possible combinations of band indices, see Fig. 2.2 for a summary of allowed scattering processes in the two-band model of the iron-based superconductors. Since they differ in their effect on, e. g., superconductivity, we categorize scattering processes into *intraband* scattering processes, characterized by the respective intraband scattering rate

$$\Gamma_\lambda := \Gamma_{\lambda\lambda,\lambda\lambda}\,, \tag{B.5}$$

and several types of *interband* scattering processes. We refer to Sec. 2.2.1 and App. C.2 for a discussion of the effect of these scattering processes on the superconducting transition temperature T_c.

B.1.2 Spatially extended effects

Let us now revoke the assumption of spatially local disorder and consider

$$\hat{\mathcal{H}}_\text{dis} = \sum_{\alpha,\alpha'}\int \text{d}\boldsymbol{r}\,\text{d}\boldsymbol{r}'\,\hat{\psi}_\alpha^\dagger(\boldsymbol{r}) W_{\alpha\alpha'}(\boldsymbol{r},\boldsymbol{r}')\hat{\psi}_{\alpha'}(\boldsymbol{r}') \tag{B.6a}$$

$$= \sum_{\alpha,\alpha'}\int \text{d}\boldsymbol{r}\,\text{d}\boldsymbol{r}'\,\hat{\psi}_\alpha^\dagger(\boldsymbol{r})\Big[\sum_{i=1}^N u_{\alpha\alpha'}(\boldsymbol{r}-\boldsymbol{R}_i,\boldsymbol{r}'-\boldsymbol{R}_i)\Big]\hat{\psi}_{\alpha'}(\boldsymbol{r}') \tag{B.6b}$$

instead. In order to consider extended effects around each impurity, the latter formulation in terms of the individual impurity potentials $u(\boldsymbol{r},\boldsymbol{r}')$ is a better starting point since it allows to express the

[1] The disorder is homogeneous in the sense that $W_{\alpha\alpha'}(\boldsymbol{r}) = W_{\alpha\alpha'}\sum_{i=1}^N \delta(\boldsymbol{r}-\boldsymbol{R}_i)$ where $\boldsymbol{R}_i$ are the positions of N randomly distributed impurities.

[2] This simplification is, for example, applicable to the family of iron-based superconductors.

correlator in terms of the individual impurity potentials,

$$\Gamma_{\alpha_1\alpha_1',\alpha_2\alpha_2'}(\boldsymbol{r}_1,\boldsymbol{r}_1';\boldsymbol{r}_2,\boldsymbol{r}_2') = \left\langle \sum_{i=1}^{N} u_{\alpha_1\alpha_1'}(\boldsymbol{r}_1-\boldsymbol{R}_i,\boldsymbol{r}_1'-\boldsymbol{R}_i) \sum_{j=1}^{N} u_{\alpha_2\alpha_2'}(\boldsymbol{r}_2-\boldsymbol{R}_j,\boldsymbol{r}_2'-\boldsymbol{R}_j) \right\rangle_{\mathrm{dis}} \tag{B.7}$$

$$= \sum_{i=1}^{N} \left\langle u_{\alpha_1\alpha_1'}(\boldsymbol{r}_1-\boldsymbol{R}_i,\boldsymbol{r}_1'-\boldsymbol{R}_i) u_{\alpha_2\alpha_2'}(\boldsymbol{r}_2-\boldsymbol{R}_i,\boldsymbol{r}_2'-\boldsymbol{R}_i) \right\rangle_{\mathrm{dis}} + \sum_{i\neq j} \left\langle u_{\alpha_1\alpha_1'}(\boldsymbol{r}_1-\boldsymbol{R}_i,\boldsymbol{r}_1'-\boldsymbol{R}_i) u_{\alpha_2\alpha_2'}(\boldsymbol{r}_2-\boldsymbol{R}_j,\boldsymbol{r}_2'-\boldsymbol{R}_j) \right\rangle_{\mathrm{dis}} , \tag{B.8}$$

where the first term contains all contributions from two scattering events at the same impurity whereas the second term contains only contributions from unrelated scattering events off different impurities. The latter contribution can be absorbed into a shift of the chemical potential, and we end up with the following generalization of the disorder correlator in momentum space

$$\Gamma_{(\alpha_1\boldsymbol{k}_1)(\alpha_1'\boldsymbol{k}_1'),(\alpha_2\boldsymbol{k}_2)(\alpha_2'\boldsymbol{k}_2')} = \sum_{i=1}^{N} \left\langle \mathrm{e}^{\mathrm{i}(\boldsymbol{k}_1-\boldsymbol{k}_1'+\boldsymbol{k}_2-\boldsymbol{k}_2')\cdot\boldsymbol{R}_i} u_{(\alpha_1\boldsymbol{k}_1)(\alpha_1'\boldsymbol{k}_1')} u_{(\alpha_2\boldsymbol{k}_2)(\alpha_2'\boldsymbol{k}_2')} \right\rangle_{\mathrm{dis}} \tag{B.9}$$

$$= n_{\mathrm{imp}} u_{(\alpha_1\boldsymbol{k}_1)(\alpha_1'\boldsymbol{k}_1')} u_{(\alpha_2\boldsymbol{k}_2)(\alpha_2'\boldsymbol{k}_2')} (2\pi)^d \,\delta(\boldsymbol{k}_1+\boldsymbol{k}_2-\boldsymbol{k}_1'-\boldsymbol{k}_2'+\boldsymbol{K}) , \tag{B.10}$$

implying that the impurity line can be expressed in terms of the matrix elements $u_{(\alpha\boldsymbol{k})(\alpha'\boldsymbol{k}')}$ of the contribution of a single impurity at $\boldsymbol{R}=\boldsymbol{0}$.

B.2 Application: iCDW impurities in iron-based superconductors

This section provides details for the discussion of scattering on a specific type of orbital-magnetic impurities, resulting from nucleation of iCDW order around nonmagnetic impurities in FeSCs, as discussed in Sec. 2.3.2.

In momentum space, the matrix element of an iCDW impurity at $\boldsymbol{R}=\boldsymbol{0}$ is given by

$$u^{\mathrm{iCDW}}_{(\lambda\boldsymbol{k})(\lambda'\boldsymbol{k}')} = \mathrm{i}\,U_0 \sum_s \mathrm{e}^{\mathrm{i}(\boldsymbol{k}-\boldsymbol{k}'+\boldsymbol{Q})\cdot\boldsymbol{R}_s} \left(\delta_{\lambda 1}\,\delta_{\lambda' 2} - \delta_{\lambda 2}\,\delta_{\lambda' 1}\right) . \tag{B.11}$$

Hence the impurity line amounts to

$$\Gamma^{\mathrm{iCDW}}_{(\lambda_1\boldsymbol{k}_1)(\lambda_1'\boldsymbol{k}_1'),(\lambda_2\boldsymbol{k}_2)(\lambda_2'\boldsymbol{k}_2')} = -n_{\mathrm{imp}} U_0^2 \sum_{s,s'} \mathrm{e}^{\mathrm{i}(\boldsymbol{k}_1-\boldsymbol{k}_1'+\boldsymbol{Q})\cdot\boldsymbol{R}_s + \mathrm{i}(\boldsymbol{k}_2-\boldsymbol{k}_2'+\boldsymbol{Q})\cdot\boldsymbol{R}_{s'}} \,\delta^{\mathrm{iCDW}}_{\lambda_1\lambda_1',\lambda_2\lambda_2'} , \tag{B.12}$$

where momentum conservation following from $(2\pi)^2\,\delta(\boldsymbol{k}_1+\boldsymbol{k}_2-\boldsymbol{k}_1'-\boldsymbol{k}_2'+\boldsymbol{K})$ is implied and we introduced

$$\delta^{\mathrm{iCDW}}_{\lambda_1\lambda_1',\lambda_2\lambda_2'} = (\delta_{\lambda_1 1}\,\delta_{\lambda_1' 2} - \delta_{\lambda_1 2}\,\delta_{\lambda_1' 1})(\delta_{\lambda_2 1}\,\delta_{\lambda_2' 2} - \delta_{\lambda_2 2}\,\delta_{\lambda_2' 1}) = \begin{cases} -1 & \text{for } \lambda_1=\lambda_2'\neq\lambda_2=\lambda_1' , \\ +1 & \text{for } \lambda_1=\lambda_2\neq\lambda_2'=\lambda_1' , \\ 0 & \text{otherwise} . \end{cases} \tag{B.13}$$

Therefore, only the interband scattering processes $\Gamma^{\mathrm{iCDW}}_{\lambda\bar{\lambda},\bar{\lambda}\lambda}$ and $\Gamma^{\mathrm{iCDW}}_{\lambda\bar{\lambda},\lambda\bar{\lambda}}$ are associated with finite scattering rates.

We are primarily interested in the phase of $\Gamma_{12,12} = \Gamma_{12} e^{i\phi}$, but start by noting that the imaginary part of the impurity line of any scattering process generated by an iCDW impurity vanishes generically in a lattice preserving inversion symmetry since

$$\begin{aligned}\operatorname{Im}\Gamma_{(\lambda_1\boldsymbol{k}_1)(\lambda_1'\boldsymbol{k}_1'),(\lambda_2\boldsymbol{k}_2)(\lambda_2'\boldsymbol{k}_2')} &= -n_{\text{imp}}U_0^2\,\delta^{\text{iCDW}}_{\lambda_1\lambda_1',\lambda_2\lambda_2'}\operatorname{Im}\Big[\sum_{s,s'} e^{i(\boldsymbol{k}_1-\boldsymbol{k}_1'+\boldsymbol{Q})\cdot\boldsymbol{R}_s+i(\boldsymbol{k}_2-\boldsymbol{k}_2'+\boldsymbol{Q})\cdot\boldsymbol{R}_{s'}}\Big] \\ &= -n_{\text{imp}}U_0^2\,\delta^{\text{iCDW}}_{\lambda_1\lambda_1',\lambda_2\lambda_2'}\sum_{s,s'}\sin\Big((\boldsymbol{k}_1-\boldsymbol{k}_1'+\boldsymbol{Q})\cdot\boldsymbol{R}_s+(\boldsymbol{k}_2-\boldsymbol{k}_2'+\boldsymbol{Q})\cdot\boldsymbol{R}_{s'}\Big) \\ &= 0 \end{aligned} \tag{B.14}$$

due to the antisymmetry of the sine function.

Keeping in mind that a global prefactor of -1 corresponds to a phase of $\phi = \pi$, we evaluate the impurity line $\Gamma_{12,12}$ for an inversion-symmetric lattice as it is appropriate for the FeSCs. As discussed in App. B.1.1, the momentum dependence within the bands can be neglected. Finally, by assuming that the impurity effects can be restricted to nearest neighbors, we obtain

$$\begin{aligned}\Gamma_{12,12} &= -n_{\text{imp}}U_0^2\,\delta^{\text{iCDW}}_{12,12}\sum_{s\in\text{NN}_{\boldsymbol{R}=\boldsymbol{0}}}1\sum_{s'\in\text{NN}_{\boldsymbol{R}=\boldsymbol{0}}}1 \\ &= -n_{\text{imp}}U_0^2N_{\text{NN}}^2 = n_{\text{imp}}U_0^2N_{\text{NN}}^2e^{i\pi}\,, \end{aligned} \tag{B.15}$$

where we denote the number of nearest neighbors by N_{NN}.

B.3 Application: patch approximation for LAO/STO

In this section, we briefly comment on how the patch approximation for the Fermi surface of the LAO/STO interface [48] can be exploited to study impurity scattering in these systems. A detailed presentation can be found in our original publication [150], and here we briefly summarize the main results.

Ref. 150 identified two symmetry constraints for the disorder correlator. Firstly, the disorder correlator should transform trivially under each operation g of the point group, implying the constraint

$$\Gamma'_{\alpha_1\alpha_1',\alpha_2\alpha_2'} = (\mathcal{R}_\psi(g))_{\alpha_1\tilde{\alpha}_1}(\mathcal{R}_\psi(g))_{\alpha_2\tilde{\alpha}_2}\Gamma'_{\tilde{\alpha}_1\tilde{\alpha}_1',\tilde{\alpha}_2\tilde{\alpha}_2'}(\mathcal{R}_\psi^\dagger(g))_{\tilde{\alpha}_2'\alpha_2'}(\mathcal{R}_\psi^\dagger(g))_{\tilde{\alpha}_1'\alpha_1'}\,, \tag{B.16}$$

where $\mathcal{R}_\psi(g)$ is the representation of g on wave functions. Secondly, the transformation behavior with respect to time reversal $\hat{\Theta} = \hat{\mathcal{T}}\hat{\mathcal{K}}$ is of interest since magnetic and nonmagnetic disorder is expected to have different effects. Nonmagnetic (i. e., symmetric w. r. t. time reversal, $\sigma = 1$) and magnetic (i. e., antisymmetric w. r. t. time reversal, $\sigma = -1$) disorder realizations are characterized by the condition

$$\Gamma'_{\alpha_1\alpha_1',\alpha_2\alpha_2'} = \sigma\mathcal{T}_{\alpha_1\tilde{\alpha}_1}\Gamma'_{\tilde{\alpha}_1'\tilde{\alpha}_1,\alpha_2\alpha_2'}(\mathcal{T}^{-1})_{\tilde{\alpha}_1'\alpha_1'}\,. \tag{B.17}$$

In Ref. 150, these symmetry constraints were used to construct the most general disorder vertex for nonmagnetic and magnetic impurities, respectively. For that purpose, the expansion

$$\Gamma_{\alpha_1\alpha_1',\alpha_2\alpha_2'} = \sum_{\mu,\mu'}C_{\mu\mu'}(w_\mu)_{\alpha_1\alpha_1'}(w_{\mu'})_{\alpha_2\alpha_2'} \tag{B.18}$$

in terms of Hermitian matrices $\{w_\mu\}$ was considered, where the expansion coefficients C are real and symmetric, $C = C^* = C^T$ as a consequence of the Hermiticity of each disorder realization W. A

convenient choice for the set of Hermitian matrices that forms the basis are the tensor products of Pauli matrices σ_i and τ_i ($i \in \{0,1,2,3\}$) in spin and orbital space, respectively. This results in the expressions (3.12) as well as (3.19) and (3.20) for the most general disorder vertices for nonmagnetic and magnetic impurities, respectively.

In order to express these disorder correlators in the patch approximation, we use the four eigenstates $\phi_{\alpha,\boldsymbol{k}}$ of the noninteracting part of the Hamiltonian $h(\boldsymbol{k})$ and introduce the operators

$$\hat{\psi}_{\alpha,\boldsymbol{k}} = (\phi_{\beta,\boldsymbol{k}})_\alpha \hat{f}_{\beta,\boldsymbol{k}} \qquad \text{and} \qquad \hat{\psi}^\dagger_{\alpha,\boldsymbol{k}} = \hat{f}^\dagger_{\beta,\boldsymbol{k}} (\phi^*_{\beta,\boldsymbol{k}})_\alpha \,. \tag{B.19}$$

After transforming the disorder correlator to the new basis, we can exploit the patch approximation: As the wave functions $\phi_{\alpha,\boldsymbol{k}}$ are approximately constant in the respective patches of the Fermi surface introduced in Fig. 3.1 (c), we assume perfect spin and orbital polarization of each patch and make the substitution $\phi_{\alpha,\boldsymbol{k}} \to \phi_{(\lambda,j,\eta)}$ and $\hat{f}_{\alpha,\boldsymbol{k}} \to \hat{f}_{(\lambda,j,\eta),\boldsymbol{k}}$. Here, λ labels the two sheets of the Fermi surface, $j \in \{1,2,3,4\}$ refers to the patches of the Fermi surface, and $\eta \in \{+,-\}$ specifies whether $k_1 + k_2 > 0$ or $k_1 + k_2 < 0$, respectively. Note that, from now on, whenever referring to the patch notation, we denote the momentum deviation from the center of the respective patch by $\boldsymbol{k}$ rather than the absolute momentum. Using the multi-index notation $\tau \equiv (\lambda, j, \eta)$, the disorder correlator in patch approximation is finally given by

$$\Gamma^{\mathrm{PA}}_{\tau_1\tau_1',\tau_2\tau_2'} = \sum_{\mu,\mu'} C_{\mu\mu'} (\phi^\dagger_{\tau_1} w_\mu \phi_{\tau_1'})(\phi^\dagger_{\tau_2} w_{\mu'} \phi_{\tau_2'}) \,. \tag{B.20}$$

(The appropriate phase convention for the eigenstates that reproduces the results from Ref. 48 is $\hat{\Theta}\phi_{(\lambda,j,\eta)} = -\mathrm{i}\eta\phi_{(\lambda,j,-\eta)}$.) This results in the tensor Γ^{PA} with 16^4 index combinations. Fortunately, for the calculation of the transition temperature, only certain combinations are important, which can be summarized into matrices $\mathcal{S}$ and $\mathcal{V}$ as introduced in Eqs. (3.8) and (3.9), respectively. In Sec. C.4, we provide two examples of such matrices in patch approximation.

Appendix C

C Pair breaking in multi-orbital superconductors

Here, we present details on the calculation of the superconducting transition temperature T_c. Thereby, this appendix complements our discussion of the robustness of s^{++} and s^{+-} pairing states in the context of iron-based superconductors (Chap. 2) and the $LaAlO_3/SrTiO_3$ interface (Chap. 3). We start with a discussion of the clean two-band model and then introduce disorder as described in App. B. Details on the application of the matrix formalism presented here can be found in Sec. C.3, while the application to the $LaAlO_3/SrTiO_3$ interface is summarized in Sec. C.4.

C.1 Two-band model

We consider a two-band model in the following, where $\lambda \in \{1,2\}$ labels the two bands. We assume superconductivity to result from interband pair hopping, described by the quartic interaction

$$\mathcal{S}_{\text{int}} = V_{\text{SC}} \sum_{j,j'} \int_{k\in\mathcal{P}_j, k'\in\mathcal{P}_{j'}} \left[\bar{\psi}_{1,j,+}(k)\bar{\psi}_{1,j,-}(-k)\psi_{2,j',-}(-k')\psi_{2,j',+}(k') + \text{G. c.}\right] . \tag{C.1}$$

Here, we artificially split (each pocket of) the Fermi surface into two half spaces, labeled by the branch index $\eta = +$ ($\eta = -$) for states with $k_1 + k_2 > 0$ ($k_1 + k_2 < 0$) in the case of a quasi-2D Fermi surface. Furthermore, we could introduce several patches of the Fermi surface and label them with $j \in \{1, \ldots, p\}$. This partitioning of the Fermi surface is done such that all states within one patch are characterized by the same orbital and spin quantum numbers. Furthermore, the states represented by the fermionic fields $\psi_{\lambda,j,+}(k)$ and $\psi_{\lambda,j,-}(-k)$ should be related by time reversal, that is, they are characterized by opposite spin. For LAO/STO, the respective partitioning is shown in Fig. 3.1 (c).

In the case of materials like the iron-based superconductors, where the Fermi surface is degenerate w. r. t. spin, we artificially split the Fermi surface in two parts, labeled by an additional index ν. Each of these parts is assigned a spin quantum number such that again, $(\lambda, \nu, j, +)$ and $(\lambda, \nu, j, -)$ are connected by time reversal. In the end, this would amount to a factor 2 which would be compensated by the a redefinition of the DOS. Hence, to simplify notation, we may omit the additional index ν in the remainder.

We introduce spinors in branch space as

$$\bar{\Psi}_{\lambda,j}(k) = \begin{pmatrix}\bar{\psi}_{\lambda,j,+}(k) & \bar{\psi}_{\lambda,j,-}(-k)\end{pmatrix} \qquad \text{and} \qquad \Psi^T_{\lambda,j}(k) = \begin{pmatrix}\psi_{\lambda,j,+}(k) & \psi_{\lambda,j,-}(-k)\end{pmatrix} \tag{C.2}$$

in order to rewrite the interaction part of the action as

$$\mathcal{S}_{\text{int}} = V_{\text{SC}} \sum_{j,j'} \int_{k\in\mathcal{P}_j, k'\in\mathcal{P}_{j'}} \left[\left(\tfrac{1}{2} \bar{\Psi}_{1,j}(k)(\mathrm{i}\hat{\tau}_2)\bar{\Psi}^T_{1,j}(k) \right) \times \left(\tfrac{1}{2} \Psi^T_{2,j'}(k')(-\mathrm{i}\hat{\tau}_2)\Psi_{2,j'}(k') \right) + \text{G. c.} \right] . \tag{C.3}$$

Here, $\hat{\tau}_2$ is a Pauli matrix in branch space and the factor $\frac{1}{2}$ stems from antisymmetrization. We further introduce the fields

$$\bar{b}_\lambda = \tfrac{1}{2} \sum_j \int_{k\in\mathcal{P}_j} \bar{\Psi}_{\lambda,j}(k)(\mathrm{i}\hat{\tau}_2)\bar{\Psi}^T_{\lambda,j}(k) \qquad \text{and} \qquad b_\lambda = \tfrac{1}{2} \sum_j \int_{k\in\mathcal{P}_j} \Psi^T_{\lambda,j}(k)(-\mathrm{i}\hat{\tau}_2)\Psi_{\lambda,j}(k) \tag{C.4}$$

and rewrite

$$\mathcal{S}_{\text{int}} = V_{\text{SC}} \begin{pmatrix} \bar{b}_1 & \bar{b}_2 \end{pmatrix} \begin{pmatrix} 0 & 1 \\ 1 & 0 \end{pmatrix} \begin{pmatrix} b_1 \\ b_2 \end{pmatrix} . \tag{C.5}$$

Since the coupling matrix is not positive definite (for neither $V_{\text{SC}} > 0$ nor $V_{\text{SC}} < 0$), we need to diagonalize the interaction part of the action before performing the decoupling for different channels separately. This can be done by introducing the fields

$$\bar{b}_\pm = \frac{1}{\sqrt{2}}(\bar{b}_1 \pm \bar{b}_2) \qquad \text{and} \qquad b_\pm = \frac{1}{\sqrt{2}}(b_1 \pm b_2) , \tag{C.6}$$

resulting in

$$\mathcal{S}_{\text{int}} = V_{\text{SC}}(\bar{b}_+ b_+ - \bar{b}_- b_-) . \tag{C.7}$$

Finally, this can be decoupled by the following Hubbard-Stratonovich transformations:

$$\mathrm{e}^{|V_{\text{SC}}|\bar{b}_\pm b_\pm} = \int \mathcal{D}[\bar{\Delta}_\pm, \Delta_\pm]\, \mathrm{e}^{-\frac{1}{|V_{\text{SC}}|}|\Delta_\pm|^2 + \bar{b}_\pm\Delta_\pm + \bar{\Delta}_\pm b_\pm} , \tag{C.8}$$

$$\mathrm{e}^{-|V_{\text{SC}}|\bar{b}_\pm b_\pm} = \int \mathcal{D}[\bar{\Delta}_\pm, \Delta_\pm]\, \mathrm{e}^{-\frac{1}{|V_{\text{SC}}|}|\Delta_\pm|^2 + \mathrm{i}\bar{b}_\pm\Delta_\pm + \mathrm{i}\bar{\Delta}_\pm b_\pm} . \tag{C.9}$$

Attractive interaction Let us first assume an attractive interaction $V_{\text{SC}} < 0$ and perform the decoupling,

$$\begin{aligned} \mathrm{e}^{-\mathcal{S}_{\text{int}}} = &\int \mathcal{D}[\bar{\Delta}_+, \Delta_+]\, \mathrm{e}^{-\frac{1}{|V_{\text{SC}}|}|\Delta_+|^2 + \frac{1}{\sqrt{2}}(\bar{b}_1+\bar{b}_2)\Delta_+ + \frac{1}{\sqrt{2}}\bar{\Delta}_+(b_1+b_2)} \\ &\times \int \mathcal{D}[\bar{\Delta}_-, \Delta_-]\, \mathrm{e}^{-\frac{1}{|V_{\text{SC}}|}|\Delta_-|^2 + \frac{\mathrm{i}}{\sqrt{2}}(\bar{b}_1-\bar{b}_2)\Delta_- + \frac{\mathrm{i}}{\sqrt{2}}\bar{\Delta}_-(b_1-b_2)} . \end{aligned} \tag{C.10}$$

Then, the interaction together with the usual noninteracting part $\mathcal{S}_0$ (as stated in Eq. (A.1)) can be brought to the form

$$\mathrm{e}^{-(\mathcal{S}_0+\mathcal{S}_{\text{int}})} = \int \mathcal{D}[\bar{\Delta}, \Delta]\, \mathrm{e}^{-\frac{1}{|V_{\text{SC}}|}(|\Delta_+|^2+|\Delta_-|^2) - \sum_{j,j'} \int_{k\in\mathcal{P}_j, k'\in\mathcal{P}_{j'}} \bar{\Psi}_{j,k}(-\mathcal{G}^{-1}_{j,j',k,k'})\Psi_{j',k'}} \tag{C.11}$$

by introducing the Nambu spinors

$$\bar{\Psi}_{k,j} = \begin{pmatrix} \bar{\Psi}_{1,j}(k) & \Psi^T_{1,j}(k) & \bar{\Psi}_{2,j}(k) & \Psi^T_{2,j}(k) \end{pmatrix} \qquad \text{and} \qquad \Psi_{k,j} = \begin{pmatrix} \Psi_{1,j}(k) \\ \bar{\Psi}^T_{1,j}(k) \\ \Psi_{2,j}(k) \\ \bar{\Psi}^T_{2,j}(k) \end{pmatrix} . \tag{C.12}$$

Furthermore, the inverse Nambu Green's function is introduced as

$$\mathcal{G}^{-1}_{j,j',k,k'} = \delta_{j,j'}\,\delta_{k,k'}(\mathcal{G}_0^{-1} + \mathcal{U})_{j,k} \tag{C.13a}$$

$$\text{with} \qquad \mathcal{G}_0^{-1} = \frac{1}{2}\begin{pmatrix} G^{-1}_{0;1,j}(k) & 0 & 0 & 0 \\ 0 & -G^{-1}_{0;1,j}(k) & 0 & 0 \\ 0 & 0 & G^{-1}_{0;2,j}(k) & 0 \\ 0 & 0 & 0 & -G^{-1}_{0;2,j}(k) \end{pmatrix} \tag{C.13b}$$

$$\text{and} \qquad \mathcal{U} = \frac{1}{2}\begin{pmatrix} 0 & (\mathrm{i}\hat{\tau}_2)\frac{\Delta_+ + \mathrm{i}\Delta_-}{\sqrt{2}} & 0 & 0 \\ (-\mathrm{i}\hat{\tau}_2)\frac{\bar{\Delta}_+ + \mathrm{i}\bar{\Delta}_-}{\sqrt{2}} & 0 & 0 & 0 \\ 0 & 0 & 0 & (\mathrm{i}\hat{\tau}_2)\frac{\Delta_+ - \mathrm{i}\Delta_-}{\sqrt{2}} \\ 0 & 0 & (-\mathrm{i}\hat{\tau}_2)\frac{\bar{\Delta}_+ - \mathrm{i}\bar{\Delta}_-}{\sqrt{2}} & 0 \end{pmatrix}. \tag{C.13c}$$

Here, the noninteracting Green's functions $G^{-1}_{0;\lambda,j}(k)$ should be understood as matrices in η-space, $[G^{-1}_{0;\lambda,j}(k)]_{\eta\eta'} = \delta_{\eta\eta'}\,G^{-1}_{0;\lambda,j,\eta}(\eta k) = \delta_{\eta\eta'}(\eta \mathrm{i}\nu_n - \varepsilon_{\lambda,j,\eta,\eta\boldsymbol{k}})$.

Repulsive interaction Analogously, we consider repulsive interaction by assuming $V_{\mathrm{SC}} > 0$. Then the factor i is associated with Δ_+ rather than with Δ_-. Therefore, the treatment of repulsive interaction only differs in the expression that we obtain for $\mathcal{U}$ here,

$$\mathcal{U} = \frac{1}{2}\begin{pmatrix} 0 & (\mathrm{i}\hat{\tau}_2)\frac{\mathrm{i}\Delta_+ + \Delta_-}{\sqrt{2}} & 0 & 0 \\ (-\mathrm{i}\hat{\tau}_2)\frac{\mathrm{i}\bar{\Delta}_+ + \bar{\Delta}_-}{\sqrt{2}} & 0 & 0 & 0 \\ 0 & 0 & 0 & (\mathrm{i}\hat{\tau}_2)\frac{\mathrm{i}\Delta_+ - \Delta_-}{\sqrt{2}} \\ 0 & 0 & (-\mathrm{i}\hat{\tau}_2)\frac{\mathrm{i}\bar{\Delta}_+ - \bar{\Delta}_-}{\sqrt{2}} & 0 \end{pmatrix}. \tag{C.14}$$

Effective action As a next step, we integrate out the fermions. Then, the partition function can be expressed as

$$\mathcal{Z} = \int \mathcal{D}[\bar{\psi},\psi]\,\mathrm{e}^{-(\mathcal{S}_0+\mathcal{S}_{\mathrm{int}})} = \int \mathcal{D}[\bar{\Delta},\Delta]\,\mathrm{e}^{-\frac{1}{|V_{\mathrm{SC}}|}(|\Delta_+|^2+|\Delta_-|^2)+\mathrm{Tr}\ln(-\mathcal{G}^{-1})} \tag{C.15}$$

$$=: \mathcal{Z}_0 \int \mathcal{D}[\bar{\Delta},\Delta]\,\mathrm{e}^{-\mathcal{S}_{\mathrm{eff}}(\bar{\Delta},\Delta)}\,. \tag{C.16}$$

In the last line, we introduced the partition function $\mathcal{Z}_0$ of a noninteracting system as

$$\mathcal{Z}_0 = \mathrm{e}^{\mathrm{Tr}\ln(-\mathcal{G}_0^{-1})} \tag{C.17}$$

by using $\ln(-\mathcal{G}^{-1}) = \ln(-\mathcal{G}_0^{-1}(\mathbb{1} + \mathcal{G}_0\mathcal{U}))$. Furthermore, we introduced the effective action as

$$\mathcal{S}_{\mathrm{eff}}[\bar{\Delta},\Delta] = \frac{1}{|V_{\mathrm{SC}}|}(|\Delta_+|^2 + |\Delta_-|^2) - \mathrm{Tr}\ln(\mathbb{1} + \mathcal{G}_0\mathcal{U}) \tag{C.18}$$

$$\approx \frac{1}{|V_{\mathrm{SC}}|}(|\Delta_+|^2 + |\Delta_-|^2) + \frac{1}{2}\,\mathrm{Tr}(\mathcal{G}_0\mathcal{U}\mathcal{G}_0\mathcal{U})\,. \tag{C.19}$$

Since the transition temperature can be obtained from the quadratic coefficient of a Ginzburg-Landau expansion, we already expanded the ln-term according to $\ln(1+x) = x - \frac{x^2}{2} + \mathcal{O}(x^3)$ in the last line. (Note that $\mathrm{Tr}(\mathcal{G}_0\mathcal{U})$ vanishes.) Using the above definitions, the trace can be evaluated straightforwardly

$$\begin{aligned}\mathrm{Tr}(\mathcal{G}_0\mathcal{U}\mathcal{G}_0\mathcal{U}) = \operatorname{sgn} V_{\mathrm{SC}} \sum_j \int_{k\in\mathcal{P}_j} \mathrm{tr}_\eta \Big[& G_{0;1,j}(k)(\mathrm{i}\hat{\tau}_2)G_{0;1,j}(k)(-\mathrm{i}\hat{\tau}_2) \\ & + G_{0;2,j}(k)(\mathrm{i}\hat{\tau}_2)G_{0;2,j}(k)(-\mathrm{i}\hat{\tau}_2)\Big]\Big(|\Delta_+|^2 - |\Delta_-|^2\Big) \\ - \sum_j \int_{k\in\mathcal{P}_j} \mathrm{tr}_\eta \Big[& G_{0;1,j}(k)(\mathrm{i}\hat{\tau}_2)G_{0;1,j}(k)(-\mathrm{i}\hat{\tau}_2) - \\ & - G_{0;2,j}(k)(\mathrm{i}\hat{\tau}_2)G_{0;2,j}(k)(-\mathrm{i}\hat{\tau}_2)\Big]\Big(\mathrm{i}\bar{\Delta}_+\Delta_- + \mathrm{i}\Delta_+\bar{\Delta}_-\Big) \qquad \text{(C.20)} \\ = \operatorname{sgn} V_{\mathrm{SC}} \Big[d^0_{11} + d^0_{22}\Big]\Big(|\Delta_+|^2 - |\Delta_-|^2\Big) & - \mathrm{i}\Big[d^0_{11} - d^0_{22}\Big]\Big(\bar{\Delta}_+\Delta_- + \bar{\Delta}_-\Delta_+\Big). \qquad \text{(C.21)}\end{aligned}$$

The factor $\frac{1}{2}$ from $|\Delta|^2/(\sqrt{2})^2$ is canceled by the factor 2 resulting from the 4×4 matrix structure here. Furthermore, another factor $\frac{1}{2}$ from $\frac{1}{2}\,\mathrm{Tr}$ will be canceled when evaluating tr_η. In the last line, we summarized the prefactors into the expressions $d_{\lambda\lambda'}$, which have a straightforward interpretation in terms of diagrams, cf. Fig. 2.3 (a). In calculating these expressions, we use that $G_{0;\lambda,j}(k)$ is diagonal in η-space, $[G_{0;\lambda,j}(k)]_{\eta\eta'} = \delta_{\eta\eta'}\, G_{0;\lambda,j,\eta}(\eta k) = \delta_{\eta\eta'}(\eta \mathrm{i}\nu_n - \varepsilon_{\lambda,j,\eta,\eta\boldsymbol{k}})^{-1}$, and furthermore

$$(\mathrm{i}\hat{\tau}_2)_{\eta\eta'}(-\mathrm{i}\hat{\tau}_2)_{\eta'\eta} = \begin{Bmatrix} 0\,, & \eta = \eta' \\ 1\,, & \bar{\eta} = \eta' \end{Bmatrix} = \delta_{\bar{\eta}\eta'}\ . \qquad \text{(C.22)}$$

We now assume that $\varepsilon_{\lambda,j,\eta,\eta\boldsymbol{k}} \equiv \varepsilon_{\lambda,j,\eta\boldsymbol{k}}$ and furthermore $\varepsilon_{\lambda,j,\boldsymbol{k}} = \varepsilon_{\lambda,j,-\boldsymbol{k}}$ which allows us to evaluate the integrals as

$$\begin{aligned} d^0_{\lambda\lambda}(T) &= 2\sum_{j=1}^{p} \int_{k\in\mathcal{P}_j} G_{0;\lambda,j,+}(k)G_{0;\lambda,j,-}(k) = 2\sum_{j=1}^{p} T\sum_{n=-\infty}^{\infty} \rho_{\lambda,j} \int \mathrm{d}\varepsilon_{\lambda,j}\, \frac{1}{\mathrm{i}\nu_n - \varepsilon_{\lambda,j}} \frac{1}{-\mathrm{i}\nu_n - \varepsilon_{\lambda,j}} \qquad \text{(C.23)} \\ &= 2\sum_{j=1}^{p} \rho_{\lambda,j}\left[\psi_0\left(\frac{1}{2} + \frac{\Lambda}{2\pi T}\right) - \psi_0\left(\frac{1}{2}\right)\right] \qquad \text{(C.24)}\end{aligned}$$

where the factor 2 is a result of tr_η. Here, in evaluating the momentum integral, we assumed a constant DOS $\rho_{\lambda,j}$ at the Fermi level in each patch. Furthermore, we introduced the cut-off Λ which is assumed to be universal on the FS. In the remainder, we assume particle-hole symmetry and therefore set $\rho_{\lambda,j} = \frac{\rho_{\mathrm{F}}}{p}$, assuming a total DOS of ρ_{F} per band. Finally, this results in

$$d^0_{11}(T) = d^0_{22}(T) = 2\rho_{\mathrm{F}}\left[\psi_0\left(\frac{1}{2} + \frac{\Lambda}{2\pi T}\right) - \psi_0\left(\frac{1}{2}\right)\right] \approx 2\rho_{\mathrm{F}} \ln\left(\frac{2\Lambda \mathrm{e}^\gamma}{\pi T}\right). \qquad \text{(C.25)}$$

The effective action up to quadratic order can hence be recast as

$$\mathcal{S}_{\mathrm{eff}}[\bar{\Delta}, \Delta] = \begin{pmatrix} \bar{\Delta}_+ & \bar{\Delta}_- \end{pmatrix} \begin{pmatrix} a_{++}(T) & a_{+-}(T) \\ a_{-+}(T) & a_{--}(T) \end{pmatrix} \begin{pmatrix} \Delta_+ \\ \Delta_- \end{pmatrix}, \qquad \text{(C.26)}$$

implying that the sign of the eigenvalues of this quadratic form determines whether the respective eigenmode condenses. The coefficients a in this expansion can be expressed in terms of the diagrams d

as

$$a_{++}(T) = \frac{2}{|V_{\mathrm{SC}}|} + \frac{1}{2}\operatorname{sgn} V_{\mathrm{SC}}\Big[d^0_{11}(T) + d^0_{22}(T)\Big] = \frac{2}{|V_{\mathrm{SC}}|} + 2\operatorname{sgn}(V_{\mathrm{SC}})\rho_{\mathrm{F}} \ln\left(\frac{2\Lambda \mathrm{e}^{\gamma}}{\pi T}\right), \tag{C.27a}$$

$$a_{--}(T) = \frac{2}{|V_{\mathrm{SC}}|} - \frac{1}{2}\operatorname{sgn} V_{\mathrm{SC}}\Big[d^0_{11}(T) + d^0_{22}(T)\Big] = \frac{2}{|V_{\mathrm{SC}}|} - 2\operatorname{sgn}(V_{\mathrm{SC}})\rho_{\mathrm{F}} \ln\left(\frac{2\Lambda \mathrm{e}^{\gamma}}{\pi T}\right), \tag{C.27b}$$

$$a_{+-}(T) = a_{-+}(T) = -\frac{\mathrm{i}}{2}\Big[d^0_{11}(T) - d^0_{22}(T)\Big] = 0\,. \tag{C.27c}$$

SC transition If the interaction is attractive ($V_{\mathrm{SC}} < 0$), the coefficient $a_{--} > 0$ remains positive for all temperatures T. Therefore, the sign-changing s-wave (associated with the order parameter Δ_-, meaning that $\Delta_1 = -\Delta_2$) will never condense. Vice versa, for a repulsive interaction ($V_{\mathrm{SC}} > 0$), the conventional s^{++} pairing state associated with Δ_+ (i. e., $\Delta_1 = \Delta_2$) can never lower the energy. The respective other mode condenses at $T_{\mathrm{c},0}$ which is determined by the sign change of the respective coefficients, leading to the BCS expression

$$T_{\mathrm{c},0} = \frac{2\Lambda \mathrm{e}^{\gamma}}{\pi} \mathrm{e}^{-\frac{1}{|V_{\mathrm{SC}}|\rho_{\mathrm{F}}}}\,. \tag{C.28}$$

C.2 Pair breaking in the two-band model

As a next step, we consider the effect of impurities on the quadratic coefficients in order to assess the role of disorder for the two different pairing states introduced in Sec. C.1. To this end, we add quenched disorder as introduced in Eqs. (1.11) and (B.2) to the action in terms of Nambu spinors given in Eq. (C.11) as

$$\mathcal{W} = \frac{1}{2}\,\delta_{\nu_n,\nu_{n'}} \begin{pmatrix} W_{1,j,\boldsymbol{k};1,j',\boldsymbol{k}'} & 0 & W_{1,j,\boldsymbol{k};2,j',\boldsymbol{k}'} & 0 \\ 0 & -W_{1,j,j\boldsymbol{k};1,j',\boldsymbol{k}'} & 0 & -W_{1,j,\boldsymbol{k};2,j',\boldsymbol{k}'} \\ W_{2,j,\boldsymbol{k};1,j',\boldsymbol{k}'} & 0 & W_{2,j,\boldsymbol{k};2,j',\boldsymbol{k}'} & 0 \\ 0 & -W_{2,j,\boldsymbol{k};1,j',\boldsymbol{k}'} & 0 & -W_{2,j,\boldsymbol{k};2,j',\boldsymbol{k}'} \end{pmatrix} \tag{C.29}$$

This means, instead of $\frac{1}{2}\operatorname{Tr}(\mathcal{G}_0\mathcal{U}\mathcal{G}_0\mathcal{U})$, we have to calculate

$$\left\langle \frac{1}{2}\operatorname{Tr}\left[(\mathcal{G}_0^{-1} + \mathcal{W})^{-1}\mathcal{U}(\mathcal{G}_0^{-1} + \mathcal{W})^{-1}\mathcal{U}\right]\right\rangle_{\mathrm{dis}}\,. \tag{C.30}$$

Performing the disorder average leaves us with expressions that depend on disorder only via the disorder correlator $\Gamma_{\alpha_1\alpha_1',\alpha_2\alpha_2'} = \left\langle W_{\alpha_1\alpha_1'} W_{\alpha_2\alpha_2'}\right\rangle_{\mathrm{dis}}$ as introduced in Eq. (B.3). The resulting contributions to the effective action that survive disorder averaging can be summarized into self energy and vertex corrections.

Self energy and vertex corrections in self-consistent Born approximation The contributions that can be summarized into self-energy contributions come from

$$\Gamma_{(\lambda,j,\eta)(\lambda',j',\eta'),(\lambda',j',\eta')(\lambda,j,\eta)} =: \mathcal{S}_{(\lambda,j,\eta)(\lambda',j',\eta')} \equiv$$

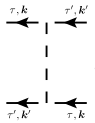

, (C.31)

whereas the vertex corrections are associated with

$$\Gamma_{(\lambda,j,\eta)(\lambda',j',\eta'),(\lambda,j,\bar{\eta})(\lambda',j',\bar{\eta}')} =: \mathcal{V}_{(\lambda,j,\eta),(\lambda',j',\eta')} \equiv \quad . \tag{C.32}$$

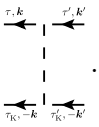

Here, we used the multi-index notation $\tau \equiv (\lambda, j, \eta)$ and denoted the corresponding Kramers partner by $\tau_{\mathrm{K}} \equiv (\lambda, j, \bar{\eta})$. This is also discussed in Sec. 2.2.1 for the two-band model of FeSCs, and in Secs. 3.1.2 and 3.1.3 for the LAO/STO interface. In the evaluation of the quadratic coefficients in the presence of disorder, we use the same assumptions as in our discussion of the clean model in Sec. C.1. In the presence of disorder, the Green's functions of the noninteracting problem are modified by a finite self energy $\Sigma_{\lambda,j,\eta}(\eta k)$, resulting in

$$G_{\lambda,j,\eta}(\eta k) = \frac{1}{\eta \mathrm{i}\nu_n - \varepsilon_{\lambda,j,\eta,\eta\boldsymbol{k}} - \Sigma_{\lambda,j,\eta}(\eta k)} \,. \tag{C.33}$$

Employing the self-consistent Born approximation (SCBA) here, we find that the self energy is given by

$$\Sigma_{\lambda,j,\eta}(\eta k) = -\mathrm{i}\pi \,\mathrm{sgn}(\eta\nu_n) \sum_{\lambda',j',\eta'} \rho_{\lambda',j'} \mathcal{S}_{(\lambda,j,\eta),(\lambda',j',\eta')} \,. \tag{C.34}$$

Correspondingly, in SCBA, i. e., upon neglecting the crossed contributions suppressed by $1/(k_{\mathrm{F}} l_{\mathrm{mfp}})$, vertex corrections can be summarized into a 'Cooperon ladder' (see Fig. 2.3 (c) for a diagrammatical representation) of all allowed scattering processes of Kramers partners, where the respective scattering processes are summarized in $\mathcal{V}$.

Since we assumed $\Gamma_{(\lambda_1,j_1,\eta_1),(\lambda_2,j_2,\eta_2,),(\lambda_3,j_3,\eta_3),(\lambda_4,j_4,\eta_4)}$ to only weakly depend on momentum (i. e., only reflected in band and patch indices), all momentum integrals decouple and it is useful to define

$$\begin{aligned} c_{\lambda,j,\eta}(\nu_n) &= \sum_{\boldsymbol{k}} G_{\lambda,j,\eta}(\boldsymbol{k},\nu_n) G_{\lambda,j,\bar{\eta}}(\boldsymbol{k},\nu_n) && \text{(C.35)} \\ &= \sum_j \rho_{\lambda,j} \int \mathrm{d}\varepsilon_{\lambda,j} \frac{1}{\eta \mathrm{i}\nu_n - \varepsilon_{\lambda,j} - \Sigma_{\lambda,j,\eta}(\eta k)} \frac{1}{\bar{\eta} \mathrm{i}\nu_n - \varepsilon_{\lambda,j} - \Sigma_{\lambda,j,\bar{\eta}}(\bar{\eta} k)} && \text{(C.36)} \\ &= \frac{\pi\rho_{\mathrm{F}}}{p|\nu_n| + \pi\frac{\rho_{\mathrm{F}}}{2} \sum_{\lambda',j',\eta'} [\mathcal{S}_{(\lambda,j,\eta),(\lambda',j',\eta')} + \mathcal{S}_{(\lambda,j,\bar{\eta}),(\lambda',j',\eta')}]} \,. && \text{(C.37)} \end{aligned}$$

At this point, we note that upon setting $\mathcal{S}_{\tau\tau'} \equiv 0$, we indeed recover the expression calculated for the corresponding clean model:

$$d^0_{\lambda\lambda} = \sum_{j,\eta} T \sum_n c_{\lambda,j,\eta}(\nu_n) = 2\rho_{\mathrm{F}} \ln\left(\frac{2\Lambda \mathrm{e}^{\gamma}}{\pi T}\right) . \tag{C.38}$$

Matrix formalism for the calculation of the coefficients Going back to Eq. (C.30), we can derive the coefficients a (as defined in Eq. (C.27)) in terms of the diagrams d which correspond to the quartic

coefficients coupling to the order parameter in the two bands, Δ_1 and Δ_2. As a result, we get

$$a_{++}(T) = \frac{2}{|V_{\mathrm{SC}}|} + \frac{1}{2}\operatorname{sgn} V_{\mathrm{SC}}\Big[d_{11}(T) + d_{22}(T) + d_{12}(T) + d_{21}(T)\Big]\,, \tag{C.39a}$$

$$a_{--}(T) = \frac{2}{|V_{\mathrm{SC}}|} - \frac{1}{2}\operatorname{sgn} V_{\mathrm{SC}}\Big[d_{11}(T) + d_{22}(T) - d_{12}(T) - d_{21}(T)\Big]\,, \tag{C.39b}$$

$$a_{+-}(T) = -\frac{\mathrm{i}}{2}\Big[d_{11}(T) - d_{22}(T) + d_{12}(T) - d_{21}(T)\Big]\,, \tag{C.39c}$$

$$a_{-+}(T) = -\frac{\mathrm{i}}{2}\Big[d_{11}(T) - d_{22}(T) - d_{12}(T) + d_{21}(T)\Big]\,. \tag{C.39d}$$

Here, as a consequence of the interband scattering process $\Gamma_{(\lambda,j,\eta)(\lambda',j',\eta'),(\lambda,j,\bar{\eta})(\lambda',j',\bar{\eta}')}$, also band-offdiagonal diagrams can arise in the presence of disorder. The corresponding diagrams are given by

$d_{\lambda\lambda'}(T) =$ 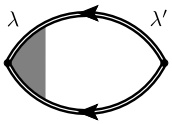

(C.40)

$$\begin{aligned}
&= \delta_{\lambda\lambda'}\, T\sum_{n} c_{\lambda,j,\eta}(\nu_n) + T\sum_{n}\sum_{j,\eta}\sum_{j',\eta'} \eta\eta' c_{(\lambda,j,\eta)}(\nu_n)\mathcal{V}_{(\lambda,j,\eta)(\lambda',j',\eta')}c_{(\lambda',j',\eta')}(\nu_n) \\
&\quad + \sum_{n}\sum_{j,\eta}\sum_{\lambda'',j'',\eta''}\sum_{j',\eta'} \eta\eta' c_{(\lambda,j,\eta)}(\nu_n)\mathcal{V}_{(\lambda,j,\eta)(\lambda'',j'',\eta'')}c_{(\lambda'',j'',\eta'')}(\nu_n)\mathcal{V}_{(\lambda'',j'',\eta'')(\lambda',j',\eta')}c_{(\lambda',j',\eta')} \\
&\quad + \dots\,,
\end{aligned} \tag{C.41}$$

where we used that

$$(-\mathrm{i}\hat{\tau}_2)_{\eta\bar{\eta}}(\mathrm{i}\hat{\tau}_2)_{\bar{\eta}'\eta'} = \eta\eta'\,. \tag{C.42}$$

As a next step, we introduce the nested matrices $\mathcal{V}$ and $\mathcal{C}$ as

$$\mathcal{V} = \Big(\mathcal{V}_{(\lambda,j,\eta)(\lambda',j',\eta')}\Big) \qquad \text{and} \qquad \mathcal{C} = \Big(\delta_{\lambda\lambda'}\,\delta_{jj'}\,\delta_{\eta\eta'}\,c_{\lambda,j,\eta}(\nu_n)\Big) \tag{C.43}$$

to conveniently calculate the diagrams within a matrix formalism. Then, the expressions for the diagrams can be stated as

$$d_{\lambda\lambda'}(T) = T\sum_{n}\sum_{j,\eta}\sum_{j',\eta'}\eta\eta'\Big[\sum_{m=0}^{\infty}(\mathcal{C}\mathcal{V})^m\mathcal{C}\Big]_{(\lambda,j,\eta)(\lambda',j',\eta')} \tag{C.44}$$

$$= T\sum_{n}\sum_{j,\eta}\sum_{j',\eta'}\eta\eta'\Big[(\mathbb{1}-\mathcal{C}\mathcal{V})^{-1}\mathcal{C}\Big]_{(\lambda,j,\eta)(\lambda',j',\eta')}\,, \tag{C.45}$$

where the matrix $\mathcal{C}$ depends implicitly on temperature via the Matsubara frequency ν_n. Within this formalism, the calculation of the diagrams reduces to the evaluation of integrals that can be performed straightforwardly since the momentum integrals decouple. Apart from that, only multiplication and inversion of $(4p)\times(4p)$ matrices is required. Consequently, the transition temperature can be calculated rather straightforwardly within this approach, although the numerical costs increase with the number of patches. The main task is the appropriate partitioning of the Fermi surface and the calculation of the corresponding scattering rates between different patches.

C.3 Application: iron-based superconductors

A straightforward calculation of the diagrams d can be found in Ref. 87. Here, we derive these results using the matrix formalism presented in Sec. C.2. In the iron-based superconductors, there is no need to introduce patches. Furthermore, for non-spin-magnetic scattering, $\mathcal{S}_{(\lambda,\eta)(\lambda',\eta')} = \delta_{\eta\eta'}\,\mathcal{S}_{(\lambda,\eta)(\lambda'\eta)}$ and $\mathcal{V}_{(\lambda,\eta)(\lambda',\eta')} = \delta_{\eta\eta'}\,\mathcal{V}_{(\lambda,\eta)(\lambda'\eta)}$ holds, together with

$$c_{(\lambda,\eta)}(\nu_n) = c_\lambda(\nu_n) = \frac{\pi\rho_\mathrm{F}}{|\nu_n| + \pi\rho_\mathrm{F}(\Gamma_\lambda + \Gamma_{12})}\,, \tag{C.46}$$

where ρ_F is the DOS at the Fermi level per band. Therefore, we introduce the 2×2 matrices

$$\mathcal{C} = \begin{pmatrix} c_1(\nu_n) & 0 \\ 0 & c_2(\nu_n) \end{pmatrix} \qquad \text{and} \qquad \mathcal{V} = \begin{pmatrix} \Gamma_1 & \Gamma_{12}\mathrm{e}^{\mathrm{i}\phi} \\ \Gamma_{12}\mathrm{e}^{-\mathrm{i}\phi} & \Gamma_2 \end{pmatrix}. \tag{C.47}$$

With these definitions, the diagrams reduce to

$$d_{\lambda\lambda'}(T) = T\sum_n \Big[(\mathbb{1} - \mathcal{C}\mathcal{V})^{-1}\mathcal{C}\Big]_{\lambda\lambda'}\,. \tag{C.48}$$

Furthermore, as a consequence of particle-hole symmetry, it holds that $d_{11} = d_{22}$ and $d_{12} = {d_{21}}^*$. Finally, the resulting expressions for the diagrams are given by

$$d_{11}(T) = \frac{\rho_\mathrm{F}}{2}\left[\ln\left(\frac{\Lambda^2\mathrm{e}^\gamma}{\pi^2T^2}\right) - \psi_0\left(\frac{1}{2} + \frac{\rho_\mathrm{F}\Gamma_{12}}{T}\right)\right] = \begin{cases} \frac{\rho_\mathrm{F}}{2}\ln\left(\frac{2\Lambda\mathrm{e}^\gamma}{\pi T}\right) & \text{for} \quad \rho_\mathrm{F}\Gamma_{12} \ll T\,, \\ \frac{\rho_\mathrm{F}}{2}\ln\left(\frac{\Lambda^2\mathrm{e}^\gamma}{\pi^2\rho_\mathrm{F}\Gamma_{12}T}\right) & \text{for} \quad \rho_\mathrm{F}\Gamma_{12} \gg T\,, \end{cases} \tag{C.49a}$$

$$d_{12}(T) = \frac{\rho_\mathrm{F}}{2}\mathrm{e}^{\mathrm{i}\phi}\left[\psi_0\left(\frac{1}{2} + \frac{\rho_\mathrm{F}\Gamma_{12}}{T}\right) - \psi_0\left(\frac{1}{2}\right)\right] = \begin{cases} \frac{\rho_\mathrm{F}}{2}\mathrm{e}^{\mathrm{i}\phi}\frac{\pi^2\rho_\mathrm{F}\Gamma_{12}}{2T} & \text{for} \quad \rho_\mathrm{F}\Gamma_{12} \ll T\,, \\ \frac{\rho_\mathrm{F}}{2}\mathrm{e}^{\mathrm{i}\phi}\ln\left(\frac{4\rho_\mathrm{F}\Gamma_{12}\mathrm{e}^\gamma}{T}\right) & \text{for} \quad \rho_\mathrm{F}\Gamma_{12} \gg T\,. \end{cases} \tag{C.49b}$$

C.4 Application: LAO/STO interface

Here, we make use of the patch approximation for the Fermi surface of the LAO/STO interface, that is, we introduce patches of the Fermi surface as explained in Chap. 3. In our calculation, we assume the DOS at the Fermi level to have the same constant value within all of the patches, $\rho_\tau = \frac{\rho_\mathrm{F}}{8}$, which corresponds to a total DOS ρ_F per band. The patch approximation results in the two 16×16 matrices $\mathcal{S}$ and $\mathcal{V}$. In Sec. B.3, we explained how the corresponding scattering rates entering the self energy and vertex corrections can be obtained using the patch approximation. Let us give the results for two exemplary terms here to illustrate how we obtained the results for the transition temperature for superconductivity in LAO/STO that are discussed in Chap. 3.

Nonmagnetic impurities The most general expression for the disorder correlator that is consistent with time-reversal symmetry is provided by Eq. (3.12). Here we exemplarily consider nonmagnetic disorder consistent with the full point group symmetry of the clean system $\tau_0\sigma_0$, where σ_i and τ_i denote Pauli matrices in spin and orbital space, respectively. The resulting matrix $\mathcal{S}$ entering the self energy

is given by

$$\mathcal{S} = \gamma^I_{A_1} \begin{pmatrix}
1&0&1&0&&&&&0&1&0&1&&&&\\
0&1&0&1&&&&&1&0&1&0&&&&\\
1&0&1&0&&&&&0&1&0&1&&&&\\
0&1&0&1&&&&&1&0&1&0&&&&\\
&&&&1&0&1&0&&&&&0&1&0&1\\
&&&&0&1&0&1&&&&&1&0&1&0\\
&&&&1&0&1&0&&&&&0&1&0&1\\
&&&&0&1&0&1&&&&&1&0&1&0\\
0&1&0&1&&&&&1&0&1&0&&&&\\
1&0&1&0&&&&&0&1&0&1&&&&\\
0&1&0&1&&&&&1&0&1&0&&&&\\
1&0&1&0&&&&&0&1&0&1&&&&\\
&&&&0&1&0&1&&&&&1&0&1&0\\
&&&&1&0&1&0&&&&&0&1&0&1\\
&&&&0&1&0&1&&&&&1&0&1&0\\
&&&&1&0&1&0&&&&&0&1&0&1
\end{pmatrix}, \tag{C.50}$$

where all entries not stated explicitly are zero, and thus were omitted for the sake of clarity. Furthermore, from the scattering rates appearing in the vertex corrections, we can build the matrix

$$\mathcal{V} = \gamma^I_{A_1} \begin{pmatrix}
1&0&1&0&&&&&0&-1&0&-1&&&&\\
0&1&0&1&&&&&-1&0&-1&0&&&&\\
1&0&1&0&&&&&0&-1&0&-1&&&&\\
0&1&0&1&&&&&-1&0&-1&0&&&&\\
&&&&1&0&1&0&&&&&0&-1&0&-1\\
&&&&0&1&0&1&&&&&-1&0&-1&0\\
&&&&1&0&1&0&&&&&0&-1&0&-1\\
&&&&0&1&0&1&&&&&-1&0&-1&0\\
0&-1&0&-1&&&&&1&0&1&0&&&&\\
-1&0&-1&0&&&&&0&1&0&1&&&&\\
0&-1&0&-1&&&&&1&0&1&0&&&&\\
-1&0&-1&0&&&&&0&1&0&1&&&&\\
&&&&0&-1&0&-1&&&&&1&0&1&0\\
&&&&-1&0&-1&0&&&&&0&1&0&1\\
&&&&0&-1&0&-1&&&&&1&0&1&0\\
&&&&-1&0&-1&0&&&&&0&1&0&1
\end{pmatrix}. \tag{C.51}$$

Using the matrix formalism presented in Sec. C.2, the expressions for the diagrams and hence the quadratic coefficients are readily obtained. The treatment of the other contributions to the nonmagnetic impurity vertex is analogous, and in the end, we obtain

$$d_{11}(T) = d_{22}(T) = \frac{\rho_\mathrm{F}}{2}\left[2\ln\left(\frac{\Lambda}{2\pi T}\right) - \psi_0\left(\frac{1}{2}\right) - \psi_0\left(\frac{1}{2} + \frac{\rho_\mathrm{F}\chi_\mathrm{inter}\Gamma}{4T}\right)\right], \tag{C.52a}$$

$$d_{12}(T) = d_{21}(T) = \frac{\rho_\mathrm{F}}{2}\left[\psi_0\left(\frac{1}{2} + \frac{\rho_\mathrm{F}\chi_\mathrm{inter}\Gamma}{4T}\right) - \psi_0\left(\frac{1}{2}\right)\right]. \tag{C.52b}$$

Here, we introduced the total scattering rate Γ due to nonmagnetic impurities, and we artificially discriminated intraband and interband scattering rates as introduced in Eq. (3.18) in order to separate the two contributions.

Magnetic impurities In addition, we considered magnetic impurities. The most general expressions for the disorder correlator resulting from magnetic order is given by Eqs. (3.19) and Eq. (3.20). Here,

we use in-plane magnetic impurities associated with $\tau_0\sigma_1$ as an example. It results in the two matrices

$$\mathcal{S} = \gamma_E^I \begin{pmatrix}
0&1&0&1&&&&&1&0&1&0&&&&\\
1&0&1&0&&&&&0&1&0&1&&&&\\
0&1&0&1&&&&&1&0&1&0&&&&\\
1&0&1&0&&&&&0&1&0&1&&&&\\
&&&&1&0&1&0&&&&&0&1&0&1\\
&&&&0&1&0&1&&&&&1&0&1&0\\
&&&&1&0&1&0&&&&&0&1&0&1\\
&&&&0&1&0&1&&&&&1&0&1&0\\
1&0&1&0&&&&&0&1&0&1&&&&\\
0&1&0&1&&&&&1&0&1&0&&&&\\
1&0&1&0&&&&&0&1&0&1&&&&\\
0&1&0&1&&&&&1&0&1&0&&&&\\
&&&&0&1&0&1&&&&&1&0&1&0\\
&&&&1&0&1&0&&&&&0&1&0&1\\
&&&&0&1&0&1&&&&&1&0&1&0\\
&&&&1&0&1&0&&&&&0&1&0&1
\end{pmatrix} \tag{C.53}$$

and

$$\mathcal{V} = \gamma_E^I \begin{pmatrix}
0&1&0&1&&&&&-1&0&-1&0&&&&\\
1&0&1&0&&&&&0&-1&0&-1&&&&\\
0&1&0&1&&&&&-1&0&-1&0&&&&\\
1&0&1&0&&&&&0&-1&0&-1&&&&\\
&&&&-1&0&-1&0&&&&&0&1&0&1\\
&&&&0&-1&0&-1&&&&&1&0&1&0\\
&&&&-1&0&-1&0&&&&&0&1&0&1\\
&&&&0&-1&0&-1&&&&&1&0&1&0\\
-1&0&-1&0&&&&&0&1&0&1&&&&\\
0&-1&0&-1&&&&&1&0&1&0&&&&\\
-1&0&-1&0&&&&&0&1&0&1&&&&\\
0&-1&0&-1&&&&&1&0&1&0&&&&\\
&&&&0&1&0&1&&&&&-1&0&-1&0\\
&&&&1&0&1&0&&&&&0&-1&0&-1\\
&&&&0&1&0&1&&&&&-1&0&-1&0\\
&&&&1&0&1&0&&&&&0&-1&0&-1
\end{pmatrix}. \tag{C.54}$$

In this case, the evaluation of the diagrams results in

$$d_{11}(T) = d_{22}(T) = \frac{\rho_\mathrm{F}}{2}\left[2\ln\left(\frac{\Lambda}{2\pi T}\right) - \psi_0\left(\frac{1}{2} + \frac{\rho_\mathrm{F}\chi_\mathrm{intra}\Gamma}{4T}\right) - \psi_0\left(\frac{1}{2} + \frac{\rho_\mathrm{F}(\chi_\mathrm{intra}+\chi_\mathrm{inter})\Gamma}{4T}\right)\right], \tag{C.55a}$$

$$d_{12}(T) = d_{21}(T) = \frac{\rho_\mathrm{F}}{2}\left[\psi_0\left(\frac{1}{2} + \frac{\rho_\mathrm{F}\chi_\mathrm{intra}\Gamma}{4T}\right) - \psi_0\left(\frac{1}{2} + \frac{\rho_\mathrm{F}(\chi_\mathrm{intra}+\chi_\mathrm{inter})\Gamma}{4T}\right)\right]. \tag{C.55b}$$

D Appendix D

Density-wave instabilities

This appendix contains additional information for our discussion of density-wave instabilities in Secs. 5.3.1 and 5.3.2. Furthermore, we provide a brief derivation of the mean-field theory for the double-$\boldsymbol{Q}$ spin-density wave order discussed in Chap. 4.

We start with the usual noninteracting part

$$\mathcal{S}_0 = \sum_{\sigma} \int_{\alpha} \bar{\psi}_{\alpha,\sigma}(-\mathrm{i}\nu_n + \varepsilon_{\boldsymbol{k}})\psi_{\alpha,\sigma}\,, \tag{D.1}$$

where α is a multi-index comprising momentum and Matsubara frequency as well as others such as band indices, except for spin which is denoted σ and shall be treated separately in the remainder. In addition, we consider a general SU(2)-invariant quartic interaction

$$\mathcal{S}_{\mathrm{int}} = \frac{1}{2}\sum_{\{\sigma_i\}} \int_{\{\alpha_i\}} V_{(\alpha_1,\sigma_1)(\alpha_2,\sigma_2),(\alpha_3,\sigma_3)(\alpha_4,\sigma_4)} \bar{\psi}_{\alpha_1,\sigma_1}\bar{\psi}_{\alpha_2,\sigma_2}\psi_{\alpha_3,\sigma_3}\psi_{\alpha_4,\sigma_4}\,\delta(\alpha_1+\alpha_2-\alpha_3-\alpha_4)\,. \tag{D.2}$$

Due to the anticommutation property of the fermionic operators, the interaction is antisymmetric under exchange of incoming as well as outgoing indices,

$$V_{(\alpha_1,\sigma_1)(\alpha_2,\sigma_2),(\alpha_3,\sigma_3)(\alpha_4,\sigma_4)} = -V_{(\alpha_1,\sigma_1)(\alpha_2,\sigma_2),(\alpha_4,\sigma_4)(\alpha_3,\sigma_3)} = -V_{(\alpha_2,\sigma_2)(\alpha_1,\sigma_1),(\alpha_3,\sigma_3)(\alpha_4,\sigma_4)}\,. \tag{D.3}$$

Such an interaction can be decomposed into charge and spin channel using

$$V_{(\alpha_1,\sigma_1)(\alpha_2,\sigma_2),(\alpha_3\sigma_3)(\alpha_4,\sigma_4)} = V^{\mathrm{ch}}_{\alpha_1\alpha_2,\alpha_3\alpha_4}\,\delta_{\sigma_1\sigma_4}\,\delta_{\sigma_2\sigma_3} + V^{\mathrm{sp}}_{\alpha_1\alpha_2,\alpha_3\alpha_4}\boldsymbol{\sigma}_{\sigma_1\sigma_4}\cdot\boldsymbol{\sigma}_{\sigma_2\sigma_3}\,. \tag{D.4}$$

Here $\boldsymbol{\sigma} = (\sigma_1,\sigma_2,\sigma_3)$, and σ_i denotes the Pauli matrices, which are the three generators of SU(2). Let us note here that the generalization to an SU(N)-invariant interaction is straightforward and involves the N^2-1 generators of SU(N), denoted by λ^i, instead of the Pauli matrices σ_i. The decoupling procedure outlined in App. A.1 can now be performed in the charge channel or in the spin channel, potentially leading to CDW order or SDW order, respectively.

Using the identity

$$\boldsymbol{\sigma}_{\sigma_1\sigma_4}\cdot\boldsymbol{\sigma}_{\sigma_2\sigma_3} = 2\,\delta_{\sigma_1\sigma_3}\,\delta_{\sigma_2\sigma_4} - \delta_{\sigma_1\sigma_4}\,\delta_{\sigma_2\sigma_3}\,, \tag{D.5}$$

the decomposition could alternatively be done in singlet and triplet channel [214],

$$V_{(\alpha_1,\sigma_1)(\alpha_2,\sigma_2),(\alpha_3\sigma_3)(\alpha_4,\sigma_4)} = V^{\mathrm{A}}_{\alpha_1\alpha_2,\alpha_3\alpha_4} I_{\sigma_1\sigma_2,\sigma_3\sigma_4} + V^{\mathrm{S}}_{\alpha_1\alpha_2,\alpha_3\alpha_4} T_{\sigma_1\sigma_2,\sigma_3\sigma_4}\,, \tag{D.6}$$

where $I_{\sigma_1\sigma_2,\sigma_3\sigma_4} = \delta_{\sigma_1\sigma_4}\delta_{\sigma_2\sigma_3} + \delta_{\sigma_1\sigma_3}\delta_{\sigma_2\sigma_4}$ is symmetric and $T_{\sigma_1\sigma_2,\sigma_3\sigma_4} = \delta_{\sigma_1\sigma_4}\delta_{\sigma_2\sigma_3} - \delta_{\sigma_1\sigma_3}\delta_{\sigma_2\sigma_4}$ is antisymmetric w. r. t. interchanging spin indices. Correspondingly, V^{A} (V^{S}) are antisymmetric (symmetric) w. r. t. the exchange of incoming and outgoing indices. This representation is better suited for an RG approach and connected to the decomposition in charge and spin channels by

$$V^{\mathrm{ch}} = \frac{1}{2}(3V^{\mathrm{A}} + V^{\mathrm{S}}), \qquad V^{\mathrm{sp}} = \frac{1}{2}(V^{\mathrm{A}} - V^{\mathrm{S}}), \tag{D.7a}$$

$$V^{\mathrm{A}} = \frac{1}{2}(V^{\mathrm{ch}} + V^{\mathrm{sp}}), \qquad V^{\mathrm{S}} = \frac{1}{2}(V^{\mathrm{ch}} - 3V^{\mathrm{sp}}). \tag{D.7b}$$

D.1 Two-band model of nested Fermi surface pockets

Let us now turn to a nested two-band model, for example the one developed for iron-based superconductors, and consider mean-field theories and fluctuation corrections for the different density-wave instabilities resulting from nesting. In the remainder, we assume the interactions to depend on momenta only via the band indices λ_i, that is $V_{(\lambda_1,\boldsymbol{k}_1,\sigma_1)(\lambda_2,\boldsymbol{k}_2,\sigma_2),(\lambda_3,\boldsymbol{k}_3,\sigma_3)(\lambda_4,\boldsymbol{k}_4,\sigma_4)} \to V_{(\lambda_1,\sigma_1)(\lambda_2,\sigma_2),(\lambda_3,\sigma_3)(\lambda_4,\sigma_4)}$.

The RG analysis at tree-level shows that only five independent coupling constants survive: $V^{\mathrm{A}}_{12,21}$, $V^{\mathrm{S}}_{12,21}$, $V^{\mathrm{S}}_{11,22}$, $V^{\mathrm{S}}_{11,11}$, and $V^{\mathrm{S}}_{22,22}$. Here, we start from the interactions in the charge and spin channel, and the connection to the couplings used in the RG approach is given in Sec. D.1.3.

D.1.1 Charge-density wave order

The interaction in the charge channel can be written in terms of fermionic operators in the two nested parts of the Fermi surface labeled by $\lambda \in \{1, 2\}$ as

$$\mathcal{S}^{\mathrm{ch}}_{\mathrm{int}} = \sum_{\sigma,\sigma'} \int_{k,k',q} \begin{pmatrix} \bar{\psi}_{1,k,\sigma}\psi_{2,k+q,\sigma} & \bar{\psi}_{2,k,\sigma}\psi_{1,k+q,\sigma} \end{pmatrix} \begin{pmatrix} V^{\mathrm{ch}}_{11,22} & V^{\mathrm{ch}}_{12,12} \\ V^{\mathrm{ch}}_{12,12} & V^{\mathrm{ch}}_{11,22} \end{pmatrix} \begin{pmatrix} \bar{\psi}_{1,k',\sigma'}\psi_{2,k'-q,\sigma'} \\ \bar{\psi}_{2,k',\sigma'}\psi_{1,k'-q,\sigma'} \end{pmatrix}, \tag{D.8}$$

where we used the above definitions of the couplings and their symmetry w. r. t. interchanging indices. Diagonalizing the matrix reveals two possibilities for a charge-density wave,

$$\mathcal{S}^{\mathrm{ch}}_{\mathrm{int}} = -\frac{1}{2}\int_q b_{+,q} V_{\mathrm{rCDW}} b_{+,-q} + \frac{1}{2}\int_q b_{-,q} V_{\mathrm{iCDW}} b_{-,-q}, \tag{D.9}$$

where we introduced the fields

$$b_{\pm,q} = \sum_{\sigma}\int_k \left(\bar{\psi}_{1,k,\sigma}\psi_{2,k+q,\sigma} \pm \bar{\psi}_{2,k,\sigma}\psi_{1,k+q,\sigma}\right) \tag{D.10}$$

and the couplings

$$V_{\mathrm{rCDW}} = -(V^{\mathrm{ch}}_{11,22} + V^{\mathrm{ch}}_{12,12}) \qquad \text{and} \qquad V_{\mathrm{iCDW}} = V^{\mathrm{ch}}_{11,22} - V^{\mathrm{ch}}_{12,12} \tag{D.11}$$

in the two CDW channels. Since $\bar{b}_{\pm,q} = \pm b_{\pm,-q}$, it holds that $b_+(\boldsymbol{r},\tau) \in \mathbb{R}$ and $\tilde{b} := \mathrm{i}b_-(\boldsymbol{r},\tau) \in \mathbb{R}$. Therefore, the first term can be decoupled by a real scalar field $\rho_+(\boldsymbol{r},\tau) \in \mathbb{R}$ whereas for the second term, we introduce an effective field $\tilde{\rho}_-(\boldsymbol{r},\tau) := \mathrm{i}\rho_-(\boldsymbol{r},\tau) \in \mathbb{R}$.

Effective action Let us assume $V_{\mathrm{rCDW}} > 0$ and $V_{\mathrm{iCDW}} > 0$ such that the interaction can be decoupled by

$$\mathrm{e}^{-\mathcal{S}_{\mathrm{int}}^{\mathrm{ch}}} = \mathrm{e}^{\frac{1}{2}\int_q b_{+,q} V_{\mathrm{rCDW}} b_{+,-q} + \frac{1}{2}\int_q \tilde{b}_{-,q} V_{\mathrm{iCDW}} \tilde{b}_{-,-q}} \tag{D.12}$$

$$= \int \mathcal{D}\rho_+ \, \mathrm{e}^{-\frac{1}{2}\int_q \rho_{+,q} \frac{1}{V_{\mathrm{rCDW}}} \rho_{+,-q} + \int_q \rho_{+,q} b_{+,-q}} \int \mathcal{D}\tilde{\rho}_- \, \mathrm{e}^{-\frac{1}{2}\int_q \tilde{\rho}_{-,q} \frac{1}{V_{\mathrm{iCDW}}} \tilde{\rho}_{-,-q} + \int_q \tilde{\rho}_{-,q} \tilde{b}_{-,-q}} . \tag{D.13}$$

Let us note here, that in case of a repulsive interaction $V_{\mathrm{CDW}} < 0$, we need to introduce a factor i for convergence $\exp[-\frac{1}{2}\int_q b_q |V_{\mathrm{CDW}}| b_{-q}] = \int \mathcal{D}\rho \, \exp[-\frac{1}{2} b_q |V_{\mathrm{CDW}}|^{-1} b_{-q} + \mathrm{i}\int_q \rho_q b_{-q}]$. This would result in an additional minus sign associated with the respective term in the quadratic coefficient, meaning that this mode could not condense since the quadratic coefficient does not change sign. If, on the other hand, $V_{\mathrm{CDW}} > 0$, we can proceed by integrating out the fermions as

$$\int \mathcal{D}[\bar{\psi},\psi] \, \mathrm{e}^{-(\mathcal{S}_0 + \mathcal{S}_{\mathrm{int}}^{\mathrm{ch}})} = \int \mathcal{D}\rho_+ \mathcal{D}\tilde{\rho}_- \, \mathrm{e}^{-\frac{1}{2}\int_q [\rho_{+,q} \frac{1}{V_{\mathrm{rCDW}}} \rho_{+,-q} + \tilde{\rho}_{-,q} \frac{1}{V_{\mathrm{iCDW}}} \tilde{\rho}_{-,-q}]}$$
$$\times \int \mathcal{D}[\bar{\psi},\psi] \, \mathrm{e}^{-\sum_{\sigma,\sigma'} \int_{k,k'} \bar{\Psi}_{k,\sigma} (-\mathcal{G}^{-1}_{\mathrm{CDW};(k,\sigma)(k',\sigma')}) \Psi_{k',\sigma'}} , \tag{D.14}$$

where we introduced the spinors

$$\bar{\Psi}_{k,\sigma} = \begin{pmatrix} \bar{\psi}_{1,k,\sigma} & \bar{\psi}_{2,k,\sigma} \end{pmatrix} \qquad \text{and} \qquad \Psi_{k',\sigma'} = \begin{pmatrix} \psi_{1,k',\sigma'} \\ \psi_{2,k',\sigma'} \end{pmatrix} \tag{D.15}$$

and the corresponding matrix Green's function

$$\mathcal{G}^{-1}_{\mathrm{CDW};(k,\sigma)(k',\sigma')} = \delta_{\sigma\sigma'} \begin{pmatrix} (\mathrm{i}\nu_n - \varepsilon_{\boldsymbol{k}}) \, \delta_{kk'} & \rho_{+,k-k'} + \mathrm{i}\tilde{\rho}_{-,k-k'} \\ \rho_{+,k-k'} - \mathrm{i}\tilde{\rho}_{-,k-k'} & (\mathrm{i}\nu_n + \varepsilon_{\boldsymbol{k}}) \, \delta_{kk'} \end{pmatrix} \tag{D.16}$$

$$= \delta_{\sigma\sigma'} (\mathrm{i}\nu_n \tau_0 \, \delta_{kk'} - \varepsilon_{\boldsymbol{k}} \tau_3 \, \delta_{kk'} + \rho_{+,k-k'} \tau_1 - \tilde{\rho}_{-,k-k'} \tau_2) . \tag{D.17}$$

Furthermore, we used the nesting condition to introduce $\varepsilon_{\boldsymbol{k}} := \varepsilon_{1,\boldsymbol{k}} = -\varepsilon_{2,\boldsymbol{k}}$. The corresponding mean-field action is given by

$$\mathcal{S}_{\mathrm{MF}}^{\mathrm{CDW}}(\rho_+, \tilde{\rho}_-) = \frac{\rho_+^2}{2V_{\mathrm{rCDW}}} + \frac{\tilde{\rho}_-^2}{2V_{\mathrm{iCDW}}} - \mathrm{Tr}\ln(-\mathcal{G}^{-1}_{\mathrm{MF}}) , \tag{D.18}$$

where

$$\mathcal{G}^{-1}_{\mathrm{MF}} = \underbrace{\mathrm{i}\nu_n \tau_0 - \varepsilon_{\boldsymbol{k}} \tau_3}_{=\mathcal{G}_0^{-1}} + \underbrace{\rho_+ \tau_1 - \tilde{\rho}_- \tau_2}_{=\mathcal{U}} . \tag{D.19}$$

Note that we omit the index 0 that denotes the mean-field value of the order parameter in the main text throughout this appendix for the sake of readability.

Transition temperature The corresponding transition temperatures for the two instabilities can be obtained from the quadratic coefficient in an expansion in terms of the order parameter, cf. the discussion of superconductivity in App. C:

$$\mathcal{S}_{\mathrm{MF}}^{\mathrm{CDW}}(\rho_+, \tilde{\rho}_-) - \mathcal{S}_{\mathrm{MF}}^{\mathrm{CDW}}(\rho_+ = 0, \tilde{\rho}_- = 0) = \Big(\frac{\rho_+^2}{2V_{\mathrm{rCDW}}} + \frac{\tilde{\rho}_-^2}{2V_{\mathrm{iCDW}}}\Big) + \frac{1}{2}\,\mathrm{Tr}(\mathcal{G}_0 \mathcal{U} \mathcal{G}_0 \mathcal{U}) \tag{D.20}$$

$$= \Big(\frac{1}{2V_{\mathrm{rCDW}}} - \int_k \frac{1}{\nu_n^2 + \varepsilon_{\boldsymbol{k}}^2}\Big)\rho_+^2 + \Big(\frac{1}{2V_{\mathrm{iCDW}}} - \int_k \frac{1}{\nu_n^2 + \varepsilon_{\boldsymbol{k}}^2}\Big)\tilde{\rho}_-^2 . \tag{D.21}$$

Therefore, the transition temperature towards the formation of CDW order is given by

$$T_{\mathrm{CDW}} = \frac{2\mathrm{e}^{\gamma}\Lambda}{\pi}\mathrm{e}^{-\frac{1}{2\rho_{\mathrm{F}}V_{\mathrm{CDW}}}}\,, \tag{D.22}$$

and either rCDW or iCDW condenses, depending on which coupling is stronger.[1]

Mean-field gap equation Furthermore, the respective mean-field gap equation (determining the value of either ρ_+ or $\tilde{\rho}_-$) can be obtained from the saddle-point condition as

$$0 = \frac{\mathrm{d}\mathcal{S}^{\mathrm{CDW}}_{\mathrm{MF}}}{\mathrm{d}\rho} = \frac{\mathrm{d}}{\mathrm{d}\rho}\Big[\frac{\rho^2}{2V_{\mathrm{CDW}}} - \mathrm{Tr}\ln(-\mathcal{G}^{-1}_{\mathrm{MF}})\Big] = 2\rho\Big[\frac{1}{2V_{\mathrm{CDW}}} - \int_k \frac{1}{\nu_n^2+\varepsilon_{\boldsymbol{k}}^2+\rho^2}\Big] \tag{D.23}$$

$$\overset{T=0}{=} 2\rho\Big[\frac{1}{2V_{\mathrm{CDW}}} - \rho_{\mathrm{F}}\ln\Big(\frac{2v_{\mathrm{F}}\Lambda}{\rho}\Big)\Big]\,, \tag{D.24}$$

which corresponds to the BCS gap equation when identifying $g \equiv 2V_{\mathrm{CDW}}$, see App. A.2 for details.

Fluctuations Let us now consider the fluctuation corrections to each of these instabilities. The matrix Green's functions can be split into mean-field and fluctuation part according to

$$\mathcal{G}^{-1}_{\mathrm{rCDW};(k,\sigma)(k',\sigma')} = \delta_{kk'}\,\delta_{\sigma\sigma'}(\mathrm{i}\nu_n\tau_0 + \rho_+\tau_1 - \varepsilon_{1,\boldsymbol{k}}\tau_3) + \delta_{\sigma\sigma'}\,\varrho_{+,k-k'}\tau_1\,, \tag{D.25}$$

$$\mathcal{G}^{-1}_{\mathrm{iCDW};(k,\sigma)(k',\sigma')} = \delta_{kk'}\,\delta_{\sigma\sigma'}(\mathrm{i}\nu_n\tau_0 - \tilde{\rho}_-\tau_2 - \varepsilon_{1,\boldsymbol{k}}\tau_3) - \delta_{\sigma\sigma'}\,\tilde{\varrho}_{-,k-k'}\tau_2\,. \tag{D.26}$$

The fluctuation corrections to the CDW mean-field action are hence given by

$$\mathrm{e}^{-(\mathcal{S}^{\mathrm{CDW}}_{\mathrm{MF}}+\mathcal{S}^{\mathrm{CDW}}_{\mathrm{fluct}})} = \mathrm{e}^{-\mathcal{S}^{\mathrm{CDW}}_{\mathrm{MF}}}\int\mathcal{D}\varrho\,\mathrm{e}^{-\frac{1}{2}\int_q \varrho_q\mathcal{D}^{-1}_{\mathrm{CDW;q}}\varrho_{-q}} = \mathrm{e}^{-\mathcal{S}^{\mathrm{CDW}}_{\mathrm{MF}}}\mathrm{e}^{-\frac{1}{2}\int_q\ln(\mathcal{D}^{-1}_{\mathrm{CDW};q})}\,, \tag{D.27}$$

where the respective propagators are given by

$$\mathcal{D}^{-1}_{\mathrm{rCDW};q} = \frac{1}{V_{\mathrm{rCDW}}} + \int_k \mathrm{tr}(\mathcal{G}^{\mathrm{rCDW}}_{\mathrm{MF};k+\frac{q}{2}}\tau_1\mathcal{G}^{\mathrm{rCDW}}_{\mathrm{MF};k-\frac{q}{2}}\tau_1) = \frac{1}{V_{\mathrm{rCDW}}} + 2\Pi^{\mathrm{n}}_q + 2\Pi^{\mathrm{a}}_q\,, \tag{D.28}$$

$$\mathcal{D}^{-1}_{\mathrm{iCDW};q} = \frac{1}{V_{\mathrm{iCDW}}} + \int_k \mathrm{tr}(\mathcal{G}^{\mathrm{iCDW}}_{\mathrm{MF};k+\frac{q}{2}}\tau_2\mathcal{G}^{\mathrm{iCDW}}_{\mathrm{MF};k-\frac{q}{2}}\tau_2) = \frac{1}{V_{\mathrm{iCDW}}} + 2\Pi^{\mathrm{n}}_q + 2\Pi^{\mathrm{a}}_q\,, \tag{D.29}$$

where of course normal and anomalous contribution have to be understood as functions of the respective order parameter ρ_+ or $\tilde{\rho}_-$ here. Therefore, as conjectured, we find that the fluctuation corrections

$$\frac{\mathrm{d}\mathcal{S}^{\mathrm{CDW}}_{\mathrm{fluct}}}{\mathrm{d}\rho^2} = \frac{1}{2}\int_q \frac{\frac{\mathrm{d}\Pi^{\mathrm{n}}_q}{\mathrm{d}\rho^2}+\frac{\mathrm{d}\Pi^{\mathrm{a}}_q}{\mathrm{d}\rho^2}}{\frac{1}{2V_{\mathrm{CDW}}}+\Pi^{\mathrm{n}}_q+\Pi^{\mathrm{a}}_q} > 0 \tag{D.30}$$

lead to sizable fluctuation corrections to the ground state energy and thereby alter the mean-field gap equation for both rCDW and iCDW order. Furthermore, in both cases, these corrections are positive, thus reducing the size of the gap as compared to its mean-field value, as discussed in Sec. 5.1. This is indeed consistent with the contribution of the amplitude mode in a neutral superfluid.

[1] From Eq. (D.20), it is obvious that for repulsive $V_{\mathrm{CDW}} < 0$, the respective mode would not condense: The factor of i that would be needed for convergence means that we would need to consider $\mathrm{Tr}[\mathcal{G}_0(\mathrm{i}\mathcal{U})\mathcal{G}_0(\mathrm{i}\mathcal{U})] = -\mathrm{Tr}[\mathcal{G}_0\mathcal{U}\mathcal{G}_0\mathcal{U}]$ instead, implying that the quadratic coefficient does not change sign.

D.1.2 Spin-density wave order

The decoupling in the spin channel can be performed as a multi-dimensional analogy to the case of CDW order. We write the interaction in the spin channel as

$$\mathcal{S}_{\text{int}}^{\text{sp}} = \sum_{\sigma_1,\sigma_2}\sum_{\sigma_1',\sigma_2'}\int_{k,k',q}\begin{pmatrix}\bar{\psi}_{1,k,\sigma_1}\boldsymbol{\sigma}_{\sigma_1\sigma_2}\psi_{2,k+q,\sigma_2} & \bar{\psi}_{2,k,\sigma_1}\boldsymbol{\sigma}_{\sigma_1\sigma_2}\psi_{1,k+q,\sigma_2}\end{pmatrix} \times \begin{pmatrix}V_{11,22}^{\text{sp}} & V_{12,12}^{\text{sp}} \\ V_{12,12}^{\text{sp}} & V_{11,22}^{\text{sp}}\end{pmatrix}\begin{pmatrix}\bar{\psi}_{1,k',\sigma_1'}\boldsymbol{\sigma}_{\sigma_1'\sigma_2'}\psi_{2,k'-q,\sigma_2'} \\ \bar{\psi}_{2,k',\sigma_1'}\boldsymbol{\sigma}_{\sigma_1'\sigma_2'}\psi_{1,k'-q,\sigma_2'}\end{pmatrix}, \tag{D.31}$$

where again, we used symmetry properties of the couplings to simplify the expression. Diagonalization of the matrix leads to two possibilities for SDW instabilities,

$$\mathcal{S}_{\text{int}}^{\text{sp}} = -\frac{1}{2}\int_q \boldsymbol{b}_{+,q}V_{\text{rSDW}}\boldsymbol{b}_{+,-q} + \frac{1}{2}\int_q \boldsymbol{b}_{-,q}V_{\text{iSDW}}\boldsymbol{b}_{-,-q}\,, \tag{D.32}$$

where we introduced the fields

$$\boldsymbol{b}_{\pm,q} = \sum_{\sigma,\sigma'}\int_k\left(\bar{\psi}_{1,k,\sigma}\boldsymbol{\sigma}_{\sigma\sigma'}\psi_{2,k+q,\sigma'} \pm \bar{\psi}_{2,k,\sigma}\boldsymbol{\sigma}_{\sigma\sigma'}\psi_{1,k+q,\sigma'}\right). \tag{D.33}$$

and the couplings

$$V_{\text{rSDW}} = -(V_{11,22}^{\text{sp}} + V_{12,12}^{\text{sp}}) \qquad \text{and} \qquad V_{\text{iSDW}} = V_{11,22}^{\text{sp}} - V_{12,12}^{\text{sp}} \tag{D.34}$$

in the two SDW channels. It holds that $\bar{\boldsymbol{b}}_{\pm,q} = \pm\boldsymbol{b}_{\pm,-q}$ and hence $\boldsymbol{b}_+(\boldsymbol{r},\tau) \in \mathbb{R}^3$ and $\tilde{\boldsymbol{b}}_-(\boldsymbol{r},\tau) := \mathrm{i}\boldsymbol{b}_-(\boldsymbol{r},\tau) \in \mathbb{R}^3$, meaning that the first term can be decoupled by introducing $\boldsymbol{M}_+(\boldsymbol{r},\tau) \in \mathbb{R}^3$ and the second by introducing $\tilde{\boldsymbol{M}}_-(\boldsymbol{r},\tau) := \mathrm{i}\boldsymbol{M}_-(\boldsymbol{r},\tau) \in \mathbb{R}^3$.

Effective action Again, we assume both $V_{\text{rSDW}} > 0$ and $V_{\text{iSDW}} > 0$ to be attractive, such that we can decouple the interaction term by a Hubbard-Stratonovich transformation as

$$\mathrm{e}^{-\mathcal{S}_{\text{int}}^{\text{sp}}} = \mathrm{e}^{\frac{1}{2}\int_q \boldsymbol{b}_{+,q}V_{\text{rSDW}}\boldsymbol{b}_{+,-q} + \frac{1}{2}\int_q \tilde{\boldsymbol{b}}_{-,q}V_{\text{iSDW}}\tilde{\boldsymbol{b}}_{-,-q}} \tag{D.35}$$

$$= \int \mathcal{D}\boldsymbol{M}_+\,\mathrm{e}^{-\frac{1}{2}\int_q \boldsymbol{M}_{+,q}\frac{1}{V_{\text{rSDW}}}\boldsymbol{M}_{+,-q} + \int_q \boldsymbol{M}_{+,q}\boldsymbol{b}_{+,-q}} \times \int \mathcal{D}\tilde{\boldsymbol{M}}_-\,\mathrm{e}^{-\frac{1}{2}\int_q \tilde{\boldsymbol{M}}_{-,q}\frac{1}{V_{\text{iSDW}}}\tilde{\boldsymbol{M}}_{-,-q} + \int_q \tilde{\boldsymbol{M}}_{-,q}\tilde{\boldsymbol{b}}_{-,-q}}\,, \tag{D.36}$$

where, again, we note that a repulsive coupling would still allow to perform a decoupling, however, the associated mode never condenses since it leads to an increase of the ground state energy at all temperatures. As usual, we can integrate out the fermions using

$$\int \mathcal{D}[\bar{\psi},\psi]\,\mathrm{e}^{-(\mathcal{S}_0+\mathcal{S}_{\text{int}}^{\text{sp}})} = \int \mathcal{D}\boldsymbol{M}_+\mathcal{D}\tilde{\boldsymbol{M}}_-\,\mathrm{e}^{-\frac{1}{2}\int_q[\boldsymbol{M}_{+,q}\frac{1}{V_{\text{rSDW}}}\boldsymbol{M}_{+,-q} + \tilde{\boldsymbol{M}}_{-,q}\frac{1}{V_{\text{iSDW}}}\tilde{\boldsymbol{M}}_{-,-q}]} \times \int \mathcal{D}[\bar{\psi},\psi]\,\mathrm{e}^{-\sum_{\sigma,\sigma'}\int_{k,k'}\bar{\Psi}_{k,\sigma}(-\mathcal{G}^{-1}_{\text{SDW};(k,\sigma)(k',\sigma')})\Psi_{k',\sigma'}} \tag{D.37}$$

with spinors

$$\bar{\Psi}_{k,\sigma} = \begin{pmatrix} \bar{\psi}_{1,k,\sigma} & \bar{\psi}_{2,k,\sigma} \end{pmatrix} \qquad \text{and} \qquad \Psi_{k',\sigma'} = \begin{pmatrix} \psi_{1,k',\sigma'} \\ \psi_{2,k',\sigma'} \end{pmatrix} \tag{D.38}$$

and the corresponding matrix Green's function

$$\mathcal{G}^{-1}_{\mathrm{SDW};(k,\sigma)(k',\sigma')} = \begin{pmatrix} (\mathrm{i}\nu_n - \varepsilon_{\boldsymbol{k}})\,\delta_{kk'}\,\delta_{\sigma\sigma'} & \boldsymbol{M}_{+,k-k'}\cdot\boldsymbol{\sigma}_{\sigma\sigma'} + \mathrm{i}\tilde{\boldsymbol{M}}_{-,k-k'}\cdot\boldsymbol{\sigma}_{\sigma\sigma'} \\ \boldsymbol{M}_{+,k-k'}\cdot\boldsymbol{\sigma}_{\sigma\sigma'} - \mathrm{i}\tilde{\boldsymbol{M}}_{-,k-k'}\cdot\boldsymbol{\sigma}_{\sigma\sigma'} & (\mathrm{i}\nu_n + \varepsilon_{\boldsymbol{k}})\,\delta_{kk'}\,\delta_{\sigma\sigma'} \end{pmatrix} \tag{D.39}$$

$$= \mathrm{i}\nu_n(\sigma_0)_{\sigma\sigma'}\tau_0\,\delta_{kk'} - \varepsilon_{\boldsymbol{k}}(\sigma_0)_{\sigma\sigma'}\tau_3\,\delta_{kk'} + \boldsymbol{M}_{+,k-k'}\cdot\boldsymbol{\sigma}_{\sigma\sigma'}\tau_1 - \tilde{\boldsymbol{M}}_{-,k-k'}\cdot\boldsymbol{\sigma}_{\sigma\sigma'}\tau_2\,, \tag{D.40}$$

where, again, we exploited the nesting condition $\varepsilon_{1,\boldsymbol{k}} = -\varepsilon_{2,\boldsymbol{k}}$. We can choose the coordinate system such that the mean-field order parameters are aligned with the z-axis, $\boldsymbol{M}_+ = M_+\boldsymbol{e}_z$ and $\tilde{\boldsymbol{M}}_- = \tilde{M}_-\boldsymbol{e}_z$, simplifying the mean-field part to

$$\mathcal{G}^{-1}_{\mathrm{MF}} = \underbrace{\mathrm{i}\nu_n\sigma_0\tau_0 - \varepsilon_{\boldsymbol{k}}\sigma_0\tau_3}_{=\mathcal{G}_0^{-1}} + \underbrace{M_+\sigma_3\tau_1 - \tilde{M}_-\sigma_3\tau_2}_{=\mathcal{U}}\,. \tag{D.41}$$

Ultimately, this results in the mean-field action

$$\mathcal{S}^{\mathrm{SDW}}_{\mathrm{MF}}(M_+,\tilde{M}_-) = \frac{M_+^2}{2V_{\mathrm{rSDW}}} + \frac{\tilde{M}_-^2}{2V_{\mathrm{iSDW}}} - \mathrm{Tr}\ln(-\mathcal{G}^{-1}_{\mathrm{MF}})\,. \tag{D.42}$$

Transition temperature Again, we can expand the mean-field part of the action to quadratic order in M_+ and $\tilde{M}_-$,

$$\mathcal{S}^{\mathrm{SDW}}_{\mathrm{MF}}(M_+,\tilde{M}_-) - \mathcal{S}^{\mathrm{SDW}}_{\mathrm{MF}}(M_+=0,\tilde{M}_-=0) = \frac{M_+^2}{2V_{\mathrm{rSDW}}} + \frac{\tilde{M}_-^2}{2V_{\mathrm{iSDW}}} + \frac{1}{2}\,\mathrm{Tr}(\mathcal{G}_0\mathcal{U}\mathcal{G}_0\mathcal{U}) \tag{D.43}$$

$$= \Big(\frac{1}{2V_{\mathrm{rSDW}}} - 2\int_k \frac{1}{\nu_n^2+\varepsilon_{\boldsymbol{k}}^2}\Big)M_+^2 + \Big(\frac{1}{2V_{\mathrm{iSDW}}} - 2\int_k \frac{1}{\nu_n^2+\varepsilon_{\boldsymbol{k}}^2}\Big)\tilde{M}_-^2\,, \tag{D.44}$$

and the sign change of the quadratic coefficient determines the respective transition temperatures

$$T_{\mathrm{SDW}} = \frac{2\mathrm{e}^{\gamma}\Lambda}{\pi}\mathrm{e}^{-\frac{1}{4\rho_{\mathrm{F}}V_{\mathrm{SDW}}}}\,. \tag{D.45}$$

Again, the mode for which the coupling V_{SDW} is larger is the one that condenses first.

Mean-field gap equation The mean-field gap equation obtained from the saddle-point equation is given by

$$0 = \frac{\mathrm{d}\mathcal{S}^{\mathrm{SDW}}_{\mathrm{MF}}}{\mathrm{d}M} = \frac{\mathrm{d}}{\mathrm{d}M}\Big[\frac{M^2}{2V_{\mathrm{SDW}}} - \mathrm{Tr}\ln(-\mathcal{G}^{-1}_{\mathrm{MF}})\Big] = 2M\Big[\frac{1}{2V_{\mathrm{SDW}}} - 2\int_k \frac{1}{\nu_n^2+\varepsilon_{\boldsymbol{k}}^2+M^2}\Big]\,, \tag{D.46}$$

which takes the form of the BCS gap equation for $g \equiv 4V_{\mathrm{SDW}}$. At $T=0$, it reduces to

$$0 = \frac{1}{2V_{\mathrm{SDW}}} - 2\rho_{\mathrm{F}}\ln\Big(\frac{2v_{\mathrm{F}}\Lambda}{M}\Big) \tag{D.47}$$

for the nontrivial solution.

Fluctuations In order to study Gaussian fluctuation corrections to either the rSDW or the iSDW mean-field gap, we split the respective Green's function into mean-field and fluctuation part once more,

$$\mathcal{G}^{-1}_{\mathrm{rSDW};(k,\sigma)(k',\sigma')} = \delta_{kk'}[\mathrm{i}\nu_n(\sigma_0)_{\sigma\sigma'}\tau_0 - \varepsilon_{\boldsymbol{k}}(\sigma_0)_{\sigma\sigma'}\tau_3 + M_+(\sigma_3)_{\sigma\sigma'}\tau_1] + \boldsymbol{m}_{+,k-k'}\cdot\boldsymbol{\sigma}_{\sigma\sigma'}\tau_1 \tag{D.48}$$

$$\mathcal{G}^{-1}_{\mathrm{iSDW};(k,\sigma)(k',\sigma')} = \delta_{kk'}[\mathrm{i}\nu_n(\sigma_0)_{\sigma\sigma'}\tau_0 - \varepsilon_{\boldsymbol{k}}(\sigma_0)_{\sigma\sigma'}\tau_3 - \tilde{M}_-(\sigma_3)_{\sigma\sigma'}\tau_2] - \tilde{\boldsymbol{m}}_{-,k-k'}\cdot\boldsymbol{\sigma}_{\sigma\sigma'}\tau_2\,. \tag{D.49}$$

Furthermore, we note that $(\boldsymbol{m}_q)_3$ is the fluctuating mode longitudinal to the respective mean-field order parameter, whereas the other two modes, $(\boldsymbol{m}_q)_1$ and $(\boldsymbol{m}_q)_2$, are transverse modes.

The fluctuation corrections to the SDW mean-field action are given by

$$\mathrm{e}^{-(\mathcal{S}^{\mathrm{SDW}}_{\mathrm{MF}}+\mathcal{S}^{\mathrm{SDW}}_{\mathrm{fluct}})} = \mathrm{e}^{-\mathcal{S}^{\mathrm{SDW}}_{\mathrm{MF}}}\int\mathcal{D}\boldsymbol{m}\,\mathrm{e}^{-\frac{1}{2}\int_q \boldsymbol{m}_q\boldsymbol{\mathcal{D}}^{-1}_{\mathrm{SDW;q}}\boldsymbol{m}_{-q}} = \mathrm{e}^{-\mathcal{S}^{\mathrm{SDW}}_{\mathrm{MF}}}\mathrm{e}^{-\frac{1}{2}\int_q \ln\det(\boldsymbol{\mathcal{D}}^{-1}_{\mathrm{SDW};q})}\,. \tag{D.50}$$

The corresponding propagator is now of matrix form with elements

$$(\mathcal{D}^{-1}_{\mathrm{rSDW};q})_{ij} = \frac{1}{V_{\mathrm{rSDW}}}\,\delta_{ij} + \int_k \mathrm{tr}[\mathcal{G}^{\mathrm{rSDW}}_{\mathrm{MF};k+\frac{q}{2}}(\sigma_i\tau_1)\mathcal{G}^{\mathrm{rSDW}}_{\mathrm{MF};k-\frac{q}{2}}(\sigma_j\tau_1)]\,, \tag{D.51}$$

$$(\mathcal{D}^{-1}_{\mathrm{iSDW};q})_{ij} = \frac{1}{V_{\mathrm{iSDW}}}\,\delta_{ij} + \int_k \mathrm{tr}[\mathcal{G}^{\mathrm{iSDW}}_{\mathrm{MF};k+\frac{q}{2}}(\sigma_i\tau_2)\mathcal{G}^{\mathrm{iSDW}}_{\mathrm{MF};k-\frac{q}{2}}(\sigma_j\tau_2)]\,. \tag{D.52}$$

The three fluctuating modes, two transverse and one longitudinal, do not couple to each other since the respective traces vanish exactly. The other traces of interest amount to

$$\mathrm{tr}[\tau_i\tau_1\tau_j\tau_1] = \begin{cases} 2 & \text{for} \quad i=j\in\{0,1\}\,,\\ -2 & \text{for} \quad i=j\in\{2,3\}\,,\\ 0 & \text{otherwise}\,,\end{cases} \tag{D.53}$$

$$\mathrm{tr}[\tau_i\tau_2\tau_j\tau_2] = \begin{cases} 2 & \text{for} \quad i=j\in\{0,2\}\,,\\ -2 & \text{for} \quad i=j\in\{1,3\}\,,\\ 0 & \text{otherwise}\,,\end{cases} \tag{D.54}$$

$$\mathrm{tr}[\sigma_0\sigma_i\sigma_0\sigma_j] = \begin{cases} 2 & \text{for} \quad i=j\,,\\ 0 & \text{otherwise}\,,\end{cases} \tag{D.55}$$

$$\mathrm{tr}[\sigma_3\sigma_i\sigma_3\sigma_j] = \begin{cases} 2 & \text{for} \quad i=j\in\{0,3\}\,,\\ -2 & \text{for} \quad i=j\in\{1,2\}\,,\\ 0 & \text{otherwise}\,.\end{cases} \tag{D.56}$$

Eq. (D.56) implies that the fluctuation propagators of the two transverse modes are equal and differ from the propagator of the longitudinal fluctuations only in the anomalous part. As a result, the inverse fluctuation propagators can be expressed in terms of

$$\Pi^{\perp}_q = 4\Pi^{\mathrm{n}}_q - 4\Pi^{\mathrm{a}}_q \tag{D.57}$$

$$\text{and} \qquad \Pi^{\parallel}_q = 4\Pi^{\mathrm{n}}_q + 4\Pi^{\mathrm{a}}_q\,, \tag{D.58}$$

where again, normal and anomalous contribution have to be understood as functions of the respective order parameter M_+ or $\tilde{M}_-$ here. Finally, the fluctuation propagator for fluctuations around both the

rSDW mean-field configuration and the iSDW mean-field configuration takes the same form,

$$\boldsymbol{\mathcal{D}}^{-1}_{\mathrm{rSDW};q} = \begin{pmatrix} \frac{1}{V_{\mathrm{rSDW}}} + \Pi^{\perp}_q & 0 & 0 \\ 0 & \frac{1}{V_{\mathrm{rSDW}}} + \Pi^{\perp}_q & 0 \\ 0 & 0 & \frac{1}{V_{\mathrm{rSDW}}} + \Pi^{\parallel}_q \end{pmatrix}, \tag{D.59}$$

$$\boldsymbol{\mathcal{D}}^{-1}_{\mathrm{iSDW};q} = \begin{pmatrix} \frac{1}{V_{\mathrm{iSDW}}} + \Pi^{\perp}_q & 0 & 0 \\ 0 & \frac{1}{V_{\mathrm{iSDW}}} + \Pi^{\perp}_q & 0 \\ 0 & 0 & \frac{1}{V_{\mathrm{iSDW}}} + \Pi^{\parallel}_q \end{pmatrix}. \tag{D.60}$$

The above form makes the connection to phase and amplitude fluctuations in a neutral superconductor as discussed in Secs. 5.2.1 and A.3 obvious: Longitudinal fluctuations correspond to amplitude fluctuations, whereas transverse fluctuations can be identified with fluctuations of the phase. Finally, the additional contribution to the action from Gaussian fluctuations reads

$$\mathcal{S}^{\mathrm{SDW}}_{\mathrm{fluct}} = \frac{1}{2}\int_q \ln\det(\boldsymbol{\mathcal{D}}^{-1}_{\mathrm{SDW};q}) = \frac{1}{2}\int_q \ln[(\frac{1}{V_{\mathrm{SDW}}} + \Pi^{\perp}_q)^2(\frac{1}{V_{\mathrm{SDW}}} + \Pi^{\parallel}_q)]\,, \tag{D.61}$$

resulting in

$$\frac{\mathrm{d}\mathcal{S}^{\mathrm{SDW}}_{\mathrm{fluct}}}{\mathrm{d}M^2} = \frac{1}{2}\int_q \left[2\frac{\frac{\mathrm{d}\Pi^{\perp}_q}{\mathrm{d}M^2}}{\frac{1}{V_{\mathrm{SDW}}} + \Pi^{\perp}_q} + \frac{\frac{\mathrm{d}\Pi^{\parallel}_q}{\mathrm{d}M^2}}{\frac{1}{V_{\mathrm{SDW}}} + \Pi^{\parallel}_q}\right]. \tag{D.62}$$

We know from our discussion of fluctuation corrections to BCS theory, that divergences arise in the regime $2M \ll \sqrt{\omega^2 + (v_{\mathrm{F}} q\cos\theta)^2}$, where we can use $\frac{1}{4V_{\mathrm{SDW}}} + \Pi^{\mathrm{n}}_q \gg \Pi^{\mathrm{a}}_q$ and $\mathrm{d}\Pi^{\mathrm{a}}_q/\mathrm{d}M^2 \gg \mathrm{d}\Pi^{\mathrm{n}}_q/\mathrm{d}M^2$ to make the result more transparent. The corresponding fluctuation corrections to the gap equation then amounts to

$$\frac{\mathrm{d}\mathcal{S}^{\mathrm{SDW}}_{\mathrm{fluct}}}{\mathrm{d}M^2} = -\frac{1}{2}\int_q \frac{(2-1)\frac{\mathrm{d}\Pi^{\mathrm{a}}_q}{\mathrm{d}M^2}}{\frac{1}{4V_{\mathrm{SDW}}} + \Pi^{\mathrm{n}}_q} < 0\,, \tag{D.63}$$

where the factor $(2-1)$ is due to the contributions from the two transverse and the one longitudinal mode which differ in the sign of the anomalous part. In conclusion, the contributions from Gaussian fluctuations to the SDW mean-field gap cannot be neglected, but in contrast to the case of CDW order, the correction is negative. Therefore, the fluctuation-corrected value of the gap is larger than its mean-field value.

D.1.3 RG analysis

Here, we briefly summarize the notation and the results of the one-loop RG analysis presented in Ref. 41 for the two-band model of iron-based superconductors at perfect nesting. The five couplings which survive at tree level, $V^{\mathrm{A}}_{12,21}$, $V^{\mathrm{S}}_{12,21}$, $V^{\mathrm{S}}_{11,22}$, $V^{\mathrm{S}}_{11,11}$, and $V^{\mathrm{S}}_{22,22}$, are connected to the notation of

Ref. 41 by

$$\frac{U_1}{2} = V^{\mathrm{S}}_{12,21} + V^{\mathrm{A}}_{12,21}\,, \tag{D.64a}$$
$$\frac{U_2}{2} = V^{\mathrm{S}}_{12,21} - V^{\mathrm{A}}_{12,21}\,, \tag{D.64b}$$
$$\frac{U_3}{2} = V^{\mathrm{S}}_{11,22}\,, \tag{D.64c}$$
$$\frac{U_4}{2} = V^{\mathrm{S}}_{11,11}\,, \tag{D.64d}$$
$$\frac{U_5}{2} = V^{\mathrm{S}}_{22,22}\,. \tag{D.64e}$$

Here, the couplings U_i flow, and their bare values are denoted by $U_i^{(0)}$. The respective couplings in charge and spin channel can be expressed as

$$V^{\mathrm{ch}}_{12,12} = -\tfrac{1}{4}(U_1 - 2U_2)\,, \qquad V^{\mathrm{sp}}_{12,12} = -\tfrac{1}{4}U_1\,, \tag{D.65a}$$
$$V^{\mathrm{ch}}_{12,21} = \tfrac{1}{4}(2U_1 - U_2)\,, \qquad V^{\mathrm{sp}}_{12,21} = -\tfrac{1}{4}U_2\,, \tag{D.65b}$$
$$V^{\mathrm{ch}}_{11,22} = \tfrac{1}{4}U_3\,, \qquad V^{\mathrm{sp}}_{11,22} = -\tfrac{1}{4}U_3\,, \tag{D.65c}$$
$$V^{\mathrm{ch}}_{11,11} = \tfrac{1}{4}U_4\,, \qquad V^{\mathrm{sp}}_{11,11} = -\tfrac{1}{4}U_4\,, \tag{D.65d}$$
$$V^{\mathrm{ch}}_{22,22} = \tfrac{1}{4}U_5 \qquad V^{\mathrm{sp}}_{22,22} = -\tfrac{1}{4}U_5\,. \tag{D.65e}$$

For perfectly nested bands, Ref. 41 estimated for the bare couplings that the following relations are satisfied in the two-band model of FeSCs: $U_1^{(0)} = U_4^{(0)} = U_5^{(0)} > 0$ and $U_2^{(0)} = U_3^{(0)}$, and furthermore, $U_1^{(0)} > U_3^{(0)}$. Furthermore, it is convenient to introduce dimensionless coupling constants by $u_i := \rho_{\mathrm{F}} U_i$. As the two intraband coupling constants u_4 and u_5 are equivalent and not of interest for density-wave order, we consider $u_4 = u_5$ in the remainder. (Moreover, the pure s^{++} and s^{+-} SC states in FeSCs also require $u_4 = u_5$.)

RG equations We considered the generalization of the RG analysis presented in Ref. 41 to the case of N-component spinors and the corresponding SU(N)-invariant interaction. This results in the following flow equations for the coupling constants:

$$\frac{\mathrm{d}u_1}{\mathrm{d}t} = u_1^2 + u_3^2\,, \tag{D.66a}$$
$$\frac{\mathrm{d}u_2}{\mathrm{d}t} = u_2(2u_1 - Nu_2) - (N-2)u_3^2\,, \tag{D.66b}$$
$$\frac{\mathrm{d}u_3}{\mathrm{d}t} = 2u_3[2u_1 - (N-1)u_2 - u_4]\,, \tag{D.66c}$$
$$\frac{\mathrm{d}u_4}{\mathrm{d}t} = -u_3^2 - u_4^2\,. \tag{D.66d}$$

These equations reveal that for $N = 2$ (as well as for $N = 1$), certain terms vanish, however, channel interference is present for arbitrary N in this model.

In Ref. 41, the flow of the coupling constants (as determined by Eq. (D.66)) is analyzed. They find that repulsive interband pair hopping ($u_3^0 > 0$) leads to competing rSDW, iCDW, and s^{+-} SC instabilities, whereas attractive interband pair hopping ($u_3^0 < 0$) leads to competing rCDW, iSDW, and s^{++} SC instabilities.

D.2 Tetragonal magnetic order

In this section, we briefly comment how the decoupling in the spin channel as performed in Sec. D.1.2 can be generalized to a four-band model with two nesting vectors $\boldsymbol{Q}_1 = (\pi, 0)$ and $\boldsymbol{Q}_2 = (0, \pi)$. We start from the quartic interaction in the spin channel which may be written in the form

$$\mathcal{S}_{\mathrm{int}}(\bar{\psi}, \psi) = -\frac{V_{\mathrm{SDW}}}{2} \sum_{i=1}^{2} \int_q \hat{\boldsymbol{S}}_{i,q} \cdot \hat{\boldsymbol{S}}_{i,-q} \,, \tag{D.67}$$

where we introduced the abbreviations

$$\hat{\boldsymbol{S}}_{1,q} = \sum_{\sigma,\sigma'} \int_k \left(\bar{\psi}_{\mathrm{h}_\Gamma,k,\sigma} \boldsymbol{\sigma}_{\sigma\sigma'} \psi_{\mathrm{e}_X,k+q,\sigma'} + \bar{\psi}_{\mathrm{e}_Y,k,\sigma} \boldsymbol{\sigma}_{\sigma\sigma'} \psi_{\mathrm{h}_M,k+q,\sigma'} + \mathrm{G.\,c.} \right) \tag{D.68a}$$

$$\text{and} \qquad \hat{\boldsymbol{S}}_{2,q} = \sum_{\sigma,\sigma'} \int_k \left(\bar{\psi}_{\mathrm{h}_\Gamma,k,\sigma} \boldsymbol{\sigma}_{\sigma\sigma'} \psi_{\mathrm{e}_Y,k+q,\sigma'} + \bar{\psi}_{\mathrm{e}_X,k,\sigma} \boldsymbol{\sigma}_{\sigma\sigma'} \psi_{\mathrm{h}_M,k+q,\sigma'} + \mathrm{G.\,c.} \right) . \tag{D.68b}$$

Here, $\hat{\boldsymbol{S}}_{i,q}$ contains only certain combinations of operators connected by the nesting vector $\boldsymbol{Q}_i$. Then, in complete analogy, we may decouple the two contributions associated with $\boldsymbol{Q}_1$ and $\boldsymbol{Q}_2$ by introducing the two independent order parameters $\boldsymbol{M}_1$ and $\boldsymbol{M}_2$, respectively. Thereby, we can write

$$\begin{aligned} \int \mathcal{D}[\bar{\psi}, \psi] \, \mathrm{e}^{-(\mathcal{S}_0 + \mathcal{S}_{\mathrm{int}})} = \int \mathcal{D}\boldsymbol{M}_1 \, \mathcal{D}\boldsymbol{M}_2 \, \mathrm{e}^{-\frac{1}{2V_{\mathrm{SDW}}} \sum_i \int_q \boldsymbol{M}_{i,q} \cdot \boldsymbol{M}_{i,-q}} \\ \times \int \mathcal{D}[\bar{\psi}, \psi] \, \mathrm{e}^{-\sum_{\sigma,\sigma'} \int_{k,k'} \bar{\Psi}_{k,\sigma} (-\mathcal{G}^{-1}_{(k,\sigma)(k'\sigma')}) \Psi_{k',\sigma'}} \,. \end{aligned} \tag{D.69}$$

Here, we introduced the spinors

$$\bar{\Psi}_{k,\sigma} = \begin{pmatrix} \bar{\psi}_{\mathrm{h}_\Gamma,k,\sigma} & \bar{\psi}_{\mathrm{e}_X,k,\sigma} & \bar{\psi}_{\mathrm{e}_Y,k,\sigma} & \bar{\psi}_{\mathrm{h}_M,k,\sigma} \end{pmatrix} \tag{D.70}$$

in band space (in contrast to superconductivity, where we need Nambu spinors). Here, for the sake of readability, we only state the mean-field version of the matrix Green's function, which reads

$$\mathcal{G}^{-1}_{\mathrm{MF};k,\sigma\sigma'} = \begin{pmatrix} (\mathrm{i}\nu_n - \varepsilon_{\mathrm{h}_\Gamma,\boldsymbol{k}}) \, \delta_{\sigma\sigma'} & \boldsymbol{M}_1 \cdot \boldsymbol{\sigma}_{\sigma\sigma'} & \boldsymbol{M}_2 \cdot \boldsymbol{\sigma}_{\sigma\sigma'} & 0 \\ \boldsymbol{M}_1 \cdot \boldsymbol{\sigma}_{\sigma\sigma'} & (\mathrm{i}\nu_n - \varepsilon_{\mathrm{e}_X,\boldsymbol{k}}) \, \delta_{\sigma\sigma'} & 0 & \boldsymbol{M}_2 \cdot \boldsymbol{\sigma}_{\sigma\sigma'} \\ \boldsymbol{M}_2 \cdot \boldsymbol{\sigma}_{\sigma\sigma'} & 0 & (\mathrm{i}\nu_n - \varepsilon_{\mathrm{e}_Y,\boldsymbol{k}}) \, \delta_{\sigma\sigma'} & \boldsymbol{M}_1 \cdot \boldsymbol{\sigma}_{\sigma\sigma'} \\ 0 & \boldsymbol{M}_2 \cdot \boldsymbol{\sigma}_{\sigma\sigma'} & \boldsymbol{M}_1 \cdot \boldsymbol{\sigma}_{\sigma\sigma'} & (\mathrm{i}\nu_n - \varepsilon_{\mathrm{h}_M,\boldsymbol{k}}) \, \delta_{\sigma\sigma'} \end{pmatrix} . \tag{D.71}$$

The dispersions $\varepsilon_{\lambda,\boldsymbol{k}}$ are given in Eq. (4.5) of the main text. Perfect nesting in the four-band model is equivalent to the condition $\varepsilon_{\boldsymbol{k}} \equiv -\varepsilon_{\mathrm{h}_\Gamma,\boldsymbol{k}} = \varepsilon_{\mathrm{e}_X,\boldsymbol{k}} = \varepsilon_{\mathrm{e}_Y,\boldsymbol{k}} = -\varepsilon_{\mathrm{h}_M,\boldsymbol{k}}$. Therefore, the matrix Green's function in a model of nested FS pockets assumes the same form as the Nambu Green's function in the case of superconductivity, however, for a physically different reason.

Coefficients of the clean four-band model Following the usual procedure, we may integrate out fermions and expand in the order parameters, which immediately results in an expansion of type (4.8),

$$\mathcal{F}(\boldsymbol{M}_1, \boldsymbol{M}_2) = \sum_i a_i |\boldsymbol{M}_i|^2 + \sum_{i,j} u_{ij} |\boldsymbol{M}_i|^2 |\boldsymbol{M}_j|^2 + 2w (\boldsymbol{M}_1 \cdot \boldsymbol{M}_2)^2 \,. \tag{D.72}$$

In the absence of impurities, the coefficients of the four-band model are given by

$$a_i = \frac{1}{4V_{\mathrm{SDW}}} + 2\int_k \Big(G_{\mathrm{h}_\Gamma,\boldsymbol{k}}(\nu_n) G_{\mathrm{e}_i,\boldsymbol{k}}(\nu_n) + G_{\mathrm{h}_M,\boldsymbol{k}}(\nu_n) G_{\mathrm{e}_{\bar{i}},\boldsymbol{k}}(\nu_n) \Big) , \tag{D.73a}$$

$$u_{ii} = \int_k \Big(G^2_{\mathrm{h}_\Gamma,\boldsymbol{k}}(\nu_n) G^2_{\mathrm{e}_i,\boldsymbol{k}}(\nu_n) + G^2_{\mathrm{h}_M,\boldsymbol{k}}(\nu_n) G^2_{\mathrm{e}_{\bar{i}},\boldsymbol{k}}(\nu_n) \Big) , \tag{D.73b}$$

$$\begin{aligned} u_{12} = u_{21} = \int_k \Big[&\Big(G^2_{\mathrm{h}_\Gamma,\boldsymbol{k}}(\nu_n) + G^2_{\mathrm{h}_M,\boldsymbol{k}}(\nu_n) \Big) G_{\mathrm{e}_X,\boldsymbol{k}}(\nu_n) G_{\mathrm{e}_Y,\boldsymbol{k}}(\nu_n) \\ &+ \Big(G^2_{\mathrm{e}_X,\boldsymbol{k}}(\nu_n) + G^2_{\mathrm{e}_Y,\boldsymbol{k}}(\nu_n) \Big) G_{\mathrm{h}_\Gamma,\boldsymbol{k}}(\nu_n) G_{\mathrm{h}_M,\boldsymbol{k}}(\nu_n) - 2 G_{\mathrm{h}_\Gamma,\boldsymbol{k}}(\nu_n) G_{\mathrm{h}_M,\boldsymbol{k}}(\nu_n) G_{\mathrm{e}_X,\boldsymbol{k}}(\nu_n) G_{\mathrm{e}_Y,\boldsymbol{k}}(\nu_n) \Big] , \end{aligned} \tag{D.73c}$$

$$w = 4\int_k G_{\mathrm{h}_\Gamma,\boldsymbol{k}}(\nu_n) G_{\mathrm{h}_M,\boldsymbol{k}}(\nu_n) G_{\mathrm{e}_X,\boldsymbol{k}}(\nu_n) G_{\mathrm{e}_Y,\boldsymbol{k}}(\nu_n) . \tag{D.73d}$$

Upon neglecting the second hole pocket at the M point, i. e., considering $E_M \to \infty$ (implying $G_{\mathrm{h}_M,\boldsymbol{k}}(\nu_n) = 0$), we recover the results of the three-band model as summarized in Eq. (4.10) and previously derived in Ref. 159, for instance.

Coefficients of the disordered three-band model Disorder can be considered in analogy to superconductivity, as described in Apps. B and C, see also Eq. (C.30). Within the three-band model of FeSCs introduced in Sec. 4.2, this results in the following expressions for the coefficients:

$$g = \mathfrak{g}_2^{(1)} - \mathfrak{g}_1^{(1)} + \mathfrak{g}_2^{(2)} - \mathfrak{g}_1^{(2)} \tag{D.74}$$

$$\begin{aligned} &= -\frac{T}{2}\sum_n \int \frac{\mathrm{d}\boldsymbol{k}}{(2\pi)^2} G^2_{\mathrm{h}_\Gamma,\boldsymbol{k}}(\nu_n) \Big(G_{\mathrm{e}_X,\boldsymbol{k}}(\nu_n) - G_{\mathrm{e}_Y,\boldsymbol{k}}(\nu_n) \Big)^2 \\ &\quad - \Gamma_{\mathrm{h}}^{\mathrm{intra}} \frac{T}{2}\sum_n \Big[\int \frac{\mathrm{d}\boldsymbol{k}}{(2\pi)^2} G^2_{\mathrm{h}_\Gamma,\boldsymbol{k}}(\nu_n) \Big(G_{\mathrm{e}_X,\boldsymbol{k}}(\nu_n) - G_{\mathrm{e}_Y,\boldsymbol{k}}(\nu_n) \Big) \Big]^2 , \end{aligned} \tag{D.75}$$

$$u = \mathfrak{g}_2^{(1)} + \mathfrak{g}_1^{(1)} + \mathfrak{g}_2^{(2)} + \mathfrak{g}_1^{(2)} \tag{D.76}$$

$$\begin{aligned} &= \frac{T}{2}\sum_n \int \frac{\mathrm{d}\boldsymbol{k}}{(2\pi)^2} G^2_{\mathrm{h}_\Gamma,\boldsymbol{k}}(\nu_n) \Big(G_{\mathrm{e}_X,\boldsymbol{k}}(\nu_n) + G_{\mathrm{e}_Y,\boldsymbol{k}}(\nu_n) \Big)^2 \\ &\quad + \Gamma_{\mathrm{h}}^{\mathrm{intra}} \frac{T}{2}\sum_n \Big[\int \frac{\mathrm{d}\boldsymbol{k}}{(2\pi)^2} G^2_{\mathrm{h}_\Gamma,\boldsymbol{k}}(\nu_n) \Big(G_{\mathrm{e}_X,\boldsymbol{k}}(\nu_n) + G_{\mathrm{e}_Y,\boldsymbol{k}}(\nu_n) \Big) \Big]^2 , \end{aligned} \tag{D.77}$$

$$w = 2\mathfrak{w} = 2\Gamma_{\mathrm{e-e}}^{\mathrm{inter}} \sum_n \Big[\int \frac{\mathrm{d}\boldsymbol{k}}{(2\pi)^2} G_{\mathrm{h}_\Gamma,\boldsymbol{k}}(\nu_n) G_{\mathrm{e}_X,\boldsymbol{k}}(\nu_n) G_{\mathrm{e}_Y,\boldsymbol{k}}(\nu_n) \Big]^2 . \tag{D.78}$$

In evaluating the momentum integrals, we use $\int \frac{\mathrm{d}\boldsymbol{k}}{(2\pi)^2} \ldots \equiv \rho_{\mathrm{F}} \int_{-\infty}^{\infty} \mathrm{d}\varepsilon \int_0^{2\pi} \frac{\mathrm{d}\theta}{2\pi} \ldots$. Furthermore, close to the limit of perfect nesting, we may expand in the small parameters $\delta_\mu/(2\pi T)$ and $\delta_m/(2\pi T)$, which finally results in the expressions presented and discussed in Chap. 4.

Appendix E

Calculation of fluctuation corrections

When evaluating fluctuations corrections to mean-field theories, one frequently encounters the following types of integrals in the inverse fluctuation propagators:

$$\Pi_q^{\mathrm{n}} := -\int \frac{\mathrm{d}\nu}{2\pi} \int_{-v_{\mathrm{F}}\Lambda}^{v_{\mathrm{F}}\Lambda} \mathrm{d}\varepsilon\, \rho(\varepsilon) \frac{\nu_+\nu_- + \varepsilon_+\varepsilon_-}{[\nu_+^2 + \varepsilon_+^2 + \Delta_0^2][\nu_-^2 + \varepsilon_-^2 + \Delta_0^2]}\,, \tag{E.1}$$

$$\Pi_q^{\mathrm{a}} := \int \frac{\mathrm{d}\nu}{2\pi} \int_{-v_{\mathrm{F}}\Lambda}^{v_{\mathrm{F}}\Lambda} \mathrm{d}\varepsilon\, \rho(\varepsilon) \frac{\Delta_0^2}{[\nu_+^2 + \varepsilon_+^2 + \Delta_0^2][\nu_-^2 + \varepsilon_-^2 + \Delta_0^2]}\,, \tag{E.2}$$

as well as
$$-\int \frac{\mathrm{d}\nu}{2\pi} \int_{-v_{\mathrm{F}}\Lambda}^{v_{\mathrm{F}}\Lambda} \mathrm{d}\varepsilon\, \rho(\varepsilon) \frac{\mathrm{i}\nu_+\varepsilon_- - \mathrm{i}\nu_-\varepsilon_+}{[\nu_+^2 + \varepsilon_+^2 + \Delta_0^2][\nu_-^2 + \varepsilon_-^2 + \Delta_0^2]}\,. \tag{E.3}$$

Here, we adopted the notation of Ref. 100 and introduced $\nu_\pm = \nu \pm \frac{\omega}{2}$ and $\varepsilon_\pm = \varepsilon_{\boldsymbol{k}\pm\frac{\boldsymbol{q}}{2}} = \varepsilon \pm v_{\mathrm{F}}\frac{q}{2}\cos\theta$, where θ is the angle between internal and external momenta $\boldsymbol{k}$ and $\boldsymbol{q}$ and we linearized the dispersion around the Fermi surface. In the remainder, we will work at particle-hole symmetry and hence assume a constant density of states $\rho(\varepsilon) = \rho_{\mathrm{F}}$ at the Fermi level, which immediately implies that the integral (E.3) vanishes. The remaining two integrals correspond to the normal and anomalous contributions as introduced in Sec. 5.2.1.

Since the fluctuation propagators have to be integrated over all frequencies and momenta up to the cutoff in the evaluation of fluctuation corrections to the mean-field gap equation, a small-q expansion is not sufficient. However, the angular integration cannot be performed for arbitrary frequency and momentum. Fortunately, it turns out that the above integrals only depend on frequency and momentum via the combination

$$r = \frac{\sqrt{\omega^2 + (v_{\mathrm{F}} q \cos\theta)^2}}{2\Delta_0}\,. \tag{E.4}$$

This allows us to consider the limits $r \ll 1$ and $r \gg 1$ separately, and find analytic expressions at least in these two limits.

In the remainder of this appendix, we exemplarily demonstrate that the anomalous part Π_q^{a} only depends on r, and subsequently summarize the results of the integrals previously obtained in the two regimes $r \ll 1$ and $r \gg 1$ by Refs. 100 and 198.

E.1 Evaluation of the integrals

We use the anomalous contribution Π_q^{a} that we introduced in our discussion of Gaussian fluctuation corrections to zero-temperature mean-field gap equations in Chap. 5 as an example on how to rewrite such integrals using Feynman's method [215]. That is, we exploit the identity

$$\frac{1}{ab} = \frac{1}{b-a}\left(\frac{1}{a}-\frac{1}{b}\right) = \frac{1}{b-a}\int_a^b \frac{\mathrm{d}x}{x^2} = \int_0^1 \frac{\mathrm{d}z}{[az+b(1-z)]^2} \tag{E.5}$$

in order to rewrite the denominator such that it contains only a single factor. For more details, we refer to Refs. 100 and 198, where these integrals have been evaluated previously. We start from

$$\Pi_q^{\mathrm{a}} = \rho_{\mathrm{F}} \int_{-\infty}^{\infty} \frac{\mathrm{d}\nu}{2\pi} \int_{-v_{\mathrm{F}}\Lambda}^{v_{\mathrm{F}}\Lambda} \mathrm{d}\varepsilon \, \frac{\Delta_0^2}{[(\underbrace{\nu+\frac{\omega}{2}}_{=\nu_+})^2 + (\underbrace{\varepsilon + v_{\mathrm{F}}\frac{q}{2}\cos\theta}_{=\varepsilon_+})^2 + \Delta_0^2][(\underbrace{\nu-\frac{\omega}{2}}_{=\nu_-})^2 + (\underbrace{\varepsilon - v_{\mathrm{F}}\frac{q}{2}\cos\theta}_{=\varepsilon_-})^2 + \Delta_0^2]} \tag{E.6}$$

$$= \rho_{\mathrm{F}} \int_{-\infty}^{\infty} \frac{\mathrm{d}\nu}{2\pi} \int_{-v_{\mathrm{F}}\Lambda}^{v_{\mathrm{F}}\Lambda} \mathrm{d}\varepsilon \int_0^1 \mathrm{d}z \, \frac{\Delta_0^2}{[(\nu_+^2+\varepsilon_+^2+\Delta_0^2)z + (\nu_-^2+\epsilon_-^2+\Delta_0^2)(1-z)]^2}$$

$$= \rho_{\mathrm{F}} \int_{-\infty}^{\infty} \frac{\mathrm{d}\nu}{2\pi} \int_{-v_{\mathrm{F}}\Lambda}^{v_{\mathrm{F}}\Lambda} \mathrm{d}\varepsilon \int_0^1 \mathrm{d}z \, \frac{\Delta_0^2}{[(\underbrace{\nu_+^2-\nu_-^2}_{=2\nu\omega} + \underbrace{\varepsilon_+^2-\varepsilon_-^2}_{=2\varepsilon v_{\mathrm{F}} q\cos\theta})z + \nu_-^2+\epsilon_-^2+\Delta_0^2]^2} \, . \tag{E.7}$$

As a next step, we complete the square in the denominator,

$$\Pi_q^{\mathrm{a}} = \rho_{\mathrm{F}} \int_{-\infty}^{\infty} \frac{\mathrm{d}\nu}{2\pi} \int_{-v_{\mathrm{F}}\Lambda}^{v_{\mathrm{F}}\Lambda} \mathrm{d}\varepsilon \int_0^1 \mathrm{d}z \, \frac{\Delta_0^2}{[\nu^2 + 2\nu(2z-1)\frac{\omega}{2} + \varepsilon^2 + 2\varepsilon(2z-1)\frac{v_{\mathrm{F}}q\cos\theta}{2} + \frac{\omega^2}{4} + \frac{(v_{\mathrm{F}}q\cos\theta)^2}{4} + \Delta_0^2]^2}$$

$$= \rho_{\mathrm{F}} \int_{-\infty}^{\infty} \frac{\mathrm{d}\nu}{2\pi} \int_{-v_{\mathrm{F}}\Lambda}^{v_{\mathrm{F}}\Lambda} \mathrm{d}\varepsilon \int_0^1 \mathrm{d}z \, \frac{\Delta_0^2}{[\tilde{\nu}^2 + \tilde{\varepsilon}^2 + \frac{\omega^2}{4}(1-(2z-1)^2) + \frac{(v_{\mathrm{F}}q\cos\theta)^2}{4}(1-(2z-1)^2) + \Delta_0^2]^2}$$

$$= \rho_{\mathrm{F}} \int_{-\infty}^{\infty} \frac{\mathrm{d}\nu}{2\pi} \int_{-v_{\mathrm{F}}\Lambda}^{v_{\mathrm{F}}\Lambda} \mathrm{d}\varepsilon \int_0^1 \mathrm{d}z \, \frac{\Delta_0^2}{[\tilde{\nu}^2 + \tilde{\varepsilon}^2 + \omega^2(z-z^2) + (v_{\mathrm{F}}q\cos\theta)^2(z-z^2) + \Delta_0^2]^2} \, , \tag{E.8}$$

where we introduced $\tilde{\nu} = \nu + (2z-1)\frac{\omega}{2}$ and $\tilde{\varepsilon} = \varepsilon + (2z-1)\frac{v_{\mathrm{F}}q\cos\theta}{2}$. Finally, we can rewrite the integrals in terms of $\tilde{\varepsilon}$ and $\tilde{\nu}$,

$$\int_{-\infty}^{\infty} \frac{\mathrm{d}\nu}{2\pi} \int_{-v_{\mathrm{F}}\Lambda}^{v_{\mathrm{F}}\Lambda} \mathrm{d}\varepsilon \ldots \to \int_{-\infty}^{\infty} \mathrm{d}\tilde{\nu} \int_{-v_{\mathrm{F}}\Lambda+(2z-1)\frac{v_{\mathrm{F}}q\cos\theta}{2}}^{v_{\mathrm{F}}\Lambda+(2z-1)\frac{v_{\mathrm{F}}q\cos\theta}{2}} \mathrm{d}\tilde{\varepsilon} \ldots \overset{q\ll\Lambda}{\to} \int_{-\infty}^{\infty} \mathrm{d}\tilde{\nu} \int_{-v_{\mathrm{F}}\Lambda}^{v_{\mathrm{F}}\Lambda} \mathrm{d}\tilde{\varepsilon} \ldots \, , \tag{E.9}$$

which results in the expression

$$\Pi_q^{\mathrm{a}} = \rho_{\mathrm{F}} \int_{-\infty}^{\infty} \frac{\mathrm{d}\tilde{\nu}}{2\pi} \int_{-v_{\mathrm{F}}\Lambda}^{v_{\mathrm{F}}\Lambda} \mathrm{d}\tilde{\varepsilon} \int_0^1 \mathrm{d}z \frac{\Delta_0^2}{[\tilde{\nu}^2 + \tilde{\varepsilon}^2 + (\omega^2 + (v_{\mathrm{F}}q\cos\theta)^2)(z-z^2) + \Delta_0^2]^2} \, . \tag{E.10}$$

Therefore, in the limit $\omega \ll v_{\mathrm{F}}\Lambda$ and $q \ll \Lambda$, the integral I depends on q and ω only via the combination $\omega^2 + (v_{\mathrm{F}}q\cos\theta)^2$, suggesting to introduce the quantity

$$r = \frac{\sqrt{\omega^2 + (v_{\mathrm{F}}q\cos\theta)^2}}{2\Delta_0} \, . \tag{E.11}$$

Therefore, for convenience, we may evaluate the energy and frequency integral at $q = 0$ (implying $\omega = 2\Delta_0 r$). For further evaluation of the frequency integral, we refer to the discussion in the appendix of Ref. 216, or to Refs. 100 and 198.

E.2 Summary of the results

For completeness, we summarize the results of the integrals Π_q^{n} and Π_q^{a} as well as their derivatives w. r. t. the order parameter in the two limits $r \ll 1$ and $r \gg 1$. For a derivation, we refer to Refs. 100 and 198, where also the analytical expressions before performing the angular integration (which cannot be done for arbitrary values of r) can be found. In Ref. 100, these integrals appear as prefactors in an expansion of the polarization bubble in terms of Pauli matrices as

$$\mathbf{\Pi}_q = \Pi_0\tau_0 + \Pi_1\tau_1 + \Pi_2\tau_2 + \Pi_3\tau_3 = \Pi_q^{\mathrm{n}}\mathbb{1} + \Pi_q^{\mathrm{a}}\tau_3\,, \tag{E.12}$$

where the last equality reflects that $\Pi_1 = 0 = \Pi_2$ holds at particle-hole symmetry.

Regime $r \ll 1$ In the limit $\sqrt{\omega^2 + (v_{\mathrm{F}} q\cos\theta)^2} \ll 2\Delta_0$, the normal and anomalous contribution to the fluctuation propagator are given by

$$\frac{1}{g} + \Pi_q^{\mathrm{n}} = \frac{\rho_{\mathrm{F}}}{2} + \frac{2}{3}\rho_{\mathrm{F}}\int_\Omega r^2\,, \qquad \frac{\mathrm{d}\Pi_q^{\mathrm{n}}}{\mathrm{d}\Delta_0^2} = \frac{\rho_{\mathrm{F}}}{2\Delta_0^2}\,, \tag{E.13a}$$

$$\Pi_q^{\mathrm{a}} = \frac{\rho_{\mathrm{F}}}{2} - \frac{1}{3}\rho_{\mathrm{F}}\int_\Omega r^2\,, \qquad \frac{\mathrm{d}\Pi_q^{\mathrm{a}}}{\mathrm{d}\Delta_0^2} = \frac{\rho_{\mathrm{F}}}{3\Delta_0^2}\int_\Omega r^2\,, \tag{E.13b}$$

where $\int_\Omega \ldots$ denotes the remaining angular integration over θ. Here, we also stated next-to-leading order corrections for Π_q^{n} and Π_q^{a} since the leading-order term cancels in $(\mathcal{D}_q^{-1})_{22}$. The results for the leading-order terms in the inverse fluctuation propagator are hence given by

$$(\mathcal{D}_q^{-1})_{11} = \rho_{\mathrm{F}}\,, \qquad \frac{\mathrm{d}}{\mathrm{d}\Delta_0^2}(\mathcal{D}_q^{-1})_{11} = \frac{\rho_{\mathrm{F}}}{2\Delta_0^2}\,, \tag{E.14a}$$

$$(\mathcal{D}_q^{-1})_{22} = \rho_{\mathrm{F}}\int_\Omega r^2\,, \qquad \frac{\mathrm{d}}{\mathrm{d}\Delta_0^2}(\mathcal{D}_q^{-1})_{22} = \frac{\rho_{\mathrm{F}}}{2\Delta_0^2}\,. \tag{E.14b}$$

Finally, the fluctuations corrections stemming from the regime of small momenta and frequencies are finite and in fact small by a factor $(\Delta_0/v_{\mathrm{F}}\Lambda)^{d-1}$ [100, 198].

Regime $r \gg 1$ On the other hand, for $2\Delta_0 \ll \sqrt{\omega^2 + (v_{\mathrm{F}} q\cos\theta)^2}$ (but of course $\omega \ll v_{\mathrm{F}}\Lambda$ and $q \ll \Lambda$), the expressions reduce to

$$\frac{1}{g} + \Pi_q^{\mathrm{n}} = \rho_{\mathrm{F}}\int_\Omega \ln r\,, \qquad \frac{\mathrm{d}\Pi_q^{\mathrm{n}}}{\mathrm{d}\Delta_0^2} = \frac{\rho_{\mathrm{F}}}{4\Delta_0^2}\int_\Omega \frac{1}{r^2}\,, \tag{E.15a}$$

$$\Pi_q^{\mathrm{a}} = \frac{\rho_{\mathrm{F}}}{2}\int_\Omega \frac{\ln r}{r^2}\,, \qquad \frac{\mathrm{d}\Pi_q^{\mathrm{a}}}{\mathrm{d}\Delta_0^2} = \frac{\rho_{\mathrm{F}}}{4\Delta_0^2}\int_\Omega \Big(\frac{2\ln r}{r^2} - \frac{1}{r^2}\Big)\,. \tag{E.15b}$$

Hence in this regime, it holds that

$$\frac{1}{g} + \Pi_q^{\mathrm{n}} \gg \Pi_q^{\mathrm{a}} \qquad \text{and} \qquad \frac{\mathrm{d}\Pi_q^{\mathrm{n}}}{\mathrm{d}\Delta_0^2} \ll \frac{\mathrm{d}\Pi_q^{\mathrm{a}}}{\mathrm{d}\Delta_0^2}\,, \tag{E.16}$$

and the corresponding expressions for the inverse fluctuation propagators are

$$(\mathcal{D}_q^{-1})_{11} = \rho_{\mathrm{F}}\int_\Omega \ln r\,, \qquad \frac{\mathrm{d}}{\mathrm{d}\Delta_0^2}(\mathcal{D}_q^{-1})_{11} = \frac{\rho_{\mathrm{F}}}{2\Delta_0^2}\int_\Omega \frac{\ln r}{r^2}\,, \tag{E.17a}$$

$$(\mathcal{D}_q^{-1})_{22} = \rho_{\mathrm{F}}\int_\Omega \ln r\,, \qquad \frac{\mathrm{d}}{\mathrm{d}\Delta_0^2}(\mathcal{D}_q^{-1})_{22} = \frac{\rho_{\mathrm{F}}}{2\Delta_0^2}\int_\Omega \Big(\frac{1}{r^2} - \frac{\ln r}{r^2}\Big)\,. \tag{E.17b}$$

In conclusion, the fluctuation corrections stemming from this regime are also small, but only because the divergent terms from amplitude and phase fluctuations in the numerator cancel. (Each correction taken separately is actually $\sim \ln(v_\mathrm{F}\Lambda/\Delta_0)$ [100].) Furthermore, the analysis of Ref. 198 showed that the large contributions originate from the regime $v_\mathrm{F}q > \omega$.

Bibliography

[1] P. W. Anderson, *More is different*, Science **177**, 393 (1972).

[2] H. K. Onnes, *The resistance of pure mercury at helium temperatures*, Comm. Phys. Lab. Univ. Leiden **120b** (1911).

[3] H. K. Onnes, *The disappearance of the resistance of mercury*, Comm. Phys. Lab. Univ. Leiden **122b** (1911).

[4] H. K. Onnes, *On the sudden change in the rate at which the resistance of mercury disappears*, Comm. Phys. Lab. Univ. Leiden **124c** (1912).

[5] W. Meißner and R. Ochsenfeld, *Ein neuer Effekt bei Eintritt der Supraleitfähigkeit*, Naturwissenschaften **21**, 787 (1933).

[6] J. G. Bednorz and K. A. Müller, *Possible High T_c Superconductivity in the Ba-La-Cu-O System*, Zeitschrift für Physik B Condensed Matter **64**, 189 (1986).

[7] Y. Kamihara, T. Watanabe, M. Hirano, and H. Hosono, *Iron-Based Layered Superconductor $La[O_{1-x}F_x]FeAs$ ($x = 0.05 - 0.12$) with $T_c = 26\,K$*, J. Am. Chem. Soc. **130**, 3296 (2008).

[8] J. Bardeen, L. N. Cooper, and J. R. Schrieffer, *Microscopic Theory of Superconductivity*, Phys. Rev. **106**, 162 (1957).

[9] J. Bardeen, L. N. Cooper, and J. R. Schrieffer, *Theory of Superconductivity*, Phys. Rev. **108**, 1175 (1957).

[10] P. W. Anderson, *Theory of Dirty Superconductors*, J. Phys. Chem. Solids **11**, 26 (1959).

[11] A. A. Abrikosov and L. P. Gor'kov, *On the theory of superconducting alloys. 1. The electrodynamics of alloys at absolute zero*, Zh. Eksp. Teor. Fiz. **35**, 1558 (1958). [Sov. Phys. JETP **8**, 1090 (1958)].

[12] A. A. Abrikosov and L. P. Gor'kov, *Superconducting alloys at finite temperatures*, Zh. Eksp. Teor. Fiz. **36**, 319 (1959). [Sov. Phys. JETP **9**, 220 (1959)].

[13] R. M. Fernandes, M. G. Vavilov, and A. V. Chubukov, *Enhancement of T_c by disorder in underdoped iron pnictide superconductors*, Phys. Rev. B **85**, 140512 (2012).

[14] Y. Wang, A. Kreisel, P. J. Hirschfeld, and V. Mishra, *Using controlled disorder to distinguish $s_\pm$ and s_{++} gap structure in Fe-based superconductors*, Phys. Rev. B **87**, 094504 (2013).

[15] Y. Mizukami, M. Konczykowski, Y. Kawamoto, S. Kurata, S. Kasahara, K. Hashimoto, V. Mishra, A. Kreisel, Y. Wang, P. J. Hirschfeld, Y. Matsuda, and T. Shibauchi, *Disorder-induced topological change of the superconducting gap structure in iron pnictides*, Nature Communications **5**, 5657 (2014).

[16] P. W. Anderson, *Absence of diffusion in certain random lattices*, Phys. Rev. **109**, 1492 (1958).

[17] L. D. Landau, *On the theory of phase transitions*, Zh. Eksp. Teor. Fiz. **7**, 19 (1937).

[18] V. L. Ginzburg and L. D. Landau, *On the theory of superconductivity*, Zh. Eksp. Teor. Fiz. **20**, 1064 (1950).

[19] J. Schmalian, *Failed theories of superconductivity*, Modern Physics Letters B **24**, 2679 (2010).

[20] F. London and H. London, *The Electromagnetic Equations of the Supraconductor*, Proceedings of the Royal Society of London A: Mathematical, Physical and Engineering Sciences **149**, 71 (1935).

[21] L. P. Gor'kov, *Microscopic derivation of the Ginzburg-Landau equations in the theory of superconductivity*, Zh. Eksp. Teor. Fiz. **36**, 1918 (1959). [Sov. Phys. JETP **9**, 1364 (1959)].

[22] Y. Nambu, *Quasi-Particles and Gauge Invariance in the Theory of Superconductivity*, Phys. Rev. **117**, 648 (1960).

[23] J. Goldstone, *Field theories with « Superconductor »solutions*, Il Nuovo Cimento (1955-1965) **19**, 154 (1961).

[24] L. N. Cooper, *Bound Electron Pairs in a Degenerate Fermi Gas*, Phys. Rev. **104**, 1189 (1956).

[25] H. Fröhlich, *Theory of the Superconducting State. I. The Ground State at the Absolute Zero of Temperature*, Phys. Rev. **79**, 845 (1950).

[26] F. Steglich, J. Aarts, C. D. Bredl, W. Lieke, D. Meschede, W. Franz, and H. Schäfer, *Superconductivity in the presence of strong pauli paramagnetism: $CeCu_2Si_2$*, Phys. Rev. Lett. **43**, 1892 (1979).

[27] H. R. Ott, H. Rudigier, Z. Fisk, and J. L. Smith, *UBe_{13}: An unconventional actinide superconductor*, Phys. Rev. Lett. **50**, 1595 (1983).

[28] G. R. Stewart, Z. Fisk, J. O. Willis, and J. L. Smith, *Possibility of coexistence of bulk superconductivity and spin fluctuations in UPt_3*, Phys. Rev. Lett. **52**, 679 (1984).

[29] D. Jérome, A. Mazaud, M. Ribault, and K. Bechgaard, *Superconductivity in a synthetic organic conductor $(TMTSF)_2PF_6$*, J. Physique Lett. **41**, 95 (1980).

[30] K. Bechgaard, K. Carneiro, M. Olsen, F. B. Rasmussen, and C. S. Jacobsen, *Zero-Pressure Organic Superconductor: Di-(Tetramethyltetraselenafulvalenium)-Perchlorate $[(TMTSF)_2ClO_4]$*, Phys. Rev. Lett. **46**, 852 (1981).

[31] L. Boeri, O. V. Dolgov, and A. A. Golubov, *Is $LaFeAsO_{1-x}F_x$ an Electron-Phonon Superconductor?*, Phys. Rev. Lett. **101**, 026403 (2008).

[32] G. Wu, Y. L. Xie, H. Chen, M. Zhong, R. H. Liu, B. C. Shi, Q. J. Li, X. F. Wang, T. Wu., Y. J. Yan, J. J. Ying, and X. H. Chen, *Superconductivity at 56 K in samarium-doped SrFeAsF*, Journal of Physics: Condensed Matter **21**, 142203 (2009).

[33] J. Paglione and R. L. Greene, *High-temperature superconductivity in iron-based materials*, Nature Physics **6**, 645 (2010).

[34] A. V. Chubukov and P. J. Hirschfeld, *Fe-based superconductors: seven years later*, Physics Today **68**, 46 (2015).

[35] Q. Si, R. Yu, and E. Abrahams, *High Temperature Superconductivity in Iron Pnictides and Chalcogenides*, Nature Rev. Mater. **1**, 16017 (2016).

[36] P. J. Hirschfeld, *Using gap symmetry and structure to reveal the pairing mechanism in Fe-based superconductors*, Comptes Rendus Physique **17**, 197 (2016).

[37] Q.-Y. Wang, Z. Li, W.-H. Zhang, Z.-C. Zhang, J.-S. Zhang, W. Li, H. Ding, Y.-B. Ou, P. Deng, K. Chang, J. Wen, C.-L. Song, K. He, J.-F. Jia, S.-H. Ji, Y.-Y. Wang, L.-L. Wang, X. Chen, X.-C. Ma, and Q.-K. Xue, *Interface-induced high-temperature superconductivity in single unit-cell FeSe films on $SrTiO_3$*, Chinese Physics Letters **29**, 037402 (2012).

[38] S. He, J. He, W. Zhang, L. Zhao, D. Liu, X. Liu, D. Mou, Y.-B. Ou, Q.-Y. Wang, Z. Li, L. Wang, Y. Peng, Y. Liu, C. Chen, L. Yu, G. Liu, X. Dong, J. Zhang, C. Chen, Z. Xu, X. Chen, X. Ma, Q. Xue, and X. J. Zhou, *Phase diagram and electronic indication of high-temperature superconductivity at 65 K in single-layer FeSe films*, Nature Materials **12**, 605 (2013).

[39] R. M. Fernandes, A. V. Chubukov, and J. Schmalian, *What drives nematic order in iron-based superconductors?*, Nature Physics **10**, 97 (2014).

[40] I. I. Mazin and J. Schmalian, *Pairing symmetry and pairing state in ferropnictides: Theoretical overview*, Physica C **469**, 614 (2009).

[41] A. V. Chubukov, D. V. Efremov, and I. Eremin, *Magnetism, superconductivity, and pairing symmetry in iron-based superconductors*, Phys. Rev. B **78**, 134512 (2008).

[42] D. Podolsky, H.-Y. Kee, and Y. B. Kim, *Collective modes and emergent symmetry of superconductivity and magnetism in the iron pnictides*, EPL **88**, 17004 (2009).

[43] J. Kang and Z. Tešanović, *Theory of the valley-density wave and hidden order in iron pnictides*, Phys. Rev. B **83**, 020505 (2011).

[44] F. Eilers, K. Grube, D. A. Zocco, T. Wolf, M. Merz, P. Schweiss, R. Heid, R. Eder, R. Yu, J.-X. Zhu, Q. Si, T. Shibauchi, and H. v. Löhneysen, *Strain-driven approach to quantum criticality in AFe_2As_2 with A=K, Rb, and Cs*, Phys. Rev. Lett. **116**, 237003 (2016).

[45] R. M. Fernandes and A. V. Chubukov, *Low-energy microscopic models for iron-based superconductors: a review*, Rep. Prog. Phys. **80**, 014503 (2017).

[46] A. Ohtomo and H. Y. Hwang, *A high-mobility electron gas at the $LaAlO_3/SrTiO_3$ heterointerface*, Nature **427**, 423 (2004).

[47] N. Reyren, S. Thiel, A. D. Caviglia, L. F. Kourkoutis, G. Hammerl, C. Richter, C. W. Schneider, T. Kopp, A.-S. Rüetschi, D. Jaccard, M. Gabay, D. A. Muller, J.-M. Triscone, and J. Mannhart, *Superconducting Interfaces Between Insulating Oxides*, Science **317**, 1196 (2007).

[48] M. S. Scheurer and J. Schmalian, *Topological superconductivity and unconventional pairing in oxide interfaces*, Nature Communications **6**, 6005 (2015).

[49] A. Brinkman, M. Huijben, M. van Zalk, J. Huijben, U. Zeitler, J. C. Maan, W. G. van der Wiel, G. Rijnders, D. H. A. Blank, and H. Hilgenkamp, *Magnetic effects at the interface between non-magnetic oxides*, Nature Materials **6**, 493 (2007).

[50] L. Lu, C. Richter, J. Mannhart, and R. C. Ashoori, *Coexistence of magnetic order and two-dimensional superconductivity at $LaAlO_3/SrTiO_3$ interfaces*, Nat Phys **7**, 762 (2011).

[51] J. A. Bert, B. Kalisky, C. Bell, M. Kim, Y. Hikita, H. Y. Hwang, and K. A. Moler, *Direct imaging of the coexistence of ferromagnetism and superconductivity at the $LaAlO_3/SrTiO_3$ interface*, Nature Physics **7**, 767 (2011).

[52] N. Nakagawa, H. Y. Hwang, and D. A. Muller, *Why some interfaces cannot be sharp*, Nat Mater **5**, 204 (2006).

[53] S. Thiel, G. Hammerl, A. Schmehl, C. W. Schneider, and J. Mannhart, *Tunable Quasi-Two-Dimensional Electron Gases in Oxide Heterostructures*, Science **313**, 1942 (2006).

[54] A. Kalabukhov, R. Gunnarsson, J. Börjesson, E. Olsson, T. Claeson, and D. Winkler, *Effect of oxygen vacancies in the $SrTiO_3$ substrate on the electrical properties of the $LaAlO_3/SrTiO_3$ interface*, Phys. Rev. B **75**, 121404 (2007).

[55] W. Siemons, G. Koster, H. Yamamoto, T. H. Geballe, D. H. A. Blank, and M. R. Beasley, *Experimental investigation of electronic properties of buried heterointerfaces of $LaAlO_3$ on $SrTiO_3$*, Phys. Rev. B **76**, 155111 (2007).

[56] Z. Q. Liu, C. J. Li, W. M. Lü, X. H. Huang, Z. Huang, S. W. Zeng, X. P. Qiu, L. S. Huang, A. Annadi, J. S. Chen, J. M. D. Coey, T. Venkatesan, and Ariando, *Origin of the Two-Dimensional Electron Gas at $LaAlO_3/SrTiO_3$ Interfaces: The Role of Oxygen Vacancies and Electronic Reconstruction*, Phys. Rev. X **3**, 021010 (2013).

[57] A. D. Caviglia, S. Gariglio, N. Reyren, D. Jaccard, T. Schneider, M. Gabay, S. Thiel, G. Hammerl, J. Mannhart, and J.-M. Triscone, *Electric field control of the $LaAlO_3/SrTiO_3$ interface ground state*, Nature **456**, 624 (2008). 10.1038/nature07576.

[58] J. A. Bert, K. C. Nowack, B. Kalisky, H. Noad, J. R. Kirtley, C. Bell, H. K. Sato, M. Hosoda, Y. Hikita, H. Y. Hwang, and K. A. Moler, *Gate-tuned superfluid density at the superconducting $LaAlO_3/SrTiO_3$ interface*, Phys. Rev. B **86**, 060503 (2012).

[59] M. Rotter, M. Tegel, I. Schellenberg, F. M. Schappacher, R. Pöttgen, J. Deisenhofer, A. Günther, F. Schrettle, A. Loidl, and D. Johrendt, *Competition of magnetism and superconductivity in underdoped $(Ba_{1-x}K_x)Fe_2As_2$*, New Journal of Physics **11**, 025014 (2009).

[60] R. M. Fernandes, D. K. Pratt, W. Tian, J. Zarestky, A. Kreyssig, S. Nandi, M. G. Kim, A. Thaler, N. Ni, P. C. Canfield, R. J. McQueeney, J. Schmalian, and A. I. Goldman, *Unconventional pairing in the iron arsenide superconductors*, Phys. Rev. B **81**, 140501 (2010).

[61] D. K. Pratt, W. Tian, A. Kreyssig, J. L. Zarestky, S. Nandi, N. Ni, S. L. Bud'ko, P. C. Canfield, A. I. Goldman, and R. J. McQueeney, *Coexistence of Competing Antiferromagnetic and Superconducting Phases in the Underdoped $Ba(Fe_{0.953}Co_{0.047})_2As_2$ Compound Using X-ray and Neutron Scattering Techniques*, Phys. Rev. Lett. **103**, 087001 (2009).

[62] A. D. Christianson, M. D. Lumsden, S. E. Nagler, G. J. MacDougall, M. A. McGuire, A. S. Sefat, R. Jin, B. C. Sales, and D. Mandrus, *Static and Dynamic Magnetism in Underdoped Superconductor* $BaFe_{1.92}Co_{0.08}As_2$, Phys. Rev. Lett. **103**, 087002 (2009).

[63] R. T. Gordon, H. Kim, N. Salovich, R. W. Giannetta, R. M. Fernandes, V. G. Kogan, T. Prozorov, S. L. Bud'ko, P. C. Canfield, M. A. Tanatar, and R. Prozorov, *Doping evolution of the absolute value of the London penetration depth and superfluid density in single crystals of* $Ba(Fe_{1-x}Co_x)_2As_2$, Phys. Rev. B **82**, 054507 (2010).

[64] D. Parker, M. G. Vavilov, A. V. Chubukov, and I. I. Mazin, *Coexistence of superconductivity and a spin-density wave in pnictide superconductors: Gap symmetry and nodal lines*, Phys. Rev. B **80**, 100508 (2009).

[65] V. Cvetkovic and Z. Tešanovic, *Multiband magnetism and superconductivity in Fe-based compounds*, EPL **85**, 37002 (2009).

[66] A. B. Vorontsov, M. G. Vavilov, and A. V. Chubukov, *Interplay between magnetism and superconductivity in the iron pnictides*, Phys. Rev. B **79**, 060508 (2009).

[67] A. B. Vorontsov, M. G. Vavilov, and A. V. Chubukov, *Superconductivity and spin-density waves in multiband metals*, Phys. Rev. B **81**, 174538 (2010).

[68] R. M. Fernandes and J. Schmalian, *Competing order and nature of the pairing state in the iron pnictides*, Phys. Rev. B **82**, 014521 (2010).

[69] M. G. Vavilov and A. V. Chubukov, *Phase diagram of iron pnictides if doping acts as a source of disorder*, Phys. Rev. B **84**, 214521 (2011).

[70] M. Hoyer, S. V. Syzranov, and J. Schmalian, *Effect of weak disorder on the phase competition in iron pnictides*, Phys. Rev. B **89**, 214504 (2014).

[71] J. G. Analytis, H-H. Kuo, R. D. McDonald, M. Wartenbe, P. M. C. Rourke, N. E. Hussey, and I. R. Fisher, *Transport near a quantum critical point in* $BaFe_2(As_{1-x}P_x)_2$, Nature Physics **10**, 194 (2014).

[72] Y. Dagan, M. M. Qazilbash, C. P. Hill, V. N. Kulkarni, and R. L. Greene, *Evidence for a Quantum Phase Transition in* $Pr_{2-x}Ce_xCuO_{4-\delta}$ *from Transport Measurements*, Phys. Rev. Lett. **92**, 167001 (2004).

[73] L. Taillefer, *Scattering and Pairing in Cuprate Superconductors*, Annual Review of Condensed Matter Physics **1**, 51 (2010).

[74] K. Hashimoto, K. Cho, T. Shibauchi, S. Kasahara, Y. Mizukami, R. Katsumata, Y. Tsuruhara, T. Terashima, H. Ikeda, M. A. Tanatar, H. Kitano, N. Salovich, R. W. Giannetta, P. Walmsley, A. Carrington, R. Prozorov, and Y. Matsuda, *A sharp peak of the zero-temperature penetration depth at optimal composition in* $BaFe_2(As_{1-x}P_x)_2$, Science **336**, 1554 (2012).

[75] A. Levchenko, M. G. Vavilov, M. Khodas, and A. V. Chubukov, *Enhancement of the London penetration depth in pnictides at the onset of spin-density-wave order under superconducting dome*, Phys. Rev. Lett. **110**, 177003 (2013).

[76] Y. Schattner, M. H. Gerlach, S. Trebst, and E. Berg, *Competing Orders in a Nearly Antiferromagnetic Metal*, Phys. Rev. Lett. **117**, 097002 (2016).

[77] R. S. Dhaka, C. Liu, R. M. Fernandes, R. Jiang, C. P. Strehlow, T. Kondo, A. Thaler, J. Schmalian, S. L. Bud'ko, P. C. Canfield, and A. Kaminski, *What Controls the Phase Diagram and Superconductivity in Ru-Substituted $BaFe_2As_2$?*, Phys. Rev. Lett. **107**, 267002 (2011).

[78] H. Wadati, I. Elfimov, and G. A. Sawatzky, *Where Are the Extra d Electrons in Transition-Metal-Substituted Iron Pnictides?*, Phys. Rev. Lett. **105**, 157004 (2010).

[79] T. Berlijn, C.-H. Lin, W. Garber, and W. Ku, *Do Transition-Metal Substitutions Dope Carriers in Iron-Based Superconductors?*, Phys. Rev. Lett. **108**, 207003 (2012).

[80] A. Herbig, R. Heid, and J. Schmalian, *Charge doping versus impurity scattering in chemically substituted iron pnictides*, Phys. Rev. B **94**, 094512 (2016).

[81] L. N. Bulaevskii and M. V. Sadovskii, *Localization and superconductivity*, JETP Lett. **39**, 640 (1984).

[82] M. V. Sadovskii, *Superconductivity and Localization*, Physics Reports **282**, 225 (1997).

[83] J. Rammer, *Quantum Transport Theory*, Perseus Books (1998).

[84] H. Bruus and K. Flensberg, *Many-Body Quantum Theory in Condensed Matter Physics: An Introduction*, Oxford University Press, USA (2004).

[85] A. Altland and B. D. Simons, *Condensed Matter Field Theory*, Cambridge University Press, 2nd ed. (2010).

[86] A. C. Potter and P. A. Lee, *Engineering a $p + ip$ superconductor: Comparison of topological insulator and Rashba spin-orbit-coupled materials*, Phys. Rev. B **83**, 184520 (2011).

[87] M. Hoyer, M. S. Scheurer, S. V. Syzranov, and J. Schmalian, *Pair breaking due to orbital magnetism in iron-based superconductors*, Phys. Rev. B **91**, 054501 (2015).

[88] A. A. Abrikosov and L. P. Gor'kov, *Contribution to the theory of superconducting alloys with paramagnetic impurites*, Zh. Eksp. Teor. Fiz. **39**, 1781 (1960). [Sov. Phys. JETP **12**, 1243 (1961)].

[89] A. A. Abrikosov, L. P. Gor'kov, and I. E. Dzyaloshinski, *Methods of Quantum Field Theory in Statistical Physics*, Dover Pubn Inc, revised english ed. (1975).

[90] T. Giamarchi, *Quantum Physics in One Dimension*, Clarendon Press (2004).

[91] L. V. Keldysh, *Diagram technique for nonequilibrium processes*, Zh. Eksp. Teor. Fiz. **47**, 1515 (1964). [Sov. Phys. JETP 20, 1018].

[92] A. Kamenev, *Field Theory of Non-Equilibrium Systems*, Cambridge University Press, 1st ed. (2011).

[93] K. B. Efetov, *Supersymmetry method in localization thoery*, Zh. Eksp. Teor. Fiz. **82**, 872 (1982). [Sov. Phys. JETP **55**, 514 (1982)].

[94] K. Efetov, *Supersymmetry in Disorder and Chaos*, Cambridge University Press (1999).

[95] S. F. Edwards and P. W. Anderson, *Theory of spin glasses*, Journal of Physics F: Metal Physics **5**, 965 (1975).

[96] A. Larkin and A. Varlamov, *Theory of Fluctuations in Superconductors*, Oxford University Press, USA (2005).

[97] R. Glover, *Ideal resistive transition of a superconductor*, Physics Letters A **25**, 542 (1967).

[98] N. D. Mermin and H. Wagner, *Absence of ferromagnetism or antiferromagnetism in one- or two-dimensional isotropic Heisenberg models*, Phys. Rev. Lett. **17**, 1133 (1966).

[99] P. C. Hohenberg, *Existence of long-range order in one and two dimensions*, Phys. Rev. **158**, 383 (1967).

[100] Š. Kos, A. J. Millis, and A. I. Larkin, *Gaussian fluctuation corrections to the BCS mean-field gap amplitude at zero temperature*, Phys. Rev. B **70**, 214531 (2004).

[101] A. E. Karkin, J. Werner, G. Behr, and B. N. Goshchitskii, *Neutron-irradiation effects in polycrystalline $LaFeAsO_{0.9}F_{0.1}$ superconductors*, Phys. Rev. B **80**, 174512 (2009).

[102] Y. Li, J. Tong, Q. Tao, C. Feng, G. Cao, W. Chen, F.-c. Zhang, and Z.-a. Xu, *Effect of a Zn impurity on T_c and its implications for pairing symmetry in $LaFeAsO_{1-x}F_x$*, New Journal of Physics **12**, 083008 (2010).

[103] J. Li, Y. Guo, S. Zhang, S. Yu, Y. Tsujimoto, H. Kontani, K. Yamaura, and E. Takayama-Muromachi, *Linear decrease of critical temperature with increasing Zn substitution in the iron-based superconductor $BaFe_{1.89-2x}Zn_{2x}Co_{0.11}As_2$*, Phys. Rev. B **84**, 020513 (2011).

[104] J. Li, Y. F. Guo, S. B. Zhang, J. Yuan, Y. Tsujimoto, X. Wang, C. I. Sathish, Y. Sun, S. Yu, W. Yi, K. Yamaura, E. Takayama-Muromachiu, Y. Shirako, M. Akaogi, and H. Kontani, *Superconductivity suppression of $Ba_{0.5}K_{0.5}Fe_{2-2x}M_{2x}As_2$ single crystals by substitution of transition metal (M = Mn, Ru, Co, Ni, Cu, and Zn)*, Phys. Rev. B **85**, 214509 (2012).

[105] K. Kirshenbaum, S. R. Saha, S. Ziemak, T. Drye, and J. Paglione, *Universal pair-breaking in transition-metal-substituted iron-pnictide superconductors*, Phys. Rev. B **86**, 140505 (2012).

[106] Y. Yamakawa, S. Onari, and H. Kontani, *Effect of realistic finite-size impurities on T_c in Fe-based superconductors based on the five-orbital tight-binding model*, Phys. Rev. B **87**, 195121 (2013).

[107] R. Prozorov, M. Kończykowski, M. A. Tanatar, A. Thaler, S. L. Bud'ko, P. C. Canfield, V. Mishra, and P. J. Hirschfeld, *Effect of Electron Irradiation on Superconductivity in Single Crystals of $Ba(Fe_{1-x}Ru_x)_2As_2$ ($x = 0.24$)*, Phys. Rev. X **4**, 041032 (2014).

[108] C. C. Tsuei and J. R. Kirtley, *Pairing symmetry in cuprate superconductors*, Rev. Mod. Phys. **72**, 969 (2000).

[109] P. J. Hirschfeld, M. M. Korshunov, and I. I. Mazin, *Gap symmetry and structure of Fe-based superconductors*, Rep. Prog. Phys. **74**, 124508 (2011).

[110] H.-J. Grafe, D. Paar, G. Lang, N. J. Curro, G. Behr, J. Werner, J. Hamann-Borrero, C. Hess, N. Leps, R. Klingeler, and B. Büchner, *^{75}As NMR Studies of Superconducting $LaFeAsO_{0.9}F_{0.1}$*, Phys. Rev. Lett. **101**, 047003 (2008).

[111] K. Matano, Z. A. Ren, X. L. Dong, L. L. Sun, Z. X. Zhao, and G.-q. Zheng, *Spin-singlet superconductivity with multiple gaps in $PrFeAsO_{0.89}F_{0.11}$*, EPL **83**, 57001 (2008).

[112] F. Ning, K. Ahilan, T. Imai, A. S. Sefat, R. Jin, M. A. McGuire, B. C. Sales, and D. Mandrus, *^{59}Co and ^{75}As NMR Investigation of Electron-Doped High T_c Superconductor $BaFe_{1.8}Co_{0.2}As_2$ ($T_c = 22$ K)*, J. Phys. Soc. Jpn **77**, 103705 (2008).

[113] Y. Shimizu, T. Yamada, T. Takami, S. Niitaka, H. Takagi, and M. Itoh, *Pressure-Induced Antiferromagnetic Fluctuations in the Pnictide Superconductor $FeSe_{0.5}Te_{0.5}$: ^{125}Te NMR Study*, J. Phys. Soc. Jpn **78**, 123709 (2009).

[114] I. I. Mazin, D. J. Singh, M. D. Johannes, and M. H. Du, *Unconventional Superconductivity with a Sign Reversal in the Order Parameter of $LaFeAsO_{1-x}F_x$*, Phys. Rev. Lett. **101**, 057003 (2008).

[115] K. Kuroki, S. Onari, R. Arita, H. Usui, Y. Tanaka, H. Kontani, and H. Aoki, *Unconventional Pairing Originating from the Disconnected Fermi Surfaces of Superconducting $LaFeAsO_{1-x}F_x$*, Phys. Rev. Lett. **101**, 087004 (2008).

[116] S. Graser, T. A. Maier, P. J. Hirschfeld, and D. J. Scalapino, *Near-degeneracy of several pairing channels in multiorbital models for the Fe pnictides*, New Journal of Physics **11**, 025016 (2009).

[117] V. Mishra, G. Boyd, S. Graser, T. Maier, P. J. Hirschfeld, and D. J. Scalapino, *Lifting of nodes by disorder in extended-s-state superconductors: Application to ferropnictides*, Phys. Rev. B **79**, 094512 (2009).

[118] M. M. Korshunov and I. Eremin, *Theory of magnetic excitations in iron-based layered superconductors*, Phys. Rev. B **78**, 140509 (2008).

[119] T. A. Maier and D. J. Scalapino, *Theory of neutron scattering as a probe of the superconducting gap in the iron pnictides*, Phys. Rev. B **78**, 020514 (2008).

[120] T. A. Maier, S. Graser, D. J. Scalapino, and P. Hirschfeld, *Neutron scattering resonance and the iron-pnictide superconducting gap*, Phys. Rev. B **79**, 134520 (2009).

[121] A. D. Christianson, E. A. Goremychkin, R. Osborn, S. Rosenkranz, M. D. Lumsden, C. D. Malliakas, I. S. Todorov, H. Claus, D. Y. Chung, M. G. Kanatzidis, R. I. Bewley, and T. Guidi, *Unconventional superconductivity in $Ba_{0.6}K_{0.4}Fe_2As_2$ from inelastic neutron scattering*, Nature **456**, 930 (2008). 10.1038/nature07625.

[122] T. Kariyado and M. Ogata, *Single-impurity problem in iron-pnictide superconductors*, J. Phys. Soc. Jpn **79**, 083704 (2010).

[123] M. N. Gastiasoro, P. J. Hirschfeld, and B. M. Andersen, *Impurity states and cooperative magnetic order in Fe-based superconductors*, Phys. Rev. B **88**, 220509 (2013).

[124] Q.-E. Wang, Z.-J. Yao, and F.-C. Zhang, *Single nonmagnetic impurity resonance in FeSe-based 122-type superconductors as a probe for pairing symmetry*, EPL **101**, 57002 (2013).

[125] S. Grothe, S. Chi, P. Dosanjh, R. Liang, W. N. Hardy, S. A. Burke, D. A. Bonn, and Y. Pennec, *Bound states of defects in superconducting LiFeAs studied by scanning tunneling spectroscopy*, Phys. Rev. B **86**, 174503 (2012).

[126] H. Yang, Z. Wang, D. Fang, Q. Deng, Q.-H. Wang, Y.-Y. Xiang, Y. Yang, and H.-H. Wen, *In-gap quasiparticle excitations induced by non-magnetic Cu impurities in $Na(Fe_{0.96}Co_{0.03}Cu_{0.01})As$ revealed by scanning tunnelling spectroscopy*, Nature Communications **4**, 2749 (2013).

[127] D. V. Efremov, M. M. Korshunov, O. V. Dolgov, A. A. Golubov, and P. J. Hirschfeld, *Disorder-induced transition between $s_\pm$ and s_{++} states in two-band superconductors*, Phys. Rev. B **84**, 180512 (2011).

[128] M. M. Korshunov, D. V. Efremov, A. A. Golubov, and O. V. Dolgov, *Unexpected impact of magnetic disorder on multiband superconductivity*, Phys. Rev. B **90**, 134517 (2014).

[129] M. B. Schilling, A. Baumgartner, B. Gorshunov, E. S. Zhukova, V. A. Dravin, K. V. Mitsen, D. V. Efremov, O. V. Dolgov, K. Iida, M. Dressel, and S. Zapf, *Tracing the $s_\pm$ symmetry in iron pnictides by controlled disorder*, Phys. Rev. B **93**, 174515 (2016).

[130] M. Tinkham, *Introduction to Superconductivity: Second Edition (Dover Books on Physics)*, Dover Publications, 2nd ed. (2004).

[131] V. G. Kogan and R. Prozorov, *Interband coupling and nonmagnetic interband scattering in $\pm s$ superconductors*, Phys. Rev. B **93**, 224515 (2016).

[132] N. Dupuis and V. M. Yakovenko, *Collective modes in a system with two spin-density waves: the Ribault phase of quasi-one-dimensional organic conductors*, Phys. Rev. B **61**, 12888 (2000).

[133] P. Schlottmann, *Non-fermi-liquid behavior in a system with a nested Fermi surface*, Phys. Rev. B **68**, 125105 (2003).

[134] J. Zhang, R. Sknepnek, R. M. Fernandes, and J. Schmalian, *Orbital coupling and superconductivity in the iron pnictides*, Phys. Rev. B **79**, 220502 (2009).

[135] H. Suhl, B. T. Matthias, and L. R. Walker, *Bardeen-Cooper-Schrieffer Theory of Superconductivity in the Case of Overlapping Bands*, Phys. Rev. Lett. **3**, 552 (1959).

[136] V. A. Moskalenko, *Superconductivity of metals with overlapping of energetic bands*, Fiz. Metal. Metalloved **8**, 503 (1959).

[137] A. A. Golubov and I. I. Mazin, *Effect of magnetic and nonmagnetic impurities on highly anisotropic superconductivity*, Phys. Rev. B **55**, 15146 (1997).

[138] S. Onari and H. Kontani, *Violation of Anderson's Theorem for the Sign-Reversing s-Wave State of Iron-Pnictide Superconductors*, Phys. Rev. Lett. **103**, 177001 (2009).

[139] M. M. Korshunov, Y. N. Togushova, and O. V. Dolgov, *Uniform Impurity Scattering in Two-Band $s_\pm$ and s_{++} Superconductors*, Journal of Superconductivity and Novel Magnetism **29**, 1089 (2016).

[140] J. Li and Y. Wang, *Magnetic impurities in the two-band $s_\pm$-wave superconductors*, EPL **88**, 17009 (2009).

[141] V. G. Kogan, *Pair breaking in iron pnictides*, Phys. Rev. B **80**, 214532 (2009).

[142] C. J. van der Beek, S. Demirdiş, D. Colson, F. Rullier-Albenque, Y. Fasano, T. Shibauchi, Y. Matsuda, S. Kasahara, P. Gierlowski, and M. Konczykowski, *Electron irradiation of Co, Ni, and P-doped $BaFe_2As_2$-type iron-based superconductors*, Journal of Physics: Conference Series **449**, 012023 (2013).

[143] M. L. Kulić and O. V. Dolgov, *Anisotropic impurities in anisotropic superconductors*, Phys. Rev. B **60**, 13062 (1999).

[144] M. N. Gastiasoro, F. Bernardini, and B. M. Andersen, *Unconventional disorder effects in correlated superconductors*, Phys. Rev. Lett. **117**, 257002 (2016).

[145] A. J. Millis, D. K. Morr, and J. Schmalian, *Local Defect in Metallic Quantum Critical Systems*, Phys. Rev. Lett. **87**, 167202 (2001).

[146] B. M. Andersen, P. J. Hirschfeld, A. P. Kampf, and M. Schmid, *Disorder-induced static antiferromagnetism in cuprate superconductors*, Phys. Rev. Lett. **99**, 147002 (2007).

[147] M. N. Gastiasoro and B. M. Andersen, *Impurity Bound States and Disorder-Induced Orbital and Magnetic Order in the s± State of Fe-Based Superconductors*, Journal of Superconductivity and Novel Magnetism **26**, 2651 (2013).

[148] M. N. Gastiasoro, P. J. Hirschfeld, and B. M. Andersen, *Origin of electronic dimers in the spin-density wave phase of Fe-based superconductors*, Phys. Rev. B **89**, 100502 (2014).

[149] K. Michaeli and L. Fu, *Spin-Orbit Locking as a Protection Mechanism of the Odd-Parity Superconducting State against Disorder*, Phys. Rev. Lett. **109**, 187003 (2012).

[150] M. S. Scheurer, M. Hoyer, and J. Schmalian, *Pair breaking in multiorbital superconductors: An application to oxide interfaces*, Phys. Rev. B **92**, 014518 (2015).

[151] M. S. Scheurer, *Mechanism, symmetry and topology of ordered phases in correlated systems*, Ph.D. thesis, Karlsruhe Institute of Technology (2016).

[152] K. Michaeli, A. C. Potter, and P. A. Lee, *Superconducting and Ferromagnetic Phases in $SrTiO_3/LaAlO_3$ Oxide Interface Structures: Possibility of Finite Momentum Pairing*, Phys. Rev. Lett. **108**, 117003 (2012).

[153] H. Boschker, C. Richter, E. Fillis-Tsirakis, C. W. Schneider, and J. Mannhart, *Electron–phonon Coupling and the Superconducting Phase Diagram of the $LaAlO_3$–$SrTiO_3$ Interface*, Scientific Reports **5**, 12309 (2015).

[154] S. N. Klimin, J. Tempere, J. T. Devreese, and D. van der Marel, *Interface superconductivity in $LaAlO_3$–$SrTiO_3$ heterostructures*, Phys. Rev. B **89**, 184514 (2014).

[155] A. F. Santander-Syro, O. Copie, T. Kondo, F. Fortuna, S. Pailhes, R. Weht, X. G. Qiu, F. Bertran, A. Nicolaou, A. Taleb-Ibrahimi, P. Le Fevre, G. Herranz, M. Bibes, N. Reyren, Y. Apertet, P. Lecoeur, A. Barthelemy, and M. J. Rozenberg, *Two-dimensional electron gas with universal subbands at the surface of $SrTiO_3$*, Nature **469**, 189 (2011).

[156] N. Pavlenko, T. Kopp, E. Y. Tsymbal, G. A. Sawatzky, and J. Mannhart, *Magnetic and superconducting phases at the $LaAlO_3/SrTiO_3$ interface: The role of interfacial Ti 3d electrons*, Phys. Rev. B **85**, 020407 (2012).

[157] N. Pavlenko, T. Kopp, E. Y. Tsymbal, J. Mannhart, and G. A. Sawatzky, *Oxygen vacancies at titanate interfaces: Two-dimensional magnetism and orbital reconstruction*, Phys. Rev. B **86**, 064431 (2012).

[158] M. Hoyer, R. M. Fernandes, A. Levchenko, and J. Schmalian, *Disorder-promoted C_4-symmetric magnetic order in iron-based superconductors*, Phys. Rev. B **93**, 144414 (2016).

[159] R. M. Fernandes, A. V. Chubukov, J. Knolle, I. Eremin, and J. Schmalian, *Preemptive nematic order, pseudogap, and orbital order in the iron pnictides*, Phys. Rev. B **85**, 024534 (2012).

[160] X. Wang and R. M. Fernandes, *Impact of local-moment fluctuations on the magnetic degeneracy of iron arsenide superconductors*, Phys. Rev. B **89**, 144502 (2014).

[161] R. M. Fernandes, S. A. Kivelson, and E. Berg, *Vestigial chiral and charge orders from bidirectional spin-density waves: Application to the iron-based superconductors*, Phys. Rev. B **93**, 014511 (2016).

[162] S. Liang, C. B. Bishop, A. Moreo, and E. Dagotto, *Isotropic in-plane quenched disorder and dilution induce a robust nematic state in electron-doped pnictides*, Phys. Rev. B **92**, 104512 (2015).

[163] J. Kang, X. Wang, A. V. Chubukov, and R. M. Fernandes, *Interplay between tetragonal magnetic order, stripe magnetism, and superconductivity in iron-based materials*, Phys. Rev. B **91**, 121104 (2015).

[164] C. Fang, H. Yao, W.-F. Tsai, J. Hu, and S. A. Kivelson, *Theory of electron nematic order in $LaFeAsO$*, Phys. Rev. B **77**, 224509 (2008).

[165] C. Xu, M. Müller, and S. Sachdev, *Ising and spin orders in the iron-based superconductors*, Phys. Rev. B **78**, 020501 (2008).

[166] J.-H. Chu, J. G. Analytis, K. De Greve, P. L. McMahon, Z. Islam, Y. Yamamoto, and I. R. Fisher, *In-plane resistivity anisotropy in an underdoped iron arsenide superconductor*, Science **329**, 824 (2010).

[167] M. A. Tanatar, E. C. Blomberg, A. Kreyssig, M. G. Kim, N. Ni, A. Thaler, S. L. Bud'ko, P. C. Canfield, A. I. Goldman, I. I. Mazin, and R. Prozorov, *Uniaxial-strain mechanical detwinning of $CaFe_2As_2$ and $BaFe_2As_2$ crystals: Optical and transport study*, Phys. Rev. B **81**, 184508 (2010).

[168] J.-H. Chu, H.-H. Kuo, J. G. Analytis, and I. R. Fisher, *Divergent nematic susceptibility in an iron arsenide superconductor*, Science **337**, 710 (2012).

[169] A. Jesche, C. Krellner, M. de Souza, M. Lang, and C. Geibel, *Coupling between the structural and magnetic transition in $CeFeAsO$*, Phys. Rev. B **81**, 134525 (2010).

[170] Takasada Shibauchi, private communication .

[171] M. G. Kim, A. Kreyssig, A. Thaler, D. K. Pratt, W. Tian, J. L. Zarestky, M. A. Green, S. L. Bud'ko, P. C. Canfield, R. J. McQueeney, and A. I. Goldman, *Antiferromagnetic ordering in the absence of structural distortion in* $Ba(Fe_{1-x}Mn_x)_2As_2$, Phys. Rev. B **82**, 220503(R) (2010).

[172] S. Avci, O. Chmaissem, J. Allred, S. Rosenkranz, I. Eremin, A. V. Chubukov, Bugaris D. E., D. Y. Chung, M. G. Kanatzidis, J.-P. Castellan, J. A. Schlueter, H. Claus, D. D. Khalyavin, P. Manuel, A. Daoud-Aladine, and R. Osborn, *Magnetically driven suppression of nematic order in an iron-based superconductor*, Nature Communications **5**, 3845 (2014).

[173] L. Wang, F. Hardy, A. E. Böhmer, T. Wolf, P. Schweiss, and C. Meingast, *Complex phase diagram of* $Ba_{1-x}Na_xFe_2As_2$*: a multitude of phases striving for the electronic entropy*, Phys. Rev. B **93**, 014514 (2016).

[174] E. Hassinger, G. Gredat, F. Valade, S. R. de Cotret, A. Juneau-Fecteau, J.-P. Reid, H. Kim, M. A. Tanatar, R. Prozorov, B. Shen, H.-H. Wen, N. Doiron-Leyraud, and L. Taillefer, *Pressure-induced Fermi-surface reconstruction in the iron-arsenide superconductor* $Ba_{1-x}K_xFe_2As_2$*: Evidence of a phase transition inside the antiferromagnetic phase*, Phys. Rev. B **86**, 140502 (2012).

[175] A. E. Böhmer, F. Hardy, L. Wang, T. Wolf, P. Schweiss, and C. Meingast, *Superconductivity-induced re-entrance of the orthorhombic distortion in* $Ba_{1-x}K_xFe_2As_2$, Nature Communications **6**, 7911 (2015).

[176] J. M. Allred, S. Avci, D. Y. Chung, H. Claus, D. D. Khalyavin, P. Manuel, K. M. Taddei, M. G. Kanatzidis, S. Rosenkranz, R. Osborn, and O. Chmaissem, *Tetragonal magnetic phase in* $Ba_{1-x}K_xFe_2As_2$ *from x-ray and neutron diffraction*, Phys. Rev. B **92**, 094515 (2015).

[177] E. Hassinger, G. Gredat, F. Valade, S. R. de Cotret, O. Cyr-Choinière, A. Juneau-Fecteau, J.-P. Reid, H. Kim, M. A. Tanatar, R. Prozorov, B. Shen, H.-H. Wen, N. Doiron-Leyraud, and L. Taillefer, *Expansion of the tetragonal magnetic phase with pressure in the iron arsenide superconductor* $Ba_{1-x}K_xFe_2As_2$, Phys. Rev. B **93**, 144401 (2016).

[178] J. M. Allred, K. M. Taddei, D. E. Bugaris, M. J. Krogstad, S. H. Lapidus, D. Y. Chung, H. Claus, M. G. Kanatzidis, D. E. Brown, J. Kang, R. M. Fernandes, I. Eremin, S. Rosenkranz, O. Chmaissem, and R. Osborn, *Double-Q spin-density wave in iron arsenide superconductors*, Nature Physics **12**, 493 (2016).

[179] X. Wang, J. Kang, and R. M. Fernandes, *Magnetic order without tetragonal-symmetry-breaking in iron arsenides: Microscopic mechanism and spin-wave spectrum*, Phys. Rev. B **91**, 024401 (2015).

[180] F. Waßer, A. Schneidewind, Y. Sidis, S. Wurmehl, S. Aswartham, B. Büchner, and M. Braden, *Spin reorientation in* $Ba_{0.65}Na_{0.35}Fe_2As_2$ *studied by single-crystal neutron diffraction*, Phys. Rev. B **91**, 060505 (2015).

[181] B. P. P. Mallett, Y. G. Pashkevich, A. Gusev, T. Wolf, and C. Bernhard, *Muon spin rotation study of the magnetic structure in the tetragonal antiferromagnetic state of weakly underdoped* $Ba_{1-x}K_xFe_2As_2$, EPL **111**, 57001 (2015).

[182] J. Lorenzana, G. Seibold, C. Ortix, and M. Grilli, *Competing orders in FeAs layers*, Phys. Rev. Lett. **101**, 186402 (2008).

[183] I. Eremin and A. V. Chubukov, *Magnetic degeneracy and hidden metallicity of the spin-density-wave state in ferropnictides*, Phys. Rev. B **81**, 024511 (2010).

[184] G. Giovannetti, C. Ortix, M. Marsman, M. Capone, J. von den Brink, and J. Lorenzana, *Proximity of iron pnictide superconductors to a quantum tricritical point*, Nature Communications **2**, 398 (2011).

[185] P. M. R. Brydon, J. Schmiedt, and C. Timm, *Microscopically derived Ginzburg-Landau theory for magnetic order in the iron pnictides*, Phys. Rev. B **84**, 214510 (2011).

[186] V. Cvetkovic and O. Vafek, *Space group symmetry, spin-orbit coupling, and the low-energy effective Hamiltonian for iron-based superconductors*, Phys. Rev. B **88**, 134510 (2013).

[187] M. N. Gastiasoro and B. M. Andersen, *Competing magnetic double-Q phases and superconductivity-induced reentrance of C_2 magnetic stripe order in iron pnictides*, Phys. Rev. B **92**, 140506 (2015).

[188] C. L. Henley, *Ordering due to disorder in a frustrated vector antiferromagnet*, Phys. Rev. Lett. **62**, 2056 (1989).

[189] P. Chandra, P. Coleman, and A. I. Larkin, *Ising transition in frustrated Heisenberg models*, Phys. Rev. Lett. **64**, 88 (1990).

[190] Q. Si and E. Abrahams, *Strong correlations and magnetic frustration in the high T_c iron pnictides*, Phys. Rev. Lett. **101**, 076401 (2008).

[191] M. H. Christensen, J. Kang, B. M. Andersen, I. Eremin, and R. M. Fernandes, *Spin reorientation driven by the interplay between spin-orbit coupling and Hund's rule coupling in iron pnictides*, Phys. Rev. B **92**, 214509 (2015).

[192] S. Maiti and A. V. Chubukov, *Renormalization group flow, competing phases, and the structure of superconducting gap in multiband models of iron-based superconductors*, Phys. Rev. B **82**, 214515 (2010).

[193] F. Rullier-Albenque, D. Colson, A. Forget, and H. Alloul, *Hall Effect and Resistivity Study of the Magnetic Transition, Carrier Content, and Fermi-Liquid Behavior in $Ba(Fe_{1-x}Co_x)_2As_2$*, Phys. Rev. Lett. **103**, 057001 (2009).

[194] L. Fang, H. Luo, P. Cheng, Z. Wang, Y. Jia, G. Mu, B. Shen, I. I. Mazin, L. Shan, C. Ren, and H.-H. Wen, *Roles of multiband effects and electron-hole asymmetry in the superconductivity and normal-state properties of $Ba(Fe_{1-x}Co_x)_2As_2$*, Phys. Rev. B **80**, 140508 (2009).

[195] M. P. Allan, A. W. Rost, A. P. Mackenzie, Y. Xie, J. C. Davis, K. Kihou, C. H. Lee, A. Iyo, H. Eisaki, and T.-M. Chuang, *Anisotropic Energy Gaps of Iron-Based Superconductivity from Intraband Quasiparticle Interference in LiFeAs*, Science **336**, 563 (2012).

[196] L. Fanfarillo, A. Cortijo, and B. Valenzuela, *Spin-orbital interplay and topology in the nematic phase of iron pnictides*, Phys. Rev. B **91**, 214515 (2015).

[197] M. H. Christensen, J. Kang, B. M. Andersen, and R. M. Fernandes, *Spin-driven nematic instability of the multiorbital Hubbard model: Application to iron-based superconductors*, Phys. Rev. B **93**, 085136 (2016).

[198] S. Fischer, *The role of Coulomb interaction for fluctuation corrections to the BCS theory of superconductivity*, Master's thesis, Karlsruhe Institute of Technology (2016).

[199] S. Fischer, M. Hecker, M. Hoyer, and J. Schmalian, *Short-distance breakdown of the Higgs mechanism and the robustness of the BCS theory for charged superconductors* (in preparation).

[200] M. Hoyer and J. Schmalian, *On the role of fluctuations for density-wave instabilities: physical origin for the failure of the mean-field description* (in preparation).

[201] A. Georges and J. S. Yedidia, *Onsager reaction terms for quantum many-body systems: Application to antiferromagnetic and superconducting order in the Hubbard model*, Phys. Rev. B **43**, 3475 (1991).

[202] P. G. J. van Dongen, *Thermodynamics of the extended Hubbard model in high dimensions*, Phys. Rev. Lett. **67**, 757 (1991).

[203] A. Martín-Rodero and F. Flores, *Solution for the U-negative Hubbard superconductor including second-order correlation effects*, Phys. Rev. B **45**, 13008 (1992).

[204] M. Y. Kuchiev and O. P. Sushkov, *Many-body correlation corrections to superconducting pairing in two dimensions*, Phys. Rev. B **53**, 443 (1996).

[205] A. Eberlein and W. Metzner, *Effective interactions and fluctuation effects in spin-singlet superfluids*, Phys. Rev. B **87**, 174523 (2013).

[206] A. Eberlein, *Fermionic two-loop functional renormalization group for correlated fermions: Method and application to the attractive Hubbard model*, Phys. Rev. B **90**, 115125 (2014).

[207] M. Hecker, *Collective modes in a superconductor in the presence of Coulomb interaction*, Master's thesis, Karlsruher Institut für Technologie (2016).

[208] D. Pekker and C. Varma, *Amplitude/Higgs Modes in Condensed Matter Physics*, Annual Review of Condensed Matter Physics **6**, 269 (2015).

[209] I. O. Kulik, O. Entin-Wohlman, and R. Orbach, *Pair susceptibility and mode propagation in superconductors: A microscopic approach*, Journal of Low Temperature Physics **43**, 591 (1981).

[210] P. W. Anderson, *Plasmons, gauge invariance, and mass*, Phys. Rev. **130**, 439 (1963).

[211] A. Paramekanti, M. Randeria, T. V. Ramakrishnan, and S. S. Mandal, *Effective actions and phase fluctuations in d-wave superconductors*, Phys. Rev. B **62**, 6786 (2000).

[212] R. E. Peierls, *Quantum Theory of Solids*, Oxford University Press (1955). (p. 108).

[213] A. W. Overhauser, *Spin Density Waves in an Electron Gas*, Phys. Rev. **128**, 1437 (1962).

[214] G. Y. Chitov and D. Sénéchal, *Renormalization-group study of interacting electrons*, Phys. Rev. B **52**, 13487 (1995).

[215] R. P. Feynman, *Space-Time Approach to Quantum Electrodynamics*, Phys. Rev. **76**, 769 (1949).

[216] V. G. Vaks, V. M. Galitskii, and A. I. Larkin, *Collective excitations in a superconductor*, Soviet Physics JETP **14**, 1177 (1962).

List of Figures

Acronyms

2D two-dimensional

AG Abrikosov-Gor'kov

ARPES angle-resolved photoemission spectroscopy

BCS Bardeen-Cooper-Schrieffer

CDW charge-density wave

CSDW charge-spin density wave

DOS density of states

FeSC iron-based superconductor

FS Fermi surface

iCDW charge-density wave with an imaginary order parameter

LAO $LaAlO_3$

NMR nuclear magnetic resonance

NN nearest neighbor

RG renormalization group

SC superconductivity

SCBA self-consistent Born approximation

SDW spin-density wave

STM scanning tunneling microscopy

STO $SrTiO_3$

SVC spin-vortex crystal

TRS time-reversal symmetry

Notation

In the following, we briefly summarize some conventions regarding the notation used throughout this thesis.

- We set $k_\mathrm{B} \equiv 1$ and $\hbar \equiv 1$, where k_B denotes the Boltzmann constant and $\hbar$ denotes the reduced Planck constant.
- We use the compact notation $k := (\mathrm{i}\nu_n, \boldsymbol{k})$ and $q := (\mathrm{i}\omega_n, \boldsymbol{q})$ for fermionic and bosonic states, respectively. Here, $\nu_n = (2n+1)\pi T$ is a fermionic Matsubara frequency whereas $\omega_n = 2n\pi T$ is a bosonic Matsubara frequency.
- $\beta = 1/T$ denotes the inverse temperature of the system.
- Furthermore, we abbreviate Matsubara summation and momentum integration as

  $$\int_k \ldots \equiv T \sum_{n=-\infty}^{\infty} \int \frac{\mathrm{d}\boldsymbol{k}}{(2\pi)^d} \ldots ,$$

  where in evaluating the diagrams, we often assume a constant density of states at the Fermi level and use

  $$\int \frac{\mathrm{d}\boldsymbol{k}}{(2\pi)^d} \ldots \equiv \rho_\mathrm{F} \int \mathrm{d}\varepsilon \int_0^{2\pi} \frac{\mathrm{d}\theta}{2\pi} \ldots .$$

  Lastly, at $T = 0$, the Matsubara summation can be substituted by a frequency integration

  $$T \sum_{n=-\infty}^{\infty} \ldots \equiv \int_{-\infty}^{\infty} \frac{\mathrm{d}\nu}{2\pi} \ldots .$$

- We use the Pauli matrices in their usual definition, together with the identity matrix $\sigma_0 \equiv \mathbb{1}_2$:

  $$\sigma_0 = \begin{pmatrix} 1 & 0 \\ 0 & 1 \end{pmatrix}, \qquad \sigma_1 = \begin{pmatrix} 0 & 1 \\ 1 & 0 \end{pmatrix}, \qquad \sigma_2 = \begin{pmatrix} 0 & -\mathrm{i} \\ \mathrm{i} & 0 \end{pmatrix}, \qquad \sigma_3 = \begin{pmatrix} 1 & 0 \\ 0 & -1 \end{pmatrix}.$$

  Throughout this thesis, Pauli matrices σ_i refer to spin whereas we use the notation τ_i for Pauli matrices in band space, orbital space, etc.
- Whenever working with indices that label two different discrete values (for example the band index $\lambda \in \{1, 2\}$ in the two-band model), we use $\bar{\lambda}$ to denote the 'opposite' of λ.
- In the patch approximation introduced in Chap. 3, we introduce the multi-index $\tau \equiv (\lambda, j, \eta)$ and its Kramers partner $\tau_\mathrm{K} \equiv (\lambda, j, \bar{\eta})$.
- In the context of fluctuation corrections at $T = 0$, we introduced the quantities

  $$r = \sqrt{\left(\frac{\omega}{2\Delta_0}\right)^2 + \left(\frac{v_\mathrm{F} q \cos\theta}{2\Delta_0}\right)^2}$$

  as well as $\nu_\pm = \nu \pm \frac{\omega}{2}$ and $\varepsilon_\pm = \varepsilon_{\boldsymbol{k} \pm \frac{\boldsymbol{q}}{2}} = \varepsilon \pm v_\mathrm{F} \frac{q}{2} \cos\theta$.

Furthermore, we compiled an overview of the notation used throughout this thesis which, however, makes no claim to be complete:

d	dimensionality of the system
d_s	spin dimensionality
$\boldsymbol{x}$	real space coordinate
$\boldsymbol{k}$, $\boldsymbol{q}$	crystal momenta
σ	spin
λ	band index
$\hat{\psi}^{(\dagger)}_{\lambda,\boldsymbol{k},\sigma}$	fermionic annihilation (creation) operator
$\varepsilon_{\lambda,\boldsymbol{k}}$	dispersion (measured from the chemical potential μ)
$\mathcal{G}^{-1}$	inverse fermionic matrix propagator
$\mathcal{D}^{-1}$	inverse fluctuation propagator
ρ_F	density of states at the Fermi level
k_F	Fermi momentum
v_F	Fermi velocity
E_F	Fermi energy
Λ	cut-off
E_C	Coulomb energy at the Fermi momentum
ω_p	plasma frequency
$\Delta(\boldsymbol{r}) \in \mathbb{C}$	order parameter for SC order (amplitude fluctuations η_1 and phase fluctuations η_2)
$\boldsymbol{M}(\boldsymbol{r}) \in \mathbb{R}^{d_\mathrm{s}}$	order parameter for SDW order (fluctuations $\boldsymbol{m}$: 1 longitudinal component, $d_\mathrm{s}-1$ transverse components)
$\rho(\boldsymbol{r}) \in \mathbb{R}$	order parameter for CDW order (fluctuations ϱ)
T_c, T_N, T_s	transition temperatures for SC, SDW order, and structural transition ($T_{\mathrm{c},0}$ denotes the SC transition temperature of the clean system)
$\langle \ldots \rangle_\mathrm{dis}$	disorder average
n_imp	impurity concentration
l_mfp	mean free path
R_loc	localization length
Γ	scattering rate (a measure of disorder strength)
Γ_c	critical scattering rate (at which superconductivity is destroyed by impurities)
ϕ	phase in the interband scattering matrix element, cf. Eq. (2.15)
a	quadratic coefficient in Ginzburg-Landau expansion
u	quartic coefficient in Ginzburg-Landau expansion
g	nematic coupling constant in Ginzburg-Landau expansion
w	planar coupling constant in Ginzburg-Landau expansion
γ	Euler-Mascheroni constant
$\psi_n(x)$	n^th derivative of the digamma function
$\zeta(x)$	Riemann zeta function
$\mathrm{U}(N)$	unitary group
$\mathrm{SU}(N)$	special unitary group
$\mathrm{O}(N)$	orthogonal group
$\mathrm{SO}(N)$	special orthogonal group

Acknowledgments

Finally, I have the pleasure to thank all those, who made this thesis possible in the first place.

First and foremost, I would like to express my deepest gratitude to my supervisor Prof. Dr. Jörg Schmalian for giving me the opportunity to do my doctorate in his group. He is a passionate and dedicated scientist and teacher and it was a lot of fun to work with him and learn from him. I am grateful for his guidance and support during the last years. Furthermore, I appreciate the fascinating research topics he introduced me to and the interesting schools and conferences I was given the opportunity to attend. I really enjoyed working at both the Institut für Theorie der Kondensierten Materie and at the Institut für Festkörperphysik for the last years. Hence I am glad that Prof. Dr. Matthieu Le Tacon agreed to be the second reviewer of this thesis – thank you very much!

I am also much obliged to my collaborators Rafael Fernandes, Sonja Fischer, Matthias Hecker, Alex Levchenko, Mathias Scheurer, Jörg Schmalian, and Sergey Syzranov. I greatly enjoyed our joint research projects and the fruitful discussions we had – I learned a lot about physics from them. Moreover, these discussions sparked many interesting ideas that were essential for the research that lead to this thesis.

Furthermore, I would like to gratefully acknowledge the helpful discussions that I had with Anna Böhmer, Alexander Herbig, Patrik Hlobil, Una Karahasanovic, Julia Link, Tim Ludwig, Peter Orth, Michael Schütt, and Philipp Weiß during our book seminars, the splendid 'pnictide breakfast discussion group', and on so many other occasions.

Likewise, I very much enjoyed the company of Matthias Bard, Nikolaos Kainaris, Elio König-Tarasevich, and Mathias Scheurer in our shared office. They were always willing to discuss physics, helped a lot when I struggled with everyday problems, and were always up for a joke.

Another big thank you goes to all my other colleagues at Institut für Theorie der Kondensierten Materie for making this a fantastic place to work at – the atmosphere is both very familiar and scientifically stimulating. I immensely benefited from their input following my seminar talks as well as their constant readiness to help with physical, technical, organizational, and private questions and problems. Moreover, I very much appreciate the many interesting conversations, memorable outings, and other adventures with them. In particular, I would like to acknowledge Andreas Poenicke for technical support as well as Matthias Bard, Stefan Beyl, Ulf Briskot, Fabienne Flatter, Pia Gagel, Matthias Hecker, Patrik Hlobil, Bhilahari Jeevanesan, Nikolaos Kainaris, Janina Klier, Markus Klug, Lars Lauke, Julia Link, Tim Ludwig, Pablo Schad, Mathias Scheurer, and Philip Wollfarth for our breaks and evenings with coffee, Skat, physics, cake, Mate, dancing, and for so much more.

Special thanks go to those who proofread parts of the manuscript and thereby helped me to improve it: Matthias Bard, Stefan Beyl, Pia Gagel, Patrik Hlobil, Bhilahari Jeevanesan, Nikolaos Kainaris, Markus Klug, Julia Link, Tim Ludwig, and Mathias Scheurer.

Last but not least, I would like to thank my family and my friends for their moral support. Especially during the writing of this thesis, they were there for me whenever I needed them, and – equally important – also understood that I needed to be left alone sometimes. In particular, I would like to thank Patrick for providing the proper music, for his advice in aesthetical questions, for his patience and encouragement, and for making me smile, as well as my parents for their unconditional support, their constant encouragement and their advice.